CONTROLLING THE INTERFACIAL BEHAVIOUR OF COLLOIDAL MICROGEL SYSTEMS

JOANNA BRONWEN THORNE

A thesis submitted in partial fulfilment of the requirements of the University of Greenwich for the Degree of Doctor of Philosophy

April 2012

DECLARATION

I certify that this work has not been accepted in substance for any degree, and is not concurrently being submitted for any degree other than that of Doctor of Philosophy being studied at the University of Greenwich. I also declare that this work is the result of my own investigations except where otherwise identified by references and that I have not plagiarised the work of others.

.... Joanna Thorne (Candidate)

.... Date

.... Professor M. J. Snowden (Supervisor)

.... Date

.... Dr B. D. Alexander (Supervisor)

.... Date

ACKNOWLEDGEMENTS

ABSTRACT

Controlling the Interfacial Behaviour of Colloidal Microgel Systems

Submitted in partial fulfilment of the requirements of the University of Greenwich
for the degree of Doctor of Philosophy by
Joanna B. Thorne

Hydrophobically modified colloidal microgel particles were prepared by a surfactant-free emulsion polymerization of *N-iso*propylacrylamide (NIPAM) with more hydrophobic vinyl ether/ester/silane co-monomers (10 % total mass monomer). Most of the resultant dispersions were novel co-polymer microgels and all exhibited a thermo-sensitive volume phase transition. Key properties of the microgels, *i.e.* size, electrophoretic mobility and volume phase transition temperature (VPTT), were determined by dynamic light scattering (DLS), laser Doppler electrophoresis, UV-visible spectrophotometry and scanning electron microscopy. The influence of co-monomer incorporation, *e.g.* structure and relative hydrophobicity, upon the physico-chemical properties of the microgel was examined. Hydrophobic modification strongly influenced size, slightly altered electrophoretic mobility and left the VPTT relatively unaffected.

The interfacial properties of the microgels were studied by tensiometry. Substantial reductions in the surface tension of water were observed for all microgels, close in magnitude to that achieved by the surfactant sodium dodecyl sulphate, but at a far lower concentration. The effect was influenced by a complex combination of parameters including size, charge, conformation, co-monomer type, temperature and solvent quality.

A DLS study of the swelling response of microgels in the presence of less polar co-solvents (short-chain alcohols) found that hydrophobic modification altered alcohol-induced de-swelling/re-entrant swelling behaviour and particle-dispersant interactions. Furthermore, the characteristic temperature-driven volume collapse above the VPTT was overcome by alcohol addition.

Finally, the stability and heteroflocculation of anionic/cationic mixtures of poly(NIPAM) microgels was studied by DLS and UV-visible spectrophotometry as a function of dispersion temperature, pH and electrolyte concentration. Electrolytes of increasing cation valency (NaCl, MgCl$_2$, LaCl$_3$) were used to reduce the particle Debye length.   Conditions conducive to preserving stability or encouraging flocculation were identified and related to the complex balance of particle interactions.

It is anticipated that the results of these investigations may support future development of microgels with applications relating to more hydrophobic environments and materials.

CONTENTS

PUBLICATIONS

Publications and presentations arising from work contained within this thesis

Thorne, J. B, Vine, G. J., Snowden, M. J. (2011) 'Microgel applications and commercial considerations', *Colloid & Polymer Science*, **289**(5–6), 625–646.

Thorne, J. B, Snowden, M. J. (2011) 'Controlled stabilization of 'smart' nanoparticle dispersions', poster at *Nanoformulation 2011*, Singapore.

Thorne, J. B, Snowden, M. J. (2011) 'Heteroflocculation behaviour of mixed-charge poly(NIPAM) microgel dispersions', poster at *Colloids and Materials 2011*, Amsterdam.

Thorne, J. B, Snowden, M. J. (2011) 'Controlling the stability of smart nanoparticle dispersions', poster at *SET for BRITAIN Finals and Exhibition*, UK

Thorne, J. B, Benée, L. S., Snowden, M. J. (2010) 'Characterization of hexane-water Pickering emulsions stabilized by hydrophobically modified poly(*N-iso*propylacrylamide)-based microgel particles', poster and oral flash presentation at *Faraday Discussion FD146: Wetting dynamics of hydrophobic and structured surfaces*, Richmond, USA.

Thorne, J. B, Benée, L. S., Snowden, M. J. (2009) 'The influence of organic solvents on the hydrodynamic diameter of hydrophobically-modified poly(NIPAM)-based microgels', oral presentation at *14th Annual UK Polymer Colloid Forum Meeting*, UK.

Thorne, J. B, Benée, L. S., Snowden, M. J. (2009) 'The influence of organic solvents on the hydrodynamic diameter of hydrophobically-modified poly(NIPAM)-based microgels', oral presentation at *2009 European Student Colloid Conference*, Spain.

Thorne, J. B, Benée, L. S., Snowden, M. J. (2008) 'Interfacial properties of colloidal microgels', poster at *UK Polymer Colloids Forum, Young Researchers Symposium*, UK.

TABLES

FIGURES

Chapter 2: Synthesis of poly(NIPAM)-based microgels

Chapter 3: Characterization of poly(NIPAM)-based microgels

Chapter 4: Investigation of the interfacial properties of hydrophobically modified poly(NIPAM) microgel particles

Chapter 6: Investigation of the heteroflocculation of mixed-charged poly(NIPAM) microgel systems

ABBREVIATIONS

% w/v	Percentage weight per volume
Π_{el}	Elastic pressure of the polymeric network
Π_{in}	Osmotic pressure of the mobile ions inside a microgel
Π_{out}	Osmotic pressure of the mobile ions in the bulk solution
$1/\kappa$	Debye length or double layer thickness
2-PrOH	2-propanol
4-VP	4-vinyl pyridine
a	Particle radius
A	Absorbance
AA	acrylic acid
APS	ammonium persulphate
BuA	butyl acrylate
CCC	Critical coagulation concentration
CFT	Critical flocculation temperature
CMC	Critical micelle concentration
CVA	4,4′-azo-bis(4-cyanovaleric acid)
D	Diffusion coefficient
D_H	Hydrodynamic diameter
DLS	Dynamic light scattering
DLVO	Derjaguin, Landau, Verwey and Overbeek theory
DVE	dodecyl vinyl ether
EP	Emulsion polymerization
EtOH	Ethanol
F	Force
f(κa)	Henry's function
I	Transmitted light intensity
I_0	Incident light intensity
iPMA	*iso*propyl methacrylate
k	Boltzmann constant
KPS	di-potassium peroxidisulphate or potassium persulphate
L	Wetted length of the plate

LCST	Lower critical solution temperature
MAA	methacrylic acid
MMA	methyl methacrylate
MBA	*N,N′*-methylenebisacrylamide
MeOH	Methanol
MPA	2,2′-azo-bis(2-methylpropionamidine) dihydrochloride
n	*n*-value
N1–6	Poly(NIPAM)
NIPAM	*N-iso*propylacrylamde
P-COO$^-$	Poly(NIPAM) microgel (N4) with carboxylate surface groups
P-NH$_3^+$	Poly(NIPAM) microgel (N4) with amine surface groups
P-SO$_3^-$	Poly(NIPAM) microgel (N4) with sulphate surface groups
PCS	Photon correlation spectroscopy
PdI	Polydispersity index
PEG	poly(ethylene glycol)
PEO	poly(ethylene oxide)
PSD	Particle size distribution
RI	Refractive index
SANS	Small-angle neutron scattering
SDS	sodium dodecyl sulphate
SEM	Scanning electron microscopy
SFEP	Surfactant-free emulsion polymerization
T	Temperature or transmittance (specified in text)
TBVE	*tert*-butyl vinyl ether
TEM	Transmission electron microscopy
TMVS	trimethyl(vinyl)silane
TPVE	*tert*-pentyl vinyl ether
TPVS	triphenyl(vinyl)silane
U_E	Electrophoretic mobility
V	Voltage
V4TBB	vinyl-4-*tert*-butyl benzoate
V_A	Energy of attractive van der Waals forces
VBE	vinyl butyl ether
VD	vinyl decanoate

VL	vinyl laurate
VP	vinyl pyridine
VPT	Volume phase transition
VPTT	Volume phase transition temperature
V_R	Energy of repulsive forces from the electrical double layer
VS	vinyl stearate
V_T	Total energy of interaction
VTMOS	vinyltrimethoxyvinylsilane
W_{min}	Minimum amount of work
x	Distance from surface or volume fraction (specified in text)
z	Ion valency
α	De-swelling ratio
γ_0	Interfacial tension
δ	Thickness of electrical double layer
ΔA	New unit area of water-air interface
ϵ	Electronic charge
ε	Dielectric constant/relative permittivity
ε_0	Permittivity of a vacuum
ζ	Zeta potential
η	Viscosity
θ	Contact angle
κ	Reciprocal of the Debye length
λ	Wavelength
σ	Surface tension
Ψ	Electric potential
Ψ_0	Electric potential at surface
Ψ_d	Stern potential
Ψ_x	Electric potential at distance x from surface

LITERATURE REVIEW

1.1 Introduction

Over the last three decades there has been great interest in hydrophilic microgels that shrink and swell in water in response to changes in environmental conditions such as pH, ionic strength and temperature.[1,2,3] These microgels are capable of the sorption/desorption of a variety of materials,[4] *e.g.* removing water from biodiesel.[5] By incorporating different monomers and cross-linkers into the structure of a microgel it is possible to adjust its swelling response to specific conditions.[6,7] The objective of this work was to alter the composition of microgel particles through the incorporation of more hydrophobic co-monomers and to investigate the impact this modification has upon the physico-chemical properties and interfacial behaviour of the microgels. This chapter is, therefore, a review of existing literature relating to the synthesis, structure, characterization and applications of microgel particles, particularly in relation to the hydrophobic modification of microgels.

1.2 Microgels

Microgel particles are discrete, intra-molecularly cross-linked polymeric gel particles, that are uniformly dispersed in a solvent medium and swollen by a good solvent.[2,8,9] Solvent quality is determined by the nature of solvent-polymer interactions, which influence polymer configuration such that a polymer will expand in a good solvent and contract in a poor solvent.[10] Baker first used the term "microgel" to describe intramolecularly cross-linked particles,[2] whilst Staudinger and Husemann[11] were the first to prepare microgel particles using divinyl benzene.[3]

This work is concerned with microgel particles based on *N-iso*propylacrylamide (NIPAM). Poly(NIPAM) microgel particles were first prepared by Pelton and Chibante,[8] who observed that the aqueous poly(NIPAM) lattices formed were swollen below the lower critical solution temperature (LCST) of linear poly(NIPAM) (32 °C) but shrunken at temperatures above the LCST. Further investigations

revealed that the shrinking and swelling behaviour occurred in response to changes in environmental conditions such as pH, ionic strength and temperature.[2] It is this key characteristic that has led to the application of microgel particles to a wide range of uses under specific environmental conditions.[3]

1.2.1 Terminology

Various terms are used interchangeably to describe microgels and other particles that differ in size, composition, structure, synthesis, dispersion medium, properties and application.[12] These terms have included microsphere,[13,14] nanogel[15] and hydrogel sphere.[16] Murray and Snowden[2] note that whilst terms such as "submicron gel bead" or "nano-particle" give an indication of the dimensions of the particles, their use has not always been confined to cross-linked structures and may therefore lead to confusion regarding the nature of the particle under consideration. This work is concerned with cross-linked NIPAM-based microgel particles in the colloidal size range, *i.e.* 1 nm – 1 μm,[17] which exhibit stimuli-responsive swelling behaviour.

1.2.2 Synthesis

A variety of methods are available for the synthesis of microgel particles.[18] These include inverse (micro)emulsion polymerization, living free-radical polymerization and radiation polymerization.[7,18] The most commonly used technique is emulsion polymerization (EP),[3,4] a versatile type of free-radical polymerization.[19] In conventional EP, surfactants inhibit particle growth to produce very small particles (typically smaller than 150 nm) with a narrow particle size distribution.[6,18] However, it is difficult to completely remove residual surfactant following EP, which led to the development of surfactant-free emulsion polymerization (SFEP), the synthesis method used in this investigation.

SFEP was first used by Goodwin *et al.*[20] to prepare non-swollen poly(styrene) latex particles and it has since become the basis of a standard synthesis method for poly(NIPAM)-based microgels.[6] To polymerize the NIPAM monomers and facilitate particle formation, SFEP requires a continuous phase with high dielectric constant (*e.g.* water) and an initiator (*e.g.* di-potassium peroxidisulphate, $K_2S_2O_8$, KPS).[6] A cross-

linker with two vinyl groups (*e.g. N,N'*-methylenebisacrylamide, MBA) is incorporated to enable formation of cross-links between polymer chains.[6,8,18] Figure 1.1 illustrates a mechanism for microgel preparation using SFEP, taken from Saunders and Vincent.[3]

$$S_2O_8^{2-} \xrightarrow{\Delta} 2(\bullet SO_4^-) \quad \textbf{(a)}$$

$$M + \bullet SO_4^- \longrightarrow \bullet MSO_4^- \quad \textbf{(b)}$$

$$M + \bullet MSO_4^- \longrightarrow \bullet M_{x+1} SO_4^- \quad \textbf{(c)}$$
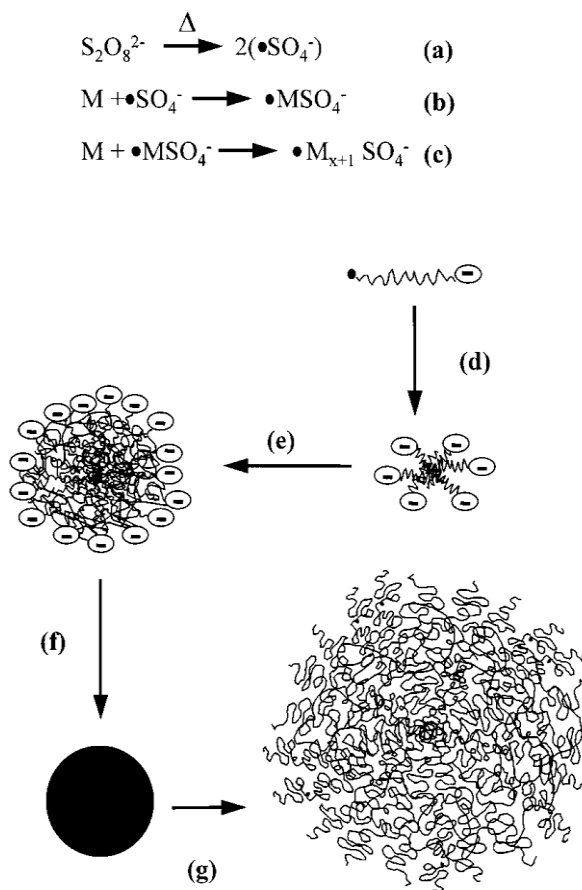
Figure 1.1 Mechanism of microgel particle preparation by SFEP, from Ref. [3]

(a) initiator decomposition; (b) initiation; (c) propagation; (d) particle nucleation; (e) particle aggregation; (f) particle swelling in a poor solvent; and (g) particle swelling in a good solvent. The counter cations and particle charges in steps (f) and (g) have been omitted for clarity. M indicates a vinyl monomer.

The mechanism begins with thermal decomposition of the initiator into free radicals that initiate polymerization (via homologous nucleation). The radicals attack the vinyl group of the monomers, which propagate into oligomers with a polymer chain attached to a charged head group derived from the initiator/free radical. In addition to being colloidally unstable, these oligomers are surface active. When their chain length exceeds the solubility limit of the solvent they nucleate into spherical micelle-like structures, with the polymer chains oriented to the core and the charged head groups stabilizing the micelle by aligning at the surface, *i.e.* the charged chain ends tend to concentrate at the particle-water interface. Links form between the polymer chains by reaction with the cross-linkers.[3,6,9]

Limited aggregation of the micelle-like nuclei takes place. This causes the surface charge density of the resulting particles to increase until the particles are colloidally stable compared with similar and larger particles, at which point the particles achieve electrostatic stabilization in the continuous phase. The particles continue to grow in size as remaining monomers and oligomers are incorporated into the structure; once the concentration of free oligomers falls below a certain threshold, growth of the particles will cease. The process ends when a free radical enters the structure and terminates the reaction.[3,6,9]

The main advantages of SFEP are that it avoids the need to remove residual surfactant following the process and it has a very short particle nucleation period (typically of minutes), which ensures a narrow particle size distribution.[6,18] The reaction is conducted under an inert atmosphere of nitrogen, whilst heating to 70 °C ensures that the initiator thermally decomposes and that the oligomers undergo phase separation to form nuclei rather than continuing to grow into longer chains.[18] It is possible to incorporate other vinyl co-monomers into the microgel structure using SFEP,[7] for example poly(NIPAM-*co*-vinyl laurate) microgels have been prepared.[21]

The nature of the monomers, co-monomers, initiators and cross-linkers comprising a particular microgel not only influences the properties of the resulting particles, but also the synthesis method required to produce them. For example, the solvent required for SFEP should have a high dielectric constant and may not be as suitable a solvent for more hydrophobic monomers such as styrene,[22] which may be more readily polymerized via EP using solvents such as ethylbenzene, toluene or tetrahydrofuran.[3] The particular characteristics of various monomers and other particle components, and their subsequent impact upon microgel structure and properties will be discussed below.

1.2.3 Structure

The microgel resulting from SFEP can be described as a uniform dispersion of discrete polymeric gel particles, in a continuous solvent medium.[3,6] The internal structure of the particles resembles a typical cross-linked network, with a porous, "sponge-like" structure.[2] Building on the details of the polymerization mechanism

outlined in Fig. 1.1, the following schematic illustrates simply the basic individual structural components of a microgel particle (Fig. 1.2).

In the spherical, micelle-like structure, the hydrophobic polymer chains tend to orientate to the interior, with their charged head groups stabilizing the structure by aligning at the surface of the sphere. The cross-linker molecules form bridges between the polymer chains, further stabilizing the structure, and some solvated polymer chains extend outwards into the continuous phase (water in this case), creating a steric barrier that is often known as the "hairy layer".[23,24,25,26] A generic model of poly(NIPAM) microgel structure discussed by Pelton and Hoare[9] suggests it is possible that, in addition to residing at or just within the surface of the sphere, some of the electrical charges may reside at the end of the solvated polymer chains. The combined presence of the electrical charges and "dangling surface chains" or "hairs" at the surface means that microgel particles are generally very resistant to aggregation, *i.e.* are colloidally stable.[9]

Key:

⟿●   Polymer chain with charged head group

────   Crosslinker

⟿   Polymer chain extending into solvent, forming 'hairy layer'
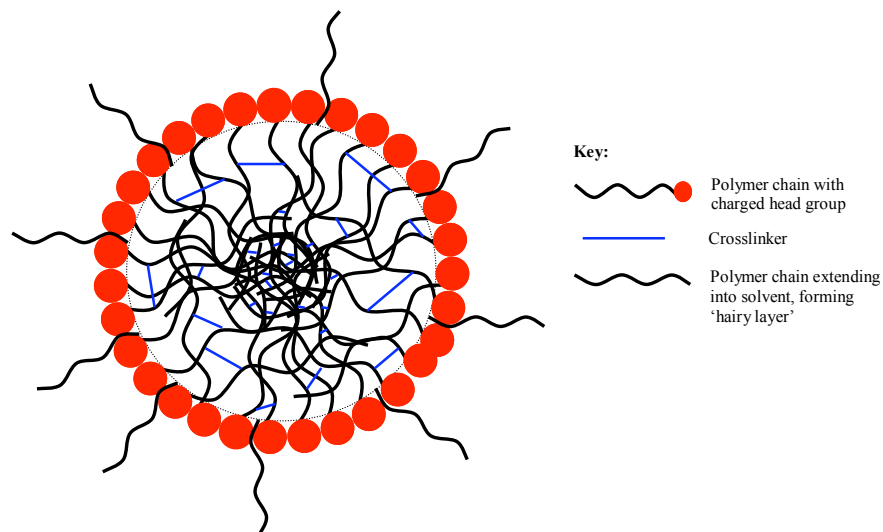
Figure 1.2 Schematic of the basic structural components of a microgel particle

1.2.3.1 Monomer/co-monomer

NIPAM is the monomer upon which most water-swellable microgel systems are based (Fig. 1.3). Similar microgels have been prepared with great effect from a range of other monomers and co-monomers. For example, particles have been successfully prepared from alternative acrylamide monomers such as *N*-ethylacrylamide[27] or *N*-*iso*propylmethacrylamide.[28] Other non-acrylamide monomers that have been used

include acrylic acid,[29] *N*-[(2-hydroxy-3-trimethylammonium)propyl]chitosan chloride,[30] methacrylic acid,[31] *N*-vinylcaprolactam,[32,33,34,35,36] methylmethacrylate[37] and styrene.[38] The key characteristic of each of these monomers is the presence of at least one vinyl group that can participate in polymerization and/or cross-linking reactions.[3,6] The term "homo-polymer" is used to refer to polymers derived from a single species of monomer,[39] hence microgels based on single monomers are known as homo-polymer microgels.[40]
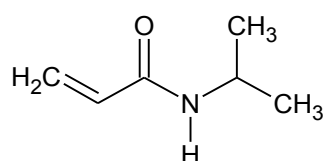
Figure 1.3 Structure of *N-iso*propylacrylamide

Additional monomers can also be co-polymerized into the microgel structure, such as butyl acrylate and methacrylic acid.[41,42] For example, Snowden *et al.*[43] prepared poly(NIPAM-*co*-acrylic acid) particles, whilst Saunders *et al.*[44] prepared pH-responsive poly(ethylacrylate-*co*-methacrylic acid-*co*-1,4-butanediol diacrylate) microgel particles for use in the restoration of damaged load-bearing tissue. Polymers derived from more than one monomer species are known as co-polymers,[45] hence microgels based on two or more microgels are termed co-polymer or hetero-polymer microgels.

Microgel particles tend to possess characteristics derived from the individual monomer(s) from which they are composed.[5,46,47] For example, linear poly(NIPAM) chains are thermosensitive, displaying conformational changes (a coil-to-globule transition) in response to changing temperature,[48,49] a property which is conveyed to poly(NIPAM)-based microgels.[50] This manifests as a volume-phase transition in which the particles switch between swollen and collapsed conformations, changing from a soft porous, network-like structure to a smaller, harder, latex-like particle.[9,51] This is described in detail in Section 1.2.4.2. The monomeric composition of a microgel will also determine whether the particles are swellable in aqueous or non-aqueous solvents.[2]

Co-monomers are utilized to alter the physico-chemical characteristics of the microgel particles.[18] For example, co-monomers such as acrylic acid can be used to introduce pH sensitivity to NIPAM-based microgels.[43] Hydrophobic and hydrophilic co-monomers can be incorporated to alter the response of microgels to temperature[24,43] and stability in solvents of different polarity.[5] For example, Hoffman *et al.*[52] co-polymerized NIPAM with a hydrophilic co-monomer (acrylamide) and a hydrophobic co-monomer (*N-tert*-butyl acrylamide), then measured the LCST of the linear co-polymers at various co-polymer inclusion ratios. It clearly showed that co-polymerization with a hydrophilic co-monomer increased the LCST whilst co-polymerization with a hydrophobic co-monomer lowered the LCST (Fig. 1.4).
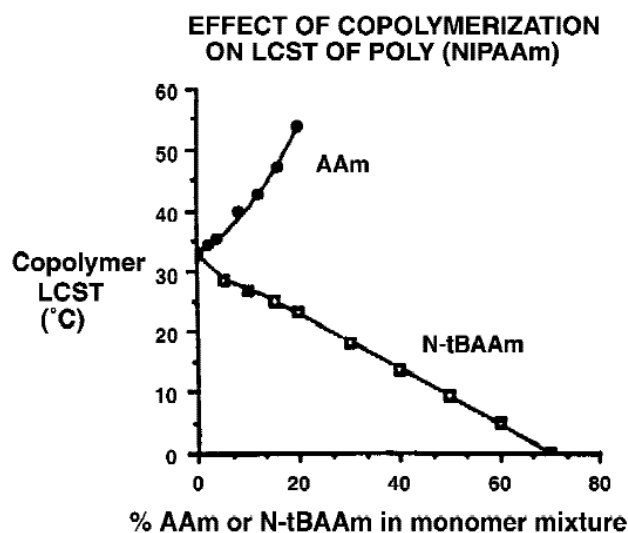
Figure 1.4   Effect upon LCST of poly(NIPAM) of co-polymerization with a hydrophilic (acrylamide, AAm) or hydrophobic (*N*-butyl acrylamide, N-tBAAm) co-monomer, taken from Ref. [52]

Examples of hydrophobic co-monomers used in poly(NIPAM) microgel synthesis include butyl acrylate,[40] 4-vinyl pyridine[46] and *iso*propyl methacrylate.[53] Co-monomers can also be used to introduce specific functional groups into the structure of a microgel, *e.g.* the pH sensitivity achieved by co-polymerizing NIPAM with acrylic acid results from the introduction of carboxylic acid groups from the co-monomer. Meunier *et al.*[54] prepared hydrophilic, cationic microgels containing amino groups by co-polymerizing NIPAM with 2-aminoethylmethacrylate hydrochloride in the presence of a cationic initiator (2,2′-azo-bis(2-methylpropion-amidine) dihydrochloride). Using such co-monomers, polymers that contain a

substantial number of ionic or ionizable groups can be produced, which are known as polyelectrolytes.[55]

The ratio of monomer to co-monomer is also significant. In the case of poly(NIPAM)-based microgels, the co-monomer content is typically restricted to 5–10 % total monomer weight, which is sufficient to significantly influence the overall properties of the resultant microgel particles.[4,5,6] At larger co-monomer inclusion ratios, the thermo-responsive characteristics of NIPAM may begin to be lost from the microgel.

Co-monomer concentration may also influence the polymerization rate. For example, Meunier *et al.*[54] observed that when synthesising poly(NIPAM-*co*-2-aminoethylmethacrylate hydrochloride), higher co-monomer concentrations led to an increased initial polymerization rate, suggesting that the cationic 2-aminoethylmethacrylate hydrochloride caused the formation of a larger number of polymerization loci during synthesis.

Various attempts to determine the structure of microgel particles with respect to monomer composition have been made as it is likely that differences in the physico-chemical properties of monomers cause differences both in reaction behaviour during synthesis and in the resultant particle structure. For example, if a co-monomer (or cross-linker) is more reactive than the monomer then it will be incorporated into the polymer chain more rapidly and the relative proportions of the two in the reaction mixture and the microgel structures themselves will vary with time.[56] A small-angle neutron scattering (SANS) investigation probing the internal structure of poly(NIPAM-*co*-butyl acrylate) particles discovered that the BuA co-monomer appeared in small hydrophobic domains within the NIPAM network.[57] Raman and nuclear magnetic resonance (NMR) spectroscopy have also been used to obtain semi-quantitative measurements of the extent of incorporation of co-monomers in co-polymer poly(NIPAM) microgels.[40]

Alkaline titration has been used to study the distribution of acrylic acid (AA) residues in poly(NIPAM-*co*-AA) particles; the results indicated that the residues are clustered within the microgel network rather than being uniformly distributed.[58] Hoare and Pelton[59] observed that the more slowly a functional group reacts with NIPAM (by

EP in presence of sodium dodecyl sulphate, SDS), the more localized the functional groups are on the microgel surface; in poly(NIPAM-*co*-vinylacetic acid), a large number of vinyl acetic acid units were found on highly mobile chain ends at or near the microgel surface. Building on this work, the same group developed a kinetic model capable of semi-quantitatively predicting the macroscopic chain and radial functional group distribution in carboxylic-acid-functionalized poly(NIPAM)-based microgels.[60] Despite these efforts, however, the precise structure of microgels remains unclear. For example, microgel surface topology is poorly described in literature, with surface-chain hair-length distribution or density rarely known.[9]

1.2.3.2 Cross-linkers

The cross-links in the structure of a microgel prevent the polymer chains, *e.g.* poly(NIPAM), dissolving in water at low temperatures.[4,61] Consequently, by controlling the degree of cross-linking within the particle network, the extent to which a microgel particle swells can be influenced (Fig. 1.5).[3] Cross-linkers also influence the rate of conformational change, with a higher cross-link density ensuring the polymer chains are held more closely together and resulting in more rapid collapse.[18]
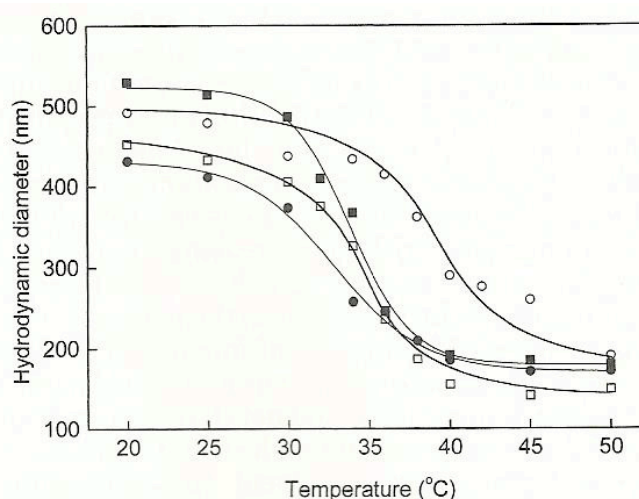
Figure 1.5   Variation in hydrodynamic diameter with temperature for poly(NIPAM) microgels prepared with different MBA cross-linker densities (■ = 5 %, □ = 10 %, ● = 20 %, ○ = 30 %), taken from Ref. [66]

There also appears to be a correlation between cross-linker density and particle size, with higher cross-linker densities resulting in smaller average particle sizes.[62] The

presence of cross-linkers means that microgels, in addition to having a finite structure, are not strictly soluble and instead form colloidal dispersions.[2] The key characteristic of monomers used for this purpose is the presence of two vinyl groups, which enable cross-link formation between polymer chains to occur.[6,8,18] Examples of commonly used cross-linkers used include divinyl benzene and *N,N'*-methylenebisacrylamide (MBA). However, self-cross-linking of poly(NIPAM) microgels can be achieved in the absence of such a cross-linker.[61,63,64,65] Prepared under otherwise similar conditions, the resultant particles differed only in possessing a lower solid content and larger swelling ratio than standard MBA-cross-linked poly(NIPAM) microgels.[65]

Cross-linker distribution is unlikely to be uniform throughout the structure: Wu *et al.*[61] studied the consumption of NIPAM and MBA during poly(NIPAM) synthesis (by EP using SDS) as a function of time and temperature and found that MBA was consumed more quickly than NIPAM. This supports the conclusions of McPhee *et al.*[67] who observed that a large proportion of MBA was incorporated during the initial growth of poly(NIPAM) particles during synthesis. This indicates that the cross-link density of the first particles formed is likely to be greater than that of particles formed later during the synthesis reaction.[61] Previously, Nieuwenhuis and Vrij[35] noted an inhomogeneous distribution of divinyl benzene cross-linker within poly(MMA) particles.

These findings indicate the likely existence of areas of high density of cross-linker, particularly towards the particle core, with a decreasing gradient of cross-linker content from the core to the surface.[26] Using dynamic light scattering and laser Doppler electrophoresis to study poly(NIPAM) particle size and electrophoretic mobilities, Daly and Saunders[63] found evidence of a highly cross-linked core and lightly cross-linked shell structure, which was later confirmed by Saunders.[64] Following an NMR study of poly(NIPAM) cross-linked with MBA, Guillermo *et al.*[26] proposed the existence of a core-shell structure, with the relative core size proportional to the MBA concentration. Meunier *et al.*[54] observed that the distribution of MBA cross-linker in cationic poly(NIPAM-*co*-2-aminoethylmethacrylate hydrochloride) particles was strongly influenced by the 2-aminoethylmethacrylate hydrochloride concentration at the start of the polymerization reaction.

Collectively these findings have implications for the pore size of the "sponge-like" structure, which possibly increases from the centre to the periphery.[3] Stieger *et al.*[65] showed that microgel segment density (and hence pore size) is not homogenous in the swollen state. Several attempts to determine microgel pore size have been made. For example, Saunders and Vincent[66] estimated from de-swelling data that the minimum pore size of poly(NIPAM) cross-linked with 4.5 wt.% MBA was 2 nm. More recently, Si *et al.*[67] used scanning electron microscopy, confocal laser scanning microscopy and a gas sorption porosity analyzer to measure the pore size of a range of poly(NIPAM-*co*-AA) microgels (with varying wt. % AA), finding that pore size ranged from 2–50 nm and could be controlled simply by changing the wt. % AA. A barrier to the precise determination of pore size is the need to firstly dry the particles but without changing their structures. Si *et al.*[67] tested several drying techniques, observing structural damage during drying by lyophilization and vacuum drying, but finding that the original internal and external poly(NIPAM-*co*-AA) microgel structure could be preserved using CO_2 supercritical drying.
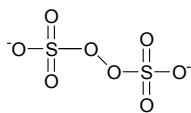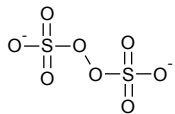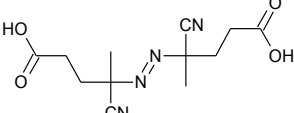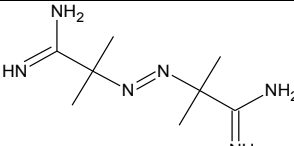
The degree of cross-linking also controls the extent to which a microgel particle can swell, a key property of poly(NIPAM) microgel particles.[3,61,68] For example, the study by Guillermo *et al.*[26] of the swelling behaviour of poly(NIPAM) particles as a function of MBA cross-linker concentration found that swelling capability was clearly governed by cross-linker content. This was in good agreement with the previously mentioned work of Wu *et al.*[61] Furthermore, Meunier *et al.*[68] identified a maximum MBA limit above which unstable thiol-containing poly(NIPAM) microgel particles resulted during polymerization.

1.2.3.3 Initiators

Thermally decomposed radical initiators are typically used in SFEP to initiate the polymerization of poly(NIPAM)-based microgels. Radical initiators are usually peroxide or azo compounds[69] and examples include di-potassium peroxidisulphate (KPS), ammonium persulphate (APS), 4,4′-azo-bis(4-cyanovaleric acid) (CVA) and 2,2′-azo-bis(2-methylpropion-amidine) dihydrochloride (MPA). Each of these decomposes to form a different free radical, which ultimately forms the charged head

groups that reside on the microgel surface and stabilize the particles, resulting in microgel species which are charged (Table 1.1).

Table 1.1 Examples of radical initiators

Initiator	Structure	Microgel surface group	Nature of microgel formed
di-potassium peroxidisulphate (KPS)		$SO_3H/$ SO_3^-	Anionic
ammonium persulphate (APS)		$SO_3H/$ SO_3^-	Anionic
4′-azo-bis(4-cyanovaleric acid) (CVA)		COOH/ COO⁻	Anionic
2,2′-azo-bis(2-methylpropionamidine) dihydrochloride (MPA)		$NH_3^+/$ NH_2	Cationic

The quantity of initiator used is also influential. Meunier *et al.*[68] prepared cationic poly(NIPAM-*co*-vinylbenzylisothiouronium chloride) particles at varying MPA concentrations and observed an increase in particle size (by quasi-elastic light scattering and transmission electron microscopy, TEM). In addition, the swelling capacity of the particles increased as the MPA concentration increased.

1.2.3.4 Structure and particle interactions at interfaces

It is important not only to understand the structure of the microgel particles themselves, but, as they are colloidal particles in dispersion, also their structure in relation to the bulk phase. The structure of the liquid in the interfacial region between the particle and the solvent is different to that of the bulk phase itself due to the influence of the surface of the particle.[70] Most substances acquire a surface charge when they come into contact with a high dielectric constant medium; this charge attracts free counter-ions from within the bulk phase and repels ions of like charge.[71]

Charged particles such as anionic and cationic microgels possess charged surface groups (originating from the initiator and possibly co-monomers from which they are

prepared), which attract a diffuse layer of counter-ions that form an "ion atmosphere" around each particle (Fig. 1.6).[70] This interfacial region is known as the electrical double layer[71] and has a defined thickness, δ.[70] The concentration of counter-ions within the electrical double layer decreases from the particle surface until it matches that of the bulk solvent and it is this point that marks the value of δ.[70]
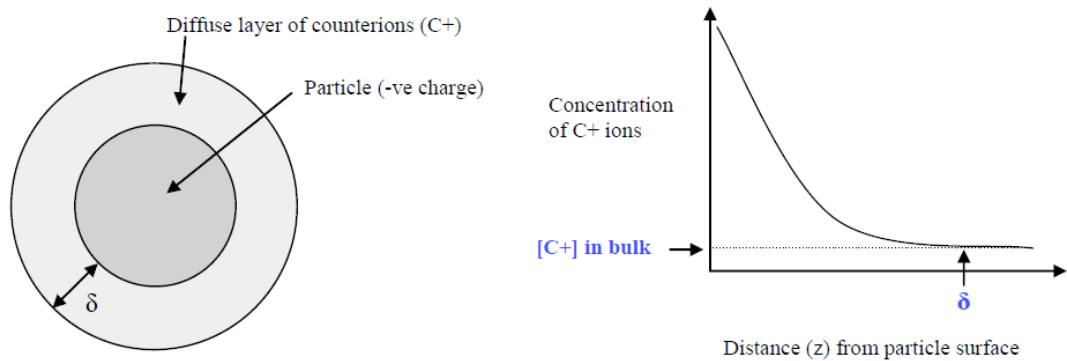
Figure 1.6 Electrical double layer for a charged particle, redrawn from Ref. [70]

The theory of the electrical double layer is concerned both with the distribution of ions throughout the layer and, as a consequence, with the magnitude of electric potentials occurring in the region.[71] According to the Stern-Gouy-Chapman theory, the distribution of counter-ions in the electrical double layer is further divided into a compact inner region and a diffuse outer region.[72]

In the diffuse region, ions are distributed according to the influence of electrical forces and random thermal motion. The inner region may contain specifically adsorbed ions, which are attached (temporarily) to the surface by electrostatic and/or van der Waals forces that are strong enough to overcome (or be unaffected by) thermal agitation and therefore remain in place.[71]

Gouy and Chapman first modelled the diffuse region of the electrical double layer (Fig. 1.7). The density of ions decreases as the distance from the surface increases, as does the electric potential (Ψ). The symbol Ψ_0 denotes the potential at the surface, whilst Ψ indicates the potential at a distance x from the surface.
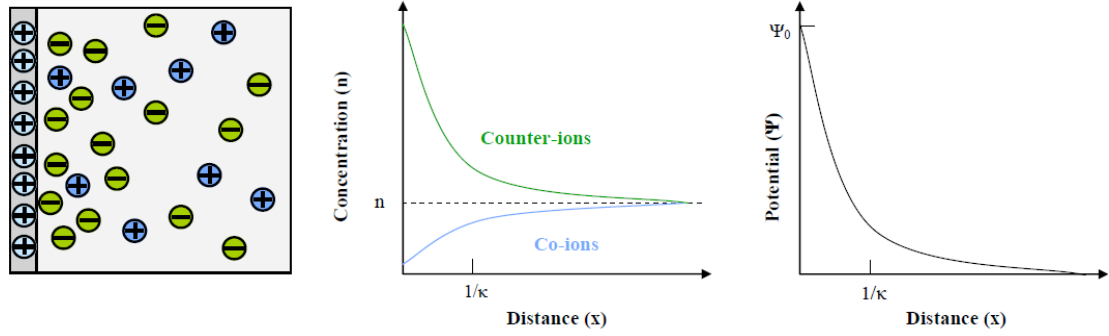
Figure 1.7 Schematic of a charged surface in electrolyte modelled by Gouy and Chapman, showing variation in ion concentration and electric potential as a function of distance from the surface, redrawn from Ref. [71]

The term $1/\kappa$ is the Debye length[72,73] and is equal to the thickness of the diffuse double layer (δ),[71,72] where κ has dimensions of reciprocal length and is a term based on factors including the temperature, dielectric constant and ionic strength of the solvent:[72,74,75]

$$\kappa = \left(\frac{2 \times 10^3 \epsilon^2 N}{\varepsilon_0 \varepsilon kT}\right)^{\frac{1}{2}} \sqrt{I}$$

[Equation 1.1]

where ϵ = electronic charge, ε_0 = permittivity of a vacuum , ε = relative permittivity (dielectric constant) of the solvent, k = Boltzmann's constant, T = temperature and I = ionic strength.

The ionic strength (I) of an electrolyte solution depends both upon the valency (z_i) and concentration (c_i, molar) of the ions in solution:[75,76,77]

$$I = \frac{1}{2}\sum_i c_i z_i^2$$

[Equation 1.2]

For example, in a 1.0 M electrolyte such as NaCl, with a 1:1 ratio of anions to cations, the concentration of each ion is equal to 1, and therefore $I = 1$. For an electrolyte such as 1.0 M $MgCl_2$, the ratio of anions to cations is 2:1, the Mg^{2+} concentration is equal to 1 and the Cl^- concentration is equal to 2, so $I = 3$.

It is therefore clear that variations in either the concentration or valency of an electrolyte ion has a direct effect upon κ and consequently upon the thickness of a double layer. Ions with higher valencies and/or concentrations will increase the ionic strength, thereby increasing the value of κ and reducing $1/\kappa$, the double layer thickness (Debye length).[71,72] For example, the Debye length of particles in a 1:1 electrolyte such as NaCl at 25 °C varies as a function of ionic strength according to:[71,72,77]

$$\kappa = (3.29 \times 10^9) z_i (c_i)^{\frac{1}{2}}$$
$$= (3.29 \times 10^9)\sqrt{I}$$

<div align="right">[Equation 1.3]</div>

The Gouy-Chapman model of the diffuse region is based on several assumptions, which limit the applicability of the model. It assumes: a flat, infinite, uniformly charged surface; the ions are point charges that follow the Boltzmann distribution; the solvent influences the double layer only via its dielectric constant, which is uniform; and only a single, symmetrical electrolyte is present.[71] These assumptions clearly limited the application of this model, particularly in the case of spherical particles in the presence of ions that are not point charges.

Stern added to the model by addressing the composition of the inner layer of the electrical double layer, proposing a Stern plane that separates the inner and diffuse regions (Fig. 1.8).[71] The distance of the Stern plane from the particle surface is approximately equal to the radius of one hydrated ion and accounts for the possibility of specifically adsorbed ions.[71] The centres of any such ions are located in the Stern layer (*i.e.* between the particle surface and the Stern plane) and form part of the compact inner region of the electrical double layer, whilst any ions whose centres reside outside the Stern plane form part of the diffuse layer.[71]

The surface of shear (shear plane) marks the boundary between the "fixed" charged surface and the "mobile" electrolyte solution.[71] It can be thought of as the effective location of the boundary of the solid/liquid interface.[72] The exact location of the shear plane, however, is unknown due to the fact that the Stern layer incorporates some solvent molecules in addition to the adsorbed ions: as a consequence, the shear plane is likely to lie slightly further away from the surface than the Stern plane.[71]
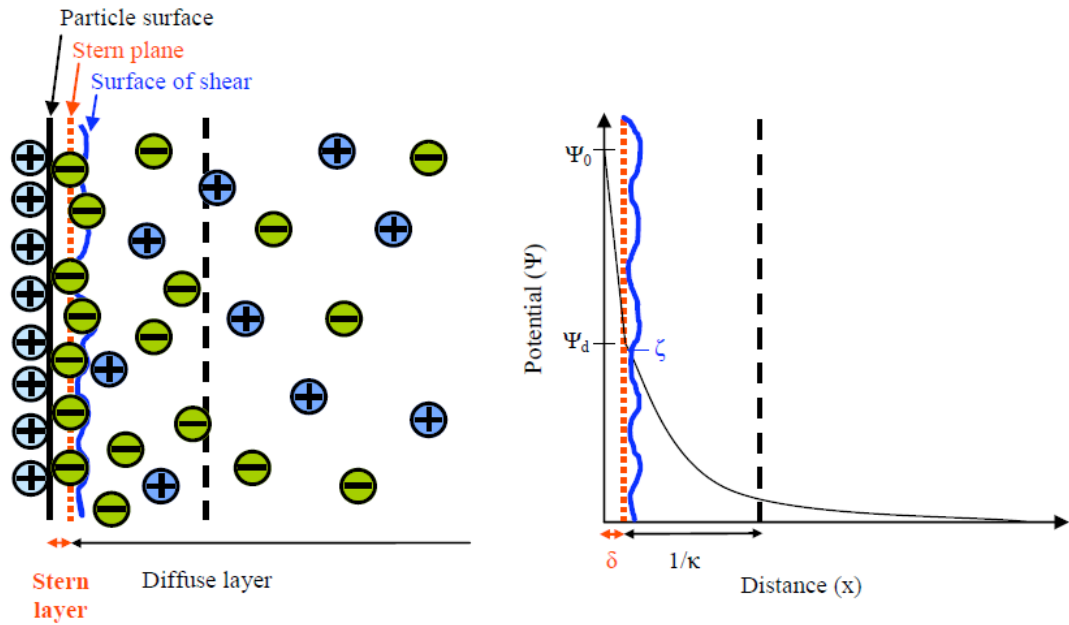
Figure 1.8 Schematic of the electrical double layer showing the Stern plane, redrawn from Ref. [71]

Once again, the potential at the surface is Ψ_o but the potential at the Stern plane, known as the Stern potential, is Ψ_d. The potential in the diffuse layer decreases as a function of distance from the surface, from Ψ_d to zero as the boundary of the diffuse layer is reached (*i.e.* no difference in potential from the bulk solvent).[71] The value of Ψ_d can be estimated from electrokinetic measurements of electrophoresis. However, electrokinetic phenomena arise from events that shear the mobile diffuse layer from the charged surface and fixed inner layer and consequently electrokinetic measurements of the zeta potential (ζ) (or charge density at the shear plane) do not provide any information about the value of Ψ_o or Ψ_d. In reality, as shown in Fig. 1.8, the value of ζ, which marks the shear plane, is only slightly less than Ψ_d, which marks the Stern plane and is therefore considered to be approximately equal to Ψ_d.[71] This is common and experimental evidence suggests that error arising from the assumption is small.[71]

The value of ζ is most commonly derived from measurements of electrophoretic mobility (U_E):[78]

$$U_E = \frac{2\varepsilon\zeta f(\kappa a)}{3\eta}$$

[Equation 1.4]

where ε is the dielectric constant, η is the viscosity and f(κa) is Henry's function.[50,79]

As previously mentioned, κ is the reciprocal of the Debye length, which represents the thickness of the diffuse layer, and a is the radius of the particle. The value of Henry's function depends on the nature of the particles being measured and consequently different approximations are suitable for different particles. The Hückel equation is appropriate for small particles in non-aqueous electrolyte media, which are considered equivalent to point charges, where the value of κa is much less than 1 and $f(\kappa a) = 1$.[71,78] Substituted into Equation 1.4, the equation for U_E becomes:

$$U_E = \frac{2\varepsilon\zeta}{3\eta}$$

[Equation 1.5]

The Smoluchowski equation is more appropriate than Hückel for large particles such as microgels, where the ratio of particle surface curvature to double layer thickness is also large ($\kappa a > 100$) and the surface is effectively flat.[71] In such cases, the diffuse layer is effectively small compared to the particle radius and $f(\kappa a) = 1.5$.[50,71,78] Substituted into Equation 1.4, the equation for U_E of larger particles becomes:[71]

$$U_E = \frac{\varepsilon\zeta}{\eta}$$

[Equation 1.6]

In the case of microgels, U_E is usually quoted rather than ζ[80] to describe the electric potential or charge density of a particle surface.[4] This is because the electrical double layer theory (and ζ) describe the behaviour of hard, spherical particles; whilst microgel particles conform with this in the collapsed state above the volume phase transition temperature (VPTT), below the VPTT they adopt a softer, swollen, deformable structure, which is not adequately described. This means that the electrical double layer of microgel particles in the swollen conformation is not sufficiently rigorously defined. Therefore, the electrical double layer model described so far only covers the behaviour at temperatures above the VPTT and modification is required to describe behaviour below the VPTT. For this reason, Oshima[81] developed a model to unite the theories of the electrophoresis of spherical hard colloidal particles and soft particles, so that the electrophoretic mobility of soft particles could be described. Despite this, an appreciation of electrical double layer

theory is crucial to understanding a range of microgel characteristics, for example, dispersion stability, which will be considered below.

1.2.4 Properties and stimuli-responsive behaviour

Microgels have been described as colloidal particles with an internal gel structure, which means they combine typical colloidal properties with the responsiveness of gels.[82] Poly(NIPAM)-based microgels have a range of physico-chemical properties derived from the monomer, cross-linker and initiator from which they are prepared. They are discrete gel-like particles in dispersion, typically prepared at a concentration of 0.5 % w/v,[2] with low viscosities, very high surface-area-to-volume ratios and rapid thermal and solution responses.[4,6] They display interesting electrical properties that result from the presence of covalently bonded charged groups originating from the initiator, and vary with changes in conditions, such as temperature and electrolyte.[4]

The "sponge-like" structure enables the microgel particles to behave like "micro-sponges", absorbing solvated materials under one set of conditions then undergoing rapid conformational changes and releasing them again following certain environmental changes.[6] This investigation is particularly concerned with the swelling behaviour of poly(NIPAM)-based microgels, which is considered in more detail below, along with the conditions which influence such behaviour. The key physico-chemical properties used to characterize microgel systems are briefly outlined in Section 1.2.4.1, before more detailed consideration of the stimuli-responsive behaviour of the particles.

1.2.4.1 Physico-chemical properties

Several physico-chemical properties are commonly used to describe and characterize the basic nature and stimuli-responsive behaviour of microgel particles. These include particle size, electrophoretic mobility and the volume-phase transition temperature.

Volume-phase transition temperature (VPTT)
The VPTT marks the point at which microgel particles switch between their swollen and collapsed conformations.[6,8,53] The standard VPTT value for poly(NIPAM)

microgel particles is 34 °C.[18] The VPTT can be strongly influenced by microgel composition (see Section 1.2.3).

Particle size

As colloidal dispersions, microgel particles should fall between 1 nm and 1 μm in size[17] and an extremely diverse range of particle sizes have been reported. A useful summary was prepared by Saunders and Vincent,[3] which detailed the collapsed and swollen sizes of particles prepared from a variety of monomers and co-monomers, varying from 50–900 nm.[3] The particle size is usually reported in terms of the hydrodynamic diameter, D_H (or radius), *i.e.* its size when dispersed in solvent. However, dehydrated sizes, such as those obtained from electron microscopy, are also reported and care must be taken to state the type of measurement alongside such values. Furthermore, the swelling ratio, which is derived from size measurements under two different solvency conditions,[9] is frequently reported and is a useful parameter. Large differences in particle size (and hence de-swelling ratio) are observed above and below the VPTT.

Electrophoretic mobility

The electrophoretic mobility (U_E) is a convenient way to express the surface charge of microgel particles (see Section 1.2.3.4).[80] As with particle sizes, a range of mobilities have been reported in the literature for particles of different composition; values can vary substantially between the swollen and shrunken particle compositions, due to the fact that volume changes alter the surface charge density of the particles and hence the mobilities. For example, the electrophoretic mobility of poly(NIPAM) particles dispersed in 1 x 10^{-3} M NaCl has been reported as - 0.20 x 10^{-8} m^2 V^{-1} s^{-1} at 25 °C, increasing to - 4.05 x 10^{-8} m^2 V^{-1} s^{-1} at 50 °C.[63]

Other properties

A wide range of other properties can be determined for microgel systems, such as dispersion viscosity and conductivity, however, only the main ones relevant to this investigation have been described in detail. There are other properties that, if known, would be of great value but are difficult to obtain. For example, although it is not impossible to determine, the molecular weight of microgel particles is rarely reported due to the fact that it is difficult to measure the average dry mass per particle and

therefore very difficult to determine the water content or number concentration of particles in a dispersion.[9]

1.2.4.2 Thermo-responsive swelling behaviour

Figure 1.9 (a) illustrates the typical thermo-responsive behaviour of poly(NIPAM). At room temperature the particle is swollen,[8] with its polymer networks extended into a soft, porous structure. Such polymer networks, immersed in a good solvent, will take in solvent molecules until the chemical potential inside and outside the structure is balanced. Swelling therefore continues until the elastic forces of the cross-links that restrict swelling are equal to the osmotic force imposed by the solvent.[6]

(a)   (b)
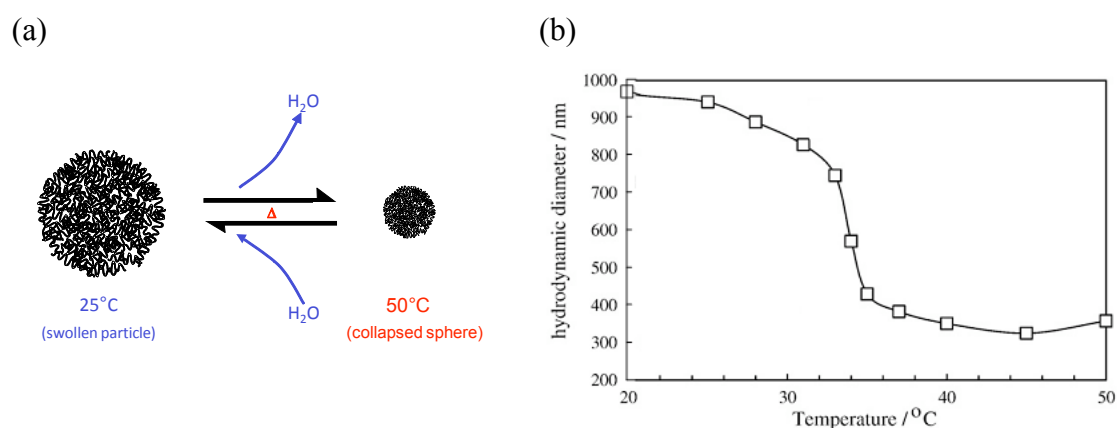
Figure 1.9   (a) Typical thermo-responsive behaviour of poly(NIPAM) microgel particles; (b) Illustration of the change in hydrodynamic diameter of poly(NIPAM) microgel particles as a function of temperature, adapted from Ref. [8]

As the temperature increases, the particle collapses, adopting a tightly packed structure more like a hard particle such as a poly(styrene) latex.[18]   Fig. 1.9 (b) illustrates a typical plot of the change in microgel particle D_H as a function of temperature.[7]   The point at which the particle switches between swollen and collapsed conformations is the VPTT,[8,53] which is usually taken to be the midpoint of the particle diameter *versus* temperature curve[3] and is 34 °C for poly(NIPAM).[18]

This behaviour results from the temperature dependence of hydrogen bonding and hydrophobic interactions between the poly(NIPAM) chains (polymer) and water (solvent).[83]   Below the VPTT, the swollen particles contain a large volume of solvent, typically more than 80 % water,[3] so substantial hydrogen bonding occurs

between the solvent molecules and the amide groups of the poly(NIPAM) backbones.[48,84] Van der Waals attraction between the swollen particles is low.[61] In addition, some chains extend outwards from the particle into the solvent, providing steric stabilization and creating what is known as the "hairy layer".[54,61] Longer-range electrostatic repulsions between the charged groups primarily at the particle surfaces also help ensure the colloidal stability of the particles in an aqueous solvent.[4,8]   At temperatures below the VPTT, the polymer-solvent interactions dominate and water is therefore considered to be a good solvent for poly(NIPAM).[3]

As the temperature rises above the VPTT, hydrogen bonding between the polymer and solvent is disrupted and water molecules become a poorer solvent for the poly(NIPAM) chains.[3]   Hydrophobic interactions between the polymer chains increase, as do inter- and intra-polymer hydrogen bonding, and together these lead to collapse of the particle structure.[3] Electrostatic repulsion between particles increases because the charge density of the surface groups grows as the particles collapse.[4,8]

Poly(NIPAM) microgels can therefore be considered as predominantly hydrophilic below the VPTT and more hydrophobic above the VPTT.[8] Microgel properties depend upon the balance of polymer-polymer and polymer-solvent interactions.[4] It is therefore possible to change the VPTT by altering the hydrophilic/hydrophobic balance of the microgel, by incorporating different co-monomers into the structure.[6,7,46]   For example, co-polymerization of NIPAM with hydrophobic *iso*propyl methacrylate (*i*PMA) results in a decreased VPTT,[53] whilst co-polymerization with hydrophilic AA results in an increased VPTT.[43,46,85,86]

The concentration of cross-linker also has a strong influence: Guillermo *et al.*[26] observed a broadening of the volume phase transition (VPT) and lowering of the VPTT of poly(NIPAM) particles as the concentration of MBA increased. It is possible to extend this to control swelling behaviour in non-aqueous solvents.[2] In this work, "hydrophobic modification" is used to describe the incorporation of co-monomers that are more hydrophobic than NIPAM into a NIPAM-based microgel. The formation/breakage of hydrogen bonds between the water molecules and hydrophilic amide groups within the poly(NIPAM) chains is therefore the key driver behind the reversible volume-phase transition of microgels.[6]

1.2.4.3 pH-responsive behaviour

Ionic (or polyelectrolyte) microgels display pH sensitivity resulting from the incorporation of at least one co-monomer that carries a charge when the pH approaches the pK_a for that species.[7,43] The co-polymerization of a polyelectrolyte co-monomer such as acrylic acid with a temperature-sensitive monomer such as NIPAM results in microgel particles sensitive to both pH and temperature, *i.e.* multi-responsive microgels.[43,63,87] Figure 1.10 illustrates the pH-driven conformational change of a polyelectrolyte-containing microgel.
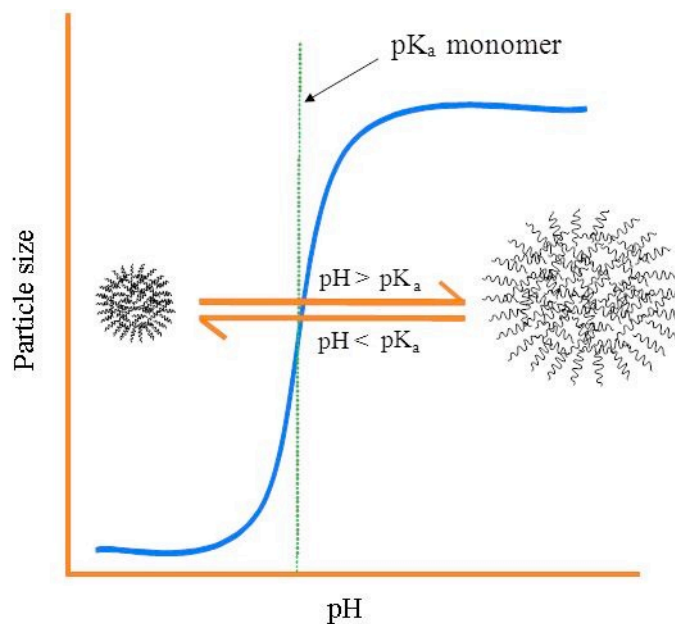
Figure 1.10 Conformational changes of a polyelectrolyte microgel as a function of pH, adapted from Ref. [6]

The mechanism of pH-driven swelling is governed by the internal osmotic pressure that results from the presence of mobile counter-ions within the particle, which oppose the internal electrostatic repulsion between the charged groups.[6,3] The balance between the internal and external pressures is described as follows:

$$\Pi_{in} + \Pi_{el} = \Pi_{out}$$

[Equation 1.7]

where Π_{in} is the osmotic pressure of the mobile ions inside the microgels, Π_{out} is the osmotic pressure of the mobile ions in the bulk solution and Π_{el} is the elastic pressure of the polymeric network.[88]

When the pH is greater than the pK_a of the polyelectrolyte group within the microgel structure, *e.g.* a carboxylate derived from a co-monomer such as AA, the acid is dissociated (ionized) and the resultant $–COO^-$ groups repel one another, causing the particle to swell. Below the pK_a (approximately 4.5 for carboxylate groups[89]) the carboxylate groups adopt the protonated –COOH form, so no electrostatic repulsion occurs between them and the microgel particles adopt a more compact structure.[6,43]

1.2.4.4 Response to changes in ionic strength

The size, charge and stability of microgel particles are influenced by the presence of electrolyte, particularly when the particles have been co-polymerized with polyelectrolyte groups. Daly and Saunders[63] measured the hydrodynamic diameter of poly(NIPAM) particles (containing carboxylic acid residues from the CVA initiator) in the presence of increasing concentrations of NaCl. It decreased as a function of both NaCl concentration and temperature. Snowden *et al.*[43] similarly demonstrated that the hydrodynamic diameter of co-polymerized poly(NIPAM-*co*-AA) microgels decreases in the presence of increasing NaCl concentration. Tan *et al.*[90] observed the same effect upon poly(methacrylic acid-*co*-ethyl acrylate) microgels cross-linked with diallyl phthalate and attributed it to a reduction in internal osmotic pressure that resulted from a charge-shielding effect of the counter-ions on the negatively charged carboxylate groups, *i.e.* the electrolyte screens the internal charge repulsion. The effect is reversed by removing the electrolyte.[43]

The effect of electrolyte upon the stability and flocculation behaviour of colloidal dispersions will be considered in further detail in Section 1.2.6.2. However, it is worth noting here the influence of temperature on the response of particle size to changes in ionic strength. As already described, conformational changes occur in response to changing temperature, which then influence the response to any changes in electrolyte concentration. For example, in the presence of low ionic strengths of an electrolyte such as NaCl, dilute microgel dispersions are colloidally stable, even when heated above the VPTT; however, at higher ionic strengths, aggregation may occur, especially above the VPTT.[7]

The nature of the electrolyte ions is significant. For example, interactions between cationic poly(2-vinylpyridine) microgels and negatively charged organic salts were shown to vary according to the number of sulphonate groups in the organic salt. The position of an anion within the Hofmeister series has also been shown to be correlated with their influence upon poly(NIPAM)-based microgels.[91,92] These effects will be considered in more detail in Section 1.2.6.

It is not only particle size that is influenced by ionic strength. Daly and Saunders[63] measured the electrophoretic mobility of poly(NIPAM) particles in the presence of increasing NaCl concentration, observing that whilst the magnitude of the electrophoretic mobility increased with temperature, it decreased as the NaCl concentration increased. Interestingly, the VPTT was found to be 5–6 °C lower than the temperature at which the pronounced changes in electrophoretic mobility occurred. This difference was attributed to electrostatic differences between the core and shell portions of the microgel structure.

1.2.4.5 Alcohol-induced swelling/de-swelling

The shrinking/swelling behaviour and associated triggers described above have related to microgel particles in water. However, the swelling of poly(NIPAM) microgel particles can be influenced by other factors, *e.g.* addition of alcohols[93] or added free polymer (Section 1.2.6.2).[84] Several groups have investigated poly(NIPAM) swelling behaviour in the presence of short-chain alcohols. For example, Crowther and Vincent[93] studied the swelling behaviour of poly(NIPAM) microgel particles (produced by SFEP with 9 % MBA cross-linker and ammonium persulphate initiator) in aqueous mixtures of methanol (MeOH), ethanol (EtOH) and 2-propanol (2-PrOH) using dynamic light scattering (DLS). At 25 °C, as the volume fraction of alcohol increased, the microgel particles collapsed, de-swelling to a minimum size at low volume fractions. However, in the more alcohol-rich region, the particles re-swelled (termed re-entrant swelling), as shown in Fig. 1.11. The volume fraction at which the greatest collapse was reached was affected by the alcohol carbon chain length, with smaller volumes of longer chain alcohols required to achieve maximum collapse.
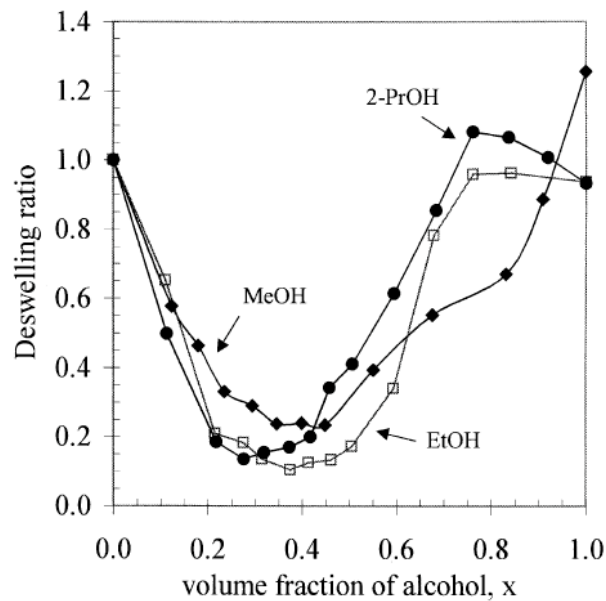
Figure 1.11 Illustration of alcohol-induced de-swelling/swelling behaviour of poly(NIPAM) microgel particles at 25 °C as a function of increasing volume fraction of MeOH (♦), EtOH ( ) and 2-PrOH (●), taken from Ref. [93]

These findings agree with a number of related studies. For example, McPhee *et al.*[67] observed poly(NIPAM) de-swelling in 0–35 % volume MeOH at 25 °C, whilst at 50 °C the particles were collapsed to a similar extent, irrespective of % volume MeOH. The main difference was that the poly(NIPAM) was prepared by EP in the presence of the surfactant SDS, so whilst the data is not directly comparable, it supports the observation of poly(NIPAM) particle de-swelling in low volume fractions of MeOH.

Further evidence comes from Mukae *et al.*[94] who observed de-swelling and re-entrant swelling in poly(NIPAM) hydrogels (macrogels) in C_1–C_4 alcohols (0.0-1.0 mole fraction) at 25 °C. Zhu and Napper[48] observed reversible de-swelling/re-entrant swelling of poly(NIPAM) chains attached to latex interfaces in aqueous MeOH/EtOH/2-PrOH dispersants (0.0–0.9 volume fraction). At 25 °C, Mielke and Zimehl[95] found similar behaviour for anionic poly(NIPAM) (prepared with SDS) below 40 % wt alcohol but observed dramatic swelling behaviour for cationic poly(NIPAM) over the same alcohol concentrations. Again, whilst not directly comparable with the Crowther and Vincent study, these findings indicate that

alcohol-induced de-swelling/re-entrant swelling is derived from the properties of the monomer/initiator from which poly(NIPAM) is prepared.

Saunders *et al.*[84] extended the work of Crowther and Vincent,[93] combining photon correlation spectroscopy (PCS or DLS) with SANS to study the alcohol-induced de-swelling of poly(NIPAM) (0.0–1.0 volume fraction MeOH and EtOH). They confirmed that de-swelling is induced by addition of alcohols at room temperature and highlighted the delicate balance between interactions favouring particle swelling and those responsible for collapse. Saunders *et al.*[96] also investigated the swelling control of poly(methyl methacrylate-*co*-methacrylic acid) microgel particles, again finding that particle swelling could be controlled by the addition of alcohols. It is therefore not just an effect observed for poly(NIPAM)-based microgels.

This de-swelling/re-entrant swelling behaviour has been explained by co-non-solvency and clathrate formation.[93] Co-non-solvency is the term used to describe the fact that individually solvents such as water and alcohols can be good solvents for particles such as microgels but in combination, over certain concentration ranges, become a poor solvent for the same particles.[48] Clathrates are tetrahedral cage-like structures of water molecules that form around an alcohol molecule.[97] In pure water, it has been suggested that water molecules form cage-like structures around hydrophobic regions of the poly(NIPAM) chains.[93,98] Otake *et al.*[98] described two phenomena that occur when hydrophobic solutes are added to water. Firstly, water molecules form cage-like structures around the hydrophobic solutes and this "hydrophobic hydration" makes the non-polar molecules soluble in water. Secondly, the non-polar molecules associate with each other through "hydrophobic interaction".

Crowther and Vincent[93] proposed that the collapse observed at low alcohol volume fractions is a consequence of the effect of added alcohol on the environment of the poly(NIPAM) chains. Water molecules are removed from the particles to form clathrate structures around the alcohol molecules, thereby promoting hydrophobic bonding between poly(NIPAM) chains (*i.e.* excluding them from the binary water-alcohol mixture) and encouraging chain collapse.[48,93] At higher alcohol volume fractions, the clathrate structure disruption frees up water molecules to re-solvate the polymer chains, contributing to the re-entrant swelling.[93] The re-entrant chain

swelling is also promoted by direct interaction of the freed alcohol molecules with hydrophobic groups within the poly(NIPAM) macromolecular structure.[48] This results from an intricate balance of interactions.[48]

The observation that smaller volumes of longer-chain alcohols were required to achieve the greatest degree of collapse[93] is supported by the findings of Onori[99] who demonstrated that as the chain length increased, the number of water molecules required to form clathrate structures around the alcohol molecules also increased. In addition, Zhu and Napper[48] found that the clathrate structures broke down at lower volume fractions for the longer-chain alcohols, meaning that re-entrant swelling commenced at lower volume fractions.

Increased temperature also influences clathrate formation, by reducing the total number of water molecules in the cage-like structures around the hydrophobic solutes, which in turn promotes the hydrophobic interactions between them.[98] This supports the idea that in pure water at 25 °C poly(NIPAM) microgel particles are swollen, encompassing very large volumes of water that hydrogen bond with the hydrophilic groups on the polymer chains, whilst at higher temperatures the hydrogen bonding is disrupted, hydrophobic interactions increase and the particles collapse (Section 1.2.4.2).

As the shrinking/swelling behaviour of microgels is of such fundamental importance to their application, a key property to be determined is the extent to which they swell, or, more conveniently, de-swell. This is usually determined from measurements of changes in the hydrodynamic diameter (D_H) of the particles using dynamic light scattering (Section 1.3.1). The extent of particle de-swelling in relation to the fully swollen hydrodynamic diameter (d_0) is expressed as the de-swelling ratio:

$$\alpha = \left(\frac{d}{d_0}\right)^3$$

[Equation 1.8]

where d is the measured D_H at a given temperature.[2]

1.2.4.6 Polymer-induced swelling/de-swelling

Microgel particle de-swelling can also be induced by the addition of free polymer to the continuous phase, which occurs via osmotic de-swelling.[84] As long as the free

polymer is excluded from the particle interior, *i.e.* remains only in the continuous phase, de-swelling may occur.[84] For example, Saunders *et al.*[84] investigated the effect of added poly(ethylene glycol) (PEG) of increasing molecular weights upon the de-swelling of poly(NIPAM) (Fig.1.12).
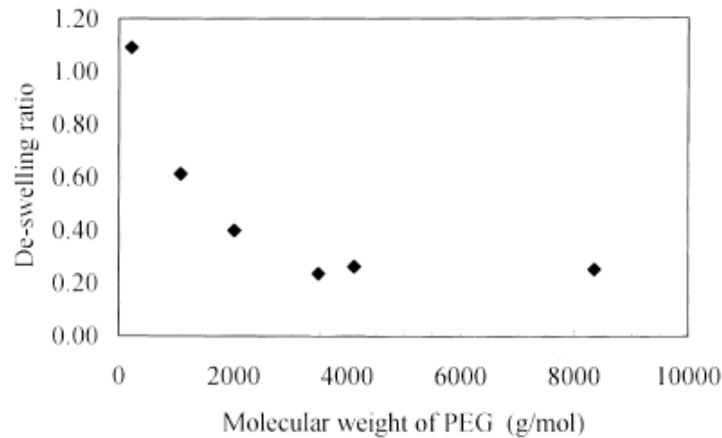
Figure 1.12 De-swelling ratio (α) of poly(NIPAM) particles (5 % wt. MBA cross-linker) as a function of molecular weight of added free PEG, taken from Ref. [84]

At the lowest molecular weight (PEG220), no de-swelling occurred because the PEG220 molecules were small enough to penetrate the interior of the poly(NIPAM) particles. However, at PEG molecular weights greater than 1080 g mol^{-1}, de-swelling occurred, with a minimum value of α (*i.e.* greatest extent of de-swelling) observed for PEG3490. At these larger molecular weights, the coil size of the free polymer is larger than the poly(NIPAM) pore size, which excludes the PEG from the microgel interior and increases the chemical potential of the continuous phase. This causes the microgel network to exclude water molecules and de-swell, which continues until the chemical potential of the solvent in the particle interior matches that of the free polymer solution.

Routh *et al.*[100] added free poly(ethylene oxide) (PEO) chains to poly(NIPAM) microgels and observed particle expansion at low PEO concentrations but particle collapse at high PEO concentrations. At low PEO concentrations, the free polymer chains permeate into the particle interior, causing an increase in osmotic pressure relative to that of the solvent, which results in particle expansion. At high PEO concentrations, however, the particles are saturated with PEO and the remaining free

PEO in the bulk solvent causes an increase in osmotic pressure relative to that in the particle interior, leading to collapse of the particles.

1.2.4.7 Influence of solvent type

Solvents of different polarity have different influences on the physical properties of linear poly(NIPAM). For example, Yu *et al.*[101] studied the variation in transition temperature of linear poly(NIPAM) in H_2O, D_2O and tetrahydrofuran (THF), finding marked differences that could be explained in terms of poly(NIPAM) solubility (THF > H_2O > D_2O) and hydrogen bonding (THF < H_2O < D_2O) in the three solvents. The linear poly(NIPAM) showed no transition temperature in THF but two critical transition temperatures in H_2O and D_2O (the latter being higher). It is therefore highly likely that different solvents have different influences upon the swelling behaviour of poly(NIPAM)-based microgels.

1.2.4.8 Other influences

Other influences or triggers for microgel stimuli-responsive behaviour include light and magnetism.[102] For example, Ménager *et al.*[103] prepared poly(acrylamide) microgel particles encapsulating magnetic particles, which, in addition to demonstrating solvent swelling, exhibited a rapid and reversible response to a weak magnetic field. Lietor-Santos *et al.*[104] showed how increased hydrostatic pressure can be used to induce de-swelling of poly(NIPAM) particles; hydrostatic pressure was found to change the entropic contribution of polymer-solvent mixing to a similar extent as temperature, but with swelling achieved on a more gradual basis than with temperature.

1.2.4.9 Particle collapse

It is worth noting that the collapse of microgel particles is thought to be related to the core-shell structure. For example, Hoare and Pelton[105] noted that the VPT of functionalized microgels appears to follow a consecutive core-shell collapse mechanism, where the core typically collapses at lower temperatures than the shell, with a significant influence upon particle size. The shell collapse is of more significance to the electrophoretic mobility of the particles, due to the location of the charges on the surface, and hence, electrophoretic mobility responds to temperature

changes more slowly than size, with the shell requiring higher temperatures to overcome the electrostatic charges in the region.

1.2.5 Interfacial behaviour

Molecules experience different interactions when at an interface than when in the bulk phase.[106] For example, water molecules at the air-water interface are subjected to unequal short-range attraction forces which result in a spontaneous net inward pull into the bulk phase and a reduction in surface free energy.[106] Liquids therefore tend to adopt shapes that minimize their surface areas, so that the maximum number of molecules are in bulk, surrounded by and interacting with neighbours. This is why droplets tend to be spherical, the conformation with the smallest surface-area-to-volume ratio.[107]

Surface-active agents (surfactants) are substances that when dissolved in a solvent have the ability to adsorb at interfaces, thereby altering the physical properties of the interfaces and changing the amount of work required to expand them,[106] *i.e.* by causing a reduction in surface tension.[108] They are amphiphilic molecules with affinity for both oil and water.[74] At low concentrations the individual surfactant molecules form orientated monolayers at the interface but at higher concentrations they also aggregate to form self-assembled structures, *e.g.* micelles.[106] These are usually clusters of 50–100 surfactant molecules whose shapes are governed by geometric and energetic considerations.[106]

Figure 1.13 illustrates the adsorption of surfactant molecules at the air-water interface, with the hydrophilic head group aligning at the interface within the water phase and the hydrophobic tails sitting in the air phase. It also shows the formation of micelles within the water phase by the surfactant molecules and the dynamic exchange of molecules between the interface, bulk phase and micelles.[74]

The point at which micelles begin to form is marked by the critical micelle concentration (CMC), which corresponds with the point at which surfactant molecules saturate the water surface. At low concentrations surfactant molecules migrate to the air-water interface and the surface tension of the water decreases

linearly with the logarithm of surfactant concentration (Fig. 1.14). When the surface starts to become saturated (around the CMC), although micelles start to form, any further increase in surfactant concentration has no further appreciable effect upon the surface tension of the water. The CMC can be determined from the surface tension *versus* surfactant concentration curve and is found at the intersection between the initial linear concentration-dependent part of the curve and the final linear concentration-independent section.[109] A classic, well-characterized surfactant is sodium dodecyl sulphate (SDS), which has a CMC of 8.3 mM.[10]
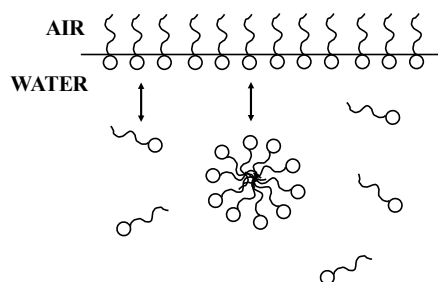
Figure 1.13 Illustration of the positioning of surfactant molecules at the air-water interface, showing the dynamic equilibration between the adsorption and micellization of surfactant molecules, redrawn from Ref. [74]
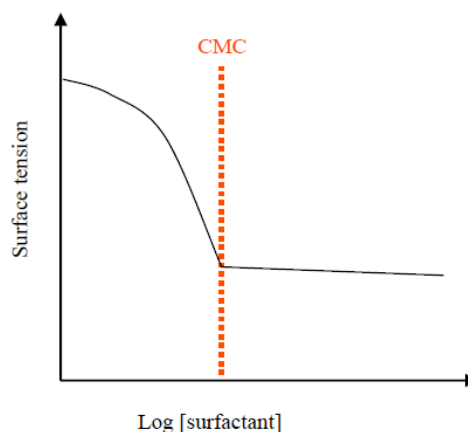
Figure 1.14 Schematic plot of the variation in critical micelle concentration as a function of surfactant concentration, adapted from Refs. [10,78]

Surfactants are typically small molecules with a hydrophilic head group and a tail group composed of a single or double, hydrophobic straight or branched hydrocarbon chain, although they may also include aromatic groups, fluorocarbons or siloxanes.[106] These structures are very different to the high molecular weight

microgel particles under investigation in this study. However, as poly(NIPAM) has both hydrophilic and hydrophobic characteristics, poly(NIPAM)-based microgel particles possess some of the key characteristics of a classic surfactant. It has been shown that colloidal particles act in many similar ways to surfactant molecules, particularly at fluid-fluid interfaces, but they do not aggregate into micelles (and therefore have no CMC) and are strongly held at interfaces.[110] Fig. 1.15 illustrates the position of particles at the air-water (or oil-water) interface.[36,110]

The hydrophilic/hydrophobic nature of a surfactant molecule is described by the hydrophile-lipophile balance (HLB) but the same tendency of spherical particles is described in terms of its wettability via the contact angle (θ).[110] This is illustrated in Fig. 1.15, where the hydrophobic nature (and θ) of the particle increases from left to right and the particle accordingly sits more in the air phase than the water phase.
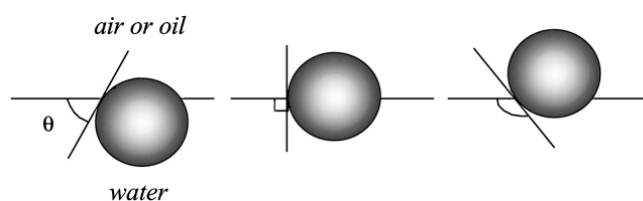
Figure 1.15 Illustration of positioning of small spherical particles at a planar air-water interface for a contact angle (measured through the aqueous phase) less than 90° (left), equal to 90° (centre) and greater than 90° (right), taken from Ref. [110]

Zhang and Pelton[111] investigated the surface activity of poly(NIPAM) microgels with varying cross-linker (MBA) concentrations and synthesis methods. In each case, the microgels lowered the surface tension of water to values close to that achieved by linear poly(NIPAM) (*i.e.* 42 mN m^{-1}) and images of the water surfaces obtained with environmental SEM provided evidence of an ordered array at the air-water interface.[4] It has also been shown that poly(NIPAM-*co*-methacrylic acid) microgels are capable of stabilizing oil-in-water emulsions and that the particles do adsorb to the oil-water interface.[112] This evidence suggests that the potential for hydrophobically modified microgels to lower surface tension at air-water and oil-water interfaces is a characteristic worthy of further investigation.

1.2.6 Dispersion stability and particle interactions

A key characteristic of microgel particles is their dispersion stability in various solvents, which is of significant interest when investigating the suitability of a microgel dispersion for a particular application.[73,113]   For example, pharmaceutical preparations require stable dispersions, whilst the drying of paint films requires flocculation to occur.[114]   Dispersion stability is governed by a balance of particle-particle and particle-solvent interactions,[113] including electrostatic repulsion, steric stabilization and attractive van der Waals forces.[61,73,115]   By considering the interactions that occur when two particles approach one another during a Brownian collision, it is possible to predict the stability of the dispersion as a whole.[73]

Dispersed particles inevitably collide due to random Brownian motion and if the particles remain in contact after the collision, they aggregate and precipitate out of dispersion.[113]   Permanent (irreversible) contact is known as coagulation, whilst temporary (reversible) contact is known as flocculation or association.[113]   These phenomena can occur in dispersions of a single microgel particle type (homoaggregation) as well as in mixed-charge colloidal dispersions (*i.e.* dispersions of two or more differently charged particles).   In the latter case, even stronger aggregation may be observed, known as heteroaggregation or heteroflocculation.[113] The onset, form and strength of the aggregation of microgel particles in dispersion can be influenced by altering the chemical environment, *e.g.* by altering solvent pH or temperature, additives such as polymer or electrolyte ion type and concentration, or by altering the composition of the particles themselves.[73,116]

The mechanisms and interactions governing the swelling behaviour of microgel particles have already been considered (Section 1.2.4), for example hydrogen bonding, hydrophobic interactions, steric stabilization and electrostatic interactions (including the structure of the electrical double layer). However, an understanding of microgel dispersion stability, in terms of its tendency to aggregate,[73] requires further consideration of the interactions and stabilization mechanisms involved.

1.2.6.1 DLVO theory

A number of forces influence colloidal dispersions such as microgels, including inertial/diffusion/shear forces and interfacial tension.[70] When considering microgel dispersion stability, interparticle forces that come into effect as particles approach one another are particularly important and, as with microgel swelling behaviour, the overall stability of the dispersion is determined by the balance between attractive and repulsive forces, which can be described through models such as the DLVO theory.

Classic DLVO theory, named after Derjaguin, Landau, Verwey and Overbeek, can be used to describe the potential energy changes that result from colloidal forces when two monodispersed, spherical particles of the same type approach one another.[113,117,118,119] The colloidal interactions involved are attractive electrostatic forces (arising from the electrical double layer and ionizable surface groups) and repulsive long-range van der Waals forces that arise between particles as a result of temporary or induced dipoles.[73] The van der Waals forces provide a constant attractive force which, if not opposed by repulsive interparticle interactions, cause the particles to aggregate.[120] The total energy of interaction, V_T, of a simple system can be described by:

$$V_T = V_A + V_R$$

[Equation 1.19]

where V_A is the energy of attractive van der Waals forces and V_R is the energy of repulsive forces from the electrical double layer.[64] If these three terms are plotted as a function of distance (x) between the two particles, an potential energy profile is obtained (Fig. 1.16).[64] The profile shows the contributions of the attractive and repulsive forces, and the overall total energy.

As two particles begin to approach one another and the separation distance between them is large, *e.g.* $x > 100$ nm, the van der Waals (V_A) and electrostatic forces (V_R) have no influence on the particles (A).[113] However, as the particles start to get closer, both V_A and V_R increase, and as V_A increases faster (*i.e.* $V_A > V_R$), it dominates and therefore V_T forms a secondary minimum (B), promoting aggregation.[113] At very small separations, V_R dominates and opposes aggregation, with V_T following a primary maximum (C), which reflects an energy barrier that must be overcome before aggregation can occur.[113] The primary maximum can be thought of as an effective

activation energy for aggregation, so for two particles to aggregate they must collide with sufficient energy to overcome the primary maximum.[73]   At even smaller separations (D), V_A once more dominates and the aggregation that occurs in this primary minimum is irreversible coagulation.[113]
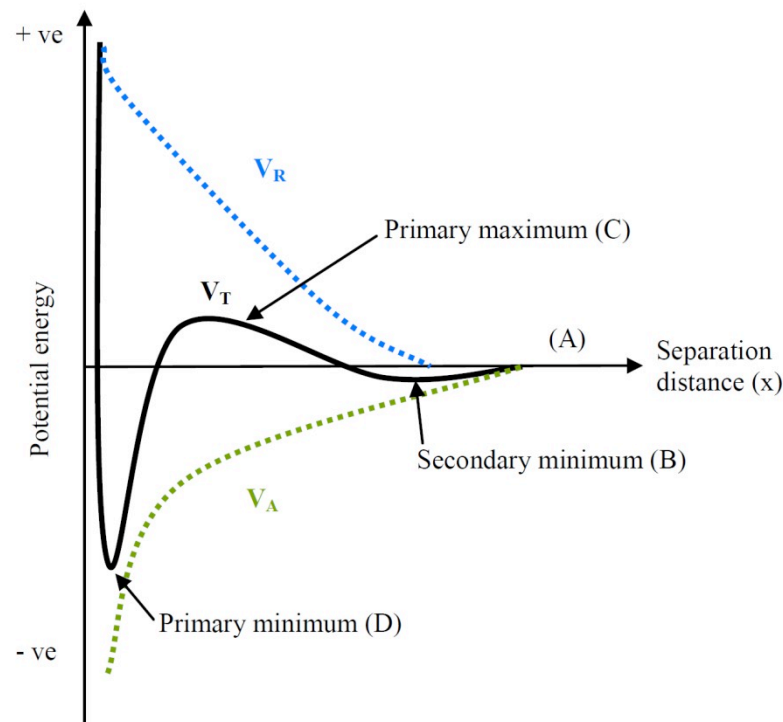
Figure 1.16   Potential energy profile of total energy of interaction between two identical particles as a function of separation distance, adapted from Refs. [64,71]

Whilst classic DLVO theory can be successfully applied to describe the interaction of two identical particles[119] in terms of van der Waals attractions and electrostatic repulsions, it has some inherent limitations.[121]   In fact, the application of classic DLVO theory can lead to anomalous predictions of interaction energy and hence to inaccurate calculations of the properties of the particle system itself.[118] For example, an atomic force microscopy study of the interaction between an immobilized layer of poly(NIPAM-*co*-AA) and a silica surface measured repulsive forces far greater in magnitude and range than predicted by DLVO theory.[25]   This discrepancy was attributed to compression/deformation of the microgel particle and the presence of the "hairy" steric layer, whose conformation was influenced by changes in solution conditions such as ionic strength and pH.[113] Furthermore, in aqueous media, particle stability will also be influenced by interaction energies contributed by water

molecules.[119]   Additional influences arise from particle curvature, shape, size and charge density.[113,118]

These additional interactions and layers of complexity are not accounted for by classical DLVO theory. Therefore great efforts have been made to extend the theory to encompass non-DLVO interactions.[117,118,119]   These interactions can be divided into two broad groups, where:[117]

- Classical DLVO theory incorporates:
    - van der Waals attractions; and
    - electrostatic repulsions.
- Extended DLVO theory also encompasses:
    - Steric interactions, with entropic and osmotic contributions;
    - Lewis acid/base interactions, which include hydrogen bonding and entropic contributions, and collectively result in structural forces, hydrophobic interactions and hydration pressures.

A single approach that incorporates all interaction types and applies to all particle systems remains elusive.[117]   However, despite the limitations of classical DLVO theory, including the fact that it does not take into account multi-body interactions, it can still be qualitatively useful in beginning to describe and predict microgel dispersion stability, especially when non-DLVO interactions are acknowledged.

1.2.6.2 Controlling microgel dispersion stability

As already described, in aqueous microgel dispersions, long-range van der Waals attractions arise between particles as a result of temporary or induced dipoles,[73,113] and this constant attractive force, if not opposed by repulsive interparticle interactions, would cause the particles to aggregate.[120]   The repulsive electrostatic interactions result from overlap of the diffuse regions of the particle electrical double layers.[70]   However, there are other potential mechanisms opposing van der Waals attraction, including steric stabilization with polymers and manipulation of electrostatic charge stabilization.   The colloidal stability of microgel dispersions is generally governed by the presence of electrical charges and "dangling surface

chains" or "hairs" on the particle surfaces,[9] so by manipulating these, the stability of the dispersion can be altered.

It is important to note that the extent of swelling of the microgel particles is also significant due to the fact that van der Waals forces are proportional to the Hamaker constant.[73] When the microgels are at room temperature in a swollen conformation, their Hamaker constant is very closely matched to that of the aqueous solvent, which means that the particles posses very low van der Waals net attraction and therefore the overall van der Waals force favouring aggregation remains minimal.[115] However, when the temperature rises above the VPTT of the particles, their collapse results in an increase in the Hamaker constant relative to that of the solvent.[3,115] This in turn leads to increased van der Waals attractive forces and favours particle aggregation.[122]

Charge stabilization

In the case of a uniformly charged homo-polymer microgel dispersion, electrostatic repulsion between the particle surfaces opposes the van der Waals attraction and favours stability of the dispersion. However, as with the van der Waals attractive forces, the conformation of the microgel particles is significant. At temperatures above the VPTT, the increased surface charge density of the particles results in increased electrostatic repulsion, favouring stability.[123] However, as previously mentioned, this stability can be manipulated by the addition of electrolyte.[73] For example, in the presence of relatively high electrolyte concentrations, *e.g.* greater than 0.05 mol dm^{-3} NaCl, poly(NIPAM) particles aggregate.[115]

In the presence of electrolyte, ions surround the charged microgel particles and effectively shield the charge.[72] As a consequence, the electrostatic charges that previously favoured stability (above and below the VPTT) are screened by the electrolyte ions, which reduces the Debye length of the electrical double layer and encourages aggregation.[115] Such aggregation above the VPTT and in the presence of electrolyte is typically reversible on cooling the dispersion back below the VPTT (*i.e.* a flocculation) where the particles redisperse.[115]

Counter-ions provided by the electrolyte dominate within the electrical double layer and as a consequence the dispersion stability is more sensitive to counter-ions than to

co-ions.[73]   For example, the stability of an anionic microgel dispersion in the presence of NaCl would be influenced more by Na^+ than Cl^-. In addition, cations tend to be more hydrated than anions and therefore are more likely to reside in bulk than the anions, which, being less hydrated, are more polarizing and more likely to be specifically adsorbed to form part of the inner layer of the electrical double layer.[71] The ion valency is also significant.[73] For example, electrolytes such as NaCl, $MgCl_2$ and $LaCl_3$ will influence the charge stability to different extents, with charged surfaces showing a preferential tendency to adsorb counter-ions, particularly those with a high charge number.[71]   According to the Shultze-Hardy rule, the critical coagulation concentration (CCC) of a given electrolyte, *i.e.* the concentration required to induce coagulation, is inversely proportional to the ion valency (z):

$$CCC \propto \frac{1}{z^n}$$

[Equation 1.10]

where $n = 6$ for high potentials or $n = 2$ for low potentials (more common).[73]

Examples of homoaggregation

Pelton and Chibante[8] studied the aggregation behaviour of poly(NIPAM) and poly(NIPAM-*co*-acrylamide) microgel "lattices" in the presence of $CaCl_2$ as a function of temperature and the proportion of acrylamide in the microgel. In 0.1 M $CaCl_2$, poly(NIPAM) particles remained dispersed at temperatures below 34 °C, but aggregated above 35 °C. At these higher temperatures, the minimum concentration of $CaCl_2$ required to induce aggregation, the CCC, was only 0.002 M.   For poly(NIPAM-*co*-acrylamide) in 0.1 M $CaCl_2$, the critical flocculation temperature (CFT), *i.e.* the temperature at which the onset of flocculation was observed, increased with increasing co-monomer (acrylamide) concentration.

Snowden and Vincent[23] investigated the temperature-induced flocculation of poly(NIPAM) in the presence of 0.1 M NaCl, observing that the particles were stable at 25 °C and flocculated at 40 °C. However, this flocculation was reversible by cooling the poly(NIPAM) back to 25 °C and the authors reported that the cycle of dispersion-flocculation-redispersion could be repeated many times. The CFT was found to decrease as the concentration of NaCl increased. Below the VPTT, the steric repulsion arising from the solvated polymer chains is sufficient to overcome the

interparticle attraction arising from the electrolyte screening of the surface charges on the particles. However, above the VPTT, the collapsed particles no longer exhibit steric repulsion but experience stronger van der Waals attractive forces, which, combined with the electrolyte charge screening, result in flocculation.

Rasmussen and Vincent[124,125] investigated the flocculation behaviour of poly(NIPAM) as a function of ionic strength in more detail by measuring the CFT as a function of NaCl concentration between 25 and 60 °C. Three clear regions of response were observed:

- At low concentrations of NaCl ($\lesssim$ 25 mM), no CFT was found because the inter-particle electrostatic repulsion was sufficient to prevent flocculation, even at temperatures well above the VPTT.

- At intermediate NaCl concentrations ($\approx$ 25–100 mM), CFTs were found to strongly decrease with increasing NaCl concentration because the electrostatic repulsion was sufficiently weakened to allow van der Waals attractive forces to cause flocculation.

- At high NaCl concentrations ($\gtrsim$100 mM), CFTs decreased linearly with increasing NaCl concentrations because the aqueous NaCl solutions become increasingly poor solvents for the poly(NIPAM) polymer chains as the NaCl concentration increases.

The flocculation behaviour of other co-polymer NIPAM-based microgels has also been studied. For example, Benée *et al.*[21] investigated the stability of anionic and cationic poly(NIPAM-*co*-vinyl laurate) microgel particles in the presence of NaCl. The incorporation of the hydrophobic vinyl laurate (VL) co-monomer influenced the stability of the dispersion. At 25 °C, the dispersion was stable but above 0.01 M an increase in *n*-value suggested a decrease in the stability of the system. At 40 °C flocculation was observed for anionic poly(NIPAM-*co*-VL) above 0.04 M NaCl and above 0.01 M NaCl for cationic poly(NIPAM-*co*-VL), both substantially lower CFCs than that observed for homo-polymer anionic poly(NIPAM) of 0.1 M NaCl. In addition, both VL microgels could not be redispersed by simple cooling. Benée *et al.* concluded that the VL was responsible for the irreversible nature of the flocculation; due to its hydrophobic nature, the hydrophobic interactions experienced by the VL-containing polymer chain during the particle collapse at 40 °C are too strong to be overcome by simple cooling and are energetically dominant.

Routh and Vincent[126] studied more hydrophilic co-polymer poly(NIPAM-*co*-AA) particles; these were observed to de-swell at high salt concentrations below the VPTT of ≈ 32 °C. Ma and Tang[101] co-polymerized NIPAM with the more hydrophilic triethyleneglycol methacrylate, incorporating polar –OH groups into the particles. The influence of the polar groups differed above and below the VPTT. As the concentration of –OH groups increased, flocculation became more difficult below the VPTT and the flocculation rate slowed, whilst above the VPTT, flocculation became more likely and the flocculation rate increased, which was attributed to increased attraction between the –OH groups at the higher temperatures.

Hou *et al.*[91] studied the effect of anions upon the aggregation behaviour of charged poly(NIPAM) microgels. Two different microgels were exposed to a range of electrolytes containing the same cation but different anions. The cationic poly(NIPAM-*co*-vinyl benzyl trimethylammonium chloride) microgel exhibited no aggregation in response to any of the anions but the anionic poly(NIPAM-*co*-sodium acrylate) was much more susceptible to aggregation induced by both kosmotropic and chaotropic anions. (Kosmotropic or "structure making" agents stabilize water structures, whilst chaotropic or "structure breaking" agents disrupt water structures.[128] The critical aggregation temperatures of poly(NIPAM-*co*-sodium acrylate) induced by each of the anions (at a given concentration) placed them in order of the Hofmeister series, *i.e.* $CO_3^{2-} > SO_4^{2-} > H_2PO_4^- > Cl^- > Br^- > NO_3^- > I^- >$ SCN^-. These effects were attributed to the indirect interfacial effects of anions near the poly(NIPAM-*co*-sodium acrylate) surface. Daly and Saunders[92] had previously shown that, unlike cations, the ability of anions (particularly those with high charge density) to dehydrate (de-swell) poly(NIPAM) particles and induce their flocculation is strongly correlated with their position in the Hofmeister series. These studies indicate that modification of poly(NIPAM) microgels by co-polymerization (using hydrophobic or hydrophilic co-monomers) can have significant influence upon the flocculation behaviour of the particles.

Examples of heteroflocculation of mixed-charge systems
The preceding discussions have only considered the aggregation behaviour of single-particulate systems of a one charge type, *e.g.* an anionic poly(NIPAM) dispersion. However, in mixed-charge systems such as the mixtures of cationic microgel particles

and anionic polystyrene latex studied by Islam *et al.*,[122] interesting aggregation behaviour is observed. Islam *et al.* added increasing concentrations of poly(NIPAM) to a fixed concentration of poly(styrene) and assessed the stability of the systems at 20 and 40 °C using *n*-values. In water at 20 °C, the mixtures were stable. The swollen cationic poly(NIPAM) particles with low charge density experienced weak electrostatic and van der Waals attractions and therefore coexisted in a stable dispersion with the anionic poly(stryrene). However, at 40 °C, the increased charge density of the collapsed cationic poly(NIPAM) particles resulted in stronger attraction of the anionic poly(styrene) particles, allowing flocculation to occur. Interestingly, stable dispersions were also observed at 40 °C but only when the cationic poly(NIPAM) was in excess compared to the anionic poly(styrene). Transmission electron microscopy (TEM) images showed anionic poly(styrene) particles surrounded by adsorbed cationic poly(NIPAM) particles (Fig. 1.17).
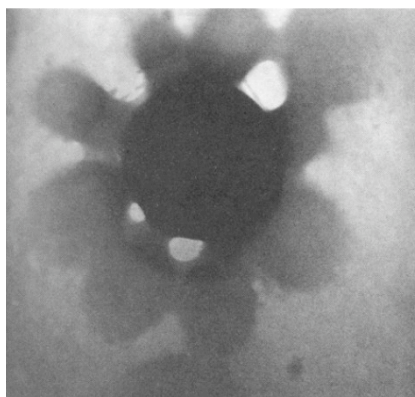
Figure 1.17 TEM of a mixture of cationic poly(NIPAM) particles surrounding an anionic poly(styrene) particle, taken from Ref. [122]

The same investigation showed that the stability of the mixtures was strongly influenced by pH and electrolyte addition. For example, at pH 10 and 40 °C, neutralization of the cationic groups on the poly(NIPAM) particles reduced electrostatic attraction to the poly(styrene) particles, thus increasing the concentration of poly(NIPAM) required to achieve flocculation (CFC) and permitting redispersion of the system upon cooling and gentle agitation. Conversely, NaCl addition reduced the CFC of poly(NIPAM) at 40 °C by reducing the electrical double layer and allowing closer, stronger interaction with the poly(styrene).

Below the VPTT, stable dispersions were maintained because the steric forces were sufficient to oppose attraction and prevent aggregation between the oppositely charged particles. Above the VPTT, the increased charge density (and subsequently greater electrostatic attraction between the particles) and absence of steric repulsion due to the particle collapse, permitted heteroaggregation of the oppositely charged particles to take place.[115] However, stable dispersions of macro-complexes were also observed above the VPTT, when the cationic microgel particles were in excess relative to the anionic polystyrene particles. The anionic latex particles were surrounded by the cationic microgel particles, creating hetero-macroparticles with a net positive charge, which was sufficient to maintain the particles in dispersion (Fig. 1.17).[115,122]

Hall *et al.*[115] studied the heteroaggregation behaviour of varying ratios of mixed cationic and anionic microgel systems as a function of temperature, pH and electrolyte concentration. Anionic homo-polymer poly(NIPAM) microgel particles were mixed with cationic co-polymer poly(NIPAM-*co*-4-VP) microgel particles. As with the poly(NIPAM)-poly(styrene) mixtures studied by Islam *et al.*,[122] stable hetero-macroparticles were observed above the VPTT of the microgels in certain mixtures (Fig. 1.18). The relative concentrations of the oppositely charged microgels were found to be crucial in determining the stability of the mixtures.
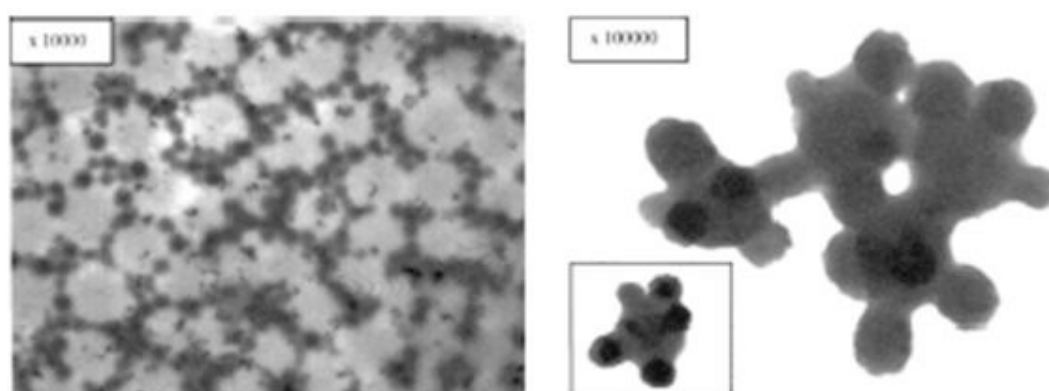
Figure 1.18 TEM images of hetero-aggregates of anionic poly(NIPAM) particles surrounded by cationic poly(NIPAM-*co*-4-VP) particles, taken from Ref. [115]

Observed in mixtures of equal concentrations of the two microgels in deionized water at pH 3. Left hand image (x10,000) shows sample dried at room temperature. Right hand image (x100,000) shows sample dried on a hot plate at 45 °C, with inset showing a single hetero-macroparticle from the same sample.

For example, although aggregation of most mixtures was observed at 20 °C, an excess concentration of cationic poly(NIPAM-*co*-4-VP) conferred stability via

formation of the hetero-macroparticles shown in Fig. 1.18. The excess cationic poly(NIPAM-*co*-4-VP) particles surrounded the larger anionic poly(NIPAM) particles, and the resultant complexes carried a net positive charge, causing repulsion between the complexes that was sufficient to maintain dispersion stability. Hall *et al.* found that this heteroaggregation was also influenced by pH and electrolyte concentration, above and below the VPTT.

More recently, Snowden *et al.*[129] noted the importance of the relative concentrations of anionic and cationic particles, stating that the change from dispersed to aggregated systems is likely to be continuous and the anionic:cationic particle ratio at which aggregation starts to occur is somewhere between 1:1 and 1:10.

The aggregation behaviour of many variations of even more complex particulate systems involving microgels have been investigated, such as Routh and Vincent[130] who studied the heteroaggregation rate of a mixture of anionic poly(NIPAM) and cationic poly(4-vinylpyridine) (4-VP) microgel particles. Hou *et al.*[131] studied mixtures of anionic poly(NIPAM-*co*-sodium acrylate) and cationic poly(NIPAM-*co*-vinyl benzyl trimethylammonium chloride) which were found not to aggregate on heating in water or the presence of monovalent cations. However, the addition of divalent metal ions had an interesting influence upon the aggregation of this mixed microgel system; below the LCST ($\approx$ 32 °C) poly(NIPAM-*co*-sodium acrylate) particles associated due to complexation between the metal ions and the carboxylate groups on the surface of the poly(NIPAM-*co*-sodium acrylate) particles, whilst above the LCST, poly(NIPAM-*co*-vinyl benzyl trimethylammonium chloride) particles adsorbed onto the associated poly(NIPAM-*co*-sodium acrylate) particles due to electrostatic attraction, forming core-shell structures.[131]

Influence of added free polymer
Dispersion stability can also be influenced by the addition of free polymer, which can promote both stabilization and aggregation by steric mechanisms.[116] In certain circumstances, more than one steric mechanism may occur, *e.g.* a polymer may participate in steric stabilization and bridging interactions.[120] For example, Fig. 1.19 illustrates how particulate dispersion stability varies in the presence of free polymer, alternating between stabilization and flocculation as the polymer concentration increases.
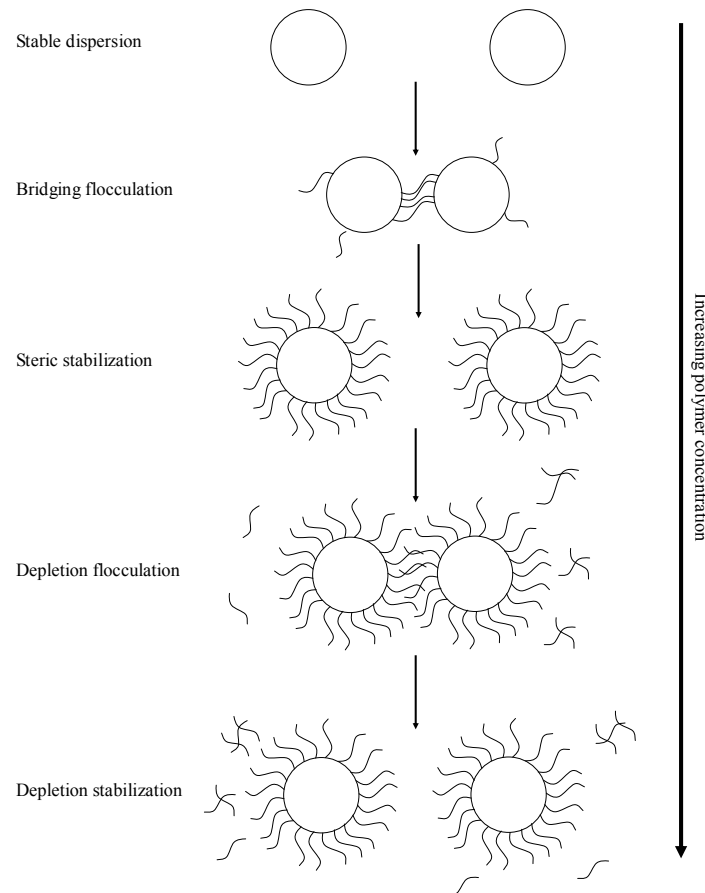
Figure 1.19 Illustration of the effects of increasing polymer concentration on the stability of a particulate dispersion, redrawn from Ref. [116]

When the particles are not yet saturated with free polymer, bridging flocculation between particles may occur when polymer molecules simultaneously adsorb to two particles.[120] At higher polymer concentrations, steric repulsion (stabilization) of dispersed particles may take place (as described in Section 1.2.6.2).[116] As the free polymer concentration rises further, depletion flocculation may occur; as particles approach, the gaps between them become too small for the free polymer, which is then excluded from the interstitial spaces between the particles, creating an osmotic potential that causes solvent to flow out from the gap in order to dilute the bulk dispersion medium, forcing the particles together and resulting in flocculation of the particles.[71,116,132] Depletion flocculation can also be induced not just by free polymer but by other inert additives such as non-ionic surfactants or small particles (*e.g.* silica).[71] Finally, at the highest polymer concentrations, depletion stabilization may occur.

Other flocculation processes include:[116]

- Incipient flocculation, where sterically stabilized particles flocculate due to decreasing solvent quality. For example, increasing temperature disrupts polymer-solvent hydrogen bonding, causing water to become a poorer solvent for microgels at higher temperatures.

- Charge-patch flocculation, where the adsorption of free polymer creates discrete anionic or cationic patches upon the particle surface, which attract neighbouring particles.

- Charge screening, where polyelectrolyte free polymers screen the particle surface charge, allowing flocculation to occur.

Snowden and Vincent[23] investigated the temperature-induced flocculation of poly(NIPAM) in the presence of non-adsorbing poly(styrene sulfonate) (PSS). At 25 °C, the poly(NIPAM) remained dispersed (up to the maximum concentration tested, 0.8 % PSS) but at 40 °C flocculation occurred from 0.6 % PSS. As with the effect of added NaCl investigated within the same study, the flocculation was found to be reversible on cooling (inversion of the sample was also required) and the cycle of dispersion-flocculation-redispersion could be repeated many times.

The addition of 0.01 M NaCl to the system further decreased the concentration of PSS required to induce flocculation, down to 0.35 %. The PSS-induced flocculation arises from depletion forces present in the system, where the exclusion of non-adsorbing PSS from the interstitial spaces between the particles (due to the fact that PSS and poly(NIPAM) are both negatively charged) exerts an osmotic pressure that forces the particles together.[116,132] Rasmussen *et al.*[125] studied the effect of added sodium poly(styrene sulfonate) (SPSS) on the flocculation of poly(NIPAM) particles, finding that the concentration of SPSS required to induce flocculation decreased as the temperature increased.

1.3   Microgel characterization

Various instrumental techniques can be used to obtain information about the physico-chemical properties of microgel particles. An excellent summary of techniques

previously used to characterize microgel particles is given in Kausar *et al.*[6] These include small-angle neutron scattering (SANS) and nuclear magnetic resonance (NMR) for structural investigations, calorimetry for studying thermodynamic properties and conductometric/potentiometric titration for measuring surface charge. The techniques utilized in this study are described below.

1.3.1 Particle size measurement

Dynamic light scattering (DLS), also known as photon correlation spectroscopy (PCS), is a light scattering technique that can be used to determine the size of particles as small as 10 nm in diameter.[79,133] It is based on the fact that particles in dispersion move due to Brownian motion, which is the random motion of particles due to bombardment by the solvent molecules surrounding them.[77] Brownian motion is related to particle size in that small particles move quickly and large particles move slowly.[79] DLS measures fluctuations in the intensity of light (photons) scattered by dispersed particles as they move randomly in and out of the path a laser beam.[133] Fast fluctuations indicate the presence of a small particle, whilst slow fluctuations indicate the presence of a large particle.[79]

The velocity of the Brownian motion of a particle is measured in terms of the translational diffusion coefficient, *D*, which indicates how quickly a substance will diffuse in a particular medium at a specific temperature and under the influence of a given concentration gradient.[108,77]

D can be related to the diameter of the particle by the Stokes-Einstein equation:

$$D_\mathrm{H} = \frac{kT}{3\pi\eta D}$$

[Equation 1.11]

where D_H is the hydrodynamic diameter, k is the Boltzmann constant, T is temperature and η is the viscosity of the dispersion medium.[77]

A laser beam illuminates a sample cell and light scattered by particles in the sample dispersion is measured at a given angle. An attenuator automatically optimizes the amount of scattered light by adjusting the intensity of the incident laser beam. This is

necessary because the intensity of scattered light must fall within a specific range for the detector to be able to successfully measure it.[79] The choice of angle at which the scattering is measured is also critical. For particle size measurements, back scattering is commonly measured at an angle of 173° (see Figure 1.20),[79] which offers several advantages over forward scattering, for example:

- it reduces the incidence of multiple scattering (where scattered light is re-scattered by dispersed particles);

- it permits measurement of samples of higher concentration due to the fact that the incident beam does not have to pass through the entire sample;

- the influence of contaminants such as dust particles tends to be greater in forward scatter due to the fact that they are often larger than the sample particles.[79]
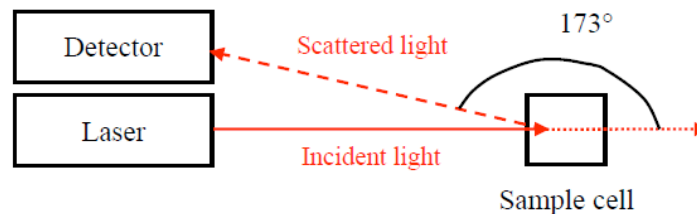
Figure 1.20 Detection of back scattered light

Changes in the intensity of the scattered light are monitored over time by a correlator and these fluctuations are used to determine size information.[79] Significant information can be obtained from a plot of the correlation coefficient (signal decay rate) against time, *e.g.* the point at which the correlation coefficient begins to decay indicates the mean size of the particle that created the intensity signal, whilst the gradient of the decay gives an indication of the polydispersity of the sample.[77]

A value for the polydispersity index (PdI) of the sample is generated, which is a dimensionless estimate of the width of the size distribution, ranging from 0–1. It can be interpreted as follows:[77]

- 0–0.05: standards or particles made to be monodisperse;

- 0.05–0.08: nearly monodisperse samples;

- 0.08–0.70: mid-range polydispersity;

- Greater than 0.70: very polydisperse, sample may be unsuitable for the technique.

1.3.1.1 Refractive index (RI)

In order to measure particle size by DLS, the RI of the dispersant must be known. This is because the translational diffusion coefficient (D), which relates the speed of movement of the particles due to Brownian motion to their hydrodynamic diameters through the Stokes-Einstein equation (Equation 1.11), is also dependent upon the RI of the dispersant medium (including any additives to the solvent), which can be seen in the scattering vector (equation not shown).[134] RI values can be measured using a refractometer or calculated empirically, *e.g.* from the Clausius-Mosotti equation.[135] The latter relates the optical properties of a material to its molecular properties, such as molecular mass and molar refractivity.[135]

The RI of a medium can be defined as the ratio of the speed of light in a vacuum to that in the medium:[108,136]

$$RI \; of \; given \; substance \; (n) = \frac{Speed \; of \; light \; in \; substance}{Speed \; of \; light \; in \; vacuum}$$

[Equation 1.12]

Light travels through different media at different speeds and when it crosses the boundary between two different media, *e.g.* air and water, the light changes direction, *i.e.* is refracted.[137] RI is wavelength and temperature dependent, generally decreasing as temperature increases, and is also affected by the presence of dissolved substances in the medium.[137] A refractometer determines the RI of a sample from the geometry of the optical path and the RI of the prism material, where the reflection of light is measured at the prism/sample interface.[136]

1.3.1.2 Dielectric constant (*ε*)

Another parameter that must be known for DLS size measurements is the dielectric constant of the dispersant medium. As with RI, the dielectric constant is related to the translational diffusion coefficient, this time via the scattering vector (of the incident laser beam),[133] which is dependent upon the dielectric properties of the medium.[134] It can be thought of as a measure of the efficiency of a solvent for separating electrolytes into ions, which is influenced by interatomic and intermolecular attractions.[138] Values for the dielectric constant of a variety of liquids at different temperatures are available in literature, *e.g.* Åkerlöf[139] published

the dielectric constants of a range of organic solvent-water mixtures at various temperatures in 1932. Addition of a co-solvent such as MeOH to water caused an almost linear reduction in dielectric constant with increasing MeOH concentration. Values such as these can enable DLS measurements of size.

1.3.1.3 Viscosity (η)

It is clear from the Stokes-Einstein equation (Equation 1.11) that knowledge of viscosity of the dispersant medium is required for DLS particle size measurements. Viscosity is a measure of the resistance of a fluid to flow, which generally decreases with temperature for water soluble polymers[56] and is greater for a solution than a pure solvent.[108] The viscosity of an aqueous alcohol mixture would therefore be expected to initially increase then decrease with alcohol concentration. Viscometers may be used to measure the viscosity of a liquid, by measuring the ease with which fluids flow through capillary tubing, *e.g.* using an Ostwald viscometer.[108] Rheometers may also be used and values for the viscosity of many liquids and binary solutions are available in literature.[140] The viscosity of a binary mixture, however, cannot easily be predicted from the viscosities of individual components.[141] This appears to be because the viscosity of a binary mixture is not simply additive, due to polar intermolecular interactions that lead to deviations.

An alternative method for determining the viscosity of mixtures uses DLS, based on the fact that, as can be seen in Equation 1.11, dispersant viscosity can be calculated if particle size and scattering (in terms of the translational diffusion coefficient, *D*) are known.[142] Dispersants can therefore be doped with standard latex particles of a known size, which can be measured using a very rough estimate of viscosity. The actual viscosity can then be back-calculated from the size measurements.

1.3.2 Electrophoretic mobility measurement

Light scattering instruments can also be used to measure the electrophoretic mobility, U_E of dispersed particles, using a combination of electrophoresis and laser Doppler velocimetry measurement techniques (also known as laser Doppler electrophoresis).[79] U_E is the velocity of a particle in an applied electric field;[79] the

theory of U_E and how it relates to zeta potential and the structure of particles in dispersion is described in Section 1.2.3.4.

Similarly to DLS particle size measurements, U_E measurement is concerned with the movement of particles in dispersion but this time the movement measured is not simply due to Brownian motion, but is electrophoretic.[79] Electrophoresis is the movement observed when an electric field is applied across an electrolyte and charged particles dispersed within the electrolyte are attracted towards the electrode of opposite charge.[79]

As with DLS size measurements, in U_E measurements a laser beam illuminates a sample cell, with attenuation if necessary, and light scattered is detected. However, in this case, the scattered light is detected at an angle of 17° (*i.e.* forward scatter) and is then compared with a reference beam. Fluctuations in the scattered light signal are monitored over time and these fluctuations are proportional to the velocity of the particles.[79] This technique also requires knowledge of sample parameters such as viscosity and dielectric constant (see Section 1.3.1).[79]

1.3.3 UV-visible absorbance/turbidity

Turbidity is a typical colloidal characteristic of microgel dispersions. It results from differences in the refractive index (RI) of the particles and the solvent. Due to the fact the microgel particle structure changes with temperature, the difference in RI between the solvent and particles also varies.[6] For example, at room temperature, the particles consist predominantly of water, so there is little difference between the RI of the solvent phase and that of the swollen particles. At higher temperatures, as water is expelled from the interior of the particles, the particle size decreases and the difference in RI between the particles and solvent grows.[4] As a consequence, the smaller, collapsed poly(NIPAM) particles scatter more light and hence the turbidity of the dispersion increases.[6]

It is therefore possible to use techniques such as UV-visible spectrophotometry to monitor particle conformational changes during the VPT by following changes in the turbidity of the dispersion. This is possible due to the fact that scattering occurs when

the size of the particles is on a comparable scale to the wavelength of light. It provides a useful means of following the temperature dependence of microgel volume-phase transitions, including determination of the VPTT.

UV-visible absorption spectroscopy is a versatile technique with many applications that is based on the measurement of the absorption of UV-visible electromagnetic radiation by solvated molecules which undergo an electronic transition.[143] However, in the case of microgels, the dispersed particles do not absorb light; instead light is scattered and the particles remain unchanged (*i.e.* no electronic transition takes place). Despite this, UV-visible spectrophotometry can still be utilized due to the fact that it measures the transmittance (*T*) of light through the sample:

$$T = \frac{I}{I_0}$$

[Equation 1.13]

where I_0 is the incident light intensity and I is the transmitted light intensity (at a specified wavelength).[108,143]

The transmittance of a single wavelength of visible light through a microgel sample, which equates to the turbidity of the sample, therefore can be monitored as a function of temperature. As it is more common to consider a sample in terms of its power to absorb rather than transmit light,[143] the absorbance (A) can be calculated from Equation 1.14.[142,143] However, it must be borne in mind that for microgels it is the transmittance of scattered light that is being measured, not absorption.

$$A = -\log_{10}(T)$$

[Equation 1.14]

The VPTT is a key physico-chemical property reported for microgel particles and it is commonly determined from UV-visible spectrophotometry/turbidity measurements. To do so, the first derivative is calculated from absorbance or transmittance data, where the peak on the first derivative plot represents the point of inflection of the absorbance (or transmittance) *versus* temperature curve[4] and indicates the VPTT of the sample.

1.3.3.1 *n*-values

The aggregation behaviour of dispersions can be determined and monitored using UV-visible spectrophotometry to measure the *n*-value of a dispersion.

$$n = \frac{d\log(Abs)}{d\log(\lambda)}$$

[Equation 1.15]

where λ = wavelength.[66,115] Measurement of the absorbance of a sample at a range of specific wavelengths enables the detection of flocculation, where a decrease in the magnitude of *n* is indicative of the occurrence of flocculation.

1.3.4 Scanning electron microscopy (SEM)

SEM can be used to determine information about the particle shape, size and dispersity of a material. It is a technique commonly used to observe the surfaces of specimens (greater than 2 nm in size) that are under high vacuum. An electron gun generates a fine electron beam that is focused onto and scanned across the specimen surface on a point-by-point basis. When the electron beam ejects loosely bound conduction electrons from the specimen surface, secondary electrons are produced from the valence electrons of sample atoms at the surface and therefore provide information about the sample surface.[144] Elastically scattered electrons may also be generated (creating a back-scattered signal). The back-scattered electrons posses greater energy than the secondary electrons and therefore provide information from a relatively greater sample depth, giving insight into compositional differences.[144] Together these two sources create signals picked up by a secondary electron detector, that are amplified and converted into an image on the display screen.[144,145]

The use of SEM to analyse microgel samples presents several particular problems. Firstly is the need for a high vacuum, which means the particles can only be observed in a dehydrated state, *i.e.* the collapsed conformation. SEM measurements therefore can only be compared with observations from other techniques made for particles in the collapsed state, above the VPTT. Furthermore, additional caution must be taken because the dehydrated particles are analysed in the (almost) total absence of solvent, whilst other techniques like DLS do so whilst the particles are still dispersed in solvent (above the VPTT). Particle deformation due to sample preparation and the high

vacuum also frequently occurs with SEM analysis, giving the particles an appearance of an oblate, spheroid shape.[66] In conclusion, SEM analysis of microgel particle size, morphology and dispersity is valuable but must be interpreted carefully.

1.3.5 Tensiometry

The effect of microgels upon the surface tension of water can be measured using tensiometric instruments such as the KRÜSS K100. The surface tension (γ_0), or surface free energy per unit area at an interface, can be defined as the minimum amount of work ($W_{\min}$) required to create a new unit area of the water-air interface (ΔA), where:[106]

$$W_{\min} = \gamma_0 \Delta A$$

[Equation 1.16]

Surface tension can be thought of as "the force acting at right angles to a line of unit length in the surface of a liquid".[146] The term "interfacial tension" can be applied to liquid-liquid or liquid-solid interfaces, whilst "surface tension" can only be applied to liquid-vapour interfaces, *e.g.* air-water.[146] Various methods exist for measuring surface tension, *e.g.* the ring and plate methods.[109]

In the plate method (Fig. 1.21) used in this investigation, a platinum plate is attached to a balance and the sample liquid beneath it is raised until the plate registers contact with the surface. At this point, the force acting on the balance, *F*, is measured and because the precise dimensions of the plate are known, the surface tension can be calculated according to:

$$\sigma = \frac{F}{L \, cos\theta}$$

[Equation 1.17]

where σ is surface tension (γ) or interfacial tension, *L* is the wetted length of the plate and θ is the contact angle. The surface of the platinum plate is roughened, facilitating optimal wetting, which means that the contact angle is virtually 0°, making $cos\theta$ equal to 1. This means that only knowledge of *F* and *L* are required to be able to calculate γ.[109]
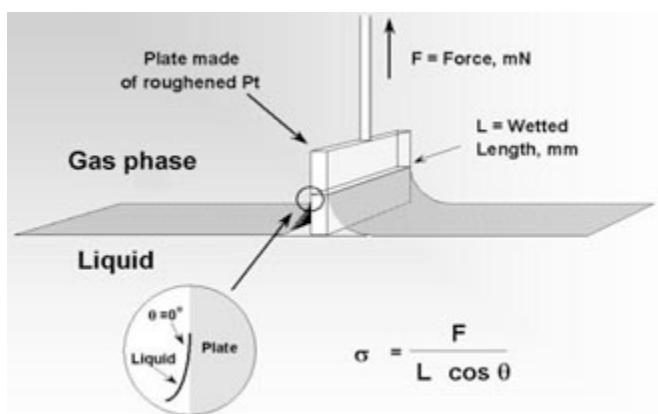
Figure 1.21 Schematic diagram of the plate method, taken from Ref. [147]

Various values for the surface tension of water are reported in literature. The *73rd Handbook of Chemistry and Physics*, for example, gives the value at 20 °C as 72.75 mN m^{-1} and at 50 °C as 67.94 mN m^{-1}.[140]

1.4   Applications

The fact that the responsive swelling properties of microgel particles can be tailored to occur in response to specific environmental conditions means that these particles show great potential in a wide variety of applications. They have already successfully been utilized in a wide range of industries, including areas such as paints, ink-jet printing, cements, enzyme immobilization, oil recovery, molecular separation, environmentally sensitive display devices and on/off molecular switches.[6] The roles of microgels in a variety of applications will be discussed below.

Pelton and Hoare[9] describe a landscape in which most microgels fall into one of two distinct groups. "Commercial" microgels are those that have already found industrial application and have been used in large quantities since the 1960s. These can be further divided into non-aqueous microgels, which have found use in areas such as paints and coatings, and alkali-swellable microgels, which have found use in the rheological control of formulated products. The other distinct group described by Pelton and Hoare can be thought of as "academic" microgels, which tend to be aqueous, home-made, poly(NIPAM)-based and produced in far smaller quantities. At present there is little cross-over between the two groups.

1.4.1 Thickeners, paints and surface coatings

In general, the rheological behaviour of microgel particles is equivalent to that of hard particles with a thin, soft shell; at low concentrations the dispersions exhibit Newtonian flow properties (*i.e.* there is no change in viscosity with increasing shear rate), but at high concentrations the dispersions exhibit a high degree of shear thinning.[18] Dispersion viscosity is also influenced by solvent quality, added linear polymers, and temperature, which collectively influence the extent of swelling that in turn dominates the shear thinning.[18,148] As microgel properties undergo volume changes with changing environmental conditions, they can therefore be used to modify dispersion viscosity, which is proportional to particle size (D_H).[148]

Due to the ease with which the rheological properties of microgel dispersions can be controlled, they have a long history and numerous applications in the surface coatings, printing, personal care product and food industries.[6,47,149] For example, microgels have been used:

- as a replacement for a volatile component of automotive surface coatings; [7,18]
- in high-performance electrodeposition paints;[150,151]
- to improve the rheological properties of industrial coatings and the weather or shock resistance of films;[2,152]
- as emulsifiers/stabilizers in complex coatings such as associative thickeners in decorative paints;[78]
- to control the rheology and physical/sensory attributes of food products, *e.g.* polysaccharide and/or protein-based microgels used to replace fat in foods;[149]
- as "super absorbers" in sanitary products;[78]
- as thickeners in cosmetics, pharmaceuticals and personal care products,[6,153,154,155,156] *e.g.* Carbopol®, a cross-linked poly(acrylic acid) microgel;[149] and
- as electrorheological fluids.[148]

1.4.2 Stimuli-responsive particulate emulsifiers

Emulsions, which can be defined as "an opaque, heterogeneous system of two immiscible liquid phases… where one of the phases is dispersed in the other as drops

of microscopic or colloidal size",[157] are very unstable but may be stabilized by the addition of surface-active materials.[157] As already described, (Section 1.2.5), colloidal particles act in many similar ways to surfactant molecules and emulsion-stabilizing properties of microgel particles have been demonstrated, making them potentially valuable in many industrial emulsion-based products, *e.g.* food, cosmetics and pharmaceuticals.[158] Lightly cross-linked poly(4-VP/silica) nanocomposite microgels have been used as effective emulsifiers of water with methyl myristate, n-dodecane and 1-undecanol,[158,159,160,161] whilst poly(NIPAM)-stat-poly(MAA) co-polymer microgels act as pH-sensitive emulsifiers.[162,163]

1.4.3 Flocculants

1.4.3.1 Waste water treatment and water purification

The processes of flocculation and coagulation have been key aspects of waste water treatment since ancient times[132] and they are still used today to remove suspended fine particulates, colloids, turbidity, natural organic matter and dissolved inorganic/organic contaminants during most water treatment.[164] A range of synthetic and natural polymers are commonly used to adsorb or bind to adjacent colloid particles to cause bridging flocculation, or to attract and adsorb oppositely charged materials, thereby decreasing the potential energy of repulsion between adjacent particles, which permits flocculation to occur.[132] As microgels are capable of the sorption/desorption of a variety of materials[4] and can be designed to flocculate under specific environmental conditions, they have the potential to assist in waste water treatment.[132]

Snowden *et al.*[165] prepared cationic and anionic poly(NIPAM) particles capable of adsorbing significant quantities of ions (ammonium nitrate, lead nitrate, cadmium nitrate, aluminium citrate and hydrochloric acid) from aqueous solution at 25 °C. The nature of the initiator used to prepare the poly(NIPAM) particles had a very strong influence on the adsorptive characteristics of the microgel due to its role in determining the surface charge groups. For example, cationic poly(NIPAM) containing quaternary ammonium groups from 2,2′-azobis(2-methylpropionamidine) dihydrochloride (MPA) removed three times more ammonium nitrate than anionic poly(NIPAM) containing carboxylate groups from CVA. Upon heating, shrinkage of

the particles led to the release of approximately 60 % of the adsorbed ions, indicating their potential value in waste water treatment and purification.

Morris *et al.*[166] demonstrated the reversible adsorption of hydrolysable lead ions by poly(NIPAM-*co*-AA) particles, which could be controlled in several ways: temperature manipulation, pH adjustment or modification of AA content. Furthermore, temperature-induced flocculation of the particles above their VPTT made the lead-ion-containing microgel particles easier to recover ready for cooling to release the lead ions, illustrating their potential use in water purification. Additional evidence suggesting the suitability of microgels for this purpose due to their absorption of metal ions comes from studies such as that by Peng and Wu,[36] who studied controllable interactions between metal cations (Hg^{2+}, Cu^{2+}, Ca^{2+} and Na^+) and thermosensitive poly(*N*-vinylcaprolactam-*co*-AA) with a view to the potential immobilization of proteins and drugs. Microgels with affinities for such ions could potentially find use in water purification.

1.4.3.2 Enhanced oil recovery

The flocculation of poly(NIPAM) microgel particles is showing promise as an "intelligent" secondary oil recovery system to enhance the recovery of oil from mature oilfields and heavy oil reserves.[12] Such secondary systems are necessary because up to 40 % of a reservoir can remain trapped underground following the primary recovery process. Usually, a fluid (*e.g.* seawater) is injected into a reservoir to push or sweep the oil out via a producer well. However, the injected fluid follows the path of least resistance and due to the presence of porous channels within the rock surrounding the reservoir, the injector fluid begins to bypass the oil and simply exits via the producer well.

To improve the sweep of the reservoir, microgel particles can be used to block the paths of least resistance, forcing the injector fluid to perform a more efficient sweep of the reservoir. These blocks are achieved by flocculating the microgel particles at high temperature (a common feature of underground oil reservoirs) and in the presence of high concentrations of electrolyte (such as that found in seawater). Upon injection, the microgel particles are at temperatures below their VPTT and remain

dispersed in a swollen conformation, with a low viscosity and density that permits passage through the porous rock. As the particles penetrate deeper into the well, generally the temperature rises, causing the particles to collapse once the VPTT has been exceeded and due to the presence of a high concentration of electrolyte, the particles flocculate and form a reversible block.[12]

Starch granules in water, which can be considered to be aqueous microgel dispersions, have already found application in oil recovery in the prevention of fluid loss following the creation of new fractures in the rock formation.[167] Degradable poly(acrylamide) microgels cross-linked with poly(ethylene glycol) have similarly been used.[167]

1.4.3.3 Water removal from biodiesel

Nur *et al.*[5] demonstrated that poly(NIPAM)-based microgel particles could be used to remove water from organic solvents such as hexane and biodiesel prepared from rape seed. A range of co-polymer microgels were observed to precipitate in hexane but on the drop-wise addition of water, the precipitated particles absorbed the water, forming a gel that could easily be recovered for re-use by filtration and centrifugation. The findings indicated that microgels might also have potential for performing the reverse application, namely removing oil from aqueous environments. As the hydrophobicity of the microgels was increased by co-polymerization, their efficiency at removing water from biodiesel decreased, suggesting the affinity of the microgel for non-aqueous materials may be increasing. A microgel with such an affinity could have a wide range of valuable applications, including the recovery/clean up of oil spills and the removal of pharmaceuticals from waste water.

1.4.4 Biomaterials/biomedical applications

Microgel particles show great potential in biomaterial applications. For example, injectable poly(MAA) microgel dispersions have been prepared that are capable of providing structural support for damaged intervertebral disc soft tissue and enabling tissue regeneration in the longer term.[168] In addition, pH-responsive

poly(ethylacrylate-*co*-methacrylic acid-*co*-1,4-butanediol diacrylate) microgel particles have been used to restore mechanical properties of damaged load-bearing soft tissue.[44] In a similar area, injectable scaffolds used to culture and proliferate cells have been successfully prepared from poly(NIPAM-*co*-2-hydroxyethyl methacrylate-*co*-acrylic acid).[169]   Furthermore, poly(NIPAM) microgels modified with a cell adhesive peptide have shown potential for the detachment and delivery of human cells: at raised temperatures, the microgels removed cells from the culture substrate, then on cooling released viable cells able to grow on new substrates.[170] Such systems may have wide-ranging applications in cell biology and tissue engineering.[170]

Other potential biomedical applications of microgels include: a synovial fluid substitute that mimics the viscoelastic properties of hyaluronic acid injections over a longer period;[171] slimming aids embedded with cationic fat binding agents that not only scavenge fatty acids but swell in the stomach, creating a feeling of fullness and hence satiety;[172] and delivery vehicles that can improve the efficiency of other biomaterials/drug delivery systems/treatments, *e.g.* poly(NIPAM)-based microgel coatings that can increase the stealthiness of magnetic iron oxide nanoparticles used in hyperthermia cancer treatments.[173]

1.4.5 Encapsulation/carrier systems

As already indicated, microgels show potential as carrier systems due to their tuneable size, high loading capacity, stability, environmental responsiveness and large surface area,[174] and it is likely they are capable of "carrying" a wide variety of materials, giving them a range of potential applications in medicine, pharmacy, biotechnology, food technology, cosmetics and detergency.[175]   For example, Sukhorukov *et al.*[175] prepared novel nanocapsules by adsorbing consecutive layers of oppositely charged polyelectrolytes onto colloidal particles such as poly(NIPAM)-based microgels, which were later sacrificed, leaving a hollow micron-sized polyelectrolyte capsule with pH-sensitive permeability that could be used to encapsulate/release materials from the hollow interior. Sukhorukov *et al.*[175] went on to suggest that hollow nanocapsules could act as artificial cell organelles. Other related capsules have included thermo-sensitive poly(NIPAM)-based nanocapsules with a core of aqueous cobalt tetrafluoroborate solution[176] and superparamagnetic

pH-sensitive multilayer hybrid hollow microspheres for targeted controlled drug release or diagnostics.[123] Microgels can also be used to "contain" or "enclose" reactions, for example acting as nano-reactors capable of modulating the catalytic activity of metal nanoparticles.[174]

1.4.6 Drug delivery

Another related potential application of microgel particles is as drug delivery vehicles. For example, Lopez *et al.*[41,42] demonstrated that poly(NIPAM) co-polymerized with BuA or MAA had potential to act as a transdermal delivery agent for drugs such as ibuprofen and salicylate. It was observed that the more hydrophobic the drug, the stronger its interaction with the microgel.[42] There is increasing interest in the role of microgels in devices that can potentially control the release of rapidly metabolized drugs or protect sensitive drugs against harsh environments.[12] For example, a poly(NIPAM-*co*-butyl methacrylate-*co*-AA) microgel shows potential as an oral delivery vehicle that can protect insulin from the low pH it encounters in the stomach; the hydrophobic butyl methacrylate promotes uptake of the hydrophobic drug, whilst incorporation of AA gives the particles pH sensitivity.[12,177] Polyanionic poly(NIPAM)-based microgels containing negatively-charged tetrazole binding sites have been prepared using molecular imprinting techniques and can bind various protonated amines, such as the local anaesthetic dibucaine and the *β*-blocker propranolol.[178]

1.5 Context

The objective of this study is to uncover the behaviour of hydrophobic microgels at oil-water interfaces by studying the interfacial and swelling properties of hydrophobically modified microgels in aqueous dispersants with of differing hydrophobicities and ionic strengths. It is anticipated that increasing understanding of the basic properties and behaviours of such microgels may provide a useful base from which potential new applications relevant to more hydrophobic environments and materials may be developed. Many existing microgel applications tend to focus

on aqueous and hydrophilic systems, but there is enormous scope for utilizing microgel particles with greater hydrophobic affinity.

1.6   Summary

As has been made clear in this literature review, a great deal is already known about microgel properties and their potential applications. However, there is much that is not fully understood, *e.g.* the distribution of cross-linker and functional groups within the particles,[9] and due to their highly tuneable physico-chemical properties, it is likely that many further applications may be found. In particular, a great deal of research has focused on hydrophilic poly(NIPAM)-based microgels but less has been reported about hydrophobically modified poly(NIPAM) microgels, with potentially greater affinity for hydrophobic environments and materials.

The aim of this project is to prepare novel hydrophobically modified poly(NIPAM)-based microgels by the incorporation of hydrophobic co-monomers and to characterize them using techniques such as DLS, UV-visible spectrophotometry and SEM. The influence of the incorporation of each co-monomer upon the physico-chemical properties of the particles will be considered. This information will then be used as the basis upon which to investigate the effect of the modifications upon the interfacial behaviours of the microgels. For example, the effect of the modified microgels upon the surface tension of water will be studied using tensiometry and the effect of the modifications upon the swelling-shrinking behaviour of the microgels in the presence of short-chain alcohols will also be investigated using DLS. In addition, the control of heteroflocculation of poly(NIPAM) microgels as a function of temperature, pH, background electrolyte and polymer addition will also be investigated. It is anticipated that an increased understanding of the basic physico-chemical properties and interfacial behaviours of hydrophobically modified microgels will aid the future development of microgels with applications relating to more hydrophobic environments and materials.

1.7   References

[1] Hoare, T., Pelton, R. (2008) *Current Opinion in Colloid & Interface Science*, **13**, 413–428.

[2] Murray, M. J., Snowden, M. J. (1995) *Advances in Colloid Interface Science,* **54**, 73–91.

[3] Saunders, B. R., Vincent, B. (1999) *Advances in Colloid Interface Science,* **80**, 1–25.

[4] Pelton, R. (2000) *Advances in Colloid Interface Science*, **85**, 1–33.

[5] Nur, H., Snowden, M. J., Cornelius, V. J., Mitchell, J. C., Harvey, P. J., Benée, L. S. (2009) *Colloids and Surfaces A: Physicochemical and Engineering Aspects*, **335**, 133–137.

[6] Kausar, N., Chowdhry, B. Z., Snowden, M. J. (2008) 'Microgels from Smart Polymers'. *In:* Galaev, I., Mattiasson, B. (Eds) *Smart Polymers: Applications in Biotechnology and Biomedicine* (2nd Edition). Boca Raton: CRC Press.

[7] Saunders, B. R., Laajam, N., Daly, E., Teow, S., Hu, X., Stepto, R. (2009) *Advances in Colloid Interface Science*, **147–148**, 251–262.

[8] Pelton, R. H., Chibante, P. (1986) *Colloids and Surfaces*, **20**(3), 247–256.

[9] Pelton, R., Hoare, T. (2011) 'Microgels and Their Synthesis: An introduction'. *In:* Fernandez-Nieves, A., Wyss, H., Mattsson, J., Weitz, D. A. (Eds) *Microgel Suspensions: Fundamentals and Applications*. Weinheim: Wiley.

[10] Holmberg, K., Jönsson, B., Kronberg, B., Lindman, B. (2003) *Surfactants and Polymers in Aqueous Solution* (2nd Edition). Chichester: Wiley.

[11] Staudinger H., Husemann, E. (1935) *Berichte der Deutschen Chemischen Gesellschaft (A and B Series)*, **68**(8) 1618–1634.

[12] Thorne, J. B., Vine, G. J., Snowden, M. J. (2011) *Colloid and Polymer Science*, **289**(5–6**)**, 625–646.

[13] Xu, S., Zhang, J., Paquet, C., Lin, Y., Kumacheva, E. (2003) *Advanced Functional Materials*, **13**(6) 468–472

[14] Ye, L., Weiss, R., Mosbach, K. (2000) *Macromolecules*, **33**(22) 8239–8245.

[15] Oh, J. K., Drumright, R., Siegwart, D. J., Matyjaszewski, K. (2008) *Progress in Polymer Science*, **33**(4) 448–477.

[16] Garner, B.W., Cai, T., Hu, Z., Neogi, A. (2008) *Optics Express*, **16**, 19410–19418.

[17] IUPAC (2006) *Compendium of Chemical Terminology* (2nd Edition), (the "Gold Book"). Compiled by McNaught, A. D., Wilkinson, A. Oxford: Blackwell (1997). XML on-line corrected version: http://goldbook.iupac.org (2006-) created by Nic, M., Jirat, J., Kosata; B., updates compiled by Jenkins, A. ISBN 0-9678550-9-8. doi:10.1351/goldbook. Last update: 2011-10-11; version: 2.3. DOI of this term: doi:10.1351/goldbook.C01172.

[18] Gracia, L. H., Snowden, M. J. (2007) 'Preparation, Properties and Applications of Colloidal Microgels'. *In:* Williams, P. A. (Ed). *Handbook of Industrial Water Soluble Polymers*. Oxford: Blackwell, 268–297.

[19] Lovell, P. A., El-Aasser, M. S. (Eds) (1997) *Emulsion Polymerization and Emulsion Polymers*. Chichester: Wiley.

[20] Goodwin, J. W., Hearn, J., Ho, C. C., Ottewill, R. H. (1973) *British Polymer Journal*, **5**(5), 347–362.

[21] Benée, L. S., Snowden, M. J., Chowdhry, B. Z. (2002) *Langmuir*, **18**, 6025–6030.

[22] Hsieh, W.-C., Wada, Y., Mitobe, T., Mitomo, H., Seko, N., Tamada, M. (2009) *Journal of the Taiwan Institute of Chemical Engineers*, **40**, 413–417.

[23] Snowden, M. J., Vincent, B. (1992) *Journal of the Chemical Society – Chemical Communications*, (16) 1103–1105.

[24] Puertas, A. M., Nieves, F. J. de las (1999) *Journal of Colloid and Interface Science*, **216**, 221–229.

[25] Woodward, N. C., Snowden, M. J., Chowdhry, B. Z., Jenkins, P., Larson, I. (2002) *Langmuir*, **18**(6), 2089–2095.

[26] Guillermo, A., Cohen Addad, J. P., Bazile, J. P., Duracher, D., Elaïssari, A., Pichot, C. (2000) *Journal of Polymer Science: Part B: Polymer Physics*, **38**, 889–898.

[27] Lowe, J. S., Chowdhry, B. Z., Parsonage, J. R., Snowden, M. J. (1998) *Polymer*, **39**, 1207–1212.

[28] Duracher, D., Elaïssari, A., Pichot, C. (1999) *Journal of Polymer Science Part A: Polymer Chemistry*, **37**, 1823–1837.

[29] Johansson, C., Hansson, P., Malmsten, M. (2007) *Journal of Colloid and Interface Science*, **316**, 350–359.

[30] Zhang, H., Mardyani, S., Chan, W. C. W., Kumacheva, E. (2006) *Biomacromolecules*, **7**, 1568–1572.

[31] Xie, H.-Q., Guan, J.-G., Guo, J.-S. (1995) *Journal of Applied Polymer Science*, **58**(5), 951–956.

[32] Gao, Y., Steve, C.F., Wu, C. (1999) *Macromolecules*, **32**(11), 3674–3677.

[33] Laukkanen, A., Wiedmer, S.K., Varjo, S., Riekkola, M.-L., Tenhu, H. (2002) *Colloid and Polymer Science*, **280**(1), 65–70.

[34] Imaz, A., Forcada, J. (2009) *European Polymer Journal*, **45**(11), 3164–3175.

[35] Peng, S., Wu, C. (2000) *Macromolecular Symposia,* **159**, 179–186.

[36] Peng, S., Wu, C. (2001) *Polymer*, **42**, 6871–6876.

[37] Nieuwenhuis, E. A., Vrij, A. (1979) *Journal of Colloid and Interface Science*, **72**(2), 321–341.

[38] Saunders, B. R., Vincent, B. (1997) *Colloid Polymer Science*, **275**, 9–17.

[39] IUPAC. Compendium of Chemical Terminology, 2nd Edition (the "Gold Book"). Compiled by A. D. McNaught and A. Wilkinson. Blackwell Scientific Publications, Oxford (1997). XML on-line corrected version: http://goldbook.iupac.org (2006-) created by M. Nic, J. Jirat, B. Kosata; updates compiled by A. Jenkins. ISBN 0-9678550-9-8. doi:10.1351/goldbook. Last update: 2010-12-22; version: 2.2. DOI of this term: doi:10.1351/goldbook.H02854.

[40] Nur, H., Cornelius, V. J., Benée, L. S., Mitchell, J. C., Day, I. J., Snowden, M. J. (2009) *Analyst*, **134**, 1366–1372.

[41] Lopez, V. Castro, Hadgraft, J., Snowden, M. J. (2005) *International Journal of Pharmaceutics*, **292**(1/2), 137.

[42] Lopez, V. Castro, Raghavan, S. L., Snowden, M. J. (2004) *Reactive & Functional Polymers*, **58**, 175–185.

[43] Snowden, M. J., Chowdhry, B. Z., Vincent, B., Morris, G. E. (1996) *Journal of the Chemical Society, Faraday Transactions*, **92**(24), 5013–5016.

[44] Saunders, J. M., Tong, T., Le Maitre, C. L., Freemont, T. J., Saunders, B. R. (2007) *Soft Matter*, **3**, 486–494.

[45] IUPAC. Compendium of Chemical Terminology, 2nd Edition (the "Gold Book"). Compiled by A. D. McNaught and A. Wilkinson. Blackwell Scientific Publications, Oxford (1997). XML on-line corrected version: http://goldbook.iupac.org (2006-) created by M. Nic, J. Jirat, B. Kosata; updates compiled by A. Jenkins. ISBN 0-9678550-9-8. doi:10.1351/goldbook. Last update: 2010-12-22; version: 2.2. DOI of this term: doi:10.1351/goldbook.C01335.

[46] Nur, H., Pinkrah, V. T., Mitchell, J. C., Benée, L. S., Snowden, M. J. (2010) *Advances in Colloid and Interface Science*, **158**, 15–20.

[47] Seidel, J., Pinkrah, V. T., Mitchell, J. C., Chowdhry, B. Z., Snowden, M. J. (2004) *Thermochimica Acta*, **414**, 47–52.

[48] Zhu, P. W., Napper, D. H. (1996) *Journal of Colloid and Interface Science*, **177**, 343–352.

[49] Qiu, X., Li, M., Kwan, C. M. S., Wu, C. (1998) *Journal of Polymer Science: Part B: Polymer Physics*, **36**, 1501–1506.

[50] Ning, H., Yuanyuan, Y., Changchun, W., Fatkin, J. (2010) *Thermo and pH Sensitive PNIPAM Coated Silica Particles Studied Using Light Scattering*, Application Note MRK1531-01. Malvern: Malvern Instruments.

[51] Amalvy, J. I., Wanless, E. J., Li, Y., Michailidou, V., Armes, S. P., Duccini, Y. (2004) *Langmuir*, **20**(21), 8992–8999.

[52] Hoffman, A. S., Stayton, P. S., Bulmus, V., Chen, G., Chen, J., Cheung, C., Chilkoti, A., Ding, Z., Dong, L., Fong, R., Lackey, C. A., Long, C. J., Miura, M., Morris, J. E., Murthy, N., Nabeshima, Y., Park, T. G., Press, O. W., Shimoboji, T., Shoemaker, S., Yang, H. J., Monji, N., Nowinski, R. C., Cole, C. A., Priest, J. H., Harris, J. M., Nakamae, K., Nishino, T., Miyata, T. (2000) *Journal of Biomedical Materials Research – Part A*, **52**(4), 577–586.

[53] Ma, X., Xi, J., Huang, X., Zhao, X., Tang, X. (2004) *Materials Letters*, **58**, 3400–3404.

[54] Meunier, F., Elaïssari, A., Pichot, C. (1995) *Polymers for Advanced Technologies*, **6**, 489–496.

[55] IUPAC (2006) Compendium of Chemical Terminology (2nd) (the "Gold Book"). Compiled by McNaught, AD, Wilkinson, A. Blackwell Scientific Publications, Oxford (1997). XML on-line corrected version: http://goldbook.iupac.org (2006-) created by Nic, M, Jirat, J, Kosata, B; updates compiled by Jenkins, A. ISBN 0-9678550-9-8. doi:10.1351/goldbook. Last update: 2009-09-07; version: 2.1.5. DOI of this term: doi:10.1351/goldbook.P04728.

[56] Cowie, J. M. G. (1991) *Polymers: Chemistry & Physics of Modern Materials* (2nd Edition). London: Blackie.

[57] Gracia, L. (2007) *Co-polymer microgels: contemporary physico-chemical, structural and analytical investigations*. Thesis (Ph.D.). University of Greenwich, London.

[58] Christensen, M. L., Keiding, K. (2005) *Colloids and Surfaces A: Physicochemical and Engineering Aspects*, **252**(1), 61–69.

[59] Hoare, T., Pelton, R. (2004) *Macromolecules*, **37**, 2544–2550.

[60] Hoare, T., McLean, D. (2006) *Journal of Physical Chemistry B*, **110**, 20327–20336.

[61] Wu, X., Pelton, R. H., Hamielec, A. E., Woods, D. R., McPhee, W. (1994) *Colloid & Polymer Science*, **272**, 467–477.

[62] Griffin, J. M., Robb, I., Bismarck, A. (2007) *Journal of Applied Polymer Science*, **104**(3), 1912–1919.

[63] Gao, J., Frisken, B. J. (2003) *Langmuir*, **19**(13), 5217–5222.

[64] Gao, J., Frisken, B. J. (2005) *Langmuir*, **21**(2), 545–551.

[65] Gao, J., Frisken, B. J. (2003) *Langmuir*, **19**(13), 5212–5216

[66] Woodward, N. C., Chowdhry, B. Z., Snowden, M. J., Leharne, S. A., Griffiths, P. C., Winnington, A. L. (2003) *Langmuir*, **19**, 3202–3211.

[67] McPhee, W., Tam, K. C., Pelton, R. (1993) *Journal of Colloid and Interface Science*, **156**, 24–30.

[63] Daly, E., Saunders, B.R. (2000) *Physical Chemistry Chemical Physics*, **2**, 3187–3193.

[64] Saunders, B. R. (2004) *Langmuir*, **20**, 3925–3932.

[65] Stieger, M., Richtering, W., Pedersen, J. S., Lindner, P. (2004) *Journal of Chemical Physics*, **120**(13), 6197–6206.

[66] Saunders, B. R., Vincent, B. (1996) *Journal of the Chemical Society, Faraday Transactions*, **92**(18), 3385–3389.

[67] Si, T., Wang, Y., Wei, W., Lv, P., Ma, G., Su, Z. (2011) *Reactive & Functional Polymers*, **71**, 728–735.

[68] Meunier, F., Pichot, C., Elaïssari, A. (2006) *Colloid & Polymer Science*, **284**, 1287–1292.

[69] Sigma-Aldrich (2011) *Free Radical Initiators* [online]. St. Louis: Sigma-Aldrich. Available from: http://www.sigmaaldrich.com/materials-science/material-science-products.html?TablePage=16374963 [Accessed 7 January 2012].

[70] Vincent, B. (2005) 'Introduction to Colloidal Dispersions'. *In*: Cosgrove, T. (Ed) *Colloid Science: Principles, Methods and Applications*. Oxford: Blackwell, pp 1–13.

[71] Shaw, D. J. (1992) *Introduction to Colloid and Surface Chemistry* (4th Edition). Oxford: Butterworth Heinemann.

[72] Riley, J. (2005) 'Charge in Colloidal Dispersions'. *In*: Cosgrove, T. (Ed) *Colloid Science: Principles, Methods and Applications*. Oxford: Blackwell, pp 14–35.

[73] Eastman, J. (2005) 'Colloid Stability'. *In:* Cosgrove, T. (Ed) *Colloid Science: Principles, Methods and Applications*. Oxford: Blackwell, pp 36–49.

[74] Morrison, I., Ross, S. (1992) *Colloidal dispersions: suspensions, emulsions and foams*. New York: Wiley.

[75] Crow, D. R. (1994) *Principles and Applications of Electrochemistry*. London: Chapman Hall.

[76] Atkins, P. W. (1990) *Atkins' Physical Chemistry* (4th Edition). Oxford: Oxford University Press.

[77] Malvern Instruments (2008) *Nano Series and HPPS Training Manual: Dynamic Light Scattering*. Malvern: Malvern Instruments.

[78] Goodwin, J. (2009) *Colloids and Interfaces with Surfactants and Polymers* (2nd Edition). Chichester: Wiley.

[79] Malvern Instruments (2008) *Zetasizer Nano Series User Manual (MAN0317, Issue 4.0)*. Malvern: Malvern Instruments.

[80] Benée, L. S. (2001) *The use of nano-particles in improved secondary oil recovery*. Thesis (Ph.D.). University of Greenwich, London.

[81] Oshima, H. (1994) *Journal of Colloid and Interface Science*, **163**, 474–483.

[82] Karg, M., Hellweg, T. (2009) *Journal of Materials Chemistry*, **19**, 8714–8727.

[83] Liu, H. Y., Zhu, X. X. (1999) *Polymer*, **40**, 6985–6990.

[84] Saunders, B. R., Crowther, H. M., Morris, G. E., Mears, S. J., Cosgrove, T., Vincent, B. (1999) *Colloids and Surfaces A: Physicochemical and Engineering Aspects*, **149**, 57–64.

[85] Zhang, Q., Zhaa, L., Maa, J., Liang, B. (2009) *Journal of Colloid and Interface Science*, 330(2), 330–336.

[86] Khan, A. (2007) *Journal of Colloid and Interface Science*, **313**, 697–704.

[87] Das, M., Kumacheva, E. (2006) *Colloid & Polymer Science*, **284**, 1073–1084.

[88] Tan, B. H., Tam, K. C., Lam, Y. C., Tan, C. B. (2005) *Advances in Colloid and Interface Science*, **113**, 111–120.

[89] Atkins, P. W. (1994) *Atkins' Physical Chemistry* (5th Edition). Oxford: Oxford University Press.

[90] Tan, B. H., Tam, K. C., Lam, Y. C., Tan, C. B. (2004) *Langmuir*, **2** (26), 11380–11386.

[91] Hou, Y., Yu, C., Liu, G., Ngai, T., Zhang, G. (2010) *Journal of Physical Chemistry*, **114**(11), 3799–3803.

[92] Daly, E., Saunders, B. R. (2000) *Langmuir*, **16**(13), 5546–5552.

[93] Crowther, H. M., Vincent, B. (1998) *Colloid & Polymer Science*, **276**, 46–51.

[94] Mukae, K., Sakuri, M., Sawamura, S., Makino, K., Kim, S. Wan, Ueda, I., Shirahama, K. (1993) *Journal of Physical Chemistry*, **97**, 737–741.

[95] Mielke, M., Zimehl, R. (1998) *Progress in Colloid Polymer Science*, **111**, 74–77.

[96] Saunders, B. R., Crowther, H. M., Vincent, B. (1997) *Macromolecules*, **30**, 482–487.

[97] Soper, A. K., Finney, J. L. (1993) *Physical Review Letters*, **71**, 4346–4349.

[98] Otake, K., Inomata, H., Konno, M., Saito, S. (1990) *Macromolecules*, **23**(1), 283–289.

[99] Onori, G. (1989) *Chemical Physics Letters*, **153**(3), 213–216, *In*: Crowther, H. M., Vincent, B. (1998) *Colloid & Polymer Science*, **276**, 46–51.

[100] Routh, A.F., Fernandez-Nieves, A., Bradley, M., Vincent, B. (2006) *Journal of Physical Chemistry*, **110**(25), 12721–12727.

[101] Yu, T. L., Lu, W. C., Liu, W. H., Lin, H. L., Chiu, C. H. (2004) *Polymer*, **45**, 5579–5589.

[102] Karg, M., Hellweg, T. (2009) *Current Opinion in Colloid & Interface Science*, **14**, 438–450.

[103] Ménager, C., Sandre, O., Mangili, J., Cabuil, V. (2004) *Polymer*, **45**, 2475–2481.

[104] Lietor-Santos, J. J., Sierra-Martin, B., Vavrin, R., Hu, Z. B., Gasser, U., Fernandez-Nieves, A. (2009) *Macromolecules*, **42**(16), 6225–6230.

[105] Hoare, T., Pelton, R. (2005) *Polymer*, **46**, 1139–1150.

[106] Eastoe, J. (2005) 'Surfactant Aggregation and Adsorption at Interfaces'. *In*: Cosgrove, T. (Ed) *Colloid Science: Principles, Methods and Applications*. Oxford: Blackwell, pp 50–76.

[107] Atkins, P., Paula, J. de (2002) *Atkins' Physical Chemistry* (7th Edition). Oxford: Oxford University Press.

[108] Chang, R. (2000) *Physical Chemistry for the Chemical and Biological Sciences*. Sausalito: University Science Books.

[109] Krüss (2005) *Tensiometer K100 MK2/SF/C Instruction Manual V2-05*. Hamburg: Krüss GmbH.

[110] Binks, B. P. (2002) *Current Opinion in Colloid & Interface Science*, **7**, 21–41.

[111] Zhang, J., Pelton, R. (1999) *Colloids and Surfaces A: Physicochemical and Engineering Aspects*, **156**,111–122.

[112] Brugger, B., Rütten, S., Phan, K.-H., Möller, M., Richtering, W. (2009) *Angewandte Chemie*, **121**, 4038–4041.

[113] Islam, A. M., Chowdhry, B. Z., Snowden, M. J. (1995) *Advances in Colloid Interface Science*, **62**, 109–136.

[114] Cosgrove, T. (2005) 'Polymers at interfaces'. *In*: Cosgrove, T. (Ed) *Colloid Science: Principles, Methods and Applications*. Oxford: Blackwell, pp 113–142.

[115] Hall, R. J., Pinkrah, V. T., Chowdhry, B. Z., Snowden, M. J. (2004) *Colloids and Surfaces A: Physicochemical and Engineering Aspects*, **233**, 25–38.

[116] Snowden, M. J. (1994) 'Flocculants'. *In*: Bloor, D., Brook, R. J., Flemings, M. C., Mahajan, S. (Eds) *The Encylcopedia of Advanced Materials*. Pergamon Press, Oxford, pp 858–862.

[117] Grasso, D., Subramaniam, K., Butkus, M., Strevett, K., Bergendahl, J. (2002) *Re/Views in Environmental Science and Technology*, **1**, 17–38.

[118] Bhattacharjee, S., Elimelech, M., Borkovec, M. (1998) *Croatica Chemica Acta*, **71**(4), 883–903.

[119] Jan van Oss, C., Norde, W., Visser, H. (1999) *Colloids and Surfaces B: Biointerfaces*, **14**, 1–2.

[120] van Duijneveld, J. (2005) 'Effect of Polymers on Colloid Stability'. *In*: Cosgrove, T. (Ed) *Colloid Science: Principles, Methods and Applications*. Oxford: Blackwell, pp 143–158.

[121] Molina-Bolívar, J. A., Galisteo-González, F., Hidalgo-Alvarez, R. (1999) *Colloids and Surfaces B: Biointerfaces*, **14**, 3–17.

[122] Islam, A. M., Chowdhry, B. Z., Snowden, M. J. (1995) *Journal of Physical Chemistry*, **99**, 14205–14206.

[123] Mu, B., Liu, P., Dong, Y., Lu, C., Wu, X. (2010) *Journal of Polymer Science Part A: Polymer Chemistry*, **48**, 3135–3144.

[124] Rasmussen, M., Vincent, B. (2004) *Reactive and Functional Polymers*, **58**, 203–211.

[125] Rasmussen, M., Routh, A., Vincent, B. (2004) *Langmuir*, **20**(9), 3536–3542.

[126] Routh, A. F., Vincent, B. (2002) *Langmuir*, **18**(14), 5366–5369.

[127] Ma, X., Tang, X. (2006) *Journal of Colloid and Interface Science*, **299**, 217–224.

[128] Lopez-Leon, T., Fernandez-Nieves, A. (2007) *Physical Review E*, **75**(1), Article number 011801.

[129] Snowden, M. J., Gracia, L. H., Nur, H. (2008) 'Heteroflocculation studies of colloidal poly(*N-iso*propylacrylamide) microgels with polystyrene latex particles: effect of particle size, temperature and surface charge'. *In:* Biggs, S., Cosgrove, T., Dowding, P. (Eds) (2008) *New Frontiers in Colloid Science – A celebration of the career of Brian Vincent*. London: RSC.

[130] Routh, A. E., Vincent, B. (2004) *Journal of Colloid and Interface Science*, **273**(2), 435–441.

[131] Hou, Y., Ye, J., Wei, X. L., Zhang, G. Z. (2009) *Journal of Physical Chemistry B*, **113**(21), 7457–7461.

[132] Bratby J (2006) *Coagulation and flocculation in water and wastewater treatment* (2nd Ed). IWA: London.

[133] Richardson, R. (2005) 'Scattering and Reflection Techniques'. *In*: Cosgrove, T. (Ed) *Colloid Science: Principles, Methods and Applications*. Oxford: Blackwell, pp 228–254.

[134] Malvern (2009) *Frequently Asked Question: Is it ok to estimate the solvent refractive index?* [online]. Malvern: Malvern Instruments. Available from: http://www.malvern.com/malvern/kbase.nsf/allbyno/KB000785/$file/FAQ%20-%20Is%20it%20OK%20to%20estimate%20the%20solvent%20refractive%20index.pdf [Accessed 16 November 2009].

[135] Malvern (2009) *Application note: Empirical methods for estimating Refractive Index values* [online]. Malvern: Malvern Instruments. Available from: http://www.malvern.com/malvern/kbase.nsf/allbyno/KB001209/$file/MRK843-01.pdf [Accessed 16 November 2009].

[136] Bellingham + Stanley (2009) *Technical Bulletin R001: Principles of Refractometry* [online]. Tunbridge Wells: Bellingham + Stanley. Available from:

http://www.bellinghamandstanley.com/general_pdfs/techb_pdfs/R001.pdf [Accessed 16 November 2009].

[137] Bellingham + Stanley (2009) *Technical Bulletin R002: Refractometers – What are they? What do they do? What are they used for?* [online]. Tunbridge Wells: Bellingham + Stanley. Available from: http://www.bellinghamandstanley.com/ general_pdfs/techb_pdfs/R002.pdf [Accessed 16 November 2009].

[138] Jouyban, A., Soltanpour, S., Chan, H. K. (2004) *International Journal of Pharmaceutics*, **269**, 353–360.

[139] Åkerlöf, G. (1932) *Journal of the American Chemical Society*, **54**(11), 4125–4139.

[140] Lide, D. R. (Ed) (1992) *CRC Handbook of Chemistry and Physics* (73rd Edition) Boca Raton: CRC Press.

[141] Mazurkiewicz, J., Tomasik, P. (1990) *Journal of Physical Organic Chemistry*, **3**, 493–502.

[142] Dean, J. R., Jones, A. M., Holmes, D., Reed, R., Weyers, J., Jones, A. (2002) *Practical Skills in Chemistry*. Harlow: Pearson (Prentice Hall).

[142] Edwards, A. A., Alexander, B. D. (2010) 'Organic Applications of UV-Visible Absorption Spectroscopy'. *In:* Lindon, J., Tranter, G. E., Koppenaal, D. (Eds) *Encyclopedia of Spectroscopy and Spectrometry*. San Diego: Academic Press.

[144] Jeol Ltd (2009) *SEM Scanning Electron Microscope A To Z: Basic Knowledge for Using the SEM* [online]. Tokyo: Jeol. Available from: http://www.jeolusa.com/tabid/320/Default.aspx?EntryId=598 [Accessed 16 November 2009].

[145] Davis, S. (2005) 'Electron Microscopy'. *In*: Cosgrove, T. (Ed) *Colloid Science: Principles, Methods and Applications*. Oxford: Blackwell, pp 266–282.

[146] Reynolds, P. (2005) 'Wetting of Surfaces'. *In*: Cosgrove, T. (Ed) *Colloid Science: Principles, Methods and Applications*. Oxford: Blackwell, pp 159–179.

[147] Krüss (2009) *Surface tension: Plate method* [online]. Hamburg: Krüss GmbH. Available from: http://www.kruss.de/en/theory/measurements/surface-tension/plate-method.html [Accessed 20 October 2009].

[148] Kawaguchi, H. (2000) *Progress in Polymer Science*, **25**, 1171–1210.

[149] Stokes, J. R. (2011) 'Rheology of Industrial Relevant Microgels'. *In:* Fernandez-Nieves, A., Wyss, H., Mattsson, J., Weitz, D. A. (Eds) *Microgel Suspensions: Fundamentals and Applications*. Weinheim: Wiley.

[150] Kim, Y. B., Kim, H.-K., Hong, J.-W. (2002) *Surface and Coatings Technology*, **153**, 284–289.

[151] Corrigan, V. G., Zawacky, S. R. (1992) *Cationic microgels and their use in electrodeposition*. US Patent 5096556.

[152] Bartsch, E., Kirsch, S., Lindner, P., Scherer, T., Stölken, S. (1998) *Berichte der Busengesellschaft főr Physikalische Chemie*, **102**, 1597–1602.

[153] Ketz, R. J., Prud'homme, R. K., Graessley, W. W. (1988) *Rheol Acta*, **27**, 531–539.

[154] Naé, H. N., Reichert, W. W. (1992) *Rheol Acta*, **31**, 351–360.

[155] Kaneda, I., Yanaki, Y. (2002) *Journal of the Society of Rheology*, **30**: 89–94.

[156] Kaneda, I., Sogabe, A., Nakajima, H. (2004) *Journal of Colloid and Interface Science*, **275**, 450–457.

[157] Binks, B. P. (1998) 'Emulsions – Recent Advances in Understanding'. *In:* Binks, B. P. (Ed) *Modern Aspects of Emulsion Science*. Cambridge: Royal Society of Chemistry, pp 1–55.

[158] Binks, B. P., Murakami, R., Armes, S. P., Fujii, S. (2005) *Angewandte Chemie International Edition*, **44**, 4795–4798.

[159] Binks, B. P., Murakami, R., Armes, S. P., Fujii, S. (2006) *Langmuir*, **22**, 2050–2057.

[160] Fujii, S., Read, E. S., Binks, B. P., Armes, S. P. (2005) *Advanced Materials*, **17**, 1014.

[161] Fujii, S., Randall, D. P., Armes, S. P. (2004) *Langmuir*, **20**, 11329.

[162] Ngai, T., Behrens, S. H., Auweter, H. (2005) *Chemical Communications*, 331–333.

[163] Ngai, T., Auweter, H., Behrens, S. H. (2006) *Macromolecules*, **39**, 8171–8177.

[164] Parsons, S., Jefferson, B. (2006) *Introduction to Potable Water Treatment Processes*. Blackwell, Oxford.

[165] Snowden, M. J., Thomas, D., Vincent, B. (1993) *Analyst*, **118**, 1367–1369.

[166] Morris, G. E., Vincent, B., Snowden, M. J. (1997) *Journal of Colloid and Interface Science*, **190**, 198–205.

[167] Ben, Y., Robb, I., Tonmukayakul, P., Wang, Q. (2011) 'Microgels for Oil Recovery'. *In:* Fernandez-Nieves, A., Wyss, H., Mattsson, J., Weitz, D. A. (Eds) *Microgel Suspensions: Fundamentals and Applications*. Weinheim: Wiley.

[168] Freemont, T. J., Saunders, B. R. (2008) *Soft Matter*, **4**, 919–924.

[169] Gan, T., Guan, Y., Zhang, Y. (2010) *Journal of Materials Chemistry*, **20**, 5937–5944.

[170] Hopkins, S., Carter, S. R., Haycock, J. W., Fullwood, N. J., MacNeil, S., Rimmer, S. (2009) *Soft Matter*, **5**, 4928–4937.

[171] Sisson, A. L., Haag, R. (2010) *Soft Matter*, **6**, 4968–4975.

[172] Rosiak, J. M., Janik, I., Kadlubowski, S., Kozicki, M., Kujawa, P., Stasica, P., Ulanski, P. (2003) *Nuclear Instruments and Methods Physics Research*, **208**, 325–330.

[173] Aqil, A., Vasseur, S., Duguet, E., Passirani, C., Benoit, J. P., Jerome, R., Jerome, C. (2008) *Journal of Materials Chemistry*, **18**, 3352–3360.

[174] Sanson, N., Reiger, J. (2010) *Polymer Chemistry*, **1**, 965–977.

[175] Sukhorukov, G., Fery, A., Möhwald, H. (2005) *Progress in Polymer Science*, **30**, 885–897.

[176] Cao, Z., Ziener, U., Landfester, K. (2010) *Macromolecules*, **43**, 6353–6360.

[177] Ramkissoon-Ganorkar, F., Liu, M., Baudys, Kim S. W. (1999) *Journal of Controlled Release*, **59**, 287.

[178] Tominey, A., Andrew, D., Oliphant, L., Rosair, G. M., Dupré, J., Kraft, A. (2006) *Chemical Communications*, 2492–2494.

SYNTHESIS OF
POLY(NIPAM)-BASED MICROGELS

2.1   Introduction

Microgels based on the monomer *N-iso*propylacrylamide (NIPAM) have been studied extensively during the last three decades. As described in Chapter 1, during this time poly(NIPAM)-based particles have been prepared by a range of synthetic methods, in combination with different co-monomers, initiators and cross-linking agents, which has resulted in an enormous diversity of particle compositions and sizes, each with subtly differing physico-chemical characteristics. The amide bonds in poly(NIPAM) chains permit substantial hydrogen bonding to occur with aqueous solvents, and as a consequence, poly(NIPAM) microgel particles are considered to be predominantly hydrophilic. This hydrophilic/hydrophobic balance can be altered by co-polymerizing NIPAM with different co-monomers. The overall aim of this work was to prepare novel hydrophobic poly(NIPAM)-based microgels by incorporating a selection of hydrophobic co-monomers, and to determine the influence of this hydrophobic modification upon the properties and interfacial behaviour of the particles. This chapter describes the synthesis of the microgel particles studied in this thesis.

2.2   Materials and methods

2.2.1 Materials

Table 2.1 summarizes details of the chemicals used to synthesise the anionic and cationic microgels studied herein. Each co-monomer possesses a vinyl group, which permits its participation in the polymerization reaction. However, the co-monomers can be further categorized into broad groups according to their structures. The categorization used in this investigation is shown in Table 2.2. The co-monomers were initially categorized according to the functional group they contain: ether (R-O-R'), ester (R-C=OOR'), silane (R-Si-(R')$_3$) or charged group (-COOH). The co-monomers were subsequently divided into straight or branched/aromatic chain groups.

Table 2.1 Details of chemicals used in microgel synthesis
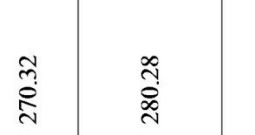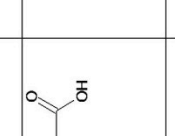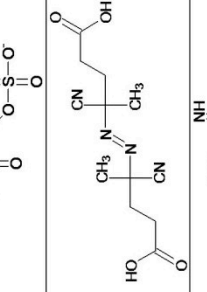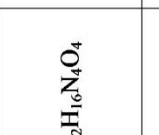
Name	Molecular formula	Structure	Molecular weight (g mol^{-1})	Source
MONOMER				
N-isopropylacrylamide (NIPAM)	$C_6H_{11}NO$		113.16	Aldrich, 415324-50G, Batches 0196BH/15106DE; and Wako, 099-03695, Lot CDL2447
CROSS-LINKER				
N,N'-methylenebisacrylamide (MBA)	$C_7H_{10}N_2O_2$		154.17	Aldrich: 14,832-6, Lot 30585-079; 14,607-2, Lot HG07719EG; 146072, Batch MKBB5122
INITIATORS				
potassium persulphate (KPS)	$K_2S_2O_8$		270.32	BDH, 298614V, Lot K23820372
4,4'-azobis(4-cyanovaleric acid) (CVA)	$C_{12}H_{16}N_4O_4$		280.28	Aldrich, 118168, Batch 1332235 14707418
2,2'-azobis(2-methylpropionamidine) dihydrochloride (MPA)	$C_8H_{18}N_6.2HCl$		271.19	Aldrich, 440914, Batch 12017DO-113
CO-MONOMERS				
vinyl ethers				
dodecyl vinyl ether (DVE)	$C_{14}H_{28}O$		212.37	Aldrich, 413496, Batch 02623AH
tert-butyl vinyl ether (TBVE)	$C_6H_{12}O$		100.16	Aldrich, 410012, Batch 12918LH-248
tert-pentyl vinyl ether (TPVE)	$C_7H_{14}O$		114.19	Aldrich, 410004, Batch 10420JF

Table continued on next page

Table 2.1 Continued...
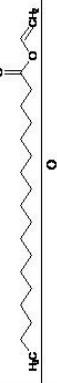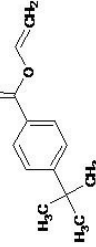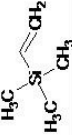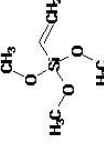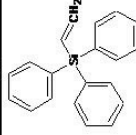
Name	Molecular formula	Structure	Molecular weight (g mol^{-1})	Source
vinyl esters				
vinyl decanoate (VD)	C$_{12}$H$_{22}$O$_2$		198.30	Aldrich, 411795, Batch S30606–405
vinyl laurate (VL)	C$_{14}$H$_{26}$O$_2$		226.36	Fluka, 61725, Lot 1082564 13906032
vinyl stearate (VS)	C$_{20}$H$_{38}$O$_2$		310.51	Aldrich, 436208, Batch 06306BR
vinyl-4-*tert*-butylbenzoate (V4TBB)	C$_{13}$H$_{16}$O$_2$		204.26	Aldrich, 380806, Batch 09613CS
vinyl silanes				
trimethyl(vinyl)silane (TMVS)	C$_5$H$_{12}$Si		100.23	Fluka, 95100
vinyltrimethoxysilane (VTMOS)	C$_5$H$_{12}$O$_3$Si		148.23	Aldrich, 235768, Batch 06897PJ
triphenyl(vinyl)silane (TPVS)	C$_{20}$H$_{18}$Si		286.44	Aldrich, 362689, Batch 03422AX
Polyelectrolyte				
methacrylic acid (MAA)	C$_4$H$_6$O$_2$		86.09	Aldrich, 155721, Batch U19881

Table 2.2 Structural categorization of co-monomers

Co-monomer	Straight chain	Branched chain/aromatic
Vinyl ether	dodecyl vinyl ether (DVE)	*tert*-butyl vinyl ether (TBVE) *tert*-pentyl vinyl ether (TPVE)
Vinyl ester	vinyl decanoate (VD) vinyl laurate (VL) vinyl stearate (VS)	vinyl-4-*tert*-butylbenzoate (V4TBB)
Vinyl silane	n/a	trimethyl(vinyl)silane (TMVS) vinyltrimethoxysilane (VTMOS) triphenyl(vinyl)silane (TPVS)
Charged	n/a	methacrylic acid (MAA)

Similarly, the radical initiators used in this study can be categorized but this time according to the functional group that originates from the initiator and resides on the microgel particle surface following the synthesis (Table 2.3).

Table 2.3 Initiator types and resultant charged groups on microgel surface

Initiator	Charged group†
di-potassium peroxidisulphate (KPS)	$-SO_3H/-SO_3^-$
4,4′-azobis(4-cyanovaleric acid) (CVA)	$-COOH/-COO^-$
2,2′-azobis(2-methylpropionamidine) dihydrochloride (MPA)	$-NH_3^+/-NH_2$

† Extent of ionization varies with dispersion pH

2.2.2 Synthesis of microgels

2.2.2.1 Anionic poly(NIPAM)-based microgels

A range of anionic poly(NIPAM)-based microgels were prepared by SFEP using the set up illustrated in Figure 2.1. This SFEP method was initially described by Goodwin *et al.*[1], but first used to prepare microgels by Pelton and Chibante.[2] In order to prepare 1 L of microgel, the monomer, co-monomer and cross-linker were added to 200 mL distilled water, whilst the initiator was added to 800 mL distilled water. The mixtures were heated to 70 °C with magnetic stirring; when both reached 70 °C the 200 mL mixture was transferred to the main reaction vessel. The reaction was allowed to proceed for six hours at 70 °C with magnetic stirring, under an atmosphere of approximately 1 bar nitrogen.

After six hours, the dispersion was cooled and filtered through damp glass wool into semi-permeable membrane tubing, so that it could be dialysed against distilled water, which was changed daily for at least seven days or until the conductivity of the

dialysate remained around 2 μS/cm.[3,4,5] The dialysed dispersions were refrigerated in sealed bottles ready for analysis.
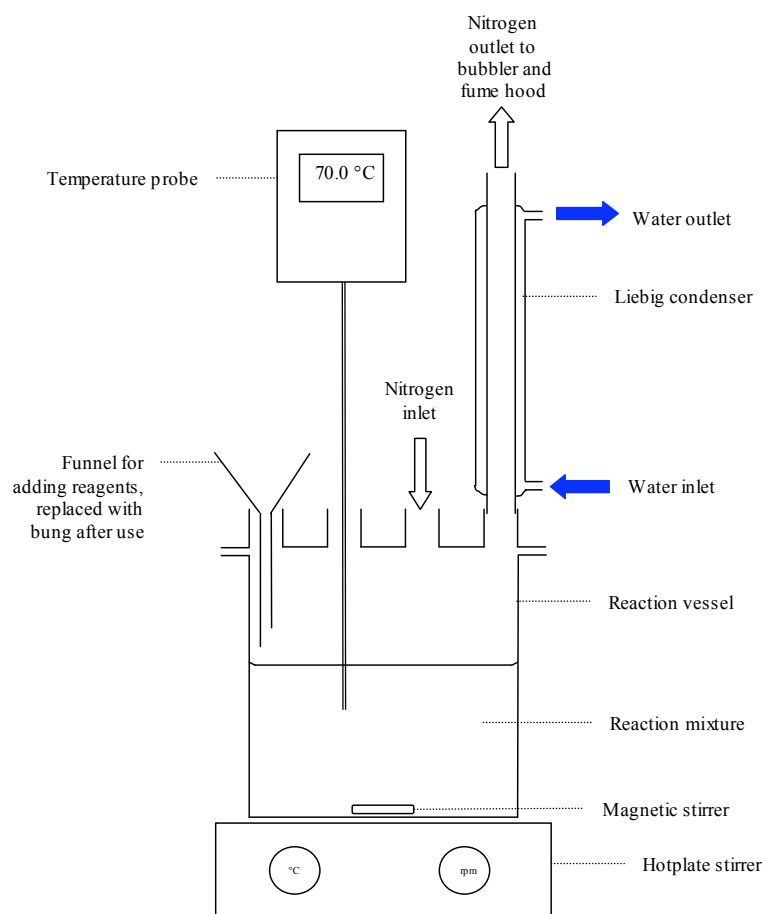
Figure 2.1 SFEP reaction set up for synthesis of poly(NIPAM)-based microgels

To increase the hydrophobic nature of each microgel, a range of hydrophobic co-monomers were incorporated at a concentration of 10 % w/w total monomer (*i.e.* base monomer NIPAM plus co-monomer). The compositions of the microgels are shown in Table 2.4. The microgel dispersions were prepared at a concentration of 0.5 % w/v, *i.e.* the equivalent of 5.0 g monomer/co-monomer in 1 L distilled water. The same cross-linker (*N,N'*-methylenebisacrylamide, MBA) and ionic initiator (potassium persulphate, KPS) were used in each preparation, both at 10 % w/w total monomer.

The homo-polymer poly(NIPAM) microgels are referred to as batches N1–6, whilst the co-polymer microgels are referred to simply by the co-monomer name, *e.g.* DVE. Unless otherwise specified, the monomer composition of the co-polymer microgels was 90 % NIPAM and 10 % co-monomer.

Table 2.4 Composition of microgels

Microgel abbreviation)	Abbreviation	NIPAM (%)	Co-monomer (%)	Initiator[†]
Poly(NIPAM)	N1 and N2	100	–	10 % KPS
Poly(NIPAM-*co*-dodecyl vinyl ether)	DVE	90	10	10 % KPS
Poly(NIPAM-*co*-*tert*-butyl vinyl ether)	TBVE	90	10	10 % KPS
Poly(NIPAM-*co*- *tert*-pentyl vinyl ether)	TPVE	90	10	10 % KPS
Poly(NIPAM-*co*-vinyl decanoate)	VD	90	10	10 % KPS
Poly(NIPAM-*co*-vinyl laurate)	VL	90	10	10 % KPS
Poly(NIPAM-*co*-vinyl stearate)	VS	90	10	10 % KPS
Poly(NIPAM-*co*-vinyl-4-*tert*-butyl benzoate)	V4TBB	90	10	10 % KPS
Poly(NIPAM-*co*-trimethyl(vinyl)silane)	TMVS	90	10	10 % KPS
Poly(NIPAM-*co*-vinyltrimethoxysilane)	VTMOS	90	10	10 % KPS
Poly(NIPAM-*co*-triphenyl(vinyl)silane)	TPVS	90	10	10 % KPS

[†] % w/w total monomer

2.2.2.2 Anionic and cationic poly(NIPAM) microgels with different initiators

In order that the effect of initiator type upon microgel properties could be investigated, homo-polymer poly(NIPAM) microgels were prepared by the SFEP method described in Section 2.2.2.1 using three different initiators at 10 % w/w total monomer:

- potassium persulphate (KPS);
- 4,4′-azobis(4-cyanovaleric acid) (CVA);
- 2,2′-azobis(2-methylpropionamidine) dihydrochloride (MPA).

The structures of the initiators are shown in Table 2.1 and the compositions of the resulting poly(NIPAM) microgels are shown in Table 2.5. The same cross-linker, MBA, was used in each preparation, at 10 % w/w monomer. Preparation of the cationic microgel N6 required that the reaction vessel first be silanized to prevent attraction of the positively-charged cationic particles to the normally negatively-charged glassware. The glassware was therefore wiped then rinsed with silanization solution (Aldrich, 85126-1L), then left to dry in an oven prior to use.

Table 2.5 Composition of poly(NIPAM) microgels with different initiators

Microgel	Abbreviation	NIPAM (%)	Co-monomer (%)	Initiator[†]
Poly(NIPAM)	N4	100	–	10 % KPS
Poly(NIPAM)	N5	100	–	10 % CVA
Poly(NIPAM)	N6	100	–	10 % MPA

[†] % w/w total monomer

2.2.2.3 Poly(NIPAM)-based microgels prepared by modified synthesis method

In addition to the microgels listed in Tables 2.4 and 2.5, two microgels were prepared by a modified SFEP method described by Ngai *et al.* [6] in which the relative proportions of monomer, co-monomer and initiator were altered, and the ratio of solvent to reagents was substantially reduced. The compositions of these microgels are shown in Table 2.6.

Table 2.6 Composition of microgels prepared with variations to SFEP method

Microgel	Abbreviation	NIPAM (%)	Co-monomer (%)	Initiator[†]
Poly(NIPAM)	N3	100	–	1 % KPS
Poly(NIPAM-*co*-methacrylic acid)	MAA	95	5	1 % KPS

[†] % w/w total monomer

In this modified method, just 300 mL of each microgel dispersion was prepared. A total mass of 6.18 g of monomer/co-monomer (6.0 g) and cross-linker (0.18 g) was dissolved in 280 mL deionized water, using mechanical stirring in a sealed reaction vessel under an atmosphere of approximately 1 bar nitrogen. The solution mixture was adjusted to pH 10 using 0.1 M NaOH, then stirred for 40 minutes at 70 °C, again under a nitrogen atmosphere. Finally, the KPS initiator (approximately 1 % w/w total monomer) was dissolved in 20 mL deionized water, which was added to the main solution mixture. The reaction was allowed to proceed for eight hours at 70 °C under continuous nitrogen purge at a stirring rate of 400 rpm.

2.3 Results and discussion

2.3.1 Synthesis of microgels

A range of stable microgel dispersions were produced (Table 2.7) then characterized using a range of techniques, the results of which are given in the following chapters.

Table 2.7 Outcomes of microgel synthesis and co-monomer logP values

Microgel	Novel co-polymer microgel	LogP[†]
N1	No	0.28
N2	No	0.28
N3	No	0.28
N4	No	0.28
N5	No	0.28
N6[*]	No	0.28
DVE	Yes	6.35
TBVE	Yes	1.74
TPVE	Yes	2.27
VD	Yes	4.98
VLi[**]	No	6.04
VLii	No	6.04
VS	Yes	9.23
V4TBB	Yes	3.94
TMVS	Yes	1.58
VTMOS	Yes	1.95
TPVS	Yes	7.02
MAA	No	0.57

[*] The only cationic microgel dispersion; [**] Prepared by Dr Lisa Benée, Dr Hani Nur and Nuntana Srispornsawan; [†] Predicted value of logP of co-monomer (or NIPAM monomer for poly(NIPAM) microgels) obtained from http://www.chemspider.com (see Appendix A).

2.3.1.1 Novel anionic hydrophobically modified microgels

Hydrophobically modified poly(NIPAM)-based microgels have been successfully prepared by various groups. For example, Ma *et al.*[7] prepared a series of poly(NIPAM-*co-iso*propyl methacrylate) microgels (≤ 30 mol% co-monomer), whilst Benée *et al.*[8] prepared poly(NIPAM-*co*-vinyl laurate) (≤ 50 % co-monomer). Lowe *et al.*[9,10] co-polymerized NIPAM with hydrophobic monomers such as methyl methacrylate and fluorinated methacrylates, whilst Nur *et al.* synthesized poly(NIPAM-*co*-butyl acrylate)[11] and poly(NIPAM-*co*-4-vinyl pyridine)[12] microgel particles.

The co-monomers used in this study (except for MAA) were selected for inclusion due to their potential for increasing the hydrophobic nature of the resultant poly(NIPAM)-based microgel particles. The logP values for NIPAM and each of the co-monomers are shown in Table 2.7. LogP values are based upon the partition coefficient, *P*, which is the ratio of the concentrations of a single solute in two immiscible solvents (octanol and water) at equilibrium.[13] They can be used as a guide to the hydrophobicity of a single, small molecule, but not for large, complex

molecules such as microgels which are not soluble. However, they can be used to compare microgel component molecules. For example, compared to the NIPAM monomer, which has a logP value of 0.278, all the co-monomers have larger logP values, which indicates they possess a more hydrophobic nature. This suggests that substituting a proportion of the NIPAM monomer (typically 10 % in this work) with a more hydrophobic co-monomer, then co-polymerizing them by SFEP, should result in microgel particles with a stronger hydrophobic nature than poly(NIPAM) alone.

The co-monomers selected for this work vary by organic chain length and structure. The incorporation of co-monomers with longer chain lengths than NIPAM should result in regions of the microgel polymer network possessing greater hydrophobicity than in the homo-polymer poly(NIPAM) alone. Different structural arrangements of the co-monomers (*e.g.* linear, branched chain or aromatic) and different functional groups (*e.g.* ester or ether) may also result in microgel particles with varying hydrophobicities. The co-monomers used in this study can be broadly categorized as shown in Table 2.2: straight or branched chain ether or ester, or silane or charged. The influence of these characteristics is discussed in later chapters.

The anionic homo-polymer poly(NIPAM) microgels (N1, N2, N3, N4 and N5) and the co-polymer VL and MAA listed in Table 2.7 are not novel particles, their synthesis having been widely reported in literature (previously described). However, the remaining nine dispersions are believed to be novel microgel dispersions as a review of the current literature indicates that none of the co-monomers have been co-polymerized with NIPAM to prepare microgel particles. Table 2.7 indicates which of the microgel dispersions are believed to be novel formulations.

There is, however, for some of the co-monomers, evidence that they have been co-polymerized with alternative base monomers, either to produce linear polymers or spherical nanoparticles. For example, Carmona *et al.*[14] prepared a range of *N*-vinyl carbazole/vinyl p-*tert* butylbenzoate co-polymers, whilst Hosoya *et al.*[15] prepared uniform macroporous polymer beads of divinyl succinate and vinyl p-*tert* butylbenzoate. TPVE co-polymers such as poly(MMA-*co*-TPVS)[16] have been produced, as have vinyl butyl ether (VBE) co-polymers such as poly(VBE-*co*-vinyl ether ethyleneglycol) and poly(VBE-*co*-*N*-vinylpyrrolidone).[17] TMVS has been

used as a cross-linker in poly(2-acrylamido-2-methyl propane sulfonic acid-*co*-acrylic acid) co-polymers,[18] and 3-methacryloxypropyltrimethoxysilane was used to cross-link poly(NIPAM) particles.[19] Reports of co-polymer hydrogels have also been made, *e.g.* NIPAM co-polymerized with silane co-monomers such as 3-methacryloyloxypropyl trimethoxysilane[20,21] or 3-methacryloxypropyltrimethoxy silane.[22]

2.3.1.2 Anionic and cationic poly(NIPAM) microgels with different initiators

Three poly(NIPAM) microgels were prepared by an identical SFEP synthesis method but using three different initiators. This resulted in the preparation of two anionic microgels (N4 and N5) and the use of silanization solution (to pre-treat the glassware) permitted the successful synthesis of a stable cationic poly(NIPAM) dispersion (N6).

2.3.1.3 Poly(NIPAM)-based microgels prepared by altered synthesis method

The method described by Ngai *et al.*[6] was used to prepare stable dispersions of N3, a homo-polymer poly(NIPAM) microgel, and MAA,[i] a co-polymer microgel. Both N3 and MAA were prepared using just 1 % KPS initiator, which was substantially less than the 10 % initiator used in to prepare all the other microgel dispersions. In addition, following the method of Ngai *et al.*, the proportion of reagents to solvent employed in the synthesis was also significantly different: a total of 6.3 g monomer/co-monomer and 0.18 g cross-linker in just 300 mL deionized water. This equated to a theoretical yield of 2.1 % w/v using 3 % w/w cross-linker compared to a yield of 0.5% w/v using 10 % w/w cross-linker in the standard SFEP method.

2.4   Summary

A range of stable hydrophobically modified poly(NIPAM)-based microgels were prepared by co-polymerization of NIPAM with 10 % co-monomer. Several batches of homo-polymer poly(NIPAM) were also prepared, with which the co-polymer microgels could be compared. Within the poly(NIPAM) batches, the initiator type and solvent:reagent ratio was varied, so that the influence of synthesis conditions

---

[i] Composition of MAA = 95 % NIPAM and 5 % MAA

could be investigated. Finally a hydrophilic microgel, MAA, was prepared for further comparison. These microgels are the subject of characterization and investigation of interfacial behaviour in the following chapters.

2.5   References

[1] Goodwin, J. W., Hearn, J., Ho, C. C., Ottewill, R. H. (1973) *British Polymer Journal*, **5**(5), 347–362.

[2] Pelton, R. H. and Chibante, P. (1986) *Colloids and Surfaces*, **20**(3), 247–256.

[3] Diaz, J. E., Barrero, A., Marquez, M., Fernandez-Nieves, A., Loscertales, I. G. (2010) *Macromolecular Rapid Communications*, **31**, 183–189.

[4] Wilkinson, M. C., Hearn, J., Steward, P. A. (1999) *Advances in Colloid and Interface Science*, **81**, 77–165.

[5] Woodward, N. C., Chowdhry, B. Z., Leharne, S. A., Snowden, M. J. (2000) *European Polymer Journal*, **36**, 1355–1364.

[6] Ngai T., Auweter H., Behrens S. H. (2006) *Macromolecules*, **39**, 8171–8177.

[7] Ma, X., Xi, J., Huang, X., Zhao, X. and Tang, X. (2004) *Materials Letters*, **58**, 3400–3404.

[8] Benée, L.S., Snowden, M.J., Chowdhry, B.Z. (2002) *Langmuir*, **18**, 6025–6030.

[9] Lowe, T. L., Virtanen, J., Tenhu, H. (1999) *Langmuir*, **15**(12), 4259–4265.

[10] Lowe, T. L., Benhaddou, M., Tenhu, H. (1999) *Macromolecular Chemistry and Physics*, **200**(1), 51–57.

[11] Nur, H., Cornelius, V.J., Benée, L.S., Mitchell, J.C., Day, I.J., Snowden, M.J. (2009) *Analyst*, **134**, 1366–1372.

[12] Nur, H., Pinkrah, V.T., Mitchell, J.C., Benée, L.S., Snowden, M.J. (2010) *Advances in Colloid and Interface Science*, **158**, 15–20.

[13] Ubarov, E. B., Isaacs, A. (1986) *The Penguin Dictionary of Science*. London: Penguin Books.

[14] Carmona, T., Fernandez-Pena, N., Pilar Tarazona, M., Saiz, E., Mendicuti, F. (2010) *European Polymer Journal*, **46**(8), 1796–1809.

[15] Hosoya, K., Kageyama, Y., Kimata, K., Araki, T., Tanaka, N., Frechet, J. M. (1996) *Journal of Polymer Science Part A – Polymer Chemistry*, **34**(13), 2767–2774.

[16] Naghash, H. J. (2010) *Journal of Applied Polymer Science*, **116**(4), 2465–2472.

[17] Zhunuspayev, D. E., Mun, G. A., Dubolazov, A. V., Nurkeeva, Z. S., Guven, O. (2007) *Nuclear Instruments and Methods in Physics Research Section B – Beam Interactions with Materials and Atoms*, **265**(1), 76–81.

[18] Atta, A. M., Gaser, A. A., Kamel, Z. F. (2010) *Journal of Dispersion Science and Technology*, **31**(11), 1456–1464.

[19] Zhang, J. T., Liu, X.-L., Fahr, A., Jandt, K. D. (2008) *Colloid and Polymer Science*, **286**, 1209–1213.

[20] Lee, W. F., Yuan, W. F. (2002) *Journal of Applied Polymer Science*, **84**(13), 2523–2532.

[21] Kurihara, S., Minagoshi, A., Nonaka, T. (1996) *Journal of Applied Polymer Science*, **62**(1), 153–159.

[22] Zhang, X. Z., Zhuo, R. X. (1999) *Colloid and Polymer Science*, **277**(11), 1079–1082.

CHARACTERIZATION OF POLY(NIPAM)-BASED MICROGELS

3.1 Introduction

The objectives of this section were first to measure the basic physico-chemical properties of the hydrophobically modified microgels prepared in Chapter 2, then to investigate whether the nature of the co-monomer has any influence upon these characteristics and, if so, to determine whether microgel physico-chemical properties could be predicted from co-monomer characteristics. The physico-chemical information would then be used to support the investigation of the hydrophobic modification upon the interfacial properties and overall behaviour of the particles.

As identified in Chapter 2, a number of the hydrophobically modified dispersions are novel preparations and therefore determining their basic physico-chemical properties was particularly important. This enabled comparison both with the unmodified poly(NIPAM) microgels synthesized in this study and with those reported in the existing literature, which in turn aided an investigation of the effect of hydrophobic modification upon microgel properties and behaviour.

3.2 Materials and methods

The physico-chemical properties of the homo-polymer and hydrophobically modified co-polymer microgels prepared in Chapter 2 were characterized using a range of techniques. The following sections describe the methods used to determine characteristics such as particle size, turbidity and electrophoretic mobility.

3.2.1 Materials

Details of the compositions of the microgels studied are given in Chapter 2 (see Tables 2.1–2.5). However, the three-dimensional structures of the co-monomers and their functional group categories are summarized in Fig. 3.1.

a) Monomer
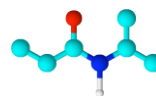
*N-iso*propylacrylamide

b) vinyl ether co-monomers
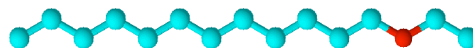
dodecyl vinyl ether
(DVE)
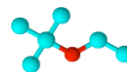
tert-butyl vinyl ether
(TBVE)
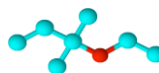
tert-pentyl vinyl ether
(TPVE)

c) vinyl ester co-monomers
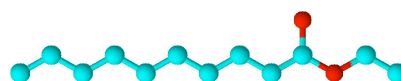
vinyl decanoate
(VD)
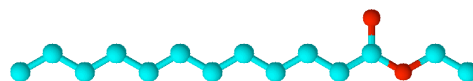
vinyl laurate
(VL)
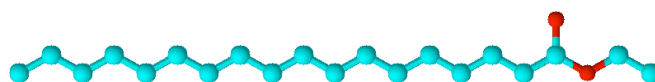
vinyl stearate
(VS)
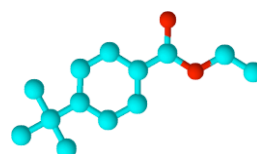
vinyl-4-*tert*-butyl
benzoate
(V4TBB)

d) vinyl silane co-monomers
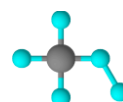
trimethyl(vinyl)silane
(TMVS)
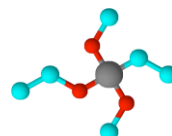
vinyltrimethoxysilane
(VTMOS)
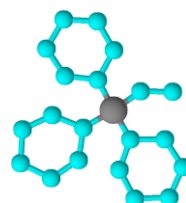
triphenyl(vinyl)silane
(TPVS)

e) polyelectrolyte co-monomers
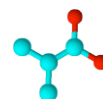
methacrylic acid
(MAA)

Figure 3.1 Monomer and co-monomer 3D structures

3.2.2 Dry weight analysis

The percentage solids content (% w/v) and percentage yield of each dispersion were determined using dry weight analysis, which requires measurement of both the dispersion mass and its solid residue after drying. Three 5 mL samples of each microgel were weighed, then placed in a Lite Scientific Raven Oven at 105 °C until all the water was judged by eye to have evaporated. The samples were removed from the oven, allowed to cool to room temperature and weighed, then returned to the oven. The process was repeated daily until three consistent masses were obtained.

The mean percentage solids for each dispersion was calculated using:

$$\% \; solids \; content \; in \; 5 \; mL = \frac{dry \; mass \; dispersion}{wet \; mass \; dispersion} \times 100$$

[Equation 3.1]

The mean percentage yield for each dispersion was calculated using:

$$\% \; yield = \frac{dry \; mass \; dispersion}{total \; reagent \; mass} \times 100$$

[Equation 3.2]

3.2.3 Particle size

A Malvern Zetasizer Nano ZS (Zetasizer) equipped with a 4 mW He-Ne laser with a fixed wavelength of 633 nm was used to measure the particle size (hydrodynamic diameter, D_H) of each microgel dispersion over a range of temperatures by dynamic light scattering (DLS). Scattered light at an angle of 173° (*i.e.* back scatter) was detected and used to determine particle D_H.

A glass cuvette was filled with 1.25 mL of microgel dispersion, which had previously been diluted 1:4 with distilled water. This ensured that the change of turbidity associated with the volume phase transition of the particles was not too great above the volume phase transition temperature (VPTT) to prevent successful measurements being made. D_H measurements were taken over a range of temperatures

encompassing the VPTT, typically from 5–60 °C. After an initial 30 minute equilibration period, five measurements were taken at 5 °C intervals over this range, with a 10 minute equilibration period prior to measurements at each interval. Measurements were taken during heating and cooling cycles.

The reliability of each measurement obtained was assessed using values such as the polydispersity index (PdI) and intensity particle size distribution (PSD). Any measurements of insufficient quality (*e.g.* PdI greater than around 0.2 or multimodal PSD) were excluded. Having determined which values were reliable, average D_H and PdI values were calculated at each temperature.

3.2.4 Turbidity

A dual-beam Cary 100 UV-visible spectrophotometer was used to measure the variation in turbidity of the microgel dispersions over a wide temperature range at a wavelength of 547 nm. The samples were diluted with filtered distilled water in a 1:4 ratio to ensure an absorbance of less than 2. For dispersions with solids content of around 0.5 % w/v, this dilution resulted in samples of approximately 0.1 % w/v. Dispersions of higher stock % w/v (*e.g.* N3 and MAA) were therefore diluted further to ensure the samples were also approximately 0.1 % w/v. Next, 3 mL aliquots were transferred to a quartz cell for measurement.

Each sample was blanked against itself then absorbance measurements were taken at 0.1 °C intervals from 5–60 °C, with the heating and cooling ramps set at a rate of 0.5 °C/minute. The samples were blanked against themselves so that the relative change in absorbance could be monitored as a function of temperature. The absorbance measurements were used to determine the VPTT for each microgel using the first derivative of the transmittance.

3.2.5 Electrophoretic mobility

The Zetasizer Nano ZS described in Section 3.2.3 was used to measure the electrophoretic mobility of each microgel dispersion using laser Doppler velocimetry. The same temperature range was employed but this time scattering was detected at an angle of 17° (*i.e.* forward scatter). A syringe was used to fill a folded capillary cell

(DTS1060C) with approximately 0.75 mL of microgel dispersion that had been diluted 1:4 with 0.1 mM NaCl in order to minimize the influence of the electrical double layer upon the mobility measurements.

After an initial 30 minute period for equilibration to temperature, an average of at least three measurements were taken at 5 °C intervals during heating and cooling runs, typically from 5–60 °C, with a 10 minute equilibration pause prior to measurement at each temperature interval. The Smoluchowski approximation and general purpose model were selected for result calculations (Section 1.2.3.4).[1]

The reliability of each measurement was assessed using information such as the phase plot and any measurements of insufficient quality (*e.g.* a poor quality phase plot) were excluded. The phase plot displays the difference between the phase of the light scattered by the particles and the phase of the reference beam as a function of time; the characteristics of good and poor quality phase plots are illustrated in Fig. 3.2. [2,3] The noisier the plot, the poorer the quality of the data. Reliable measurements were then used to calculate average values and standard deviations at each temperature.
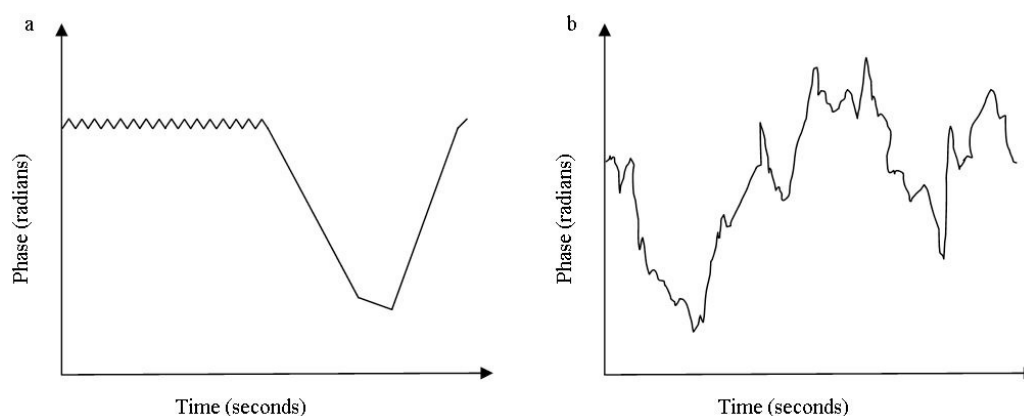
Figure 3.2 Illustration of a good (a) and poor (b) quality phase plot, adapted from Ref. [2]

3.2.6 Scanning electron microscopy

A Cambridge Stereoscan S-360 scanning electron microscope (SEM) was used to study the size and polydispersity of selected microgel dispersions. Samples were prepared by diluting each dispersion with distilled water (typically in a 1:10 ratio), a

tiny drop of which was placed on the centre of a glass cover slip and left to air dry into a thin film. This was necessary as samples must be dehydrated for SEM analysis due to the vacuum employed in the sample chamber. However, this means the microgels adopt a shrunken conformation due to the loss of water, which must be taken into account when comparing SEM size results with those obtained from techniques such as DLS. The samples were sputter coated with gold prior to obtaining SEM images and particle diameter measurements with the SEM.

3.3   Results and discussion

This section begins with the dry weight analysis results and discussion for all dispersions. It is followed by a presentation of the results and a discussion of the size, electrophoretic mobility and VPTT results for the six different poly(NIPAM) dispersions prepared in this study. Finally, the results for the hydrophobically modified microgels are presented and discussed with a view to establishing the relative effects of hydrophobic modification of poly(NIPAM) microgel particles.

Although, as made clear in Chapter 1, the physico-chemical properties of homo-polymer poly(NIPAM) microgels have been extensively reported in literature, it was necessary to characterize the specific poly(NIPAM) dispersions synthesized in this study for a number of reasons:

- to verify the microgels had properties and behaviours comparable to literature;
- to provide a baseline with which to compare the modified microgels;
- to check the influence of synthesis conditions upon the particle properties;
- to select a dispersion with which to compare the modified microgels;
- to consider how dispersion polydispersity and particle size distribution vary through the volume phase transition; and
- to provide supporting information for further investigations (Chapters 4–6).

As set out in Chapter 2, the poly(NIPAM) microgels are referred to as batches N1–6, whilst the co-polymer microgels are referred to simply by the co-monomer name, *e.g.* DVE. Unless otherwise specified, the monomer composition of the co-polymer

microgels was 90 % NIPAM and 10 % co-monomer. A summary of the poly(NIPAM) batches is given in Table 3.1.

Table 3.1 Summary of initiators used in poly(NIPAM) batches

Initiator	Batch
KPS	N1, N2, N3[†], N4
CVA	N5
MPA	N6

[†] Prepared by alternative synthesis method with different ratio of reagents:solvent (Section 2.2.2.3)

3.3.1 Dry weight analysis

The dispersion percentage solids content (% w/v) and percentage yield are shown in Table 3.2. Microgel dispersion concentrations are typically reported in terms of % w/v, where 1 L of microgel dispersion prepared from 5 g NIPAM, plus 10 % cross-linker (0.5 g) and 10 % initiator (0.5 g) would have a theoretical concentration of 0.5 % w/v, *i.e.* 5 g NIPAM monomer in 1 L solvent. However, if the masses of initiator and cross-linker are also taken into account, the total reagent mass of 6 g in 1 L could result in a maximum dispersion concentration of 0.6 % w/v. The values in Table 3.2 take into account the mass of the initiator and cross-linker, as well as the monomer/co-monomer.

The mean percentage solids content (% w/v) of the microgels prepared by the standard SFEP method (with a total reagent mass of 6 g in 1 L solvent) ranged from 0.47–0.64 % w/v. The expected maximum value of 0.6 % w/v was exceeded for only two microgels: VTMOS (0.61 $\pm$ 0.01 % w/v) and TPVS (0.64 $\pm$ 0.01 % w/v). The percentage yields for all the microgels are therefore high, with the majority greater than 90 %.

Several of the calculated yields exceeded 100 %. This may be explained by a number of factors, the most likely of which is that the samples were not fully dehydrated in the oven prior to measurement of the dry masses. It has been shown that freeze-dried microgels can never be fully dehydrated[4] and therefore it is possible that some water remains in the "dried" particles, resulting in a higher than predicted dry mass. Several repeat measurements were made in order to investigate whether measurements within the expected range could be obtained. Even longer drying

periods may help resolve the issue but further work is required to clarify this, such as thermogravimetric analysis.

Table 3.2 Dispersion percentage solids content and percentage yield

Microgel	Mean solids content (% w/v ± 1 s.d.)	Mean % yield (± 1 s.d.)
poly(NIPAM)		
N2	0.58 ± 0.01	98.8 ± 2.1
N3[*]	2.30 ± 0.01	106.5 ± 0.6
N4	0.60 ± 0.01	100.8 ± 1.5
N5	0.55 ± 0.01	92.2 ± 1.8
N6	0.53 ± 0.01	90.0 ± 1.8
vinyl ethers		
DVE	0.47 ± 0.01	79.6 ± 1.7
TBVE	0.58 ± 0.01	99.1 ± 1.3
TPVE	0.55 ± 0.01	94.1 ± 1.9
vinyl esters		
VD	0.55 ± 0.01	93.6 ± 1.1
VL	0.51 ± 0.01	86.0 ± 2.3
V4TBB	0.53 ± 0.02	89.3 ± 2.4
vinyl silanes		
TMVS	0.60 ± 0.01	104.8 ± 2.3
VTMOS	0.61 ± 0.01	104.0 ± 0.9
TPVS	0.64 ± 0.01	107.0 ± 2.1
polyelectrolyte		
MAA[*†]	1.38 ± 0.01	64.6 ± 0.8

[*] Alternative SFEP method used, with higher mass of reagents and therefore far greater theoretical maximum percentage solids content of greater than 2 % w/v ; [†] MAA composition = 95 % NIPAM and 5% MAA.

A similar situation arose with the two microgels prepared by the modified SFEP method (N3 and MAA). In the synthesis of these two dispersions, the total reagent mass was greater than 6.18 g but the total volume of solvent used was only 300 mL, giving a theoretical maximum percentage solids concentration of around 2.06 %. The yield of MAA (64.6 ± 0.8 %) resulted in a dispersion concentration of 1.38 ± 0.01 % w/v, well within the expected range, but the N3 yield (106.5 ± 0.6 %) resulted in a dispersion concentration outside the expected range (2.30 ± 0.01 % w/v). The N3 values could be explained by the same factors as discussed above for the standard SFEP microgels.

The fact that the modified SFEP preparation of MAA resulted in a far lower percentage yield than the standard SFEP microgel yields may be a result of the

ten-fold smaller quantity of initiator employed. With only 1 % initiator (instead of 10 %) used to prepare MAA, far fewer nucleation sites would be created during the polymerization process. In addition, the ratio of reagent to solvent volume was far greater in the modified SFEP method, which, combined with the smaller number of nucleation sites, may account for the lower yield. Any un-reacted reagents should have been removed by dialysis and therefore would not comprise part of the final dry mass measured.

3.3.2 Characterization of homo-polymer poly(NIPAM) microgels

The results and discussion in this section concern only the poly(NIPAM) dispersions (N1–6) (see Table 3.1). The co-polymer microgels are discussed in Section 3.3.3.

3.3.2.1 Particle size in water

Particle size in terms of the hydrodynamic diameter, D_H, is a key physico-chemical property commonly reported for microgels. Figure 3.3 shows the D_H of N4 particles upon heating and cooling (5–60 °C). It shows that the particles undergo a reversible volume phase transition (VPT) at around 35 °C, which is similar to the VPTT values for poly(NIPAM) stated in the literature[5] and the VPTT values calculated from turbidity measurements in this study (Table 3.4). The D_H of N4 ranged from roughly 540 nm at low temperatures, through a period of a rapid decrease in size at around 35 °C, to roughly 250 nm at higher temperatures.

Below the VPTT, the particles are swollen, with a substantial amount of solvent occupying the interstitial spaces between the polymer chains. Stability of the swollen particles results from hydrogen bonding between the solvent molecules and polymer chains, combined with low attractive van der Waals forces between the particles. As the temperature approaches the VPTT, the hydrogen bonding between polymer and solvent is disrupted and the chains collapse as polymer-polymer hydrophobic interactions begin to dominate over the polymer-solvent interactions. Stability of the particles in dispersion is aided by the presence of solvated polymer chains extending into solution, which provide steric stabilization.[6,7]

Above the VPTT, a large proportion of the solvent previously entrapped in the particles is excluded from the now collapsed interstitial spaces and the microgels adopt harder sphere-like structures. Despite the fact there is no longer any steric stabilization,[8,9] the dispersion remains stable due to increased electrostatic repulsion between the particles, which results from the greater charge density at the surface of the collapsed particles. The VPT is reversible on cooling; the polymer-solvent hydrogen bonding increases once more, polymer-polymer hydrophobic interactions are disrupted and the particles return to their original swollen conformation due to ingress of solvent.
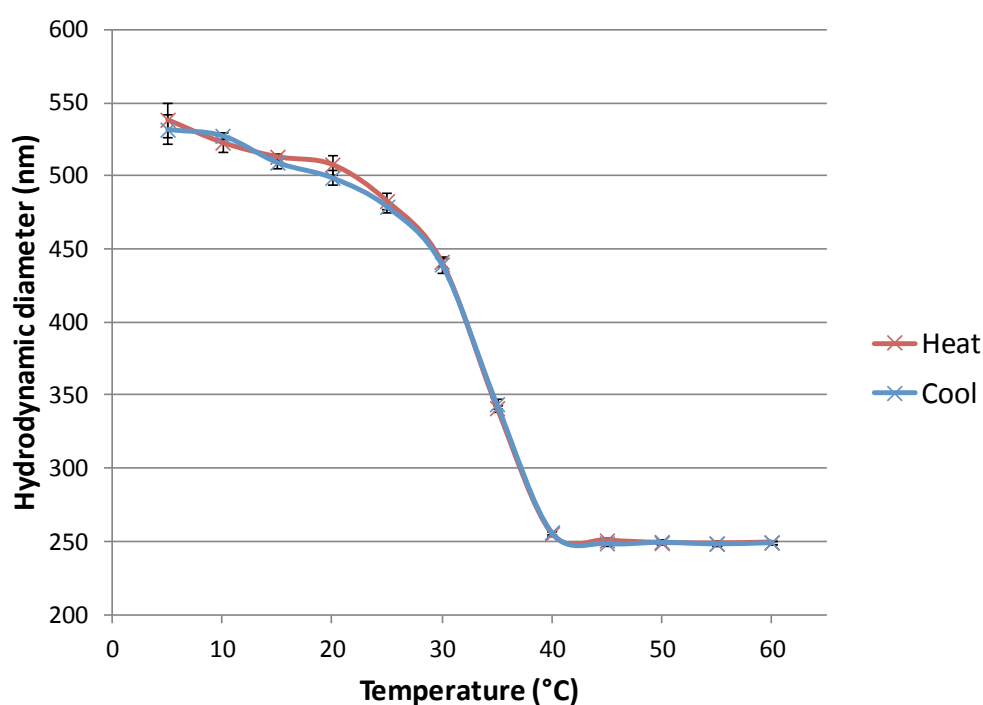
Figure 3.3 D_H **of N4 particles as a function of temperature (5 °C intervals) (± 1 s.d.)**

There is very good agreement between the heating and cooling curves in Fig. 3.3, which show only very slight hysteresis and confirm the reversible nature of the VPT. The error bars suggest that there is no substantial difference between the two curves. Hysteresis, *i.e.* the slower re-swelling observed upon cooling, may be attributed to differences in the rate of equilibration to temperature between the heating and cooling runs. Hysteresis can be minimized by using slow heating/cooling rates and allowing sufficient equilibration time at each temperature before making measurements.

Similarly-shaped curves were obtained for all the other poly(NIPAM) microgels (data not shown) but with variations in the overall swollen and collapsed particle sizes. The D_H measurements of all the poly(NIPAM) microgels are summarized in Table 3.3 and Fig. 3.4. The results confirm that, like N4, all the poly(NIPAM) microgels undergo a reversible volume phase transition: at lower temperatures (5 and 25 °C), below the VPTT of poly(NIPAM), the particles adopted a swollen conformation, with only relatively small reductions in particle size occurring from 5-25 °C.

Table 3.3 Poly(NIPAM) particle sizes and polydispersity index values

Microgel	5 °C		25 °C		50 °C	
(initiator)	D_H (nm)	PdI	D_H (nm)	PdI	D_H (nm)	PdI
N1 (KPS)	–	–	579 ± 5	–	318 ± 2	–
N2 (KPS)	532 ± 12	0.09 ± 0.05	466 ± 6	0.03 ± 0.02	263 ± 3	0.06 ± 0.02
N3 (KPS)[†]	721 ± 22	0.06 ± 0.03	625 ± 6	0.03 ± 0.03	310 ± 1	0.02 ± 0.01
N4 (KPS)	539 ± 12	0.05 ± 0.03	483 ± 6	0.03 ± 0.03	249 ± 1	0.01 ± 0.01
N5 (CVA)	458 ± 6	0.04 ± 0.02	378 ± 3	0.14 ± 0.02	224 ± 1	0.01 ± 0.01
N6 (MPA)	459 ± 6	0.12 ± 0.03	410 ± 5	0.08 ± 0.02	218 ± 1	0.06 ± 0.00

– Indicates data not available; [†] Indicates particles prepared by modified synthesis method (Section 2.2.2.3).
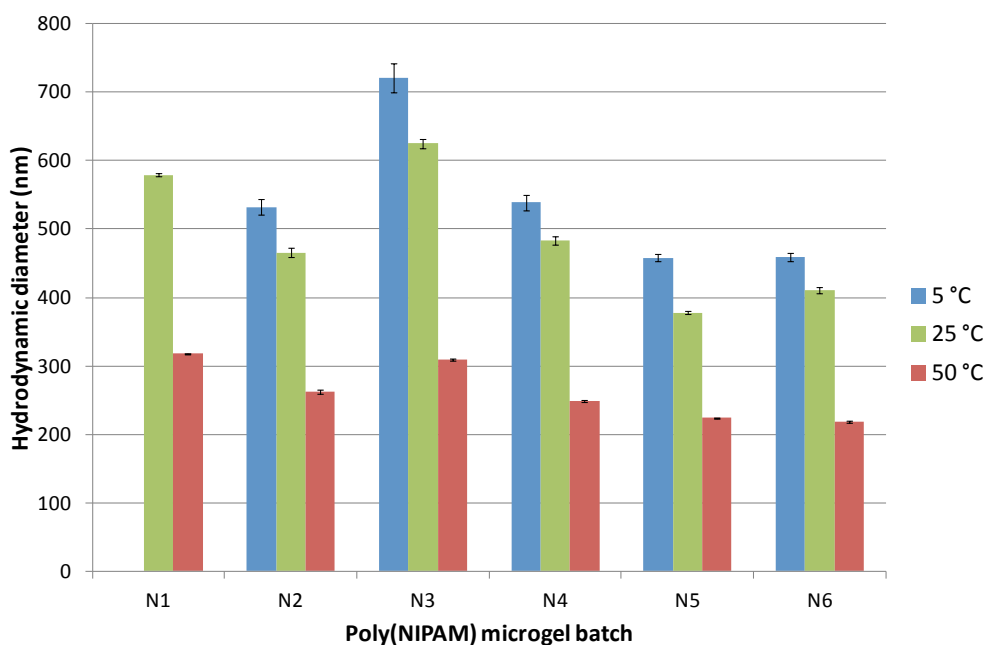
Figure 3.4 D_H of N1–6 microgel particles in water at 5, 25 and 50 °C (± 1 s.d.)

At 50 °C, above the VPTT, the particles collapsed to substantially smaller particle sizes. The data also confirmed that a wide range of poly(NIPAM) particle sizes can

be readily achieved using the same basic reagents but in different quantities, with different initiators and different synthesis methods.

Batches N1, N2 and N4 were prepared by the same method with the same composition, but the particle size varied by up to 113 nm (25 °C) and 69 nm (50 °C). These differences may have resulted from slight variations in synthesis conditions, *e.g.* stirring rate. However, the synthesis conditions for N4, N5 and N6 were identical and yet there was still variation in particle size, particularly at 5 and 25 °C. This may result from the different initiators employed as all other variables were held constant.

There was variation in D_H between all batches, particularly below the VPTT, but the N3 particles were clearly larger than all the other poly(NIPAM) microgels below the VPTT. These were prepared by the modified synthesis method, with a much higher monomer concentration (approximately 2 % w/v) and far less initiator (1 % mass of monomer), which may be the cause of the variation in D_H.

A wide range of poly(NIPAM) particle sizes have been reported in literature. A useful summary is given in Saunders and Vincent.[10] For example, the sizes of the poly(NIPAM) lattices first reported by Pelton and Chibante ranged from 0.5-1.0 µm by transmission electron microscopy (TEM) for the dehydrated (and therefore collapsed) particles.[11] In contrast, Kiminta and Luckham[12] reported poly(NIPAM) particle sizes measured by photon correlation spectroscopy (PCS) ranging from 470 nm at 25 °C to 50 nm at 65 °C. The N1–6 measurements in Fig. 3.4 and Table 3.3 fall within reported ranges.[10]

Differences between sizes described in literature may be attributed to factors such as variations in the composition of the mixtures of monomer/cross-linker/initiator or the synthesis conditions employed in each case. In this study, N4 was selected as the standard poly(NIPAM) dispersion with which the modified co-polymer microgels were later compared because it most closely matched the average size of all the poly(NIPAM) batches prepared.

In this work, D_H was measured at 5 °C intervals from 5–60 °C. However, to check whether measurements at smaller intervals would deviate from the overall trend, the

D_H of N4 was measured at 1 °C intervals and compared with the 5 °C interval data (Fig. 3.5). There was very little difference although the 1 °C measurements reveal that the VPT is sharper than is suggested by the 5 °C measurements. However, 5 °C intervals were considered sufficient to obtain good details of the overall trends.
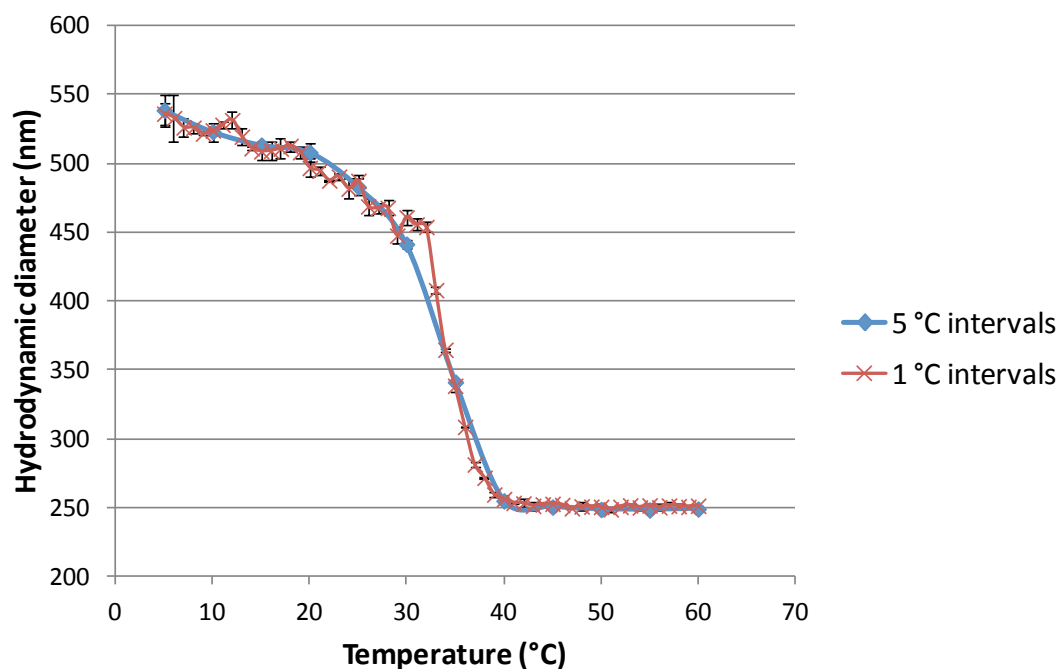
Figure 3.5 N4 particle D_H as a function of temperature, measured at 1 and 5 °C intervals (± 1 s.d.)

The polydispersity index (PdI) is a dimensionless estimate of the width of the particle size distribution, ranging from 0–1, which gives an indication of the extent to which the particles in a dispersion are of uniform size.[13] Values close to zero indicate that the sample is monodisperse, whilst larger values indicate that the sample is increasingly polydisperse, *i.e.* multiple particle sizes have been detected (Section 1.3.1). Table 3.3 shows that all but two of the PdI measurements for all poly(NIPAM) batches at 5, 25 and 50 °C were less than 0.08; according to the definitions given in Section 1.3.1, this indicates the particles were nearly monodisperse. The two exceptions were only slightly larger.

Figure 3.6 shows PdI changes as a function of temperature for N4. As expected, the greatest PdI values were observed during the VPT, as the particles begin to collapse. Below the VPTT the PdI values of the swollen particles are smaller but still fairly

varied. Above the VPTT, the particles showed far more uniform PdI values and less variation.
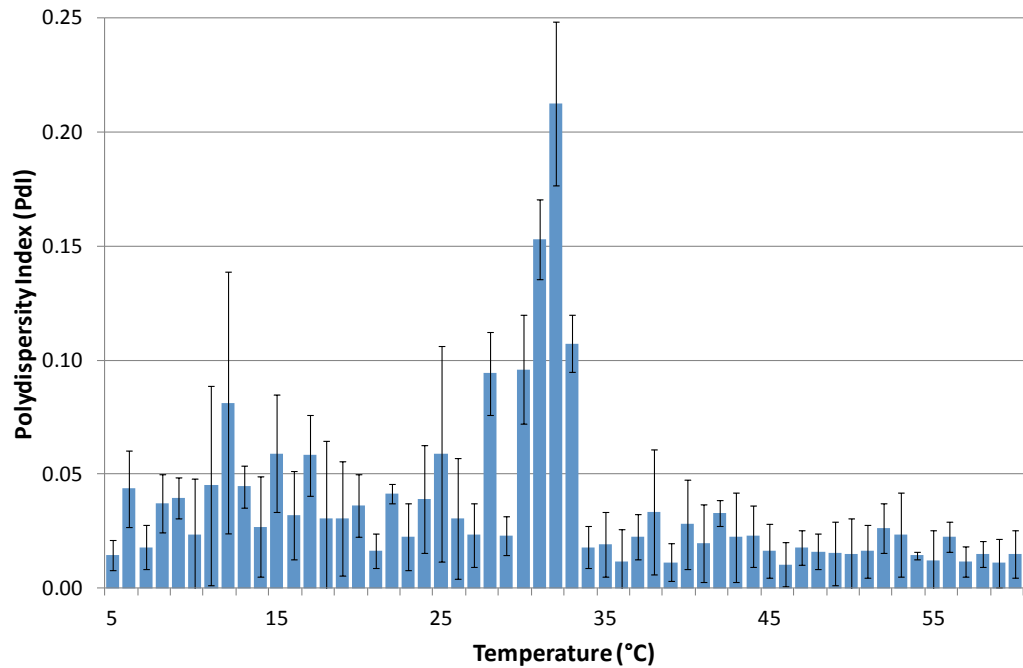
Figure 3.6 Variation in PdI of of N4 particle D_H measurements as a function of temperature (± 1 s.d.)
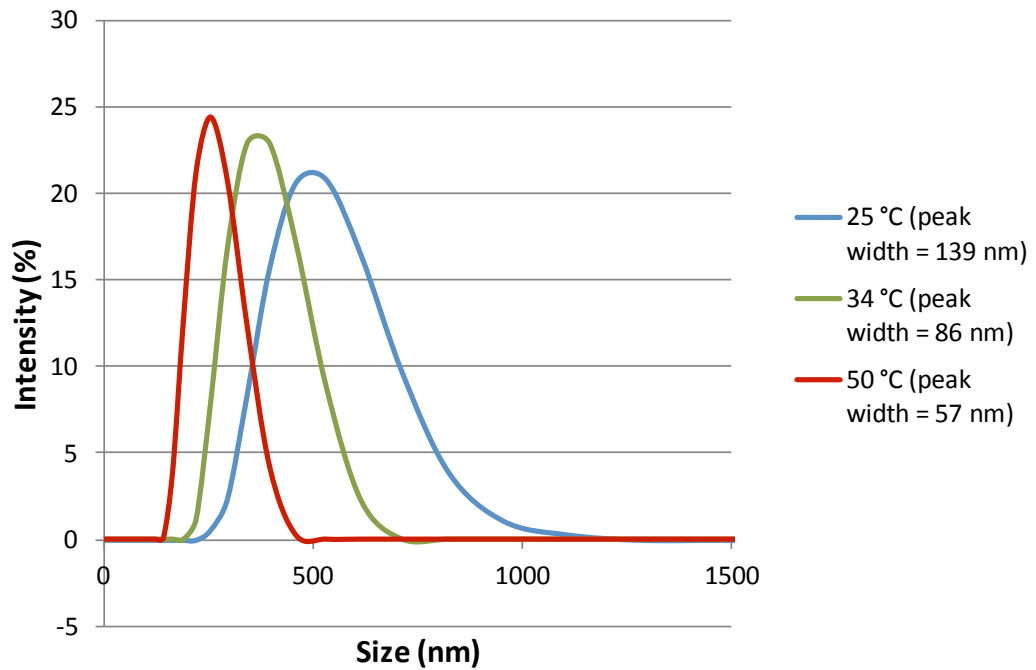
Figure 3.7 N4 intensity particle size distribution data at 25, 34 and 50 °C

99

Further information about the particles can be obtained from the particle size distribution. Figure 3.7 shows the intensity size distribution for N4 at 25, 34 and 50 °C, *i.e.* across the VPT. At each temperature the distribution has just one peak, indicating the dispersion is monodisperse. As the temperature increases, the peak size and width decreases, which correlates with both the D_H (Fig. 3.5) and PdI data (Fig. 3.6). At temperatures below and around the VPTT, there is greater variation in particle size and PdI than above the VPTT, when the collapsed particles are more uniform. The presence of more than one peak in any size distribution would be indicative of a polydisperse sample or the occurrence of flocculation. The data showed that the N1–N6 particles had, as anticipated from literature, reasonable PdI values, *i.e.* were fairly monodisperse.

3.3.2.2 Volume phase transition temperature

The variation in absorbance of visible light (wavelength 547 nm) by the poly(NIPAM) microgels was measured as a function of temperature (typically from 5–60 °C) and plotted as percent transmittance, showing the change in dispersion turbidity with increasing temperature. The first derivative of transmittance was used to calculate the VPTT for each microgel. Figure 3.8 shows a fall in percent transmittance of N4 as the temperature increased, with a period of rapid decrease from 30–35 °C.

The data confirms that at low temperatures the particles were swollen, meaning that the difference in refractive index (RI) between the particle and the solvent is small. A large proportion of the light is therefore transmitted through the slightly turbid dispersion. At higher temperatures the particles collapse and the particle RI becomes greater than that of the solvent. Here, more light is scattered by the smaller, harder particles and therefore less light is transmitted through the now very turbid sample.

A small degree of hysteresis was observed between the heating and cooling curves for N4, particularly during the VPT, but there was generally good agreement between the two. The slight hysteresis in the percent transmittance increase for the cooling curve (*i.e.* as the temperature fell from 60–5 °C), which is a function of the heating/cooling rate and sample equilibration time, can be minimized as with the particle size

measurements (Fig. 3.3) by using slower heating/cooling rates and allowing sufficient equilibration time at each temperature before making measurements.
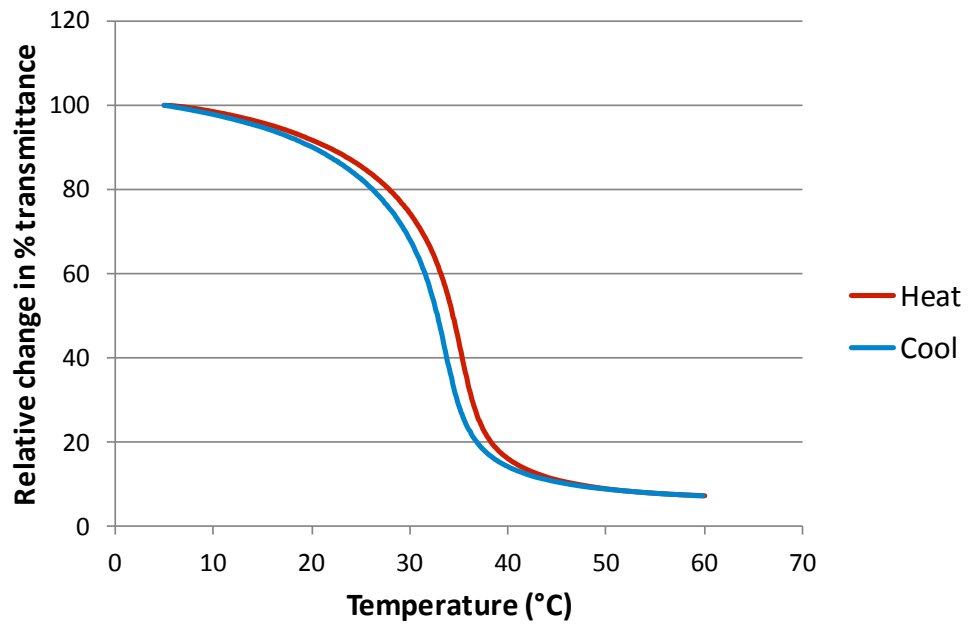
Figure 3.8 Relative change in percentage transmittance of N4 dispersion on heating/cooling from 5–60 °C
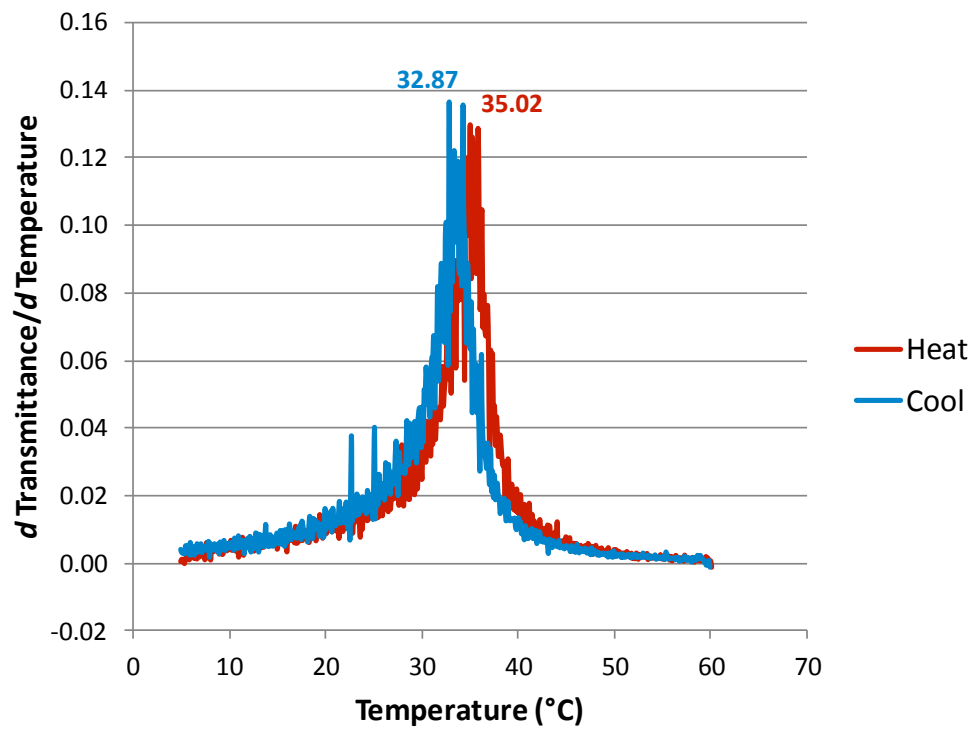
Figure 3.9 First derivative plot of transmittance of N4 dispersion as a function of temperature

Figure 3.9 shows the first derivative plot of transmittance for the N4 dispersion, which was used to determine the temperature at which the change in transmittance was most rapid, which corresponds to the VPTT. The heating and cooling curves showed that the average VPTT was around 34 °C for N4, in good agreement with values in literature.[5,14]

The first derivative plots of transmittance produced slightly different VPTT values for N4: 35 °C on heating and 33 °C on cooling, or 34 °C on average. The lower cooling value is likely to be due to hysteresis as explained above. Variations of plus or minus a few degrees in the precipitation temperature of linear poly(NIPAM) that depend upon the particular conditions have been reported.[15] The VPTT values of N1–6 are detailed in Table 3.4. The data indicate that initiator type and synthesis method (different for N3) do not influence the VPTT of poly(NIPAM) particles with 10 % MBA cross-linker.

Table 3.4 VPTT of poly(NIPAM) dispersions obtained from first derivatives of transmittance measurements

Microgel	Initiator	VPTT (°C)[*]
N1	KPS	34
N2	KPS	34
N3	KPS	34
N4	KPS	34
N5	CVA	34[†]
N6	MPA	34

[*] Average of heat and cool curve values
[†] Cool curve VPTT value only

3.3.2.3 Electrophoretic mobility

The electrophoretic mobility of a selection of poly(NIPAM) microgels was measured as a function of temperature and the results at 5, 25 and 50 °C are summarized in Table 3.5. It is clear that the magnitude of the electrophoretic mobility (charge density) increases with temperature, with a particularly large increase following the VPT. This indicates, as expected, that as the particle structure collapses through the VPT, the surface charge density of the particles increases. The values compare well with literature, *e.g.* Daly *et al.*[16] reported values of 0.20 x 10^{-8} m^2 V^{-1} s^{-1} at 25 °C and 4.05 x 10^{-8} m^2 V^{-1} s^{-1} for poly(NIPAM).

Table 3.5 also highlights the influence of initiator type upon microgel surface charge. The three microgels prepared using anionic initiators (N3, N4 and N5) carry negative charges, whilst the microgel prepared with a cationic initiator (N6) carries a positive surface charge. Furthermore, the nature of the initiator appeared to influence surface charge, with use of the CVA initiator (N5) resulting in electrophoretic mobility values of greater magnitude than the KPS initiator (N4) at 5 and 25 °C. As both microgels were prepared by otherwise identical methods, the difference in electrophoretic mobility is likely to be due the initiator type used. Further discussion of the influence of initiator type is made in Chapter 6.

Table 3.5 Electrophoretic mobility of microgel particles at 5, 25 and 50 °C

Microgel	Initiator	EM (10^{-8}m^{2}s^{-1}V^{-1} ± 1 s.d.)		
		5 °C	25 °C	50 °C
N3	KPS	-0.18 ± 0.01	-0.32 ± 0.00	-3.94 ± 0.02
N4	KPS	-0.66 ± 0.01	-1.11 ± 0.02	- 4.05[†]
N5	CVA	-0.91 ± 0.01	-1.43 ± 0.03	-3.99 ± 0.04
N6	MPA	+0.39 ± 0.01	+0.62 ± 0.02	+3.75 ± 0.09

[†] Only one record was sufficiently reliable, so no s.d. was calculated for this data point.

The N3 and N4 microgels were both prepared using KPS initiator, but by different synthesis methods (Section 2.2.2). The difference in magnitude of surface charges at all temperatures suggests that the synthesis method (and solvent:reagent ratio) also influence electrophoretic mobility of the particles.

3.3.3 Characterization of hydrophobically modified co-polymer microgels

The results and discussion in this section relate to the co-polymer microgels, all of which are composed of 90 % NIPAM and 10 % co-monomer, unless otherwise specified. Results for the homo-polymer microgel N4 are included for comparison.

3.3.3.1 Particle size in water

The sizes of the co-polymer microgel particles in water at 5, 25 and 50 °C are summarized in Table 3.6 and Fig. 3.10. The data confirmed that all the co-polymer microgels undergo a volume phase transition similar to that observed for the homo-polymer poly(NIPAM). The measurements for the two previously reported co-polymer microgels (VL and MAA – see Table 3.6) compare favourably with sizes

reported in the literature.[17,18,19] In combination with the poly(NIPAM) size data in Table 3.3, a few general conclusions can be drawn from comparison of the D_H of all the particles at 5, 25 and 50 °C.

Table 3.6 Co-polymer microgel particle sizes and PdI values

Microgel (logP value)[†]	5 °C		25 °C		50 °C	
	D_H (nm)	PdI	D_H (nm)	PdI	D_H (nm)	PdI
poly(NIPAM)						
N4 (0.28)	539 ± 12	0.05 ± 0.03	483 ± 6	0.03 ± 0.03	249 ± 1	0.01 ± 0.01
vinyl ethers						
DVE (6.35)	565 ± 11	0.06 ± 0.04	511 ± 6	0.03 ± 0.02	249 ± 2	0.03 ± 0.02
TBVE (1.74)	593 ± 11	0.06 ± 0.02	526 ± 5	0.02 ± 0.01	292 ± 3	0.03 ± 0.02
TPVE (2.27)	560 ± 8	0.05 ± 0.03	501 ± 5	0.01 ± 0.02	273 ± 3	0.01 ± 0.02
vinyl esters						
VD (4.98)	540 ± 8	0.04 ± 0.05	494 ± 2	0.03 ± 0.03	260 ± 1	0.01 ± 0.01
VLi[*] (6.04)	–	–	487 ± 7	0.07 ± 0.03	291 ± 3	0.25 ± 0.02
VLii (6.04)	–	–	530 ± 5	0.14 ± 0.03	243 ± 1	0.01 ± 0.01
VS (9.23)	482 ± 8	0.04 ± 0.04	423 ± 3	0.04 ± 0.01	227 ± 2	0.02 ± 0.01
V4TBB (3.94)	503 ± 5	0.05 ± 0.01	397 ± 5	0.03 ± 0.02	293 ± 3	0.02 ± 0.01
vinyl silanes						
TMVS (1.58)	603 ± 6	0.05 ± 0.04	542 ± 5	0.02 ± 0.02	300 ± 1	0.02 ± 0.02
VTMOS (1.95)	606 ± 13	0.11 ± 0.05	543 ± 4	0.05 ± 0.02	302 ± 2	0.02 ± 0.01
TPVS (7.02)	763 ± 10	0.05 ± 0.05	653 ± 10	0.13 ± 0.04	370 ± 3	0.03 ± 0.02
polyelectrolyte						
MAA[‡] (0.57)	281 ± 3	0.11 ± 0.04	248 ± 1	0.07 ± 0.02	135 ± 1	0.11 ± 0.01

[†] Predicted logP value of co-monomer (or NIPAM monomer for poly(NIPAM) microgels) obtained from http://www.chemspider.com (see Appendix A); [*] Prepared by Dr Lisa Benée, Dr Hani Nur and Nuntana Srispornsawan; – Data not available; [‡] Composition of MAA = 95 % NIPAM and 5 % MAA.

Firstly, D_H at 5 °C is greater than at 25 °C. This indicates that microgels are not in the fully swollen conformation at 25 °C and will swell further as the temperature is decreased because the water becomes an even better solvent for the particles, with a greater degree of hydrogen bonding taking place. This is influenced by numerous solvent characteristics including solvent density, viscosity, structure/ordering and the enthalpy/entropy of the system as a whole. The observation of larger D_H values below 25 °C may have implications for the reporting of values such as the de-swelling ratio, which is typically based on D_H values at 25 and 50 °C, the temperatures generally used in literature to represent the swollen and collapsed particle sizes. However, although D_H values are typically larger at 5 °C than 25 °C, the relative difference between the two is small in comparison to the difference between 25 and 50 °C (Tables 3.6 and 3.7).
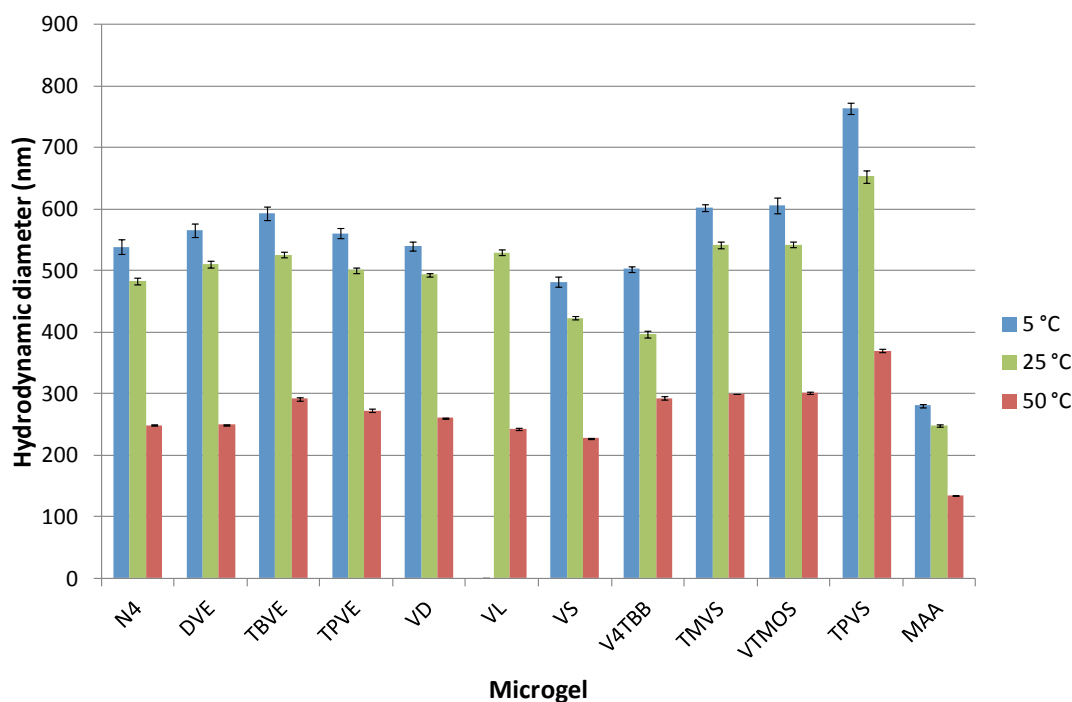
Figure 3.10 D_H **of microgel particles in water at 5, 25 and 50 °C (± 1 s.d.)**

Secondly, the 50 °C D_H measurements are more uniform (*i.e.* fall within a smaller size range) than at 25 and 5 °C. This may reflect the fact that above the VPTT, particles adopt a collapsed, hard, latex-like spherical conformation, which is less likely to show size variation than particles below the VPTT with a softer, more porous, flexible network-like structure.

Finally, the variation in D_H between the different microgels, particularly at 25 °C, suggests that incorporation of a hydrophobic co-monomer alters the extent of swelling of the particles. The influence of co-monomer type and relative hydrophobicity upon microgel properties will be considered in detail (Section 3.3.4) after presentation of other key data for the co-polymer microgels properties, including the VPTT and electrophoretic mobility.

The extent of de-swelling of each microgel from 5–50 °C and 25–50 °C, *i.e.* across the VPT, is summarized in Table 3.7 in the form of relative size changes and de-swelling ratios (*α*). The similarity in *α* values for the majority of microgels is striking. It suggests that the de-swelling transitions of the co-polymer microgels are not driven by the physico-chemical characteristics of the co-monomers *per se*.

Table 3.7 Particle de-swelling ratios from 5–50 °C and 25–50 °C

Microgel	LogP	De-swelling ratio (α)		Size change
		5–50 °C	25–50 °C	25–50 °C (nm)
poly(NIPAM)				
N1	0.28	–	0.2	261
N2	0.28	0.1	0.2	203
N3	0.28	0.1	0.1	315
N4	0.28	0.1	0.1	234
N5	0.28	0.1	0.2	154
N6	0.28	0.1	0.2	192
vinyl ethers				
DVE	6.35	0.1	0.1	262
TBVE	1.74	0.1	0.2	234
TPVE	2.27	0.1	0.2	228
vinyl esters				
VD	4.98	0.1	0.2	234
VL	6.04	0.1	0.1	287
VS	9.23	0.1	0.2	196
V4TBB	3.94	0.2	0.4	104
vinyl silanes				
TMVS	1.58	0.1	0.2	242
VTMOS	1.95	0.1	0.2	241
TPVS	7.02	0.1	0.2	283
polyelectrolyte				
MAA	0.57	0.1	0.2	113

α = de-swelling ratio (Equation 1.8) of collapsed particle size compared
to swollen particle calculated from data in Table 3.6

As discussed in Chapter 1, the extent of swelling is strongly influenced by the degree of cross-linking in a particle. All the microgels studied contained the same type and quantity of cross-linker (*N,N'*-methylenebisacrylamide, MBA at 10 % w/w total monomer). It is therefore possible that the similarity in values is a result of the constant degree of cross-linking present in each particle. Furthermore, 10 % is a relatively high cross-linker inclusion ratio and it is possible that this rate is sufficient to overcome or "hide" any influence the co-monomers might have upon de-swelling. Preparation and characterization of the same co-polymer microgels but at lower cross-linker inclusion ratios (*e.g.* 2.5 % w/w and 5.0 % w/w total monomer) may help establish whether the co-monomers do influence de-swelling.

The only co-polymer microgel to stand out in terms of de-swelling ratio was V4TBB, with $\alpha = 0.4$; it also exhibited the smallest relative size change between 25 and 50 °C. It is possible that the aromatic moieties created sufficient steric hindrance to prevent de-swelling occurring to the same extent as the other homo-polymer and co-polymer microgels, despite containing the same amount of MBA. This is evidence that co-monomers may influence de-swelling behaviour, which might become more apparent for the other co-polymer microgels at lower cross-linker inclusion rates.

3.3.3.2 Particle size by SEM

SEM images were obtained for three microgels to study the variation in particle size in the shrunken (dehydrated) state (Fig. 3.11) and to compare with DLS measurements.

(a) N1   (b) DVE

(c) V4TBB   (d) V4TBB
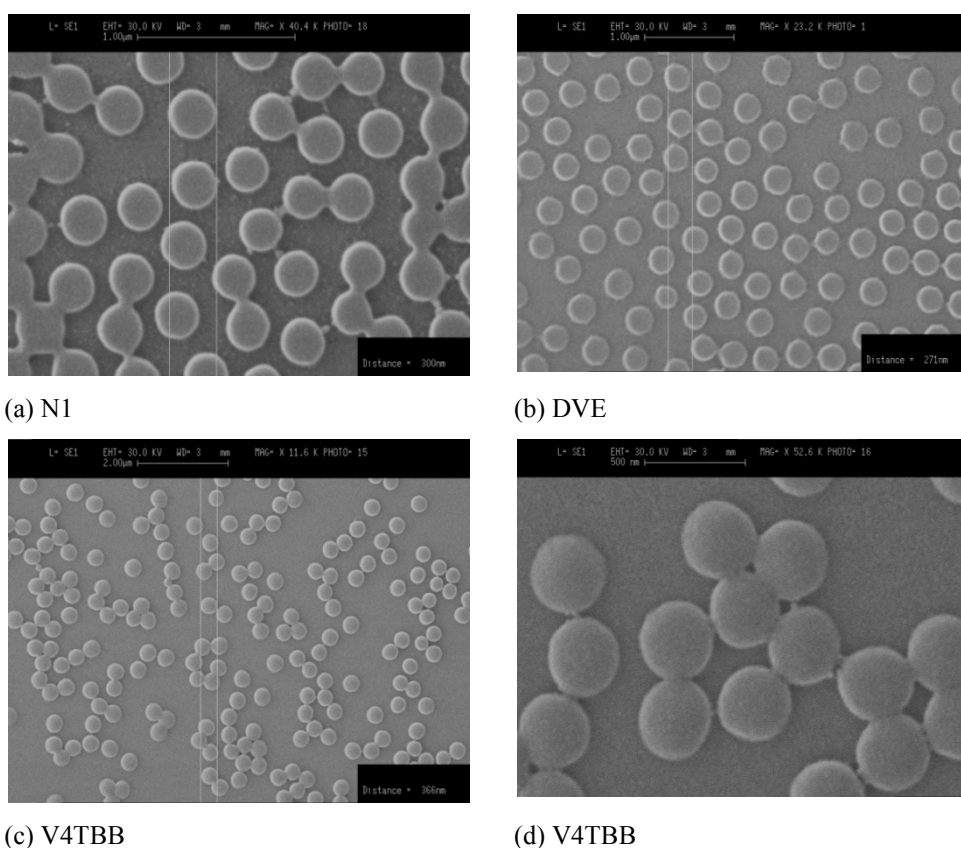
Figure 3.11 Scanning electron micrographs of selected microgels

The measured particle diameters are summarized in Table 3.8. Comparison was made with the 50 °C D_H DLS measurements because the particles had to be dehydrated to be analysed by SEM and therefore were measured in the collapsed conformation.

Table 3.8 Microgel particle diameters measured from SEM images

Microgel	Particle diameter by SEM (nm)	D_H by DLS at 50 °C (nm)
N1	300	318
DVE	271	249
V4TBB	366	293

Measurements of particle size taken from the SEM images show reasonable agreement with the 50 °C D_H measurements obtained by DLS for N1 and DVE. However, the difference for V4TBB was larger. The SEM images clearly show smooth, uniform, spherical, mono-disperse particles, with occasional bridges between them. Figure 4.11.d shows a closer view of the V4TBB particles, which appear slightly flattened – this is in accordance with the oblate spheroid shape of poly(NIPAM) observed by Saunders and Vincent using SEM.[20] This means that although diameters measured by SEM can give a general indication of the particle size, they cannot be considered accurate because of the particle deformation that is occurring.[10]

3.3.3.3 Volume phase transition temperature

Table 3.9 summarizes the VPTT values derived from transmittance measurements for each of the co-polymer microgels; N4 is included for comparison. Compared to N1–N6 (Table 3.4), the co-polymer microgels showed slightly more variation in VPTT. However, apart from two microgels (DVE and V4TBB) the VPTT of all the particles fell within 34 ± 1 °C, *i.e.* in line with literature values for homo-polymer poly(NIPAM). This suggests that incorporation of 10 % co-monomer did not have substantial affect upon the VPTT, at least for these compositions (*i.e.* 10 % w/w cross-linker). The measured values for the non-novel microgels VL and MAA compare favourably with values reported in the literature.[17,18,19]

In the case of more hydrophilic MAA, the slight increase in VPTT observed was expected as incorporation of a hydrophilic co-monomer has been shown to raise the VPTT.[21] Conversely, it was anticipated that incorporation of a more hydrophobic co-monomer would reduce the VPTT.[22] Of the nine hydrophobic co-polymer microgels measured, one showed an increase in VPTT (DVE), five showed no change, two showed a slight decrease (TBVE and VTMOS) and one showed a substantial decrease (V4TBB).

Table 3.9 VPTT of co-polymer microgels

Microgel	VPTT (°C)
poly(NIPAM)	
N4	34
vinyl ethers	
DVE	36
TBVE	33
TPVE	34
vinyl esters	
VD	34
VL	34
V4TBB	23[*]
vinyl silanes	
TMVS	34
VTMOS	33
TPVS	34
polyelectrolyte	
MAA[i]	35

All values calculated from average of heat and cool curves at heating rate of 0.5 °C/min unless otherwise specified. [*] Average of heat and cool curves at heating rate of 0.2 °C /min: the value at 0.5 °C/min (cool curve only) was 21 °C. [i] MAA composition = 95 % NIPAM and 5 % MAA.

The similarity between the majority of co-polymer microgels (VPTT = 34 ± 1 °C) may be explained by the fact that incorporation of just 5–10 % co-monomer (*i.e.* replacement of 5–10 % NIPAM monomer) is not sufficient to cause a substantial variation in VPTT or any significant differences in polymer-solvent interactions between the particles and water. It is possible that a larger proportion of co-monomer would show a greater effect. However, the same % w/w incorporation of V4TBB resulted in particles with a far smaller VPTT (23 °C). As suggested in the discussion of poly(NIPAM) VPPTs (Section 3.3.3.3), the lack of variability observed between co-polymer microgel VPTT values may be due to the relatively high proportion of cross-linker incorporated into the particles, which may mask any influence upon the volume phase transition the co-monomers might have. Again, investigation of co-polymer microgels with lower cross-linker inclusion rates may be informative.

The shapes of the volume phase transition curves are also informative. For example, Fig. 3.12 shows that the shape of the transition of V4TBB is clearly different to that of N4 and MAA. At the lowest temperatures, the relative change in transmittance for N4 and MAA became very small and therefore the curves began to reach a plateau

close to 100 %. However, the data for V4TBB in Fig. 3.12 shows no such plateau, which suggests that the particles may have not have adopted or have only just reached the fully swollen conformation. It was concluded that a precise VPTT could not be defined for V4TBB, despite repeat measurements over the same temperature range. However, the VPTT was clearly much lower than 34 °C.
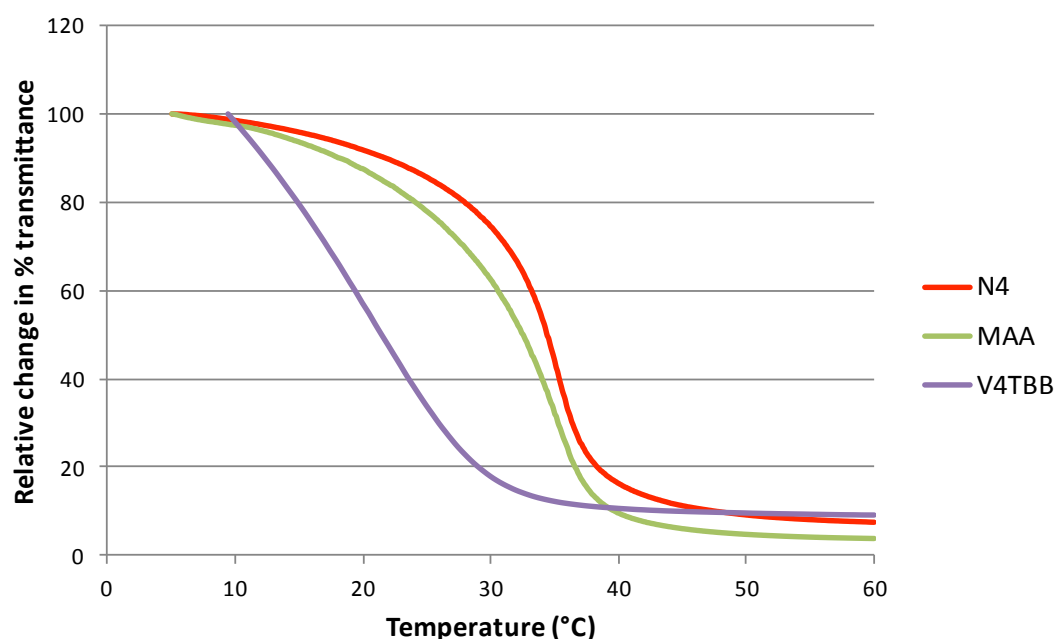
Figure 3.12   Comparison of turbidity data for N4, MAA and V4TBB

However, the size data (cooling) for V4TBB plotted alongside the turbidity data in Fig. 3.13 suggests a similar situation, where the particles may be closer to adopting the fully swollen size than the 10 °C turbidity data suggests. It can therefore be concluded that the VPTT of V4TBB is likely to be lower than that of the other microgels, *i.e.* less than 34 °C, because the minimum D_H (or fully collapsed state) is reached at a far lower temperature than the other microgels. This suggests that the measured VPTT of 23 °C may be a reasonable estimate. The VPTT calculated from the D_H measurements at 5 °C measurement intervals (from 5–60 °C) shown in Fig. 3.13 was 25 °C, providing supporting evidence that the VPTT of V4TBB is substantially lower than the other hydrophobically modified microgels. Further work is required to confirm this.

In general, the change in turbidity as a function of temperature observed for the microgels is largely driven by the thermosensitive NIPAM monomer, rather than any

contribution from the co-monomers. With NIPAM comprising the majority of the structure of the particles, the small contribution (5–10 %) from the hydrophobic co-monomers appears to be insufficient to lead to substantial changes in VPTT. However, the large reduction in VPTT resulting from the incorporation of V4TBB suggests that the relative structure and hydrophobicity of the different co-monomers may have significant influence upon the VPT of the resultant microgel particles.
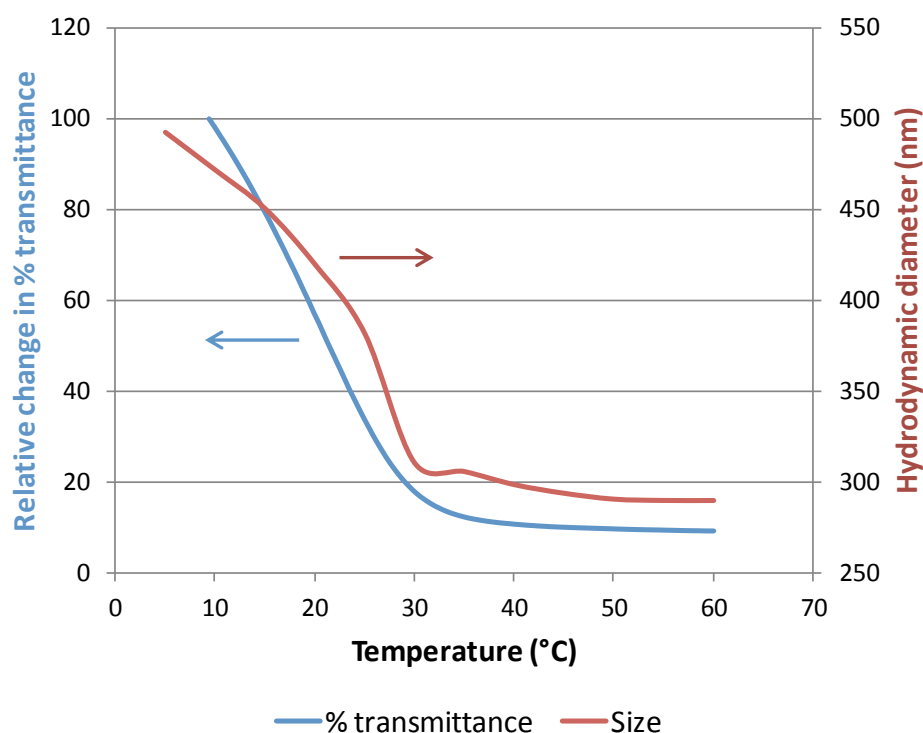
Figure 3.13 Percent transmittance and D_H of V4TBB particles on cooling

3.3.3.4 Electrophoretic mobility

The electrophoretic mobility of the hydrophobically modified microgel dispersions was measured as a function of temperature. The results at 5, 25 and 50 °C are summarized in Table 3.10, with N4 included for comparative purposes. As with the poly(NIPAM) microgels, the magnitude of the electrophoretic mobility increased as the temperature increased and the particle structure collapsed, resulting in an increase in charge density. The data shows substantial variation in the charge density of each microgel compared to N4. In general, the magnitude of electrophoretic mobility tends to be greater for the co-polymer microgels than N4. It was also clearly greatest for all particles in the collapsed state (above the VPTT).

Table 3.10 Electrophoretic mobility of microgel particles at 5, 25 and 50 °C

Microgel	Electrophoretic mobility ($10^{-8}\,m^2s^{-1}V^{-1} \pm 1$ s.d.)		
	5 °C	25 °C	50 °C
poly(NIPAM)			
N4	-0.66 ± 0.01	-1.11 ± 0.02	-4.05[*]
vinyl ethers			
DVE	-0.51 ± 0.02	-0.81 ± 0.01	-3.73 ± 0.00
TBVE	-0.80 ± 0.02	-1.06 ± 0.02	-4.10 ± 0.04
TPVE	-0.83 ± 0.02	-1.30 ± 0.05	-4.26 ± 0.12
vinyl esters			
VD	-1.18 ± 0.11	-1.00 ± 0.03	-3.87 ± 0.06
VL	-0.85 ± 0.00	-1.28 ± 0.02	-4.31 ± 0.01
VS	-0.12 ± 0.01	-0.19 ± 0.01	-2.77 ± 0.04
V4TBB	-0.90 ± 0.03	-1.63 ± 0.02	-3.83 ± 0.05
vinyl silanes			
TMVS	-0.93 ± 0.01	-1.39 ± 0.01	-4.24 ± 0.11
VTMOS	-0.72 ± 0.03	-1.19 ± 0.01	-3.90 ± 0.05
TPVS	-0.83 ± 0.01	-1.32 ± 0.03	-4.64 ± 0.02
polyelectrolyte			
MAA[i]	-0.30 ± 0.01	-0.70 ± 0.27	-3.08 ± 0.10

[*] Only one record sufficiently reliable, therefore no s.d. could be calculated.
[i] MAA composition = 95 % NIPAM and 5 % MAA
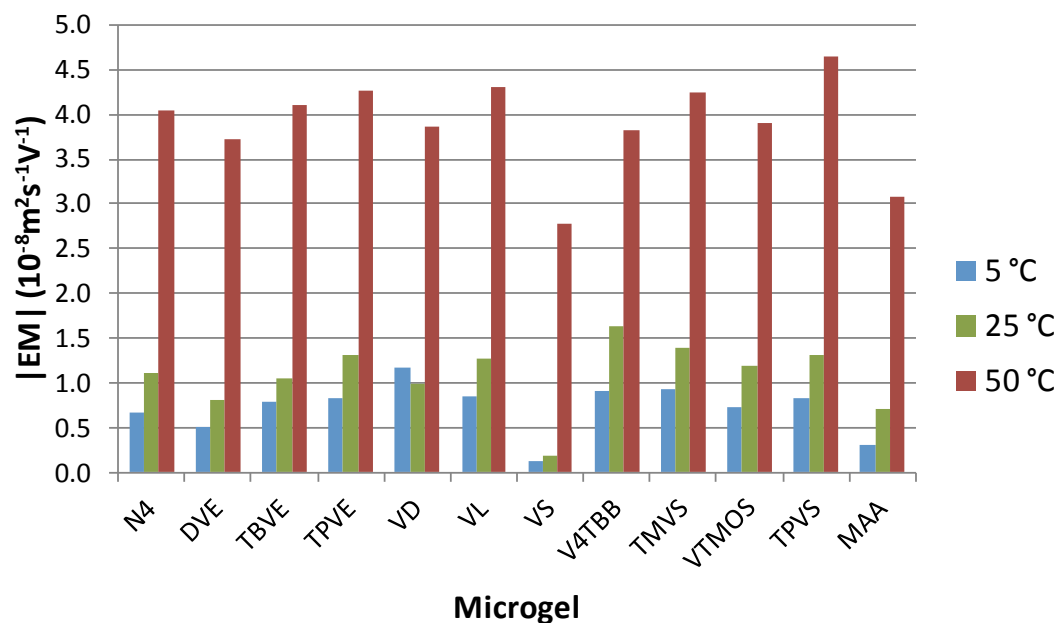
Figure 3.14 Magnitude of electrophoretic mobility of anionic microgel particles at 5, 25 and 50 °C (charge sign removed for clarity)

3.3.4 Analysis of influence of co-monomer type upon particle properties

In this section the relative influence of different co-monomer types upon the physico-chemical characteristics of the microgel particles will be considered. The data was analysed by co-monomer group to find out whether any group-specific behaviours were apparent. The aim was to determine whether the nature of the co-monomer influences microgel physico-chemical properties and, if so, whether physico-chemical properties can in any way be predicted from co-monomer characteristics.

3.3.4.1 Vinyl ether microgels

Firstly, the D_H values of the particles in water were plotted as a function of temperature (heating only) for each co-monomer category, *i.e.* vinyl ethers (Fig. 3.15), vinyl esters (Fig. 3.16) and vinyl silanes (Fig. 3.17). Poly(NIPAM) particles were also compared by initiator type (Fig. 3.18) and with a polyelectrolyte microgel (Fig. 3.19). In each case, the heating curve for N4 was included to facilitate comparison and help illustrate the effect of the inclusion of each co-monomer type.
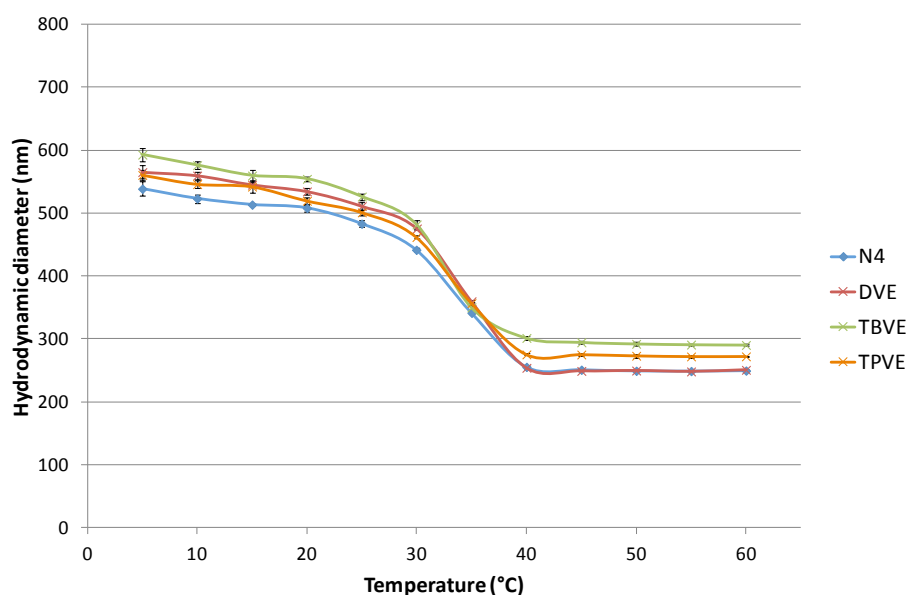
Figure 3.15 D_H in water of vinyl ether co-monomer microgel particles as a function of temperature, compared to N4 (heating only) (± 1 s.d.)

The variation in D_H as a function of temperature for NIPAM-*co*-vinyl ether microgels compared to homo-polymer N4 is shown in Fig. 3.15. The ether microgels were generally larger than the N4 microgel, where TBVE > DVE/TPVE > N4. The size

range was slightly smaller below the VPT (33 nm at 5 °C, 25 nm at 25 °C) than above the VPT (43 nm at 50 °C). In the region of the VPTT (indicated by the 35 °C data points), the microgels were very similar in size. Co-polymerization of NIPAM with 10 % of the linear or branched chain vinyl ether co-monomers therefore tended to produce larger particles at all temperatures (apart from for DVE at 50 °C and close to the VPTT).

The extent of de-swelling of each microgel between 25 and 50 °C, *i.e.* across the VPT, was summarized in Table 3.7, which specifies the size change and the de-swelling ratio (α). DVE ($\alpha = 0.1$) de-swelled to the greatest extent from 25–50 °C, very slightly more than N4. TBVE and TPVE (both $\alpha = 0.2$) de-swelled slightly less than N4. This suggests that co-polymerized linear ether co-monomers such as DVE may permit greater de-swelling than branched-chain ether co-monomers such as TBVE and TPVE. If true, this could be accounted for by the linear DVE co-monomers permitting closer packing than the branched-chain co-monomers.

There was very little difference in VPTT between the vinyl ether microgels (Table 3.9). However, the linear DVE exhibited a slightly higher VPTT (36 °C) than the branched chain TBVE and TPVE, whose VPTTs both fell within the 34 ± 1 °C expected for poly(NIPAM). A similar separation between the linear and branched chain co-monomers was observed for the electrophoretic mobility values, with the magnitude of TBVE and TPVE being larger and more closely related than DVE (Table 3.10).

3.3.4.2 Vinyl ester microgels

The variation in D_H as a function of temperature for NIPAM-*co*-vinyl ester microgels compared to homo-polymer N4 is shown in Fig. 3.16. Unlike the NIPAM-*co*-ether microgels, the co-polymerization generally produced particles smaller than N4, particularly below the VPTT. VL appeared to be the exception, being slightly larger than N4 from approximately 20–35 °C, the range over which data is available for that dispersion. Again the size range tended to be greater below the VPTT than above it, but this time a much broader range was observed immediately prior to the VPTT itself. The longest straight chain ester co-monomer, VS, exhibited the smallest D_H above and below the VPTT, with the shorter VD and VL resulting in larger particle sizes.
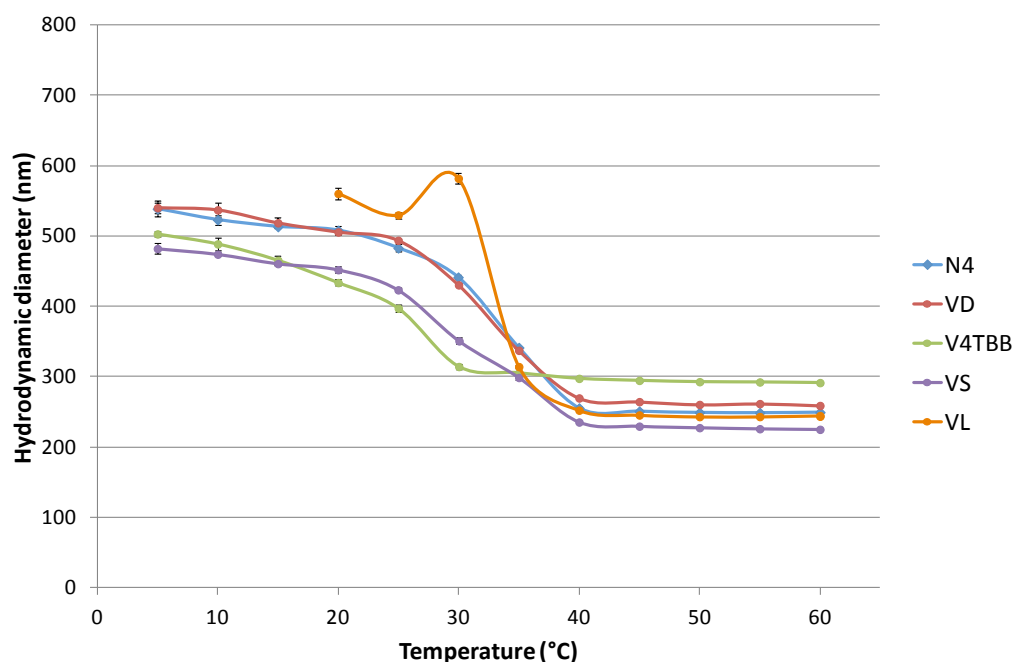
Figure 3.16 D_H **in water of vinyl ester co-monomer microgel particles as a function of temperature, compared to N4 (heating only) (± 1 s.d)**

The particles containing the aromatic co-monomer V4TBB displayed a substantially smaller range of D_H than the other ether microgels. Interestingly, as indicated by the VPTT data (Table 3.9) the volume phase transition occurred over a broader range of temperatures, with a substantially lower VPTT. The particles appeared to reach their collapsed conformation at least 10 °C lower, *i.e.* around 30 °C instead of 40 °C. In addition, the V4TBB data begins with less of a stable plateau at 5 °C. This is further evidence that the VPT of V4TBB takes place at a substantially lower temperature than the other microgels.

Table 3.7 shows that the linear ester co-monomer microgels VD and VS (both $\alpha = 0.2$) de-swelled to a similar extent as N4. VL appeared to de-swell slightly more ($\alpha = 0.1$) but this could be an artefact of the slightly unexpected data shape. Further measurements of the D_H of VL are required to clarify this, although the measured D_H are in reasonable agreement with sizes reported by Benée *et al.* (693 nm at 20 °C, 282 nm at 50 °C).[19] However, V4TBB de-swelled substantially less ($\alpha = 0.4$). This is further evidence of a difference between the influence of linear and aromatic ester co-monomers, where the extent of de-swelling may be more restricted when an aromatic co-monomer is incorporated into the polymer network.

As with the vinyl ether microgels, there was very little difference in VPTT between the straight chain vinyl ester microgels (Table 3.9). However, as already discussed, the aromatic V4TBB exhibited a substantially lower VPTT (23 °C). There was no discernable pattern between the electrophoretic mobilities of the linear and branched chain microgels.

3.3.4.3 Vinyl silane microgels

The variation in D_H as a function of temperature for NIPAM-*co*-vinyl silane microgels compared to homo-polymer N4 is shown in Fig. 3.17. In all three cases, the co-polymerization produced particles substantially larger than N4. TMVS and VTMOS were almost identical in D_H but the aromatic-containing TPVS was much larger. The range of D_H was greater below the VPTT (160 nm at 5 °C and 111 nm at 25 °C) than above it (70 nm at 50 °C).
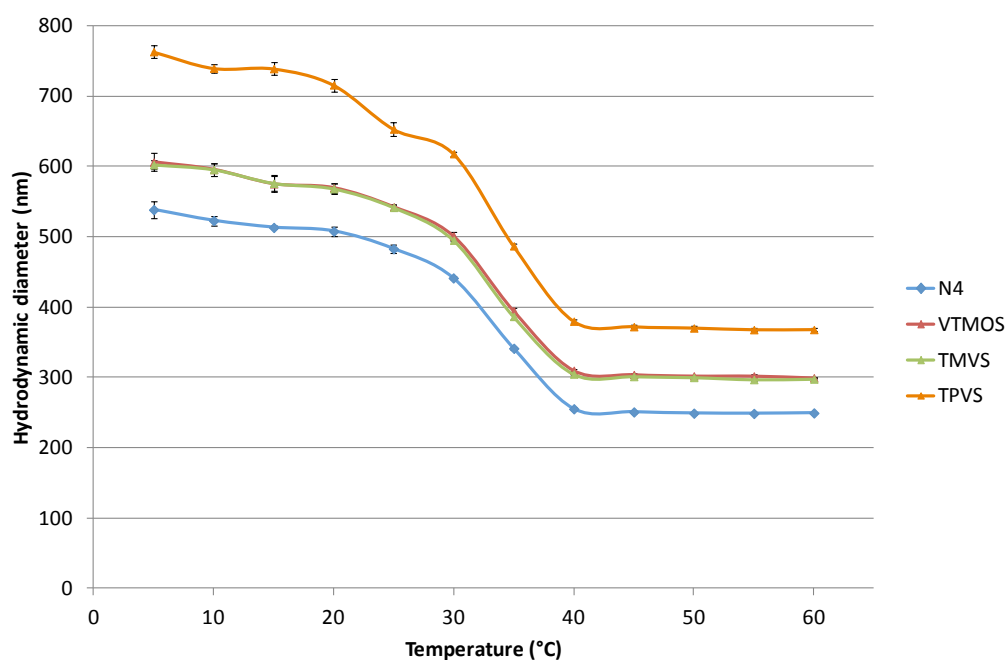
Figure 3.17 D_H **in water of vinyl silane co-monomer microgel particles as a function of temperature, compared to standard N4 (heating only) (± 1 s.d.)**

The extent of de-swelling for all the vinyl silane co-monomer microgels ($\alpha = 0.2$) was slightly less than that observed for N4 ($\alpha = 0.1$) (Table 3.7). Co-polymerization of NIPAM with 10 % vinyl silane therefore appeared to result in particles which undergo less de-swelling than poly(NIPAM) alone. The co-monomers may help

create a more rigid, less de-swellable structure, with steric hindrance preventing the same extent of collapse.

There was very little difference in VPTT between the vinyl silane microgels, all of which can be considered as slightly branched (rather than linear) (Table 3.9). The situation with electrophoretic mobility values was similar, with no discernable pattern relating to structure.

3.3.4.4 Poly(NIPAM) microgels prepared with different initiators

The D_H variation for three poly(NIPAM) microgels prepared with different initiators is shown in Fig. 3.18. As with the incorporation of a co-monomer, the use of different initiators appears to alter the particle size, with use of CVA and MPA resulting in N5 and N6 particles (respectively) that exhibit smaller D_H than N4 (KPS). In general, use of an initiator other than KPS resulted in smaller microgel particles, with N5 and N6 similarly sized below and above the VPTT (despite their opposite charges). As with other groups, the differences with N4 were greater at lower temperatures when the particles were swollen. The α values (Table 3.7) indicate that the extent of de-swelling of N4 ($\alpha = 0.1$) was slightly greater than N5 and N6 ($\alpha = 0.2$).
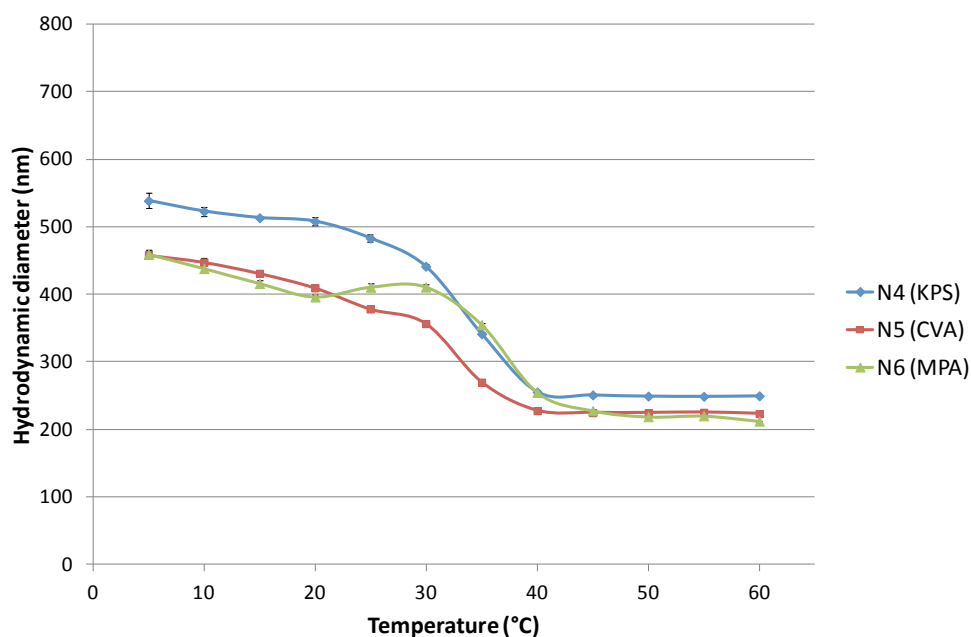
Figure 3.18 *D_H* **in water of poly(NIPAM) microgel particles prepared with different initiators as a function of temperature (heating only) (± 1 s.d)**

The similar size of N5 and N6 compared to N4 may be influenced by the initiator structure as a whole. When KPS thermally decomposes it produces two $\bullet SO_4^-$ radicals. However, when the CVA and MPA initiators decompose, the radical groups have much larger R-group structures attached ($\bullet$R-COOH and $\bullet$R-NH$_2$ respectively) which, although different in terms of composition, are similar in carbon chain length. The incorporation of the R-groups at the surface may alter the extent to which the particles can swell.

3.3.4.5 Polyelectrolyte microgel

Figure 3.19 compares the temperature-dependent variation in D_H of N4 with that of the more hydrophilic, polyelectrolyte MAA. Co-polymerization with the co-monomer MAA (methacrylic acid) results in substantially smaller microgel particles at all temperatures, which undergo a similar extent of de-swelling ($\alpha = 0.14$ for N4 and $\alpha = 0.16$ for MAA) (Table 3.7). However, the VPT of the MAA is far broader and covers a narrower size range than N4.
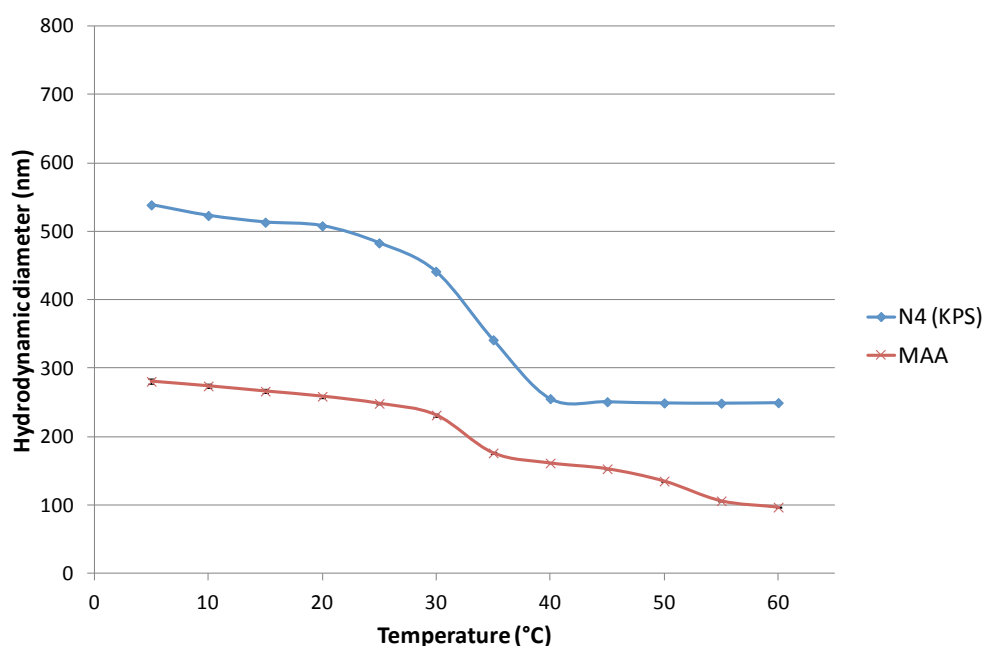
Figure 3.19 D_H in water of poly(NIPAM) microgel particles prepared with different charges as a function of temperature (heating only) ($\pm$ 1 s.d.)

As MAA contains charged co-monomers as well as charged surface groups from the initiators, it is considered to be more hydrophilic than the other microgels and

therefore anticipated to be larger in size due to more favourable polymer-solvent reactions. The smaller MAA particle size may be attributed to the fact that it was produced by a different synthesis method, as well as the polyelectrolyte nature of the co-monomer. The D_H values in Fig. 3.19 compare favourably with data reported in literature: around 240 nm at 25 °C and 175 nm at 50 °C.[17] Furthermore, the homo-polymer poly(NIPAM) microgel prepared by the authors was substantially larger than the co-polymer MAA microgels.

3.3.4.6 Potential co-monomer influence upon microgel properties

The results so far suggest that incorporating a hydrophobic co-monomer at 10 % w/w total monomer does influence particle size. However, the similarity of the VPTT and de-swelling values for the co-polymer microgels (apart from V4TBB) indicates that the particle swelling behaviour is less influenced by the co-monomers at these compositions (*i.e.* 10 % w/w co-monomer and 10 % w/w KPS cross-linker). In order to investigate the significance of co-monomer nature upon microgel properties in more detail, the data was re-examined in terms of co-monomer relative structure, size, functional group and hydrophobicity.

Firstly, the relationship between particle size and co-monomer structure/size (Table 3.6 and Fig. 3.1) was considered because co-polymerization of NIPAM with a co-monomer could be expected to influence the structure of the resulting polymer network. At its simplest, incorporation of large co-monomers might result in a more open network structure, whilst smaller co-monomers might allow for a more compact network structure. Alternatively, linear co-monomers might pack into the structure more efficiently than branched or aromatic co-monomers.

The clearest supporting evidence for such a structural effect comes from the vinyl silane co-polymer microgels, all of which were larger than homo-polymer N4 (Fig. 3.17). The TPVS co-monomer, which includes three aromatic moieties and is the largest and least flexible of the vinyl silane molecules, produced the largest particles. TMVS and VTMOS, which are more closely related in terms of structure and occupy a smaller volume (Appendix B), produced similarly-sized, smaller particles. Due to the aromatic groups it contains, TPVS is sterically very different to TMVS and VTMOS,

which will lead to different packing behaviour and hence to possible differences in the manner of particle collapse due to steric hindrance. A study of poly(methyl methacrylate) gel particles found that co-polymerization with TPVS resulted in larger particle sizes and that the degree of swelling increased with TPVS concentration.[23]

Amongst the ester co-monomers (Fig. 3.1.c), it was the aromatic V4TBB co-monomer that again produced particles with substantially different size and also swelling behaviour. This time, however, the aromatic co-monomer produced the smallest particles at 25 °C with a substantially reduced degree of de-swelling ($\alpha = 0.40$), whilst the linear VD, VL and VS produced substantially larger particles, capable of around 3–4 times greater de-swelling ($\alpha = 0.1$, similar to that of N4) (Table 3.7). The single aromatic ring possibly may permit more efficient network packing and collapse than both the linear esters and the three-ring silane TPVS. It is also shorter and therefore less hydrophobic. The linear co-monomers produced similarly-sized particles, but VS, with the longest carbon chain length, produced the smallest particles. The ester co-monomers decreased particle size and de-swelling compared to poly(NIPAM), whilst the silane co-monomers increased particle size but decreased de-swelling. The ether co-monomers (Fig. 3.1.b) all produced co-polymer microgels larger than N4 but there was no clear difference between the linear DVE and the branched TBVE/TPVE (Fig. 3.15). As with all the other co-monomers, the extent of de-swelling was reduced.

Previous research suggested that co-polymerization of NIPAM with hydrophobic co-monomers might result in particles smaller than homo-polymer poly(NIPAM),[22] due to stronger hydrophobic interaction between the greater proportion of hydrophobic domains within the network structure and decreased hydrogen bonding between the polymer chains and solvent. However, this was not always the case. For example, co-polymerization with the ether and silane co-monomers tended to produce larger particles than homo-polymer poly(NIPAM). It is possible that the structural/steric restrictions imposed by these co-monomers limit the effect of the increased hydrophobic interactions, leading to increased particle size, *i.e.* the structure is held more open sterically and therefore the particle is larger. For example, the vinyl ester microgel V4TBB had one of the smallest particle sizes below the VPTT but had the largest particle size above the VPTT; this suggests that the aromatic co-monomer moieties may limit the extent to which the particles de-swell.

It is likely that the picture is far more complex than this, however. If the two aromatic microgels, V4TBB and TPVS are compared, it is clear that incorporation of TPVS results in far larger particles than homo-polymer poly(NIPAM), but with a similar extent of de-swelling, the smaller V4TBB co-monomer results in far smaller particles with a substantially reduced extent of de-swelling. With three aromatic moieties, TPVS is likely to be less flexible and encounter far more steric hindrance than V4TBB with only a single aromatic group and greater flexibility. The molar volumes shown in Appendix B reflect the fact that TPVS is likely to occupy a greater amount of space within the microgel network, with less flexibility in structure resulting in less dense polymer chain packing.

Comparison of the three vinyl silane microgels supports this, with the smaller, more compact TMVS and VTMOS adopting smaller particle sizes at all temperatures, but showing a similar overall extent of de-swelling. Although all the microgels were prepared on a percentage weight basis, *i.e.* the proportion of co-monomer in each microgel was 10 % w/w total monomer, it is worth considering the relative number of co-monomer molecules incorporated into each microgel. Calculation of the mole fraction of co-monomer in each microgel is informative (Appendix B). This shows that a far smaller mole fraction (0.04) of TPVS was incorporated than of the other two vinyl silanes, which both have a mole fraction of 0.08. This indicates that despite a smaller number of TPVS molecules being incorporated compared to TMVS and VTMOS, its influence upon particle size is much greater, *i.e.* the TPVS microgel is much larger than TMVS, VTMOS or N4.

The mole fraction of V4TBB incorporated was slightly greater at 0.06 than TPVS (0.04) and yet, as already discussed, the particle size was substantially smaller. This suggests that the structure and volume of V4TBB results in less steric hindrance than TPVS. It is clear that a complex balance between co-monomer size, volume and flexibility is influential.

The second aspect to consider is whether the different functional groups contained in the co-monomers exert any influence, *i.e.* the ether (R-O-R'), ester (R-C=OOR') and silane (R-Si-(R')$_3$) groups distributed throughout the particle structure. For example, compared to N4, the vinyl ester co-monomers tended to decrease particle size whilst

the similarly-sized vinyl ether co-monomers tended to increase particle size. However, these differences are relatively small and the de-swelling ratios were very close (Table 3.7). It is therefore difficult to draw firm conclusions and any possible relationship with functional group type is far less clear than the potential structural influences discussed above. However, the different functional groups could alter aspects such as polymerization rate during synthesis, co-monomer location within the structure, inter-chain network spacing and particle interactions with the solvent, all of which would influence the final particle size at any given temperature. It is clear that the situation is not simple and further work is required.

The third aspect to consider is the potential influence of relative hydrophobicities of the co-monomers and resultant co-polymer microgels, and their subsequent interactions with each other and the solvent. In theory, microgel particles of differing hydrophobicities should interact differently with solvent molecules, for example the structural ordering of water around the polymer chains within the particle and around other water molecules is likely to vary. This in turn is related to aspects such as solvent density and viscosity, and extent of particle solvation and hydrogen bonding, and therefore to particle swelling.

Co-polymerization of the more hydrophilic NIPAM with more hydrophobic co-monomers should result in a greater proportion of hydrophobic domains within the structure. When Ma *et al.*[22] observed that co-polymerization of NIPAM with hydrophobic *iso*propyl methacrylate (*i*PMA) resulted in a lowering of the VPTT (*i.e.* a change in swelling behaviour of the particles) they attributed it to a reduction in hydrogen bonding between the now more hydrophobic polymer chains and the solvent, and increased hydrophobic interactions between the NIPAM *iso*propyl groups and *i*PMA.

It was therefore anticipated in this study that co-polymerization might result in altered swelling behaviours (*e.g.* reduced α values). As co-monomer hydrophobicity increases, a decrease in polymer-solvent hydrogen bonding and increase in polymer-polymer hydrophobic interactions was postulated that might lead to differing extents of de-swelling and possibly the adoption of closer-packed structures with consequently smaller particle sizes (depending on steric restrictions). However, whilst substantial

variation in D_H between the co-polymer microgels was observed, the α and VPTT values were very close (apart from V4TBB) (Tables 3.7 and 3.9). The lack of variation within the VPTT and α values suggests that (apart from V4TBB) there was very little difference in swelling behaviour between the different co-polymer microgels. The turbidity and size curves for each microgel are similar in shape, even though, as previously discussed, there is substantial variation in the overall shrunken/swollen particle diameters. This suggests that variation in co-monomer hydrophobicity may have a more substantial effect upon particle size than swelling behaviour.

This possibility was investigated using logP values to estimate the relative hydrophobicity of the co-monomers (Tables 3.6 and 3.7). Although the logP values relate only to the monomer/co-monomer and not to the microgel particle as a whole, they can be used as a guide to the likely relative hydrophobicities of the microgel particles. For example, the monomer NIPAM has a logP value of 0.28 and therefore it is anticipated that the polymer chains of a co-polymer microgel containing 90 % NIPAM and 10 % of a more hydrophobic co-monomer (*e.g.* DVE with a logP of 6.35) are likely to have a greater proportion of hydrophobic domains than a polymer chain composed purely of NIPAM. To investigate this further, D_H values at 5, 25 and 50 °C were plotted against logP for each of the co-monomer groups (Figs. 3.20, 3.21 and 3.22). Trend lines were added to aid visual determination of general tendencies rather than absolute trends.

The plots tentatively suggest that within each group the relative hydrophobicity of the co-monomers may show a relationship with particle size. The vinyl silane microgels appeared to increase in size with increasing co-monomer logP, whilst the vinyl ether and ester microgels possibly show non-linear behaviour with respect to logP. For example, the vinyl ether microgels with the lowest logP decreased in size, then increased at higher logP values. The opposite trend was apparent for the vinyl ester microgels.

Above the VPT (*i.e.* the 50 °C measurements) the ether and silane particles showed the same patterns as below the VPT, just with reduced particle sizes as expected. However, the ester microgels showed a reversal in trend above the VPT, with size

decreasing with increasing logP. All three groups showed clear differences in size with increasing temperature, where size at 5 °C > 25 °C > 50 °C.
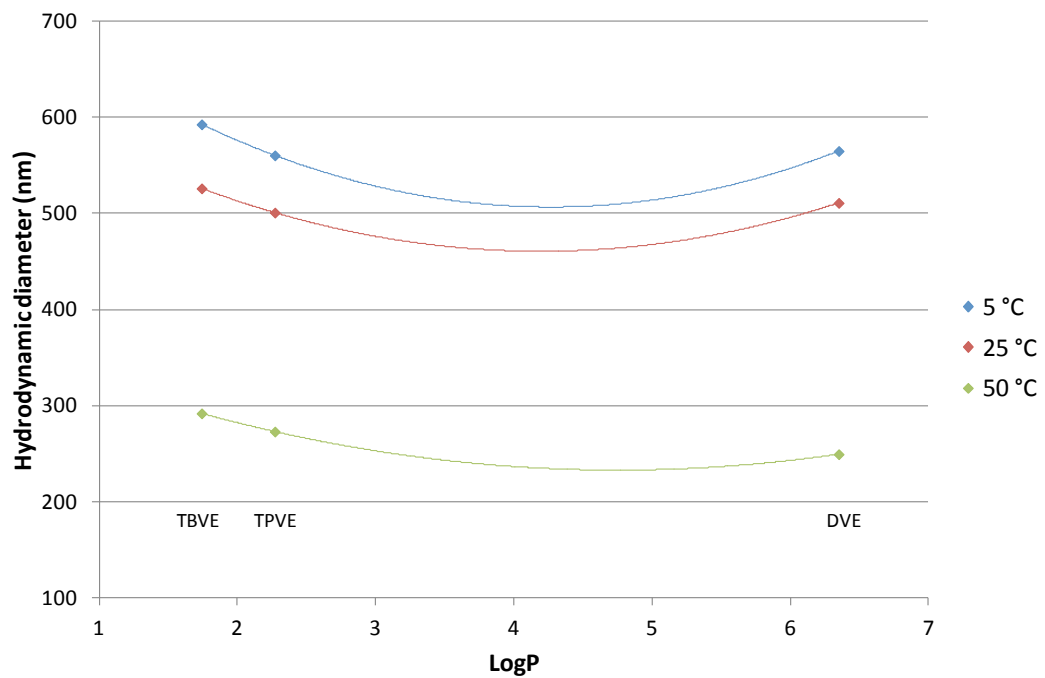
Figure 3.20 D_H **of vinyl ether co-monomer microgels as a function of logP**

Trend lines added only as a visual aid.
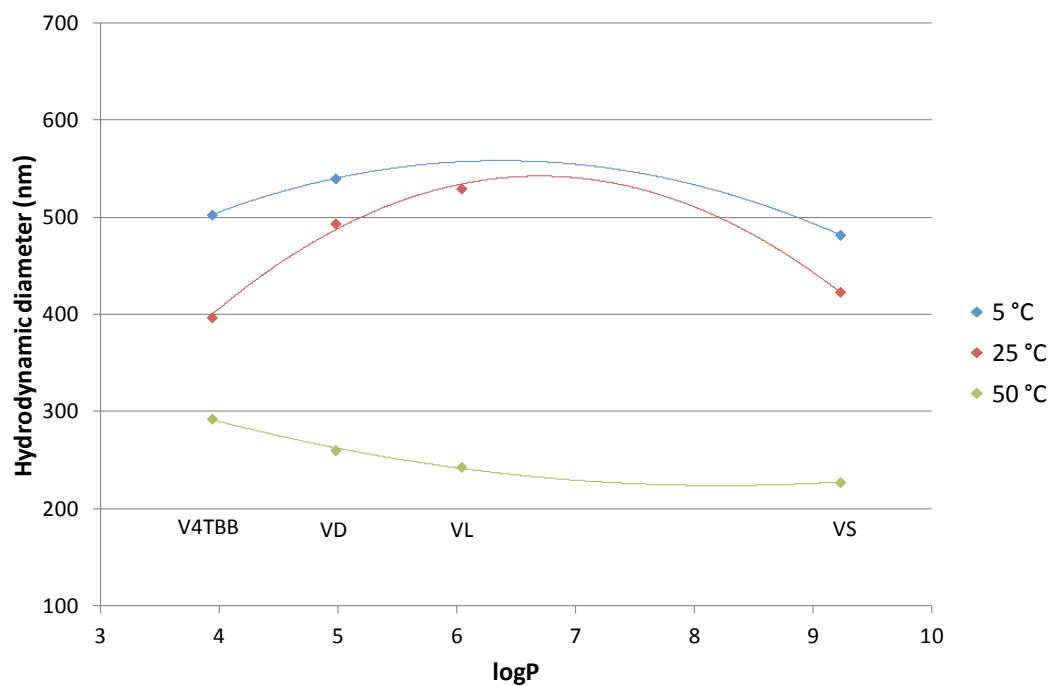
Figure 3.21 D_H **of vinyl ester co-monomer microgels as a function of logP**

Trend lines added only as a visual aid.
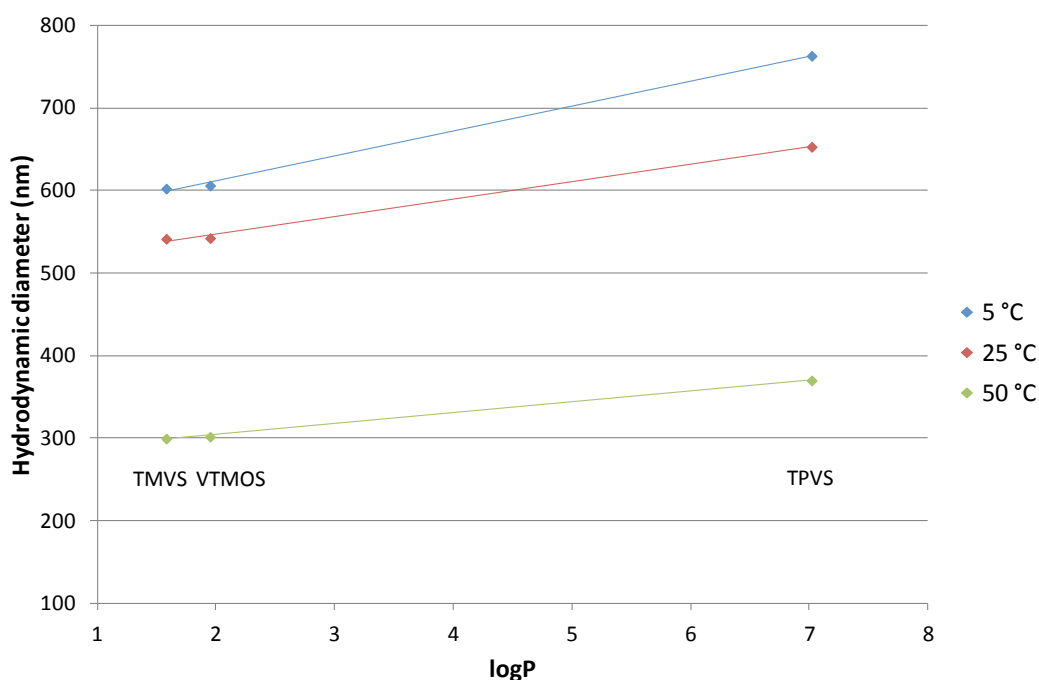
Figure 3.22 *D*_H of vinyl silane co-monomer microgels as a function of logP

Trend lines added only as a visual aid.

All the microgels shown in Figures 3.20–3.22 were prepared by the same synthesis method, using the same monomer, initiator and cross-linker, and with the same proportion of co-monomer (10 % w/w). Therefore the main difference between the particles was the specific co-monomer used in each case. The size differences are therefore likely be related to the co-monomer, *e.g.* its size or characteristics such as hydrophobicity.

Ideally a greater range of co-monomer microgels would be tested to establish the trends in more detail. In addition, it must be remembered that the logP values used are those for the co-monomer not the microgel particles themselves and therefore can only be used as a guide to the particle hydrophobicity. As previously described for cross-linker incorporation (Section 1.2.3.2), the co-monomers may not be distributed uniformly throughout a particle or in the same way in each particle in a dispersion, and the co-monomer/monomer reactivity ratios may also influence structure. Determination of the hydrophobicity of microgel particles as a whole requires further work.

In a similar exercise, the particle de-swelling ratio (α) was plotted against logP and similar trends that are possibly linear were observed (data not shown). The relative extent of de-swelling from 5–25 °C and 5–50 °C is summarized in Table 3.7. Most

striking is that the values are almost identical for all the particles, irrespective of co-monomer hydrophobicity, with a 90 % reduction in volume from 5–50 °C. Interestingly, the only particle to deviate from this was the aromatic-containing V4TBB. This is further evidence that the aromatic moieties in V4TBB influence particle collapse in a slightly different manner to the straight and branched chain co-monomers, which, despite differences in size and hydrophobicity, do not appear to differ in extent of de-swelling.

Grouping the VPTT values by logP value also did not highlight any further trends within the data, due to the lack of variation within the values. Therefore there was no apparent correlation between co-monomer and the VPTT, with only V4TBB appearing to have a substantial influence. However, further evidence for the influence of co-monomer structure comes from the VPTT data in particular, where, as discussed above, there appeared to be slight differences in the VPTT between linear and branched chain molecules, particularly for the vinyl ether and vinyl ester groups. For example, the branched TBVE and TPVE exhibited slightly lower VPTTs than linear DVE, whilst the branched V4TBB exhibited a substantially lower VPTT than the other linear vinyl ester microgels.
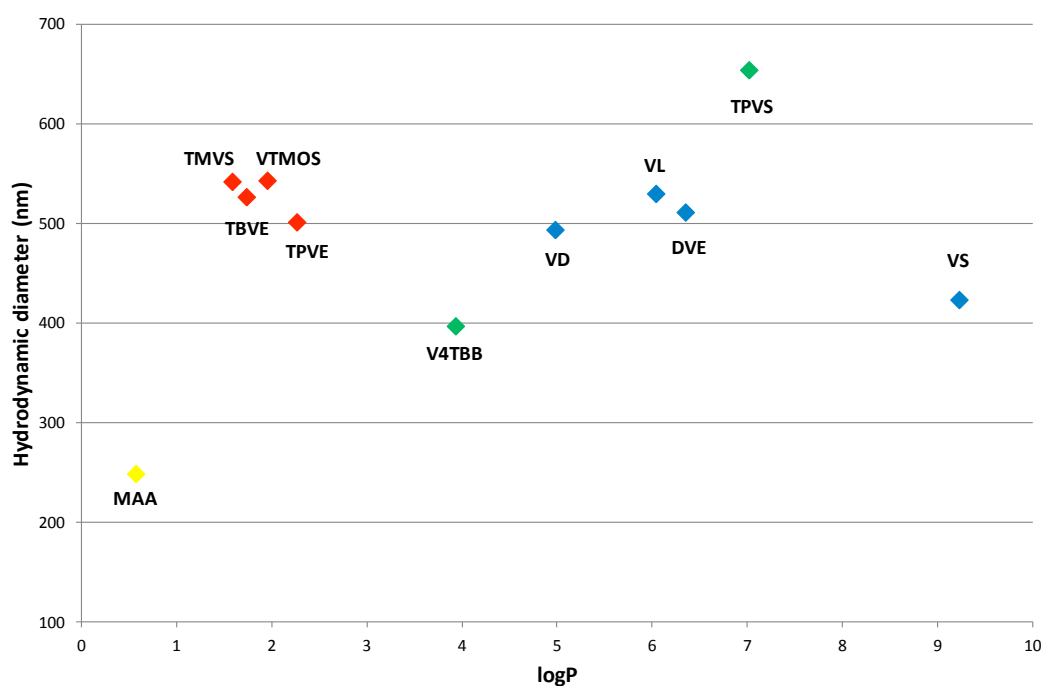
Figure 3.23 Particle size as a function of co-monomer logP at 25 °C

Co-monomer structure type: ◆ = linear; ◆ = branched; ◆ = aromatic; ◆ = polyelectrolyte.

In order to look at potential differences between branched-chain and linear co-monomer influences, particle sizes and electrophoretic mobilities were plotted against logP for all the particles. A tendency for the non-aromatic branched co-monomer microgels (TBVE, TPVE, TMVS and VTMOS) to cluster together emerged (Fig. 3.23 and 3.24).
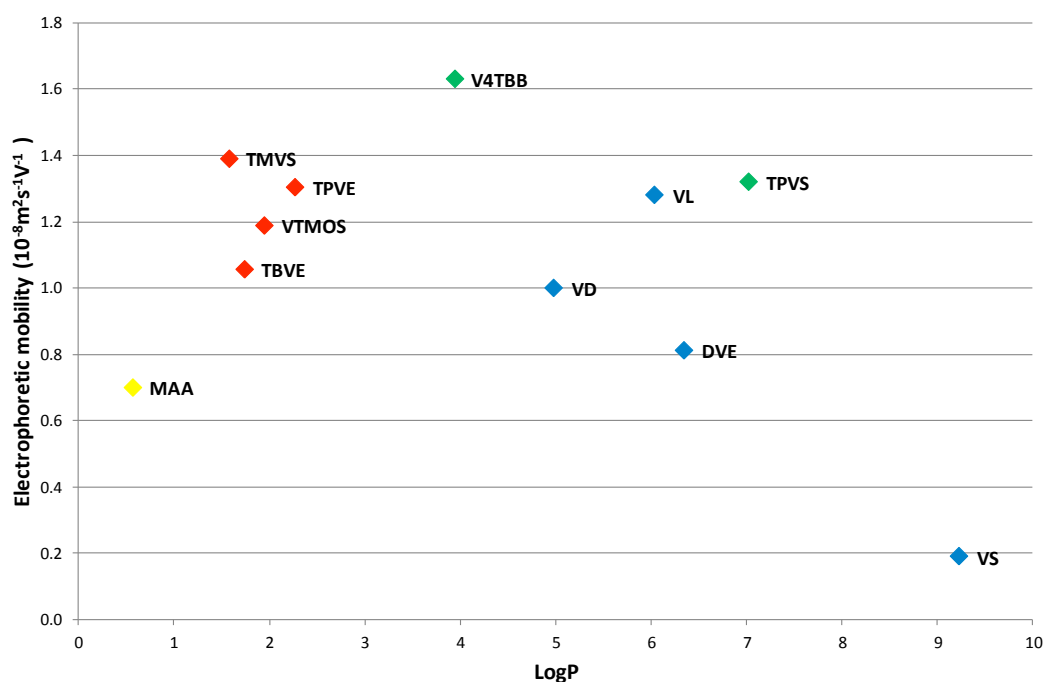
Figure 3.24 Electrophoretic mobility as a function of co-monomer logP at 25 °C

Co-monomer structure type: ♦ = linear; ♦ = branched; ♦ = aromatic; ♦ = polyelectrolyte.

The situation is less clear for the aromatic co-monomer microgels (TPVS and TMVS) but the linear co-monomer microgels (VD, VL, DVE and VS) also appear to show a slight grouping. Whilst not conclusive, this is further supporting evidence that the physical structure of co-monomers once incorporated into the polymer chains of the particle network may influence characteristics such as particle size and electrophoretic mobility, and that this influence may be more substantial than hydrophobicity or functional group alone at these co-monomer and cross-linker inclusion rates.

3.4   Summary

The basic physico-chemical characteristics of a number of homo-polymer and hydrophobically modified poly(NIPAM) microgel dispersions have been determined

experimentally, including size, VPTT and electrophoretic mobility. All the co-polymer particles exhibited a volume phase transition similar to that observed for poly(NIPAM), adopting a swollen conformation at temperatures below the volume phase transition temperature of poly(NIPAM) and a collapsed conformation at higher temperatures.

Hydrophobic modification of poly(NIPAM) microgels appeared to substantially influence particle D_H. The synthesis method, relative proportions of solvent:initiator:reagent, and initiator type were also influential. Electrophoretic mobility was influenced to a lesser extent by hydrophobic modification and appeared to be more strongly determined by initiator type. The VPTT generally appeared relatively unaffected by incorporation of 10 % co-monomer. SEM confirmed that smooth, mono-disperse microgel dispersions had been prepared.

A key aim of this chapter was to investigate the variation in microgel physico-chemical properties according to specific co-monomer characteristics such as relative size, structure and hydrophobicity. The structure and composition of the co-monomer appeared to influence particle size strongly. For example, compared to poly(NIPAM) alone, incorporation of vinyl ether or vinyl silane co-monomers increased the particle size, whilst vinyl ester co-monomers tended to reduce particle size. The hydrophobically modified particles were therefore not necessarily smaller as might be expected (due to greater hydrophobic interactions between the added hydrophobic domains, leading to the adoption of a more compact structure). Slight differences in VPTT were observed between linear and branched/aromatic co-monomer microgels, *e.g.* V4TBB displayed a broader transition with a substantially lower VPTT than the other linear vinyl ester microgels.

Co-monomer logP values were used as a guide to the potential the hydrophobicity of the microgel particles. Whilst there was no direct correlation between logP and size or electrophoretic mobility, some differences between and trends within the co-monomer types emerged. For example, incorporation of a vinyl silane co-monomer increases particle size and the size tends to increase with increasing vinyl silane logP.

It was not possible to determine precise relationships between particle characteristics and co-monomer properties such as functional group, structure, hydrophobicity or

other molecular descriptors, such as flexibility. It was therefore not possible to directly predict microgel properties from specific co-monomer characteristics. However, it was clear that co-polymerization with these hydrophobic co-monomers could substantially alter the properties compared to homo-polymer poly(NIPAM) and very general conclusions could be drawn. For example, incorporation of a vinyl silane or vinyl ether co-monomer is likely to increase the D_H of the resultant microgel compared to homo-polymer poly(NIPAM). Further investigation may permit clearer elucidation of these relationships.

Finally, the physico-chemical properties reported in this chapter provided a solid base of information from which to investigate the effect of hydrophobic modification upon the behaviour of poly(NIPAM)-based microgels, such as the swelling response in the presence of alcohol co-solvents. The results of these investigations are reported in the following chapters.

3.5   References

[1] Shaw, D.J. (1992) *Introduction to Colloid and Surface Chemistry* (4th Ed.). Oxford: Butterworth Heinemann.

[2] Malvern Instruments (2008) *Nano Series and HPPS Training Manual: Zeta Potential*. Malvern: Malvern Instruments.

[3] Malvern Instruments (2008) *Zetasizer Nano Series User Manual (MAN0317, Issue 4.0)*. Malvern: Malvern Instruments.

[4] Nur, H., Snowden, M. J., Cornelius, V. J., Mitchell, J. C., Harvey, P. J., Benée, L. S. (2009) *Colloids and Surfaces A: Physicochemical and Engineering Aspects*, **335**, 133–137.

[5] Gracia, L. H., Snowden, M. J. (2007) 'Preparation, Properties and Applications of Colloidal Microgels'. *In:* Williams, P. A. (Ed). *Handbook of Industrial Water Soluble Polymers*. Oxford: Blackwell, 268–297.

[6] Meunier, F., Elaïssari, A., Pichot, C. (1995) *Polymers for Advanced Technologies*, **6**, 489–496.

[7] Wu, X., Pelton, R. H., Hamielec, A. E., Woods, D. R., McPhee, W. (1994) *Colloid & Polymer Science*, **272**, 467–477.

[8] Hall, R. J., Pinkrah, V. T., Chowdhry, B. Z., Snowden, M. J. (2004) *Colloids and Surfaces A: Physicochemical and Engineering Aspects*, **233**, 25–38.

[9] Islam, A. M., Chowdhry, B. Z., Snowden, M. J. (1995) *Journal of Physical Chemistry*, **99**, 14205–14206.

[10] Saunders, B. R., Vincent, B. (1999) *Advances in Colloid & Interface Science*, **80**, 1–25.

[11] Pelton, R. H., Chibante, P. (1986) *Colloids and Surfaces*, **20**(3), 247–256.

[12] Kiminta, O., Luckham, P. F., Lenon, S. (1995) *Polymer*, **36**(25), 4827–4831.

[13] Malvern Instruments (2008) *Nano Series and HPPS Training Manual: Dynamic Light Scattering*. Malvern: Malvern Instruments.

[14] Wu, J., Zhou, B., Hu, Z. (2003) *Physical Review Letters*, **90**(4), 48304–48307.

[15] Tauer, K., Gau, D., Schulze, S., Völkel, A., Dimova, R. (2009) *Colloid & Polymer Science*, **287**, 299–312.

[16] Daly, E., Saunders, B.R. (2000) *Physical Chemistry Chemical Physics*, **2**, 3187–3193.

[17] Ngai, T., Auweter, H., Behrens, S. H. (2006) *Macromolecules*, **39**, 8171–8177.

[18] Ngai, T., Behrens, S. H., Auweter, H. (2005) *Chemical Communications*, 331–333.

[19] Benée, L. S., Snowden, M. J., Chowdhry, B. Z. (2002) *Langmuir*, **18**, 6025–6030.

[20] Saunders, B. R., Vincent, B. (1996) *Journal of the Chemical Society, Faraday Transactions*, **92**, 3385–3389.

[21] Puertas, A. M., Nieves, F. J. de las (1999) *Journal of Colloid and Interface Science*, **216**, 221–229.

[22] Ma, X., Xi, J., Huang, X., Zhao, X. and Tang, X. (2004) *Materials Letters*, **58**, 3400–3404.

[23] Naghash, H. J. (2010) *Journal of Applied Polymer Science*, **116**, 2465–2472.

INVESTIGATION OF THE INTERFACIAL PROPERTIES OF HYDROPHOBICALLY MODIFIED POLY(NIPAM) MICROGEL PARTICLES

4.1 Introduction

Following the synthesis and basic physico-chemical characterization of the hydrophobically modified poly(NIPAM) microgel particles described in Chapters 2 and 3, the aim of the work described in this chapter was to investigate the interfacial behaviour of the particles, particularly any influence they might have upon the surface tension of water (air-water interface). It was hypothesized that as the hydrophobic nature of the particles increased, due to co-polymerization with co-monomers more hydrophobic than NIPAM, the positioning of the particles at interfaces and hence their influence upon interfacial tension would vary.

As described in Chapter 1, surface activity of both linear poly(NIPAM) and homo-polymer poly(NIPAM) microgels has been reported in literature, both of which were shown to reduce the surface tension of water to values around 42 mN m^{-1}.[1,2] It has also been shown that poly(NIPAM-*co*-methacrylic acid),[3,4] poly(NIPAM-*co*-dimethylamino ethyl methacrylate)[5] and poly(NIPAM)[6] microgels are capable of stabilizing oil-in-water emulsions by adsorbing at the oil-water interface. Such evidence illustrates that poly(NIPAM)-based microgels possess interfacial properties and the aim of this work was to determine the extent to which hydrophobic modification alters their interfacial behaviour. It was anticipated that by altering the hydrophobic-hydrophilic balance of the microgel particles, properties such as the capacity of the particles to lower surface tension would vary accordingly.

It is worth noting that although the properties and surface activity of surfactants are well characterized, the capacity of particles to reduce surface tension is less definitively understood. Indeed, according to Pelton[5] there are only a few examples of surface active particles. However, what is certain is that particles sit at interfaces. For example, Zhang and Pelton[6] used environmental scanning electron microscopy to image an ordered array of poly(NIPAM) microgel particles at an air-water interface.

The position of particles at a surface is determined by a complex interplay between parameters such as size and charge. This positioning is likely to significantly influence any surface tension lowering capacity of particles. Figure 4.1 illustrates how particles can either freely "float" in one phase at an interface or can bridge the interface, becoming "immersed" or "confined" between the two phases.[7]
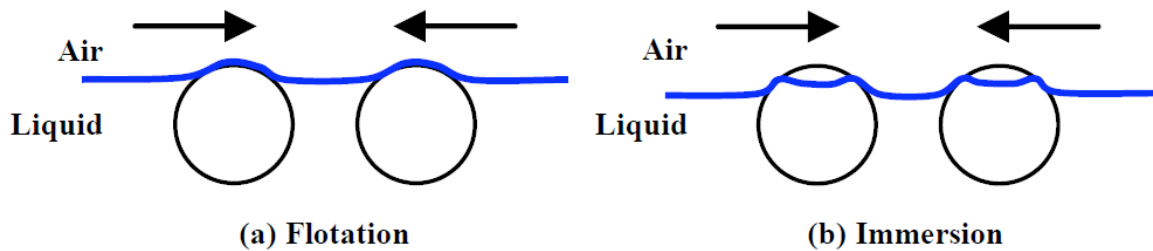
Figure 4.1   Illustration of possible positions of particles at air-water interfaces, adapted from Ref. [7]. Arrows represent attractive lateral capillary forces.

When a particle makes contact with a fluid phase boundary, the shape of the interface is perturbed and a deformation of the interface results in lateral capillary forces that alter the surface tension.[7,8] As attractive capillary forces between particles increase, the amount of work (W) required to deform the interface (ΔA) increases, which in turn increases the surface tension (γ), where:[9,10]

$$W \;=\; \gamma \Delta A$$

[Equation 4.1]

A useful summary of the potential sources of the attractive lateral capillary forces is offered by Kralchevsky and Danov,[11] including flotation capillary forces, capillary immersion forces, forces between capillary multipoles and electric-field induced capillary forces. In the case of floating particles (Fig. 4.1.a), floatation capillary forces arise due to the weight of the particles, which causes perturbations of the surface.[11,12] Hydrostatic pressure arises from the perturbations, causing attractive capillary forces between the particles. The particles attract one another in order to reduce the total deformation of the surface.[12] These are proportional to the particle weight and size (force is proportional to the radius to the sixth power) and therefore are negligible for particles smaller than 10 μm in diameter.[7,8] At less than 1 μm in diameter, microgel particles are not influenced significantly by gravity and would therefore not be affected by these forces.

However, in the case of particle "immersion" between two phases (Fig. 4.1.b), the attractive capillary forces are related to the wetting properties of the particles (force $\propto$ radius squared) and are significant for particles as small as a few nm in diameter.[7,8] Therefore it is likely that microgel "immersion" positions are influenced by the particle wetting properties. Immersion capillary forces result from the overlap of interfacial deformations related to the wetting properties of the particle and therefore are influenced by the particle position at the surface (contact angle and contact line) rather than gravity.[11] Capillary multipole forces are also related to deformations of the contact line on the particle surface, which may result from an uneven particle surface, *e.g.* due to the surface being rough, angular or heterogeneous.[11,12]

Surface deformations can also arise as a result of the electric fields around charged particles.[11,12] Due to their surface charges, the particles are subjected to an electrodipping force, which drives the particles towards the phase of greatest dielectric constant (*i.e.* towards water at the air-water interface). There is then a balance between the direct repulsion of two like-charged particles and the attractive electrocapillary forces that arise from the electric-field driven surface deformations. As microgel particles are charged species with diameters far smaller than 10 μm, the potential forces that might be behind any surface tension lowering capacity could well include the attractive electrocapillary and capillary immersion forces.

In addition, the interfacial properties of a colloidal dispersion can be considered from other perspectives. For example the energy (*E*) required to move a particle of radius *r* from the interface between two phases (α and β) can be described in terms of the contact angle (*θ*) the particle makes with the interface:[7]

$$E = \pi r^2 \gamma_{\alpha\beta}(1 - \cos\theta)^2$$

[Equation 4.2]

Equation 4.2 explains why particles are strongly held at interfaces.[12,13] As the particle size increases, the energy required to detach the particle from the surface increases, which is associated with an increase in surface tension.[13] Colloidal particles are therefore strongly bound to fluid interfaces[12] and particles with diameters larger than 10 nm (with typical $\gamma_{\alpha\beta}$ and *θ* close to 90 °) are considered irreversibly adsorbed.[14] Expressions such as Equations 4.1 and 4.2 indicate how particle properties influence the surface tension of a colloidal dispersion,

including particle size, position at an interface (contact angle), hydrophobicity and wetting properties. Other influences/forces include interparticle repulsion due to dipoles resulting from the presence of polar surface groups or the asymmetric distribution of free ions around the part of the particle immersed in the water phase.[15] Interparticle separation and the surface tension of the liquid phase itself are also significant.[8] It therefore becomes apparent that altering the composition of a microgel particle and therefore influencing its size, charge, hydrophobicity, *etc*, could alter the surface tension of the dispersion.

For example, the size of a particle determines how many can physically fit into a unit surface area, with the number of particles required to saturate a surface decreasing as a function of particle size. Far fewer microgel particles with a diameter of 500 nm will be required to saturate a surface compared with a surfactant of only a few nm in length. The relative hydrophobicity of a particle will influence its wetting properties and its position at the interface. Figure 1.15 illustrates how a predominantly hydrophilic particle will sit more in the water phase than in the air phase, whilst a more hydrophobic particle will favour the air phase. This also indicates how the relative packing density of particles can be influenced not only by size but also by position at the interface according to the area of the air-water interface occupied by a particle.
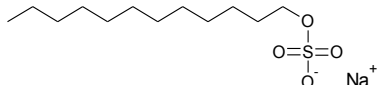
Particles with charged surfaces will experience interparticle repulsion at the interface, again altering packing density and surface tension. The influence of interparticle forces have been detected over relatively large separations, even on the mm scale[7] and therefore direct changes to the surface charge (*e.g.* through changes to particle composition) or indirect influences (*e.g.* the addition of electrolyte) to the solvent may have significant effects on surface tension. The results of this investigation will be evaluated from such perspectives.

4.2 Materials

The behaviour of a range of microgels was investigated at air-water interfaces and compared to that of a classic surfactant, sodium dodecyl sulphate (SDS). The preparation and characterization of the microgels used in this investigation are described in Chapters 2 and 3, whilst details of the SDS, which was used as supplied, are shown in Table 4.1. The poly(NIPAM) microgels are referred to as batches N1–6, whilst the co-polymer microgels

are referred to simply by the co-monomer name, *e.g.* DVE (see Tables 2.4–2.6). Unless otherwise specified, the monomer composition of the co-polymer microgels was 90 % NIPAM and 10 % co-monomer.

Table 4.1 Surfactant details

Name	Structure	Source
Sodium dodecyl sulphate (SDS)		Aldrich, L6026, Lot 101K0036

4.3 Methods

The extent to which the hydrophobically modified microgels are capable of lowering the surface tension at air-water interfaces was investigated using a KRÜSS Processor Tensiometer K100. The KRÜSS standard (Wilhelmy) plate was used to measure surface tension as a function of microgel concentration. The instrument automatically dilutes the initial sample and measures surface tension at pre-determined dilution steps. The sample was automatically stirred after each dilution step and allowed to equilibrate before the mean of five surface tension measurements was taken at each concentration.

Firstly, the effect of the surfactant SDS upon the surface tension of water was measured as a function of SDS concentration at 25 °C and 40 °C, so that the effect of the microgels could later be compared with that of this classic, well-characterized surfactant. For this purpose, a 20 mM stock solution of SDS was prepared and the dilution steps are shown in Table 4.2.

Table 4.2 SDS dilutions studied with KRÜSS Tensiometer

Step	SDS concentration (mM)	SDS concentration (mg L^{-1})
0	20	5768
1	18	5191
2	16	4614
3	14	4037
4	12	3461
5	10	2884
6	8	2307
7	6	1730
8	4	1154
9	2	577

Whilst accurate molar concentrations can be calculated for SDS dilutions, because microgels are the result of polymerization reactions, absolute molecular weights are not known and therefore molar concentrations cannot be determined. Microgel concentrations are conventionally given in terms of % w/v, which can be converted to mg L^{-1} values, as can the SDS molar values. This facilitated comparison of the surface tension measurements for the two different types of system.

An initial investigation of the effect of a small selection of microgels upon the surface tension of water was then undertaken. Measurements were made at 25 °C and 40 °C, *i.e.* temperatures above and below the volume phase transition temperature (VPTT) of each microgel to study the effect of particle conformation upon surface tension. A limited range of microgel concentrations was studied: 0.002–200 mg L^{-1} (Table 4.3).

Table 4.3 Example microgel dilutions studied with KRÜSS Tensiometer

Step	Microgel concentration (% w/v)	Microgel concentration (mg L^{-1})
0	0.020	200
1	0.018	180
2	0.016	160
3	0.014	140
4	0.012	120
5	0.010	100
6	0.008	80
7	0.006	60
8	0.004	40
9	0.002	20

The next step was to investigate the range of dispersion concentrations over which the microgels influence the surface tension of water. The surface tension of dispersions of a selection of microgels was measured over a far wider range of concentrations (*e.g.* 0.0001–5000 mg L^{-1}) to determine where the surface tension lowering effect of microgels begins.

Having determined a suitable concentration range over which to compare the surface tension lowering capacity, the effect of a wide range of microgels at 25 °C was measured. The surface tensions were compared at a set microgel concentration, *e.g.* at 1000 mg L^{-1}. A more detailed investigation into the effect of temperature was then undertaken. The surface tension of a small selection of microgels at a fixed concentration (around 1000 mg L^{-1}) was measured as a function of temperature (from approximately 25–50 °C).

Finally, the surface tension of an undiluted sample of the poly(NIPAM) microgel N4 was measured through several heating and cooling cycles. The Wilhelmy plate was cleaned (by rinsing in deionized water and flaming) at strategic points, *i.e.* a "clean" measurement was made at the start of measurements at a new temperature. In between cleanings, several follow up measurements were made with the "dirty" plate at each temperature.

4.4 Results

4.4.1 Influence of SDS on surface tension

The effect SDS upon the surface tension of water was measured to provide a baseline with which to compare the microgels (Fig. 4.2). The surface tension rapidly decreased from 72-73 mN m^{-1}[16,17] (for pure water) with increasing SDS concentration until a clear critical micelle concentration (CMC) observed, between 1730–2307 mg L^{-1} (6–8 mM) SDS. From this point the surface tension stabilized at 38 mN m^{-1}, with very little difference between the measurements taken at 25 and 40 °C. This compares well with literature values for the CMC of SDS (approximately 8 mM)[16,18] as does the reduction in surface tension achieved with SDS, which is reported to lie around 30–45 mN m^{-1}.[19,20,21]
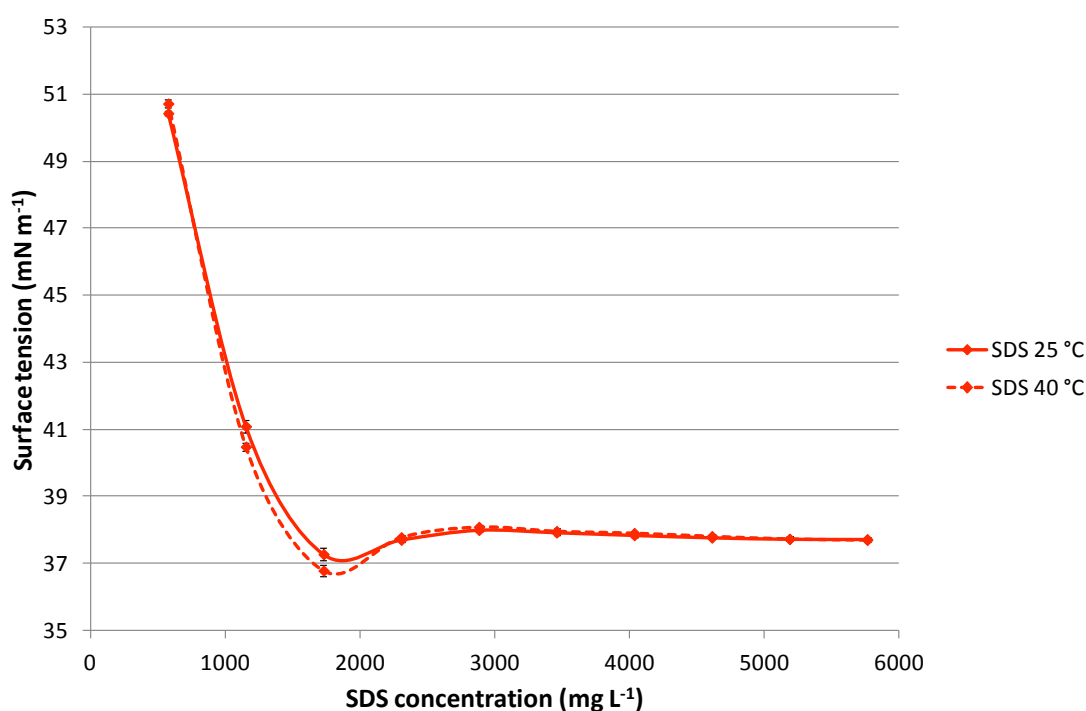
Figure 4.2 Effect of SDS upon surface tension of water at 25 °C and 40 °C (± 1 s.d.)

4.4.2 Influence of microgels on surface tension above and below the VPTT

The effect of a small selection of microgels (N1, V4TBB, DVE and VL) upon the surface tension of water was measured at 25 °C (particles swollen) and 40 °C (particles collapsed) to establish first whether microgels lower surface tension and then, if so, whether the interfacial behaviour is related to size or conformation. Figure 4.3 shows surface tension measurements as a function of microgel concentration at 25 °C and 40 °C. At the lower temperature, the microgels were in the swollen conformation and substantially lowered the surface tension to 41–44 mN m^{-1}. These results show good agreement with a study that found that poly(NIPAM)-based microgels lowered the surface tension of water to values close to those obtained with linear poly(NIPAM), *i.e.* 42 mN m^{-1}.[2]

Slight differences between the effects of individual microgels at 25 °C were apparent. For example, N1 lowered the surface tension to a lesser extent than VL and DVE, which both achieved a similar reduction, whilst V4TBB achieved an even greater reduction. This follows the trend in particle size previously observed (Tables 3.3 and 3.6), where the size of N1 > DVE > VL > V4TBB. The incorporation of a hydrophobic co-monomer appeared to affect the extent to which a microgel is capable of lowering the surface tension of water.
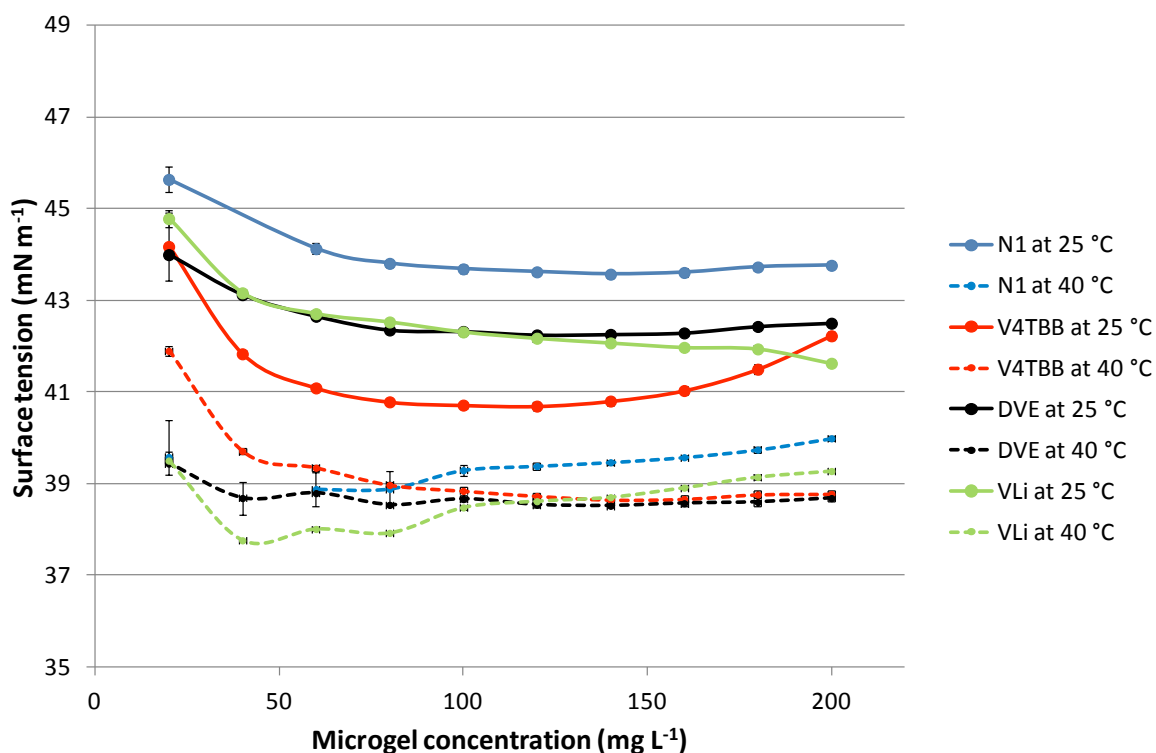
Figure 4.3 Effect of microgels upon surface tension of water at 25 °C and 40 °C (± 1 s.d.)

At 40 °C, all the microgels were in the collapsed conformation (confirmed by particle size and VPTT data, Sections 3.3.2.1 and 3.3.2.2) and lowered the surface tension to an even greater extent, from approximately 69.6 mN m^{-1}[22] (for pure water at 40 °C) to around 39 mN m^{-1} at 100 mg L^{-1} of each microgel. Again, the co-monomer microgels lowered surface tension to a greater extent than homo-polymer N1. However, the pattern of reduction with respect to microgel size was less distinct than at 25 °C and the range of surface tensions observed was much smaller. This suggests that particle size and structure may be important, *i.e.* at 40 °C when there was less variation in particle size (Tables 3.3 and 3.6) the measured surface tensions were far closer than at 25 °C when the variations in particle size and conformation were greater.

There was a significant difference between the effects of SDS and the microgels, which lowered surface tension to a similar extent as SDS (after its CMC), particularly at 40 °C. Most interestingly, however, the microgels achieved this comparable reduction at a significantly lower concentration than SDS. The microgel concentration required to reach this point was as low as 40 mg L^{-1}, compared to more than 1730 mg L^{-1} for SDS. This may reflect the fact that spherical particles are more strongly held at interfaces[13] and therefore may influence the surface tension more rapidly than the surfactant molecules, which are in dynamic equilibrium at the surface.[23]

4.4.3 Concentration of microgel particles required to lower surface tension

Figure 4.3 showed the surface tension of N1 dispersions from around 2–200 mg L^{-1} microgel. Although a slight increase in surface tension became apparent at the lowest microgel concentrations, the measured surface tension ($\approx$ 46 mN m^{-1}) was still substantially lower than that of pure water (72.3 mN m^{-1}),[16,17] suggesting that significant reductions in surface tension might persist at even lower concentrations. Measurements were therefore made to determine the minimum concentration of microgel required to achieve a significant reduction in surface tension at 25 °C. Figure 4.4.a shows the surface tension of N4 dispersions at concentrations from approximately 0.0001–2000 mg L^{-1}. Figure 4.4.b shows the same data but focuses on lower concentrations, from 0–200 mg L^{-1}, to facilitate comparison with Figures 4.2 and 4.3.

As seen in Fig. 4.2, surfactants such as SDS reach a CMC, from which point micellization of surfactant molecules begins and the surface tension takes on an approximately constant

value.[16] Particles such as microgels do not form micelles, but will saturate the surface and thereafter attain an approximately constant surface tension (although some particles increase surface tension at higher concentrations – both with respect to the surface tension of pure water and/or with respect to the surface tension previously reduced at lower particle concentrations).[7,24]
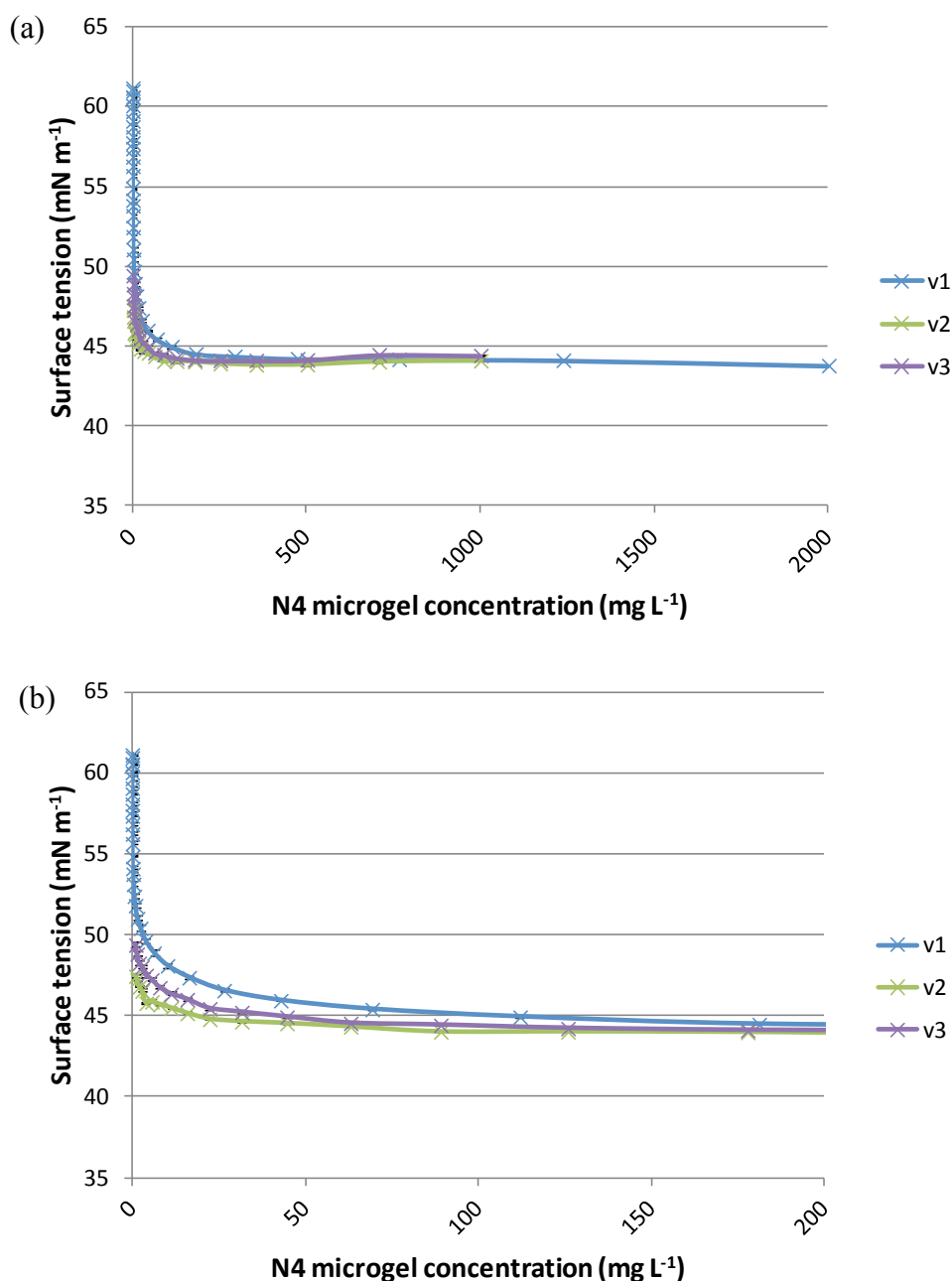
Figure 4.4 Repeat measurements of effect of N4 concentration upon surface tension of water at 25 °C (± 1 s.d.): (a) 0–2000 mg L^{-1} N4; (b) 0–200 mg L^{-1} N4.

Figure 4.4 shows the surface tension of a different poly(NIPAM) batch, N4, over a far wider concentration range. The plateau in surface tension (approximately 44 mN m^{-1}) observed from 40–200 mg L^{-1} N1 in Fig. 4.3 persisted at much higher N4 concentrations, up to at least 2000 mg L^{-1}. It also continued well below 100 mg L^{-1}; even at very low concentrations, *e.g.* 0.0001 mg L^{-1}, the measured surface tension (around 61 mN m^{-1}) was still much lower than that of pure water. Figure 4.5.b shows the region in more detail, confirming that the minimum surface tension (45 mN m^{-1}) was reached at concentrations as low as 25 mg L^{-1}.

In order to confirm that these observations were reproducible between measurements and different batches, the N2 poly(NIPAM) dispersion was re-tested over similar concentration ranges (Fig. 4.5). Although there was more variability between measurements than previously observed, a similar overall trend was apparent, with N2 reducing surface tension to approximately 42–44 mN m^{-1} from around 100 mg L^{-1} microgel. At the lowest microgel concentrations (0–20 mg L^{-1}) the overall trends were the same, *i.e.* the surface tension was substantially reduced even at the smallest microgel concentrations and reductions in surface tension were similar between poly(NIPAM) batches and repeat measurements.
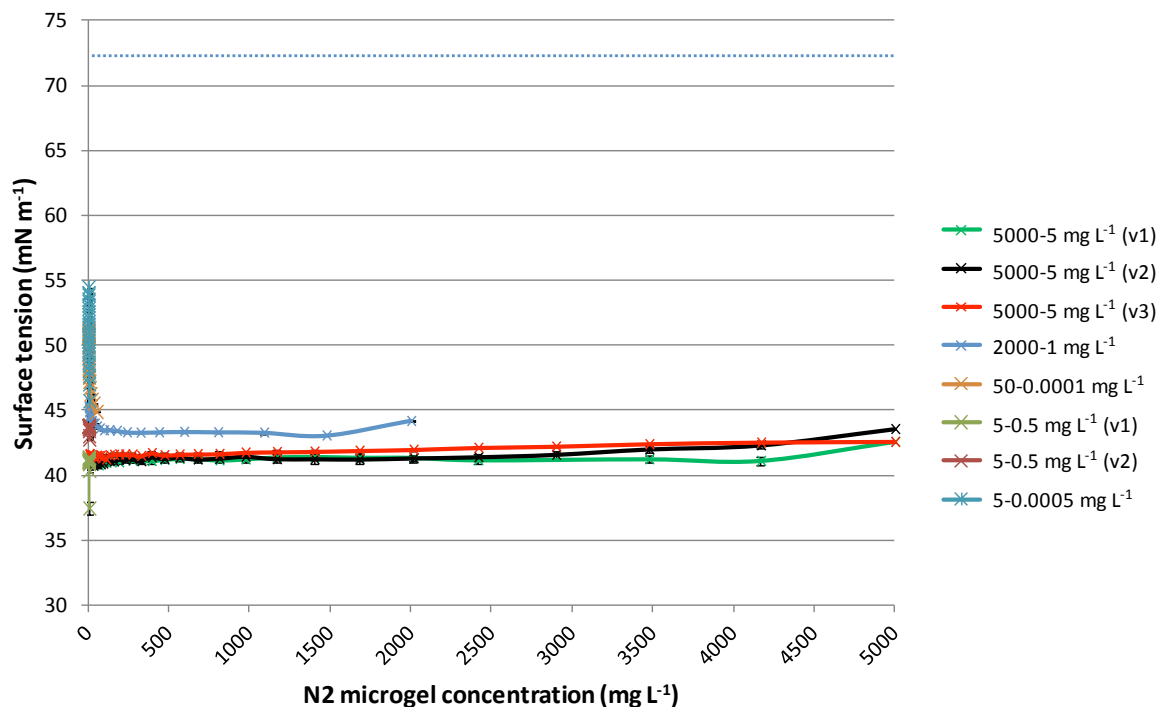
Figure 4.5 Repeat measurements of effect of concentration of N2 upon surface tension of water at 25 °C (± 1 s.d.) Blue dotted line shows approximate surface tension of pure water.

The data presented over the broader microgel concentration ranges (Figs. 4.5 and 4.6) suggests that by 50 mg L^{-1} each microgel dispersion had achieved its maximum reduction in surface tension, which remained constant as the concentration increased further. This suggested that additional increases in microgel concentration may have no further influence upon the dispersion surface tension. A slight increase in surface tension was observed at the highest concentrations of N2 (> 4000 mg L^{-1}) in Fig. 4.5. However, this could be an artefact of the experimental technique, which was observed on several occasions (*e.g.* see Fig. 4.3). Further, it could be related to the phenomenon described for titania suspensions by Dong and Johnson,[7] where an increase in surface tension was observed over a certain increasing concentration range. However, such an increase was frequently observed (data not shown), irrespective of the starting concentration (from which the instrument automatically diluted the sample according to pre-specified steps), which suggests it was more likely to be an effect arising from the technique used. Further investigation at higher concentrations would be required to establish whether a similar effect to that of the titania particles exists.
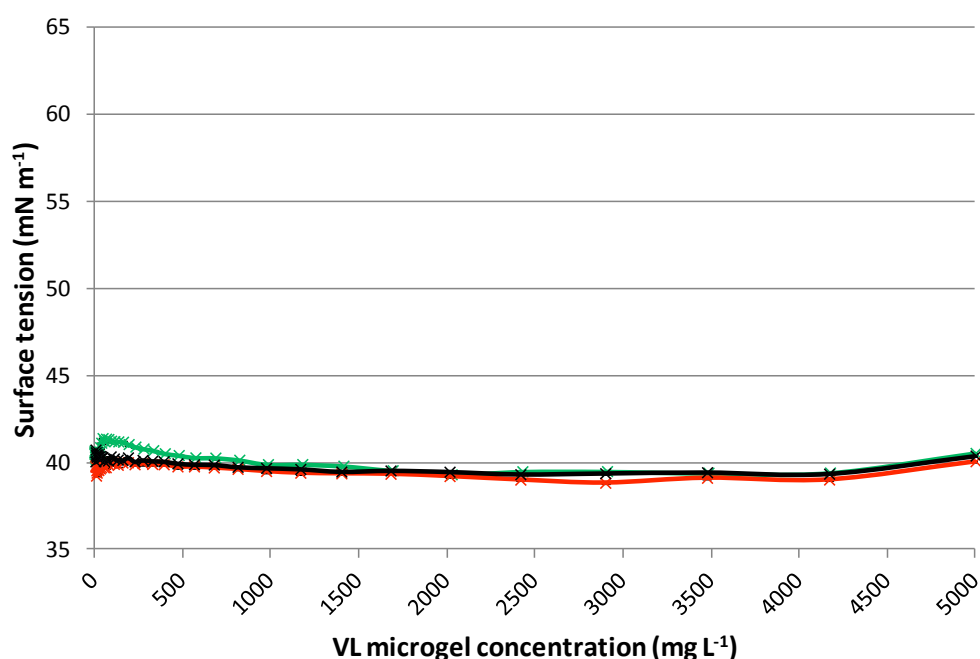
Figure 4.6   Repeat measurements of effect of concentration of VL ($\approx$ 0–5000 mg L^{-1}) upon surface tension of water at 25 °C ($\pm$ 1 s.d.)

Figure 4.6 shows that co-polymer microgels such as VL also achieve a stable minimum surface tension at low concentrations, well below 100 mg L^{-1}. It was therefore concluded that for a comparison of the effects of different co-polymer microgels to be drawn, a surface tension value at 1000 mg L^{-1} would be used.

4.4.4 Effect of co-polymer microgels upon surface tension

A summary of the surface tensions (at 1000 mg L^{-1}) of all the microgels measured at 25 °C (as a function of concentration, usually 1–2000 mg L^{-1}) is given in Table 4.4. The data show that at 1000 mg L^{-1}, each of the co-polymer microgels lowered the surface tension of water to at least a similar extent as the homo-polymer poly(NIPAM) microgels and, in several cases, achieved substantially lower surface tensions. The data for the homo-polymer microgels (N2–6) are plotted in Fig. 4.7.

Table 4.4 Dispersion surface tensions at 1000 mg L^{-1} microgel concentrations at 25 °C

Microgel	Monomer or co-monomer LogP*	Surface tension at data point closest to 1000 mg L^{-1} (mN m^{-1})†		Surface tension at 1000 mg L^{-1} estimated from data plot (mN m^{-1})	D_H at 25 °C* (nm)	Electrophoretic mobility at 25 °C* (10^{-8}m^{2}s^{-1}V^{-1})
N2	0.28	43.4	(1089)	43.3	466	–
N3	0.28	41.5	(820)	41.5	625	-0.32
N4	0.28	44.1	(1237)	44.2	483	-1.11
N5	0.28	44.1	(1130)	44.2	378	-0.91
N6	0.28	43.4	(1089)	43.3	410	+0.62
DVE	6.35	40.1	(974)	40.0	511	-0.81
TBVE	1.74	44.0	(1089)	44.0	526	-1.06
TPVE	2.27	43.9	(1089)	43.8	501	-1.30
VL	6.04	39.9	(984)	39.9	530	-1.28
V4TBB	3.94	40.7	(100)‡	40.7‡	397	-1.63
TMVS	1.58	42.9	(1089)	42.8	542	-1.39
VTMOS	1.95	40.1	(974)	40.0	543	-1.19
TPVS	7.02	43.9	(1089)	43.9	653	-1.32
MAA	0.57	43.5	(1089)	43.6	248	-0.70

* Data from Tables 4.3, 4.5, 4.6, 4.10; † Figures in brackets represent concentration in mg L^{-1} at actual data point; ‡ Data point at 100 mg L^{-1} rather than 1000 mg L^{-1}.

The surface tension values at 1000 mg L^{-1} ranged from 41.5–44 mN m^{-1}. The largest of the poly(NIPAM) microgels, N3 (625 ± 6.6 nm) showed the greatest reduction in surface tension; the other, substantially smaller microgels reduced surface tension to a lesser extent. This is opposite to the conclusion drawn from Fig. 4.3, that the smaller the microgel particle, the greater the reduction in surface tension. However, N3 was synthesized by a different method to that used for the smaller microgels, using a significantly larger ratio of reagents to solvent volume and a far smaller proportion of initiator (Section 2.2.2.3). This suggests that the surface charge may also influence the interfacial properties of a microgel.
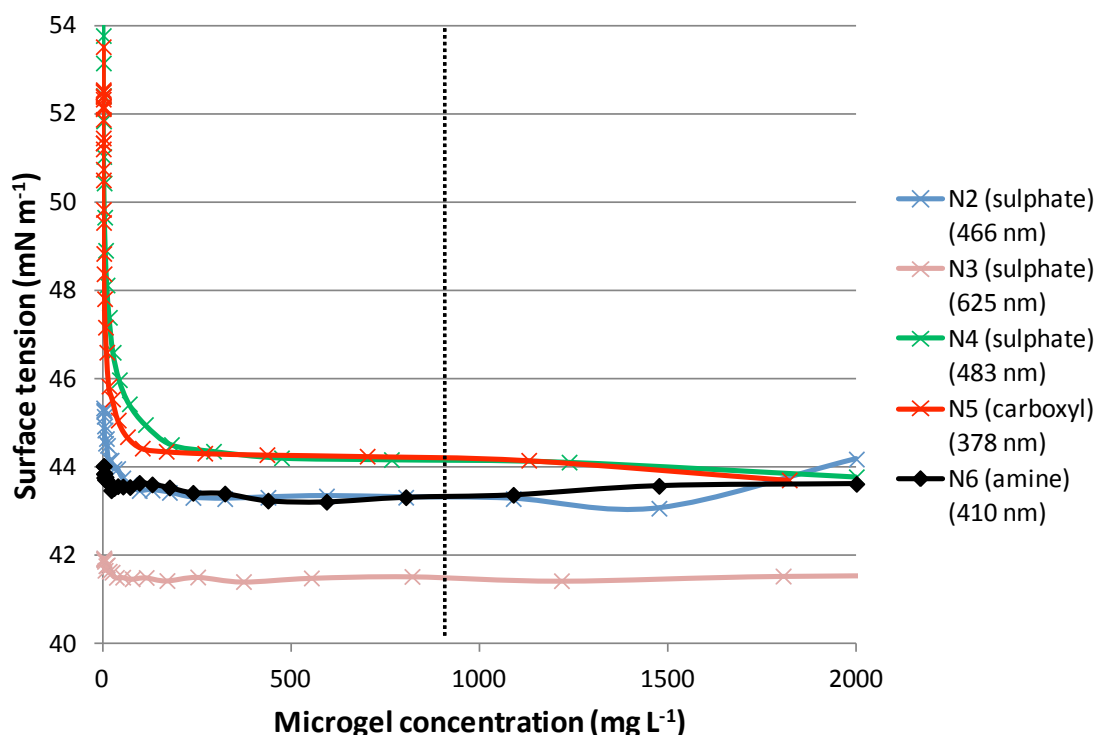
Figure 4.7 Effect of poly(NIPAM) particles upon the surface tension of water at 25 °C

Data points for anionic microgels are denoted × whilst data points for the cationic microgel are denoted by ♦. First set of brackets in legend indicates surface charge group type and second set of brackets shows corresponding particle D_H.

Figure 4.7 may also suggest a possible difference according to charge type for the three poly(NIPAM) microgels synthesized under identical conditions but differing only in initiator used (*i.e.* N4, N5 and N6). The anionically charged (but differently sized) N4 and N5 achieved almost identical reductions in surface tension at all concentrations, but the cationically charged (and intermediately sized) N6 reduced the surface tension by a greater amount. As discussed in Section 3.3.2.3 (Table 3.4) the magnitude of the charge (electrophoretic mobility) of the two anionic microgels was substantially greater (almost double) than that of the cationic microgel, which may also be significant.

4.4.4.1 Potential influence of specific co-polymer microgel characteristics

In order to investigate whether there was any correlation between co-polymer microgel characteristics and the extent of surface tension reduction, the data in Table 4.4 was analysed as a function of particle size and electrophoretic mobility (plots not shown). There was no correlation between particle size and surface tension. This is contrary to the initial findings from Fig. 4.3, where certain co-polymer microgels were found to reduce surface tension to a greater extent than homo-polymer N1. This apparent contradiction may be

explained by the fact that only three co-polymer microgels were tested in Fig. 4.3 and contrasted with a poly(NIPAM) microgel (N1) that was relatively large (579 nm at 25 °C) compared with the other poly(NIPAM) microgels (Table 4.3).

The process was repeated for the electrophoretic mobility data and once again, there was no clear correlation between particle charge and extent of surface tension reduction (data not shown). However, a slight possible trend began to emerge for the homo-polymer microgels (Fig. 4.8). As the magnitude of the charge increased, the dispersion surface charge initially increased before reaching a plateau above 1.0×10^{-8} $m^2s^{-1}V^{-1}$. This suggests that over a certain range, particle charge density might therefore have more influence upon surface tension than particle size. It also is indicative of a far more complex relationship than a simple direct correlation between a single particle characteristic and dispersion surface tension. However, further work is required to clarify the situation.
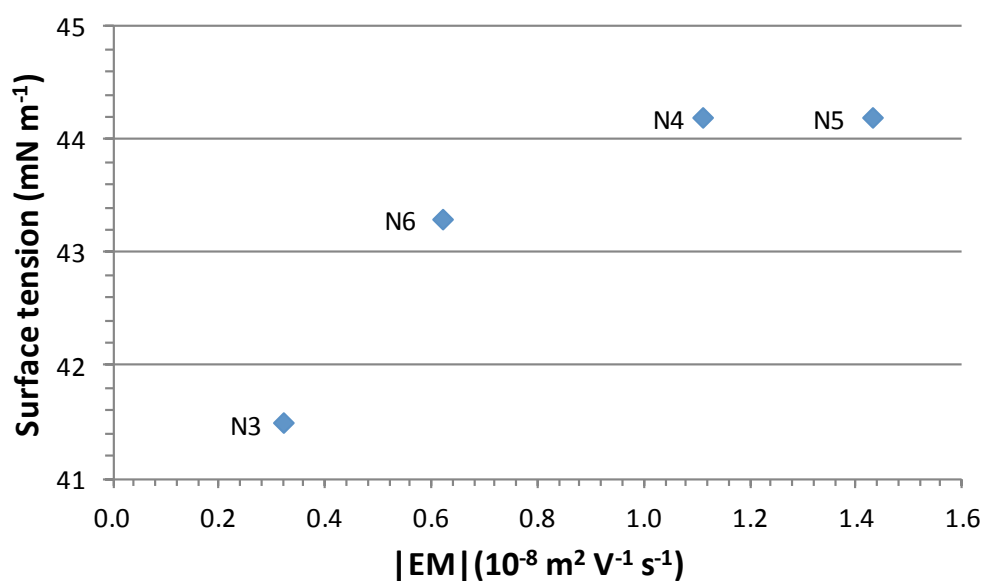
Figure 4.8 Variation in surface tension of 1000 mg L^{-1} poly(NIPAM) microgel dispersions as a function of electrophoretic mobility magnitude

Comparison of the data in Table 4.4 by functional group (*i.e.* vinyl ether/ester/silane) aided investigation of the influence of co-monomer type. All the co-polymer microgels lowered the surface tension of water to at least a similar extent as homo-polymer N2 and at similar particle concentrations. There was very little difference in effect between N2 and the branched chain vinyl ether microgels (TBVE and TPVE), which lowered the surface tension

to around 43–44 mN m^{-1} at 1000 mg L^{-1} microgel. However, the straight chain ether DVE microgel reduced the surface tension by a greater amount (approximately 40 mN m^{-1}). A similar trend was apparent for the vinyl esters, with the straight chain vinyl laurate microgel (VL) lowering the surface tension substantially more than N2 and to a similar extent as DVE, which also contains a linear C$_{12}$ co-monomer. One of the vinyl silane microgels (VTMOS) stood out by lowering the surface tension more substantially than the similarly sized TMVS and the much larger TPVS. As VTMOS was not the largest vinyl silane microgel, the greater decrease in surface tension could not be attributed purely to size differences between the particles and it was likely that another influence was at work, such as co-monomer hydrophobicity, because VTMOS is a more polar molecule than TPVS but similar to TMVS. These observations indicate that the co-monomer structure might be influential, *e.g.* straight chain versus branched chain.
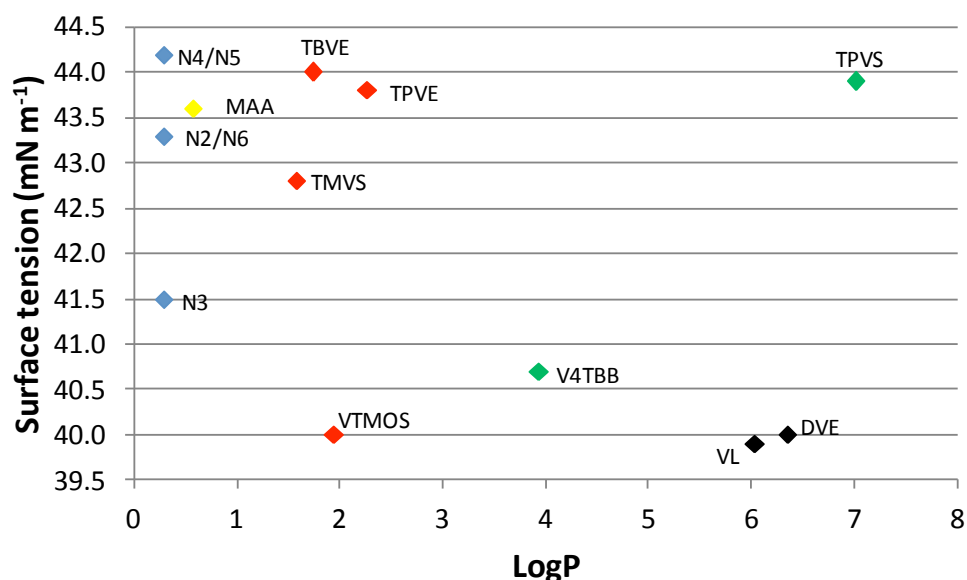
Figure 4.9 Variation in surface tension of 1000 mg L^{-1} anionic microgel dispersions at 25 °C as a function of logP. Co-monomer structure type: ◆ = poly(NIPAM) microgels; ◆ = branched; ◆ = linear; ◆ = aromatic; ◆ = polyelectrolyte. Note: value for V4TBB measured at 100 mg L^{-1} (see Table 5.4).

In order to determine whether co-monomer hydrophobicity might influence surface tension, the data were compared with the co-monomer logP (Fig. 4.9). Although the microgels with co-monomer logP values closest to that of the NIPAM monomer (0.28) generally had surface tensions similar to homo-polymer poly(NIPAM) and two of the microgels with the largest logP values (VL = 6.04 and DVE = 6.35) had the lowest surface tensions, there were several exceptions and no clear correlation between surface tension and co-monomer logP.

Overall, the comparison of surface tension values with particle size, charge and co-monomer hydrophobicity suggests that the extent to which surface tension is lowered depends on a variety of factors and that the interfacial behaviour of co-polymer microgels cannot be correlated with individual particle characteristics. This is because on moving between different microgels, more than one variable may change (*e.g.* size and electrophoretic mobility values are likely to vary). Despite this, however, it is possible that size may have an effect, as discussed below.

4.4.5 Influence of temperature

The results in Section 4.4.3 and 4.4.4 focused on the behaviour of microgels at a temperature below the VPTT (25 °C). However, as previously discussed, surface tension measurements made at 40 °C (Fig. 4.3) indicated that particles in the collapsed conformation caused a more substantial reduction in surface tension and suggested that particle size and structure was significant. In order to investigate this further and study changes through the volume phase transition, more detailed measurements were made as a function of temperature for three microgels (Fig. 4.10).
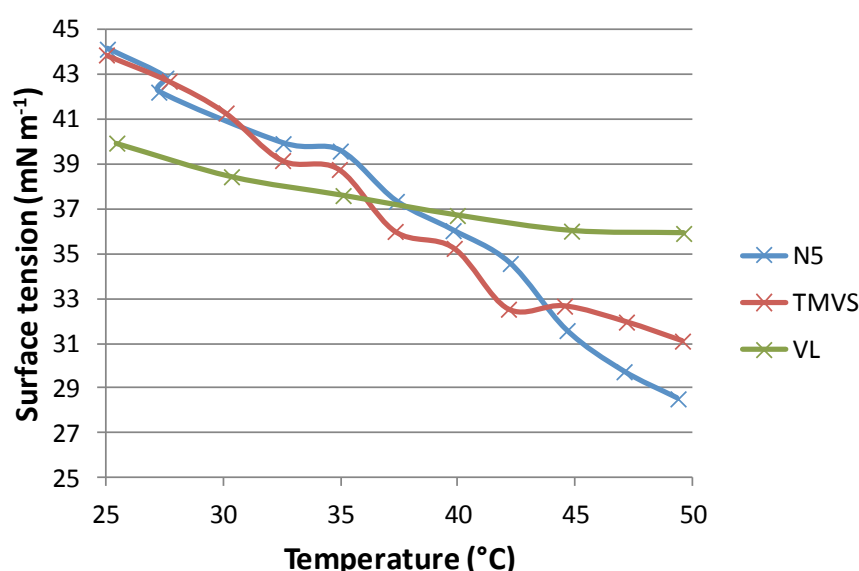
Figure 4.10 Surface tension of microgel dispersions as a function of temperature

A clear and roughly linear decrease in surface tension with increasing temperature was observed for all three microgels. However, the rate and extent of the decrease in surface tension varied between the particles. Although the surface tension of water alone is strongly

influenced by temperature, the change between 25 °C and 40 °C is relatively small, falling from 72.3 mN m^{-1} at 25 °C[16,17] to 67.94 mN m^{-1} at 50 °C[22] (compared to the reductions in surface tensions of up to 12 mN m^{-1} observed for microgel N5 in Fig. 4.10). This indicates that the reduction observed for the microgel dispersions over this temperature range cannot simply be due to changes in solvent surface tension and other factors must be influential.

For example, the homo-polymer N5, with the lowest hydrophobicity (estimated from logP values, Table 4.4) showed the greatest overall decrease in response to temperature, whilst co-polymer VL, with the greatest hydrophobicity showed the least response to temperature. The particle with the greatest hydrophilicity will participate in the greatest amount of hydrogen bonding with the solvent and therefore may be more susceptible to temperature, suggesting that particle hydrophobicity influences the extent to which it will lower surface tension.

The extent of de-swelling, measured by the de-swelling ratio (α, see Table 3.7) also corresponds with the response of surface tension to temperature. The homo-polymer N5 exhibited the smallest extent of de-swelling ($\alpha = 0.21$) but the greatest reduction in surface tension from 25–50 °C. As the extent of de-swelling increased (N5 < TMVS < VL), the relative reductions in surface tension decreased (N5 > TMVS > VL). This is evidence that the size/volume of the particles is significant and this effect may be explained by alterations in the packing density of the particles at the surface. Once again this is likely to be related to extent of hydrogen bonding and the decrease in solvent quality as temperature increases.

Interestingly, the trends appeared to relate to a cross-over point lying between 30–36 °C, *i.e.* around the microgel VPTTs (Tables 4.4 and 4.9). For example, below the VPTT (*e.g.* at 25 °C), the particles with the lowest hydrophobicity and greatest charge (N5) had the least effect upon surface tension, whilst the particle with the greatest hydrophobicity and lowest charge (VL) had the greatest effect upon surface tension. Above the cross-over point and above the VPTT (*e.g.* at 50 °C), the influence of the particles was reversed. The VL particles now had the greatest charge but the least effect upon surface tension, whilst N5 had the smaller charge but greater effect upon surface tension. These results indicate that the various factors contributing to the capacity of a particle to lower surface tension are significantly influenced by temperature and particle conformation and charge. It also suggests that whilst the difference between particles may be less above the VPTT, there is still a difference between them relating to size, charge and hydrophobicity. Monteux *et al.*[5]

observed that the interfacial tension of poly(NIPAM-*co*-dimethylamino ethyl methacrylate) microgels at dodecane-water interfaces decreased at low temperatures then increased at higher temperatures, reaching a minimum around the VPTT. This is different to the behaviour shown in Fig. 4.10. Monteux *et al.* also proposed that aggregates of microgel particles form above the VPTT and aid destabilization of emulsions rather than desorb from the interface.

The influence of repeated heating and cooling cycles upon the surface tension of the homo-polymer N4 microgel is shown in Fig. 4.11. Measurements of the surface tension of the sample were made at room temperature (RT) (below VPTT), then above the VPTT and during cooling back to RT. The sample was then reheated and cooled once more. The objectives were twofold: first to determine whether decrease in surface tension observed upon heating was reversible; and second whether the cleanliness/dirtiness of the plate was influential. As it is possible that particles might remain adhered to the plate following a measurement and therefore represent contaminants for subsequent measurements, at each temperature the plate was cleaned prior to the first measurement (denoted by "clean" in Fig. 4.11), then several repeat measurements were made without cleaning (average denoted by "dirty" in Fig. 4.11). The data demonstrates that the fall in surface tension with increasing temperature observed in Fig. 4.3 and 4.10 is reversible. The reduction in surface tension observed when a microgel is heated above its VPTT is reversible upon re-cooling and through several heat and cool cycles.

Looking firstly at the "clean" data (blue bars) in Fig.4.11 (in which cleaning of the plate between measurements ensured that no particles or other contaminants remained adhered to the plate) the reversible effect is apparent, with a substantial reduction in surface tension observed each time the microgel is heated above the VPTT. However, the RT measurements following a heating cycle do not return to the original RT values, *i.e.* the difference between the heating and cooling values decreases as the number of cycles increases. As is also clear from Fig. 4.10, the dispersion surface tension appears very sensitive to small changes in temperature. Further work is required to follow heating and cooling cycles more accurately, but this initial data does suggest that the additional reduction in surface tension observed when the microgels are heated above the VPTT is a reversible, repeatable process.
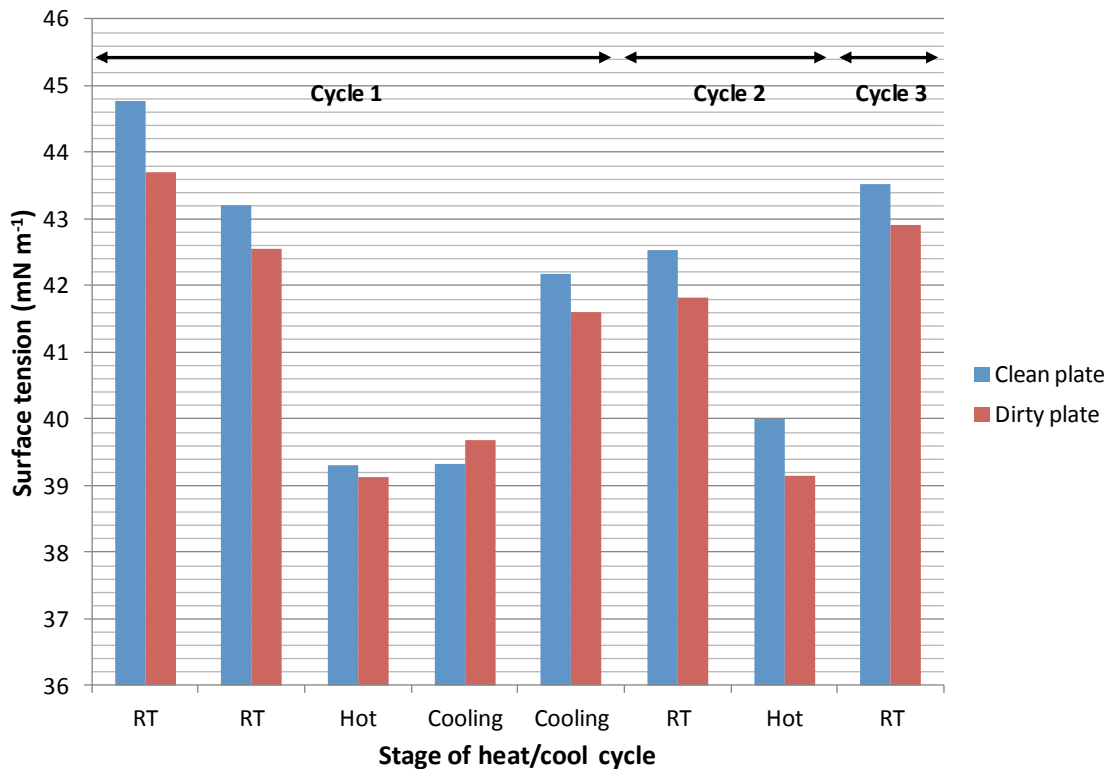
Figure 4.11 **Variation in surface tension of undiluted N4 microgel dispersion through several heating and cooling cycles, showing difference between "clean" and "dirty" plate**

Each data point represents cumulative average surface tension at 15th of 30 repeat measurements. RT = room temperature (approximately 25 °C); HOT = temperature above VPTT (at least 40 °C); COOLING = temperature falling from HOT back to RT; clean = Wilhelmy plate cleaned prior to specific measurement; dirty = Wilhelmy plate not cleaned between repeat measurements at same temperature.

In order to establish the significance of the extent of cleanliness of the Wilhelmy plate during measurements, Fig. 4.11 compares the average surface tension measurements made with a clean plate (rinsed in deionized water, flame dried then allowed to cool) (blue bars) with the average of several repeat measurements at the same temperature made without further cleaning the plate (red bars). In all but one case, the surface tension measurements at a particular temperature made with the clean plate are higher than the following repeat measurements made with the "dirty" plate. This suggests that the cleanliness of the plate is significant. The variation in values at a particular stage of the heat/cool cycle may also be influenced by variations in temperature, *e.g.* the rapid cooling of the sample following the first HOT measurement. Repeat measurements with more accurate temperature control would help clarify this.

4.5   Discussion

The results suggest that the surface tension of water is lowered in the presence of microgel particles and that this is influenced by a range of parameters including particle size, charge, conformation and co-monomer type. Temperature in particular shows an effect and because particle conformation varies above and below the VPTT, particle size, conformation and interactions with the solvent are likely to be relevant factors. However, no correlations between individual co-monomer characteristics (*e.g.* size, electrophoretic mobility or logP) were found, although there was a suggestion that size and in particular charge are influential. However, before these are considered in more detail, the question of whether or not it is the microgel particles themselves that are causing the reduction, rather than impurities or changes inherent to the solvent, must first be addressed.

As already alluded to in the introduction to this chapter, there is some debate as to whether particles are capable of lowering surface tension. Indeed there are several alternative mechanisms by which the surface tension of the microgel dispersions could be lowered. For example, surface tension measurements are extremely sensitive to the presence of contaminants, which could originate from either insufficient dialysis/cleaning of the dispersions following synthesis or contamination from the atmosphere (*e.g.* dust particles) during measurements. Alternatively, the microgel particles could adhere to the Wilhelmy plate, altering the contact angle made between the plate and the surface and therefore resulting in anomalous surface tension measurements (see Equation 1.14).

Although the microgels tested in this study were carefully dialysed against distilled water (Section 2.2.2.1) it is possible that some contaminants left over from the synthesis reaction may still be present. More extensive dialysis over longer periods and additional cleaning processes (*e.g.* centrifugation) may help ensure the microgel dispersions are free of contaminants.[6,25] Great care was taken during measurements to ensure the cleanliness of the equipment used and limit the exposure of the samples to the atmosphere, however, this remains a potential source of contaminants.

Nevertheless, the data presented in Fig. 4.11 offers an initial insight into whether the microgel particles adhere to the Wilhelmy plate during measurements. It is clear from the difference between the "clean" and "dirty" values at each temperature in Fig. 4.11 that the

surface tension readings for the N4 dispersion were reduced when repeat measurements were made without cleaning the plate. However, the difference between the "clean" and "dirty" values in each case was less than 1 mN m^{-1}. This is a small change compared to the overall reduction in surface tension from that of pure water (more than 72 mN m^{-1}) to that observed for the microgel dispersion (39–45 mN m^{-1}). Although some particle adherence to the plate appears to be occurring, it is highly unlikely that it accounts entirely for the overall reduction in surface tension.

These results are preliminary and further work is required to explore the findings fully. Several simple experiments would be informative but have not been achievable within the timeframe of this project. For example, pendant drop-shape analysis would permit the measurement of dispersion surface tension without the presence of a probe to which particles may adhere and could therefore confirm whether or not plate contamination substantially interferes with the results. Furthermore, measurement of the surface tension of the supernatant dispersion medium (containing no particles) following centrifugation should determine whether the particles are driving the reduction in surface tension. In the mean time, however, these preliminary findings suggest that the microgel particles do demonstrate some interfacial activity and appear to reduce the surface tension of water. The following discussion will focus on the results from this perspective.

Although no clear correlations between individual particle characteristics and surface tension values were found, a few general tendencies began to emerge from the data. For example, particle charge (electrophoretic mobility) appeared to correlate slightly with the surface tension of homo-polymer poly(NIPAM) dispersions (Fig. 4.8), the largest poly(NIPAM) (N3) had the lowest surface tension (Fig. 4.7) and the linear co-monomer ether and ester (DVE and VL) produced particles that lowered surface tension more than N2 or the branched chain co-monomer microgels (*e.g.* TBVE and TPVE).

A key objective of this section of work was to determine whether hydrophobic modification with 10 % w/w of a range of co-monomers would alter the interfacial behaviour of the microgel dispersions. However, the results suggest that the co-monomers at this inclusion ratio (in the presence of 10 % w/w cross-linker and 10 % w/w initiator) is not enough to substantially alter the surface tension reducing capacity of the particles. As seen in previous chapters, at 10 % co-monomer inclusion, it is the 90 % NIPAM that governs the behaviour

of the resulting microgel. It is therefore possible that different NIPAM/co-monomer/cross-linker/initiator compositions would give different results and future work would explore this further. At this stage, however, it can be concluded that although co-polymerization with 10 % co-monomer of any type does modify the surface activity of poly(NIPAM)-based microgels to at least a small extent, it is not possible to discern clearly substantial differences between specific co-monomer types and characteristics.

Nevertheless, returning to the analysis of the 10 % w/w co-monomer, these results do suggest that the relationship between particle characteristics and surface activity are very complex, particularly as additional influences such as solvent quality and dispersion temperature must be taken into account. Collectively a wide range of factors will impact upon aspects such as particle position and packing at the interface and therefore have the scope to influence surface tension.

For example, Fig. 4.3 clearly shows that at 40 °C (above the VPTT), the particles reduced the surface tension of water further than at 25 °C. Whilst this could be simply an effect of particle size, with smaller particles having a greater effect than larger particles, it could also be affected by related properties:

- Microgel particle structure is very different below (swollen, soft, porous, network-like structure) and above (collapsed, latex-like hard structure) the VPTT. These conformational differences significantly alter polymer-solvent interactions and it is possible that the interface could be more favourable for the swollen, solvent-filled particles,[26] which have more in common with the solvent phase than when in the collapsed conformation.

- At 40 °C, due to particle collapse and increased polymer-polymer hydrophobic interactions, the hydrophobic nature of the particles increases, potentially influencing particle positions at the interface, *i.e.* changing the contact angle (Fig. 1.15).

- Increased temperature also makes water a poorer quality solvent for poly(NIPAM)-based microgel particles, due to hydrogen bond disruption. Therefore water at 40 °C might become a slightly more favourable solvent for the hydrophobically modified co-polymer microgels than for the more hydrophilic homo-polymer poly(NIPAM), subsequently impacting their relative positions at the interface.

- The charge density of the particles increases dramatically as the particles pass through the volume phase transition, which is likely to increase inter-particle repulsion and separation at the interface, possibly facilitating deformation and decreasing surface tension.

- The origin of the charge type (from the initiator) and the co-monomer used clearly influence particle characteristic such as size and electrophoretic mobility, and the co-monomer also alters the relative hydrophobicity of the particles (Chapter 3).

Studies of other particle types, *e.g.* silica and polystyrene spheres, have identified clear relationships between parameters such as particle size and surface tension.[7,24] However, due to their extreme sensitivity to environmental influences such as solvent quality and temperature, less is known about the behaviour of hydrophobically modified microgel particles, which may not be as straightforward as for other particle types. For example, would other particle types of comparable size achieve similar reductions in surface tension? Or is particle composition a more significant influence than absolute size?

Okubo[24] systematically studied the surface tension of silica and polystyrene sphere dispersions as a function of particle size and concentration. The more polar silica spheres were shown to have only a small effect on surface tension ($\Delta\gamma \approx 2$ mN m^{-1}), which was virtually independent of particle size or concentration. However, the more hydrophobic polystyrene spheres had a more substantial effect ($\Delta\gamma \approx 20$ mN m^{-1}), particularly for particles of 100–200 nm diameter and at high particle concentrations. From these results alone, it is clear that particle size alone cannot be the only driver of surface tension. Okubo attributed the differences between silica and polystyrene to the differences in their surface properties.

The results for the microgels display several striking differences to polystyrene and silica. Firstly, they achieved substantially greater reductions in surface tension ($\Delta\gamma \approx 30$ mN m^{-1}). Secondly, the silica and polystyrene particles had comparatively negligible effect when particle diameter exceeded 200 nm, but far larger microgel particles substantially reduced surface tension, *e.g.* the N3 dispersion (1000 mg L^{-1} at 25 °C) had a particle size of 625 nm and lowered the surface tension to 41.5 mN m^{-1} (Table 4.4).

Thirdly, the concentration of particles required to reduce surface tension differed substantially. Okubo noted the onset of reduced surface tension tended to occur from volume fractions in the range of $x = 0.001$–0.01, with a subsequent increase in surface

tension observed at higher particle concentrations, which has also been observed for other colloidal dispersions.[7,24] Figure 4.4.b shows that poly(NIPAM) particles induced large reductions in surface tension at particle concentrations as low as 0.0001 mg L^{-1} (equivalent to a tiny volume fractions of $x = 1 \times 10^{-8}$). Whilst microgel particles show a concentration effect, it appears far broader and further work is required to determine whether an increase in surface tension would occur at higher concentrations.

Fourthly, up to 100 nm diameter, Okubo's polystyrene particles showed increasing surface activity (and therefore decreasing surface tension) with increasing particle size. However, from 100–200 nm the reverse was true, with surface tension increasing with increasing particle size, reaching a plateau above 200 nm. There was no such trend for the microgels.

Finally, it could therefore be anticipated that the behaviour of the two sets of particles might show greater similarities when the microgels are in the collapsed conformation but in fact the opposite is true, with the collapsed microgels showing even greater reductions in surface tension at 40 °C. There is no straightforward explanation for this but it is likely to be related to the extreme sensitivity of microgel particles to changes in environmental conditions. One possible mechanism might be related to the postulated adsorption of aggregates of poly(NIPAM-*co*-dimethylamino ethyl methacrylate) particles at dodecane-water interfaces above the VPTT, which may promote coalescence of the emulsion.[5]

These observations indicate that a reduction in surface tension cannot simply be a function of the particle size. If it were, dispersions of silica, polystyrene and poly(NIPAM) particles of the same size would have similar surface tensions. This is further evidence of the potential significance of surface charge. The data in Fig. 4.4 and Table 4.4 showed that the co-polymer microgels (at 1000 mg L^{-1}) tended to have slightly lower surface tensions that the homo-polymer poly(NIPAM) microgels. However, in several cases the difference was slight and overall the greatest difference was just 4 mN m^{-1}. This again suggests that hydrophobic modification with just 10 % co-monomer has little effect upon the surface tension reducing properties of microgels when considered in isolation. A combination of factors is likely to be responsible.

However, as shown in Chapter 3, the incorporation of a hydrophobic co-monomer did influence physico-chemical characteristics such as size and charge, and therefore might be

indirectly having an effect upon surface tension. A simple investigation of the potential influence of combined characteristics was therefore made to investigate whether any relationships between combinations of particle characteristics could be identified. The surface tension values were roughly grouped by relative size (small/large), electrophoretic mobility (low/high) and logP (hydrophilic/hydrophobic). In attempt to view the effect of size, charge and hydrophobicity together, a schematic representation of the average surface tension in each category was drawn up (Fig. 4.12).
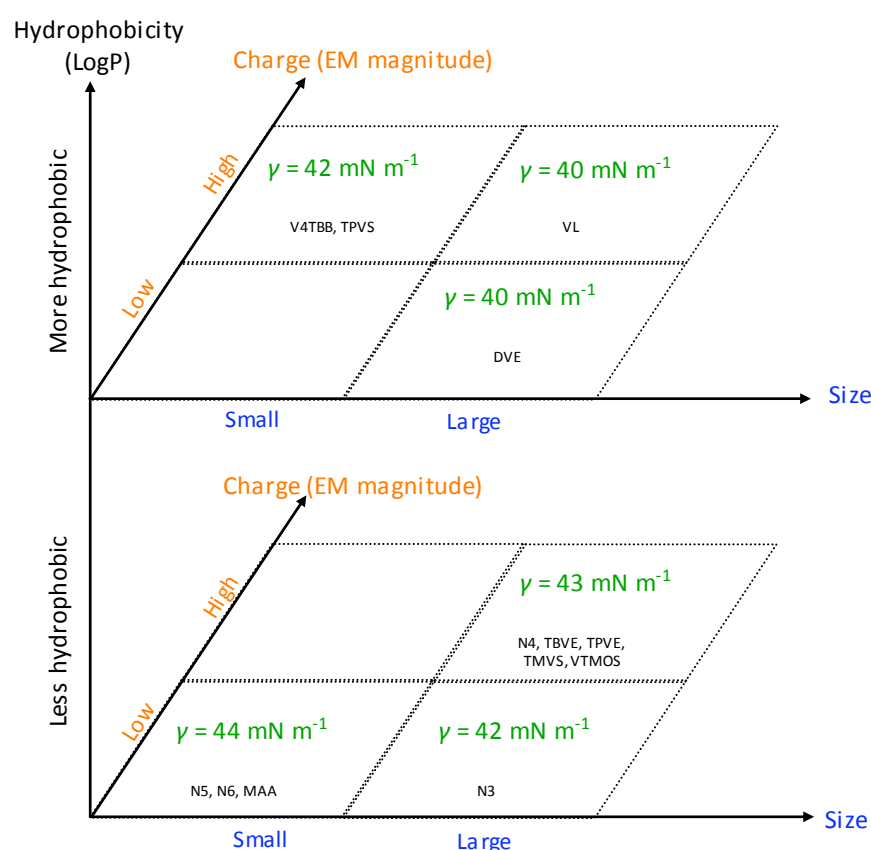
Figure 4.12 Schematic representation of average surface tension (at 25 °C) categorized by size, charge and hydrophobicity

This suggested that the greatest reductions in surface tension were observed for large, more hydrophobic particles of any charge. Smaller reductions were seen for hydrophilic particles, with larger particles, particularly those with low charge, achieving greater reductions in surface tension. Interestingly, a tendency for structurally similar co-monomers to have similar effects is apparent: the aromatic V4TBB and TPVS form one group (42 mN m^{-1}), whilst the linear DVE and VL form another (40 mN m^{-1}) and the branched chain TBVE, TPVE, TMVS and VTMOS are also clustered together (43 mN m^{-1}).

Clearly the relative differences in surface tension between the groups are small and the groups are arbitrary, so at best this approach only gives an indication of general trends and further work is required to quantify the relationships. However, it may give an indication where patterns might emerge from the data. For example, particle size and charge magnitude appear to be possibly more influential for the hydrophilic microgels, compared to the hydrophobic microgels, which may be more effective at lowering surface tension irrespective of size or charge.

The results have shown that most of the co-polymer microgels tended to lower surface tension to a greater extent than the homo-polymer poly(NIPAM) microgels. Poly(NIPAM) is considered predominantly hydrophilic and therefore is likely to favour the aqueous phase at the interface. By comparison, due to the less hydrophilic nature of the co-polymer microgels, their position at the interface is likely to reflect a balance of a greater tendency to be favour the air phase with the slight reduced tendency to reside in the aqueous phase. As a consequence, the contact angle of the co-polymer particles is likely to be greater than for the poly(NIPAM) microgel particles and therefore the area of the air-water interface occupied by the particles will vary, possibly influencing the packing density of the particles.

However, likely to be of more significance to the packing density are the relative size and charge of the particles. In terms of simple geometry, it is possible to pack a greater number of small particles into a given surface area than larger particles. However, the charged surface of the microgels will lead to interparticle repulsion, which will increase as surface charge increases and lead to less dense packing at the surface. So packing density can alter as a function of contact angle, particle size and particle charge. As the number of particles at the interface increases, the number of interparticle forces (*e.g.* attractive capillary forces) increases, in turn increasing the amount of work required to change the surface area and resulting in an increase in surface tension.[7] An interface saturated with a large number of small particles could be considered more resilient to deformation than the same interface being packed with a smaller number of large particles. It has been shown that poly(NIPAM) microgels form multilayers within the aqueous phase of an octanol-water emulsion, which increases surface cohesiveness and stability against coalescence.[6] Alternatively, an interface saturated with poly(NIPAM) particles of electrophoretic mobility that is above a certain threshold (greater than 1.0×10^{-8} m^2 V^{-1} s^{-1}) may be more resilient to deformation than the same interface packed with particles of lower charge electrophoretic

mobility (and therefore lower charge density), altering the balance between interparticle repulsions and the attractive capillary forces that arise from the electric-field driven surface deformations (Section 4.1).

Another factor to be taken into account is the relative solvent content of the particles. At 25 °C water is a better solvent for the more hydrophilic poly(NIPAM) particles than the less hydrophilic co-polymer microgels, so hydrogen bonding between the microgel polymer chains and the solvent is likely to be reduced. Particles interacting more favourably with (and containing more) solvent may be less likely to move to the interface and reduce surface tension, which could be another reason for the greater reductions in surface tension observed for the co-polymer microgels.

The trend of decreasing surface tension with increasing temperature (Fig. 4.10) supports this because as the temperature increases, hydrogen bonding is disrupted and water becomes a poorer solvent for the particles. This may encourage particles to migrate to the surface, resulting in the greater reductions in surface tension observed above the VPTT. Furthermore, the magnitude of the response of the microgel particles in Fig. 4.10 to increasing temperature reduced as the relative hydrophobicity of the particles increased (estimated by co-monomer logP), *i.e.* the more hydrophilic N5 showed a greater response to the falling solvent quality than the more hydrophobic TMVS and the even more hydrophobic VL.

The reduction in surface tension with temperature cannot simply be attributed to changes in surface tension of water alone: whilst this does decrease with temperature, the change in surface tension of water between 25 °C and 40 °C is less than 5 mN m^{-1}[22] but as previously shown the microgel dispersions had surface tensions around 30 mN m^{-1} less than pure water. Similarly, due to the fact that microgel particles undergo a volume phase transition, the fall in surface tension with increasing temperature cannot be solely explained by solvent quality due to the fact that the particles occupy substantially smaller volumes above the VPTT, which, as already discussed, will influence packing density. However, as the volume phase transition is driven by changes in polymer-solvent interactions, these two aspects are closely related.

It is interesting that although the changes in surface tension observed on heating were reversible on re-cooling, the dispersion did not reach the original room temperature values after a heat/cool cycle (Fig. 4.11). This may be related to the clear temperature sensitivity

of the particles (Fig. 4.10) and the lack of accurate temperature recording in Fig. 4.11, *i.e.* the room temperature and temperatures above the VPTT may not have been entirely consistent and a small temperature change can make a big difference. However, it could also be related to particle packing density. During the initial room temperature measurements, the interface is likely to have been saturated with swollen microgel particles. On heating, these particles will have collapsed and reduced in diameter, creating space at the interface for additional particles. As described by Equation 4.2, the particles are effectively irreversibly adsorbed to the interface and therefore when cooled, although the particles re-swell, they are likely to all remain adsorbed to the interface. If true, this could result in additional deformation of the surface which in turn would result in lower surface tension values, hence explaining why the dispersion does not return to the original RT values. The collapse of the hairy layer (and subsequent loss of steric repulsion) upon heating may also be influential. Investigation of the influence of core-shell polystyrene-poly(NIPAM) particles might be informative in this regard.

As outlined in Chapter 1, microgels have many potential applications, which include acting as stimuli-responsive stabilizers for emulsions[3,4] and waste water purification.[27,28,29] In areas of industrial application such as these, understanding of the attachment and detachment of colloids to interfaces, including their influence upon surface tension, is important.[30] An increased understanding of the relationship between microgel properties and interfacial behaviour should enable the design of microgel particles tailored to influence specific interfaces under particular environmental conditions. The results presented in this chapter represent a first step towards this.

4.6   Summary

Microgel particles appear to lower the surface tension of water to a similar extent as the surfactant SDS but at a far lower concentration. The reduction in surface tension is greater than that which has been observed for other particles such as polystyrene and silica spheres and also occurs from lower particle volume fractions. Hydrophobic modification of the microgel particles appears to increase the extent to which the surface tension is reduced. However, it is not possible to predict the influence of hydrophobic modification upon surface tension at 10 % co-monomer inclusion in a controllable way at present.

The apparent decrease in surface tension is not simply a function of individual properties such as particle size; instead it seems to result from a combination of influences including particle size, charge, hydrophobicity and conformation, solvent quality and dispersion temperature. In general, the greater the hydrophobicity of the particles (estimated from co-monomer logP), the greater the reduction in surface tension, irrespective of size or charge; the role of size and charge appear to be more significant for hydrophilic particles. Temperature has a clear effect upon microgel dispersion surface temperature, with swollen particles below the VPTT reducing surface tension less than collapsed particles above the VPTT. Once again, there appears to be significant combined influences of size, conformation, charge and hydrophobicity upon this effect. Further work is required to establish unequivocally whether microgel particles lower surface tension and then to more precisely determine these influences and establish how microgels of specific composition and properties can be designed to influence surface tension in a particular way.

4.7   References

[1] Zhang, J., Pelton, R. (1999) *Langmuir*, **15**(23), 8032–8036.

[2] Zhang, J., Pelton, R. (1999) *Colloids and Surfaces A: Physicochemical and Engineering Aspects*, **156**, 111–122.

[3] Brugger, B., Rütten, S., Phan, K.-H., Möller, M., Richtering, W. (2009) *Angewandte Chemie*, **121**, 4038–4041.

[4] Brugger, B., Rosen, B. A., Richtering, W. (2008) *Langmuir*, **24**(21), 12202–12208.

[5] Pelton, R. (2000) *Advances in Colloid and Interface Science*, **85**, 1–33.

[6] Monteux, C., Marlière, C., Paris, P., Pantoustier, N., Sanson, N., Perrin, P. (2010) *Langmuir*, **26**(17), 13839–13846.

[7] Zhang, J., Pelton, R. (1999) *Langmuir*, **15**(17), 5662–5669.

[6] Destribats, M., Lapeyre, V., Sellier, E., Leal-Calderon, F., Schmitt, V., Ravaine, V. (2011) *Langmuir*, **27**(23), 14096–14107.

[7] Dong, L., Johnson, D. (2003) *Langmuir*, **19**, 10205–10209.

[8] Kralchevsky, P. A., Nagayama, K. (2000) *Advances in Colloid and Interface Science*, **85**, 145–192.

[9] Dong, L.C., Johnson, D. T. (2003) *Journal of Dispersion Science and Technology, Special Issue – 77th Colloid and Surface Science Symposium*, **25**(5), 575–583.

[10] Eastoe, J. (2005) 'Surfactant Aggregation and Adsorption at Interfaces'. In: Cosgrove, T. (Ed) *Colloid Science: Principles, Methods and Applications*. Oxford: Blackwell, pp 50–76.

[11] Kralchevsky, P. A., Danov, K. D. (2010) 'Interactions between particles at a fluid interface'. In: Starov, V. M. (2010) *Nanoscience: Colloidal and interfacial aspects, Surfactant Science Series*, **147**, 397–435.

[12] McGorty, R., Fung, J., Kaz, D., Manoharan, V. N. (2010) *Materials Today*, **13**(6), 34–42.

[13] Binks, B. (2002) *Current Opinion in Colloid and Interface Science*, **7**, 21–41.

[14] Binks, B. P., Dyab, A. K. F., Fletcher, P. D. I. (2007) *Physical Chemistry Chemical Physics*, **9**, 6391–6397.

[15] Horozov, T. S., Binks, B. P. (2005) *Colloids and Surfaces A: Physiochemical and Engineering Aspects*, **267**, 64–73.

[16] Holmberg, K., Jönsson, B., Kronberg, B., Lindman, B. (2003) *Surfactants and Polymers in Aqueous Solution* (2nd Ed). Chichester: Wiley.

[17] KRÜSS GmbH (2006) *Laboratory Desktop* 3.1.1.2623 [software]. Hamburg: KRÜSS GmbH.

[18] Esposito, C., Colicchio, P., Facchiano, A., Ragone, R. (1998) *Journal of Colloid and Interface Science*, **200**, 310–312.

[19] Xu, Q., Nakajima, M., Ichikawa, S., Nakamura, N., Roy, P., Okadome, H., Shiina, T. (2009) *Journal of Colloid and Interface Science*, **332**(1), 208–214.

[20] Gurkov, T. D., Dimitrova, D. T., Marinova, K. G., Bilke-Crause, C., Gerber, C., Ivanov, I. B. (2005*) Colloids and Surfaces A: Physicochemical and Engineering Aspects*, **261**, 29–38.

[21] Wantke, K, -D., Fruhner, H., Örtegren, J. (2003) *Colloids and Surfaces A: Physicochemical and Engineering Aspects*, **221**, 185–195.

[22] Lide, D. R. (Ed) (1992) *CRC Handbook of Chemistry and Physics* (73rd Ed.) Boca Raton: CRC Press.

[23] Morrison, I., Ross, S. (1992) *Colloidal dispersions: suspensions, emulsions and foams*. New York: Wiley.

[24] Okubu, T. (1995) *Journal of Colloid and Interface Science*, **171**, 55–62.

[25] Wilkinson, M. C., Hearn, J., Steward, P. A. (1999) *Advances in Colloid and Interface Science*, **81**, 77–165.

[26] Saunders, B. R., Vincent, B. (1999), *Advances in Colloid and Interface Science,* **80**, 1–25.

[27] Snowden, M. J., Thomas, D., Vincent, B. (1993) *Analyst*, **118**, 1367–1369.

[28] Morris, G. E., Vincent, B., Snowden, M. J. (1997) *Journal of Colloid and Interface Science*, **190**, 198–205.

[29] Peng, S., Wu, C. (2001) *Polymer*, **42**, 6871–6876.

[30] Suarez, C. G., Noordmans, J., van de Mei, H.C., Busscher, H. J. (1999) *Physical Chemistry Chemical Physics*, **18**(1), 4423–4427.

INFLUENCE OF SHORT-CHAIN ALCOHOL CO-SOLVENTS ON HYDROPHOBICALLY MODIFIED POLY(NIPAM) MICROGEL PARTICLES

5.1 Introduction

Following the basic physico-chemical characterization of the hydrophobically modified poly(NIPAM)-based microgels described in Chapter 3 and the investigation of their behaviour with respect to interfacial tension described in Chapter 4, the objective of the work described in this chapter was to study how hydrophobically modified particles interact with more hydrophobic co-solvents. It was hypothesized that the increasingly hydrophobic natures of the modified microgels would alter the response of the particles to the presence of solvents less polar than water, compared to unmodified, hydrophilic poly(NIPAM). It was anticipated that investigation of variation in the swelling behaviour of modified microgels would help determine whether the modifications altered interactions between the microgel and solvents.

As described in Section 1.2.4.5, several research groups have investigated the behaviour of poly(NIPAM) in the presence of short-chain alcohols such as methanol (MeOH), ethanol (EtOH) and 2-propanol (2-PrOH). De-swelling of the poly(NIPAM) particles was observed at low volume fractions of added alcohol, whilst re-entrant swelling occurred at higher volume fractions, both of which were explained by the phenomenon of co-non-solvency.[1] As the response of poly(NIPAM) to added alcohols had already been determined in the literature, short-chain alcohols were selected to act as the less polar solvents with which to test the microgels.

5.2 Materials

The swelling behaviour of poly(NIPAM) (N2) particles was compared with that of two equivalent batches of poly(NIPAM-*co*-vinyl laurate) (VL) particles, whilst dispersed in

163

aqueous binary mixtures of short-chain alcohols. Details of the microgels are given in Table 2.4. Table 5.1 shows the structures and properties of the short-chain alcohols used in this investigation. A 60 nm standard latex bead was used, as supplied, in experiments to determine the viscosity of alcohol-water mixtures (Duke Scientific Corporation Nanosphere Size Standard 60.0 ± 2.7 nm, 3060A, Lot 28620).

Table 5.1 Properties of alcohol co-solvents compared to water

Chemical	Formula	ε (25 °C)	ε (50 °C)	η (cP) (25 °C)	η (cP) (50 °C)	RI (25 °C)	RI (50 °C)
MeOH	CH_3OH	31.50	27.44	0.544	–	1.326	–
EtOH	CH_3CH_2OH	24.30	20.87	1.074	0.694	1.359	–
2-PrOH	$(CH_3)_2CHOH$	18.00	15.06	2.038	1.028	1.375	–
Water	H_2O	78.50	69.85	0.890	0.547	1.333 (20 °C)	1.329

ε = dielectric constant; η = viscosity; RI = refractive index; – = value not available. All ε values taken from Ref. [2]; η and RI values from Ref. [3].

5.3 Methods

The Zetasizer Nano ZS was used as described in Section 3.2.3 to measure the hydrodynamic diameter (D_H) of the poly(NIPAM) microgel, N2, and the poly(NIPAM-*co*-vinyl laurate) microgel, VL, as a function of increasing mass fraction of added MeOH, EtOH and 2-PrOH. A suitable method was developed over a period of many repeated measurements, initially based on that used by Crowther and Vincent.[1] An initial set of measurements of the variation of the D_H of N2 and VL in MeOH and EtOH was used to assess the behaviour of the microgels in aqueous alcohol dispersions and to guide development of the method. A second set of measurements were then made for both microgels in MeOH, EtOH and 2-PrOH, at 25 °C and 50 °C. Prior to these measurements, the alcohol/water mixtures in which the N2 and VL particles were to be dispersed had to be characterized. The information obtained was required to enable D_H measurements to be made with the Zetasizer Nano ZS.

5.3.1 Dispersant preparation

Aqueous binary mixtures of MeOH, EtOH and 2-PrOH were prepared at the compositions shown in Table 5.2. The 10 mL quantities of dispersants were prepared by volume, then the mass of each component of the sample was recorded to allow calculation of an accurate percentage mass alcohol value for each mixture. Although existing data in the literature is

generally reported in terms of the volume fraction (x) of added alcohol (x = 0–1), the Zetasizer complex solvent builder function required details in the form of percentage mass, so the results are reported in same form.

Table 5.2 Composition of aqueous binary mixtures of MeOH, EtOH and 2-PrOH used in RI measurements and viscosity back-calculations

Sample no.	% volume alcohol	% mass MeOH	% mass EtOH	% mass 2-PrOH
i	0	0	0	0
ii	10	8	8	8
iii	20	16	16	16
iv	30	25	25	25
v	40	34	34	34
vi	50	43	44	43
vii	60	53	54	54
viii	70	64	65	64
ix	80	75	75	75
x	90	87	87	87

The prefix M, E or P before the sample number subscript (i–x) indicates the alcohol in the mixture, *i.e.* M = MeOH, E = EtOH and P = 2-PrOH; *e.g.* M_i–M_x denotes the ten aqueous MeOH mixtures.

The dispersants were prepared ranging from 0–90 % volume alcohol; the remaining 10 % was due to the volume of aqueous microgel dispersion that would be added to the final sample mixtures for testing. It was assumed that 1 mL aqueous microgel dispersion was equivalent to 1 mL distilled water plus microgel particles. The dispersants were placed on a tube rotator to mix overnight (for at least 14 hours) prior to testing.

5.3.2 Dispersant characterization

The dynamic light scattering (DLS) system used, the Zetasizer Nano ZS, requires the input of various material and dispersant properties prior to making size measurements of microgel particles in a solvent mixture. These are the viscosity (η), refractive index (RI) and dielectric constant (ε) of the dispersants at specific temperatures. The software associated with the instrument contains relevant details of standard solvents and common additives[4] but the majority of the dispersants compositions investigated in this study were not covered. It was therefore necessary to determine experimentally the η, RI and ε for each dispersant at several temperatures so that specific values could be input prior to D_H measurement.

5.3.2.1 Dispersant refractive index measurements

The RI values of the aqueous MeOH, EtOH and 2-PrOH dispersants (named M_i–M_x, E_i–E_x and P_i–P_x respectively) were measured directly at 25 and 50 °C using a Bellingham & Stanley RFM390 Refractometer, with an attached Rheotek circulating water bath used to maintain a constant temperature. A few drops of dispersant M_i were placed onto the refractometer lens and five consecutive measurements of the RI were recorded. This was repeated twice to give 15 measurements of the RI of M_i. The process was then repeated to obtain 15 RI measurements for each of the remaining dispersants (M_{ii}–M_x, E_i–E_x and P_i–P_x) at 25 and 50 °C. For each dispersant, the mean of the 15 measurements at each temperature was calculated. These values were plotted against percentage mass alcohol in the dispersant and used to interpolate RI values for every whole number percentage mass alcohol from 0–100 % at 25 °C and 50 °C. The interpolated values are tabulated in Appendix C. It is worth noting that M_i, E_i and P_i were in fact 100 % water, which gave an opportunity for verifying the accuracy of the instrument against literature values for the RI of water.

5.3.2.2 Dispersant dielectric constant

Dielectric constant (ε) values for aqueous mixtures of MeOH, EtOH and 2-PrOH over a range of mass fractions of alcohol at 25 and 50 °C were obtained from literature.[2] These values were plotted and lines of best fit were obtained, which were then used to interpolate ε values for every whole number from 0–100 % mass alcohol. The equations and values are given in Appendix D.

5.3.2.3 Back-calculation of dispersant viscosity

Latex doping and DLS using the Zetasizer Nano ZS were used to obtain η values for each aqueous alcohol dispersant at 25 and 50 °C, based on the fact that size measurements reported by the Zetasizer for a material are directly proportional to the η of the dispersant in which the material is dispersed.[5] Literature values for the pure solvent η were initially used to obtain η estimates, then latex doping with 60 nm standard latex particles was used to obtain a better approximation of the η value for each dispersant mixture.

Approximately 1 mL of dispersant was placed in a clean disposable cuvette using a plastic pipette. Two drops of standard latex were added. A cuvette lid prevented dispersant loss

through evaporation. Each dispersant was equilibrated to 25 °C before five particle size measurements were taken. The dispersants were then equilibrated to 50 °C for 10 minutes before five further particle size measurements were taken. The particle sizes were then fitted by adjustment of the dispersant η until the target latex particle size (60 nm) was reported, which indicated the actual η of the dispersant being tested. These back-calculated η values were plotted and trend lines allowed interpolation of η values for every whole number percentage mass alcohol (0–100 %) (Appendix E).

5.3.3 *Preparation of samples of microgels in dispersants*

Once the necessary dispersant parameters were determined, the first batch of samples of N2 and VL microgel particles were prepared in dispersant concentrations of 0, 20, 40, 60, 80 and 90 % volume MeOH and EtOH. A second batch of N2 and VL particles in 0, 10, 20, 30, 40, 50, 60, 70, 80 and 85 % volume MeOH, EtOH and 2-PrOH were later prepared. As with the dispersants, all samples were prepared by volume but the masses of each component were recorded so that the percentage mass alcohol could be calculated. The precise percentage mass compositions of each sample are shown in Appendix F.

In the first batch of samples, the original microgel dispersion concentration of approximately 0.5 % w/v was diluted 1 in 10 parts with the aqueous alcohol dispersants, which gave an approximate microgel concentration of 0.05 % w/v in each sample. In the second batch of samples, a higher concentration of microgel particles was required, so the microgel samples were diluted 3 in 10 parts with the dispersants, giving an approximate microgel concentration of 0.15 % w/v. The samples were placed on a rotator overnight to mix thoroughly and equilibrate.

5.3.4 D_H *measurement*

For measurements of the first batch of samples (Appendix F), approximately 1 mL of a sample was placed in a clean, disposable cuvette using a plastic pipette. A cuvette lid was used to prevent solvent loss due to evaporation. Each filled cuvette was pre-equilibrated in a 25 °C water bath for at least 10 minutes before being placed in the Zetasizer for a further equilibration of 2 minutes, then five D_H measurements. This process was repeated for each sample following an equilibration of at least 30 minutes in a 50 °C water bath, prior to being

replaced in the Zetasizer for a further equilibration of 2 minutes and five repeat D_H measurements.

The D_H of the second batch of samples (Appendix F) was measured in an almost identical manner. The main difference was that instead of using water baths, the 25 °C and 50 °C equilibration periods took place entirely in the Zetasizer, ensuring more uniform treatment of each sample. In a single measurement run, each sample underwent: equilibration at 25 °C for 10 minutes; five D_H measurements at 25 °C; heating to 50 °C; equilibration at 50 °C for 10 minutes; then five D_H measurements at 50 °C. The D_H of all samples was measured at 25 °C and 50 °C so that the behaviour of the microgel particles could be investigated above and below their VPTTs.

5.3.5 DLS data quality

The DTS Nano 5.00 software was used to assess measurement quality. Any data that did not meet the standard required was omitted or replaced with an acceptable repeat measurement.

5.4   Results and discussion

The particle sizes of N2 and VL were measured using DLS in the presence of increasing concentrations of the short-chain alcohols MeOH, EtOH and 2-PrOH.

5.4.1 Dispersant characterization

Several parameters relating to the alcohol-water dispersants had to be determined to enable particle size measurement by DLS to take place. The results of the characterization of the dispersant RI, ε and η are described below.

5.4.1.1 Dispersant RI values

The RI measurements obtained for each set of dispersants at 25 °C and 50 °C are plotted in Fig. 5.1. It shows that the RI measurements of the 0 % mass alcohol samples compare favourably with literature values for the RI of pure water (1.333) (Table 5.1). Increasing RI was observed with increasing alcohol concentration for all three solvents, however, RI

decreased from approximately 50 % MeOH and 80 % EtOH. No decrease in RI was observed for 2-PrOH. The RI of the pure solvents increases with increasing chain length and therefore the difference between the RI of each one and pure water therefore also increases. This accounts for the decreases in RI at the highest alcohol concentrations observed for MeOH and EtOH, and the absence of a decrease in RI for 2-PrOH.

In addition, as the alcohol chain length increased, the measured RI increased, with greater RI values observed for 2-PrOH than EtOH, which in turn had greater RI values than MeOH. The RIs observed for the solvents varied with temperature, with lower RIs measured at 50 °C than at 25 °C, as expected from theory.[6] Furthermore, the difference between 25 °C and 50 °C measurements increased with increasing alcohol concentrations for all three solvents. These findings agree with the observations of Herráez and Belda.[7] The data was used to predict the RI values of the aqueous alcohol dispersant mixtures that would later contain microgel particles (Appendix C).
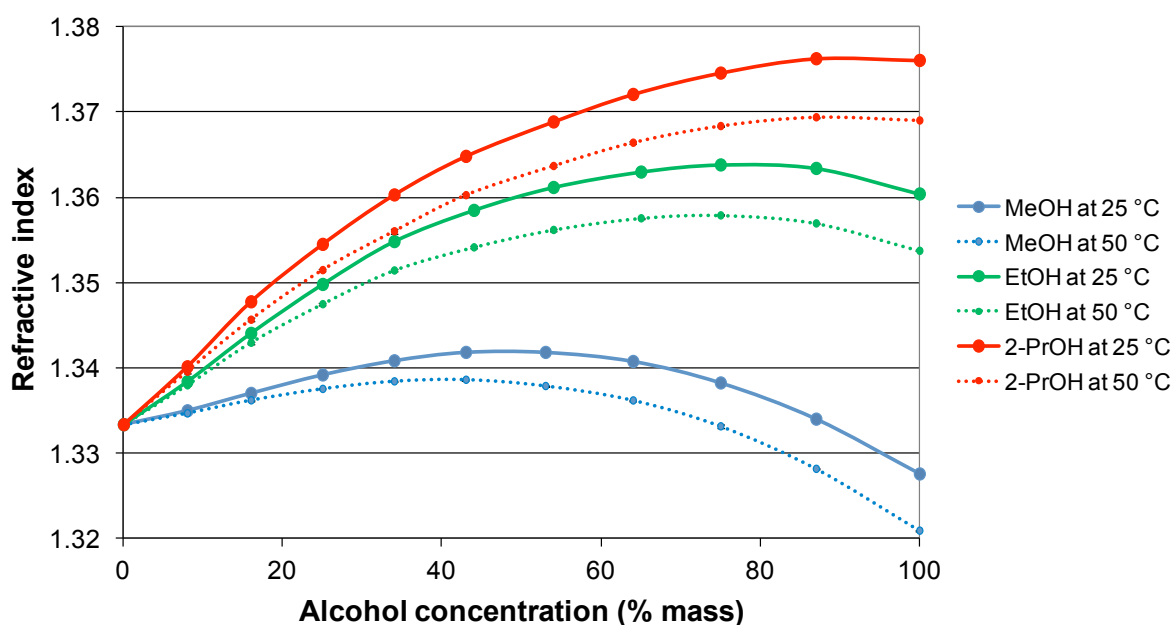
Figure 5.1 RI of aqueous alcohol mixtures as a function of alcohol concentration (± 1 s.d.)

5.4.1.2 Estimation of dispersant dielectric constants

Figure 5.2 illustrates dielectric constant (ε) values for aqueous MeOH, EtOH and 2-PrOH mixtures obtained from literature (Appendix D).[2] These were used to predict values for the

specific aqueous alcohol mixtures used in this experiment so that the D_H of microgel particles dispersed in the mixtures could be measured using DLS.

Figure 5.2 shows ε decreases as percentage mass alcohol increases for all three solvents, at both temperatures. For MeOH, the relationship is almost linear but for EtOH and to a slightly greater extent for 2-PrOH, a small increase in ε at the highest percentage mass alcohol was observed. The ε values are smaller at 50 °C compared to 25 °C; this might reflect a temperature-driven disruption of alcohol-water clathrate structures, which takes place more readily at higher temperatures.
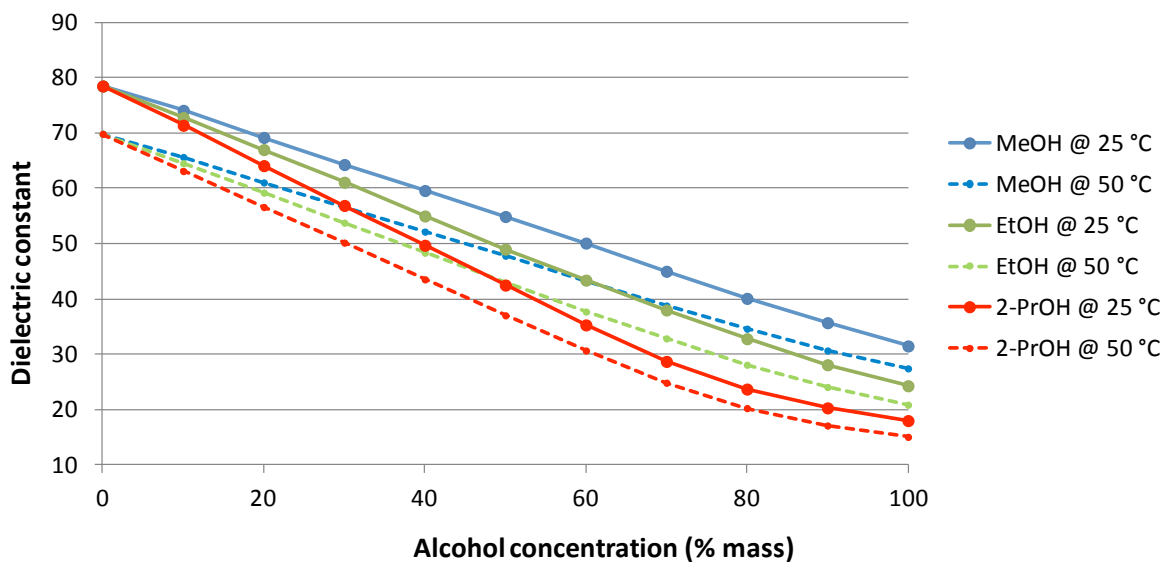
Figure 5.2 Dielectric constant of aqueous mixtures of MeOH, EtOH and 2-PrOH, taken from Ref. [2]

5.4.1.3 Dispersant viscosity values

The back-calculated viscosities measured for each aqueous alcohol mixture are plotted in Fig. 5.3. These were used to predict viscosity values for each of the dispersants in which microgel particles were later dispersed in order to measure particle size. The predicted values are detailed in Appendix E.

The plots in Fig. 5.3 show that at both temperatures, as anticipated from theory,[8] the viscosity (η) initially increased with percentage mass alcohol, then decreased at higher values of percentage mass alcohol. As the alcohol chain length increased, viscosity increased, which shows agreement with literature.[9] The plots also show lower viscosity

values at 50 °C than at 25 °C. The measured viscosity values for the pure solvents (*i.e.* at 0 % and 100 % mass alcohol) show good agreement with literature values (Table 2.2).
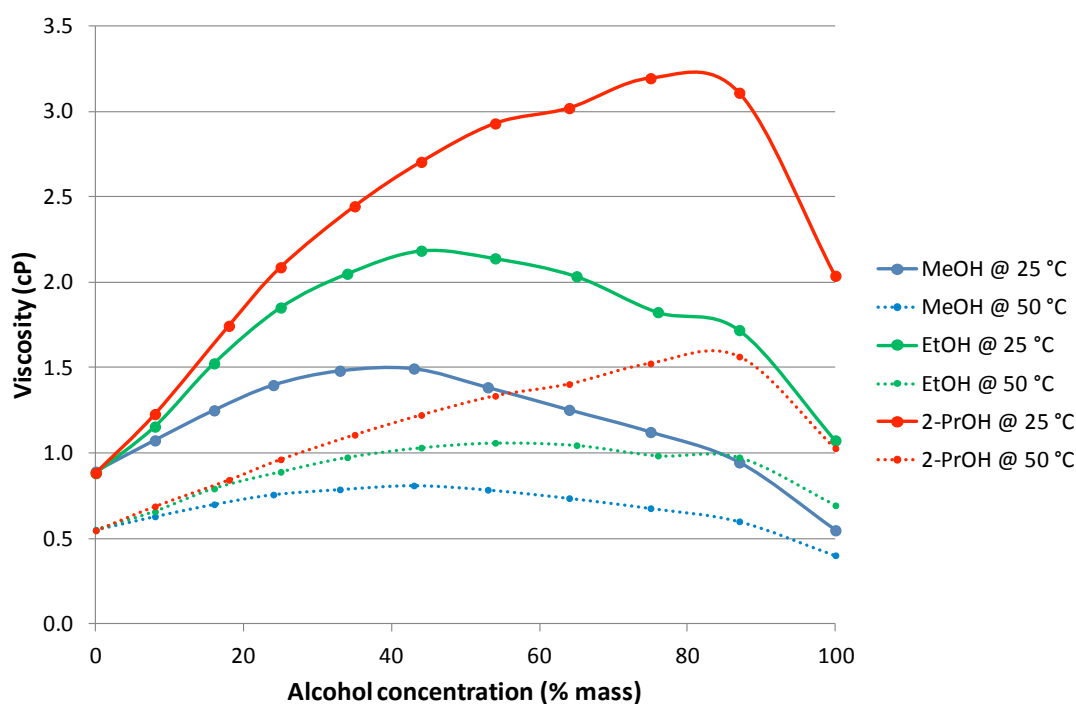
Figure 5.3   Viscosities of aqueous alcohol mixtures back-calculated from DLS using latex doping at 25 °C and 50 °C

5.4.2 Microgel particle size in aqueous alcohol dispersants

5.4.2.1 Initial measurements of N2 and VL in MeOH and EtOH mixtures at 25 °C

The results of DLS measurements of the D_H of N2 and VL particles in aqueous MeOH and EtOH dispersants, using the parameters determined in Section 5.4.1, are reported below. De-swelling ratios (α) were calculated from the D_H data as described in Section 1.2.4.5 and plotted against percentage mass alcohol. Figure 5.4 shows N2 de-swelling ratios against increasing percentage mass MeOH and EtOH.

It should be noted that the red data point (▲) at 87 % mass alcohol for N2 in EtOH in Fig. 5.4 is an approximate value which represents data that did not meet the quality criteria required by the DTS software. However, it is included here (and in Figures 5.5 and 5.6) to give an indication of the likely particle size of N2 at 87 % EtOH. These measurements were repeated several times but it was not possible to obtain data that met the quality criteria. The PdI

values were frequently greater than 0.2 and the distribution peaks were not monomodal, indicating the possible presence of flocculated particles. However, the position of the data point was similar for each repeat. It also follows a similar trend to that observed for N2 in MeOH and to results published in literature,[1] so it is likely that the data is correct.
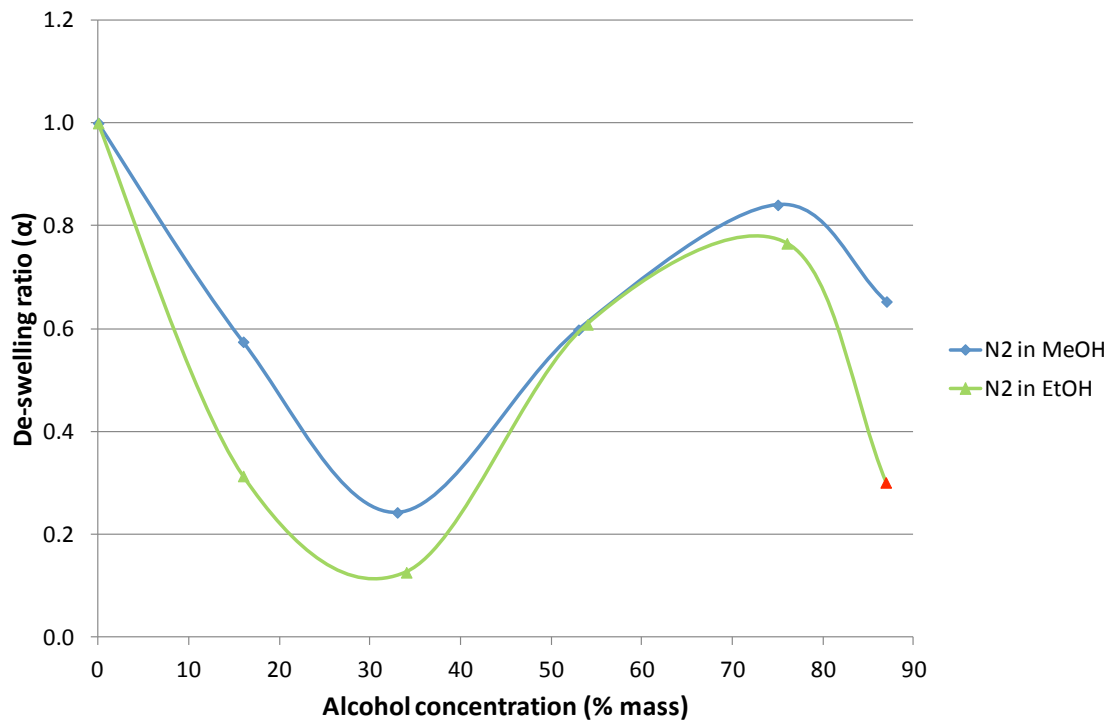
Figure 5.4   De-swelling ratio of N2 microgel particles in aqueous MeOH and EtOH dispersants at 25 °C ▲ See explanation in text above.

As expected from literature,[1] clear de-swelling and re-entrant swelling were observed for N2 in both MeOH and EtOH at 25 °C. The extent of de-swelling was greatest in EtOH but the extent of re-entrant swelling was similar for both solvents. Crowther and Vincent[1] observed that the volume fraction of alcohol required to reach the maximum extent of de-swelling (collapse) decreased as the alcohol chain length increased. On first inspection it appears that the minima in Fig. 5.4 are very similar for N2 in MeOH and EtOH, contradicting the results anticipated from literature (Section 1.2.4.5), *i.e.* the findings of Crowther and Vincent, [1] Onori *et al.*[10] and Zhu and Napper.[11]

On closer inspection, it is possible that the EtOH minimum may have been reached at a lower percentage mass alcohol than in MeOH but this cannot be determined from this set of data. All that can be concluded is that the minimum for MeOH lies below 33 % mass alcohol and

the minimum for EtOH lies below 34 % mass alcohol. Measurement of D_H at smaller percentage mass alcohol intervals should help clarify this; this became a modification of the method used to measure the second set of samples (Section 5.3.3). A second de-swelling was observed for N2 in both solvents above 70 % mass alcohol. A similar second de-swelling is apparent for poly(NIPAM) above 0.75 volume fraction of EtOH and 2-PrOH in the results of Crowther and Vincent,[1] shown in Fig. 1.11 (page 25). In general, these initial results show good agreement with published data for poly(NIPAM) microgels.
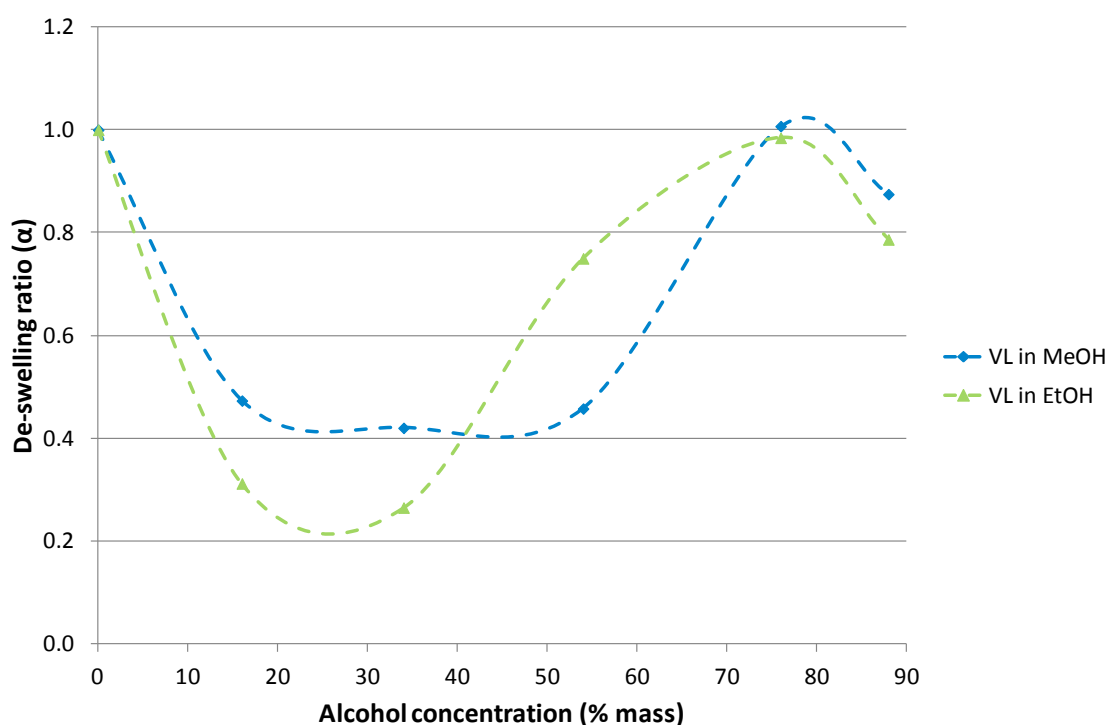
Figure 5.5 De-swelling ratio of VL microgel particles in aqueous MeOH and EtOH dispersants at 25 °C

The next step was to establish whether the hydrophobically modified VL exhibited similar behaviour. Figure 5.5 shows the de-swelling ratios (α) for VL as a function of percentage mass MeOH and EtOH. De-swelling and re-entrant swelling were again clearly apparent, with greater de-swelling observed for VL in EtOH than in MeOH, a similar extent of re-entrant swelling found in both solvents, and a second period of de-swelling above 70 % mass of both solvents. However, the VL curves were broader and flatter than those observed for N2, with minima potentially further apart. The data also suggests that maximum de-swelling may have been reached at a lower percentage mass of EtOH than MeOH, and that VL remained in the fully collapsed state over a wider range of MeOH concentrations than EtOH.

However, once again, the data point intervals are too wide to determine precisely the range of maximum de-swelling or the point at which the maximum extent of de-swelling lies.

Despite this, the initial results (Fig. 5.5) indicate that VL shows similar behaviour to that reported for poly(NIPAM) in the presence of increasing concentrations of MeOH and EtOH.[1,10,11,12,13]   Although there are no reports of alcohol-induced de-swelling and re-entrant swelling behaviour of poly(NIPAM-*co*-VL) microgels in the literature with which to compare these VL results, the data does broadly display the same trends as those reported for poly(NIPAM). However, Saunders *et al.*[14] published evidence of similar behaviour for the more hydrophilic poly(methyl methacrylate-*co*-methacrylic acid) particles, indicating that it is not a phenomenon limited to just poly(NIPAM) microgels.
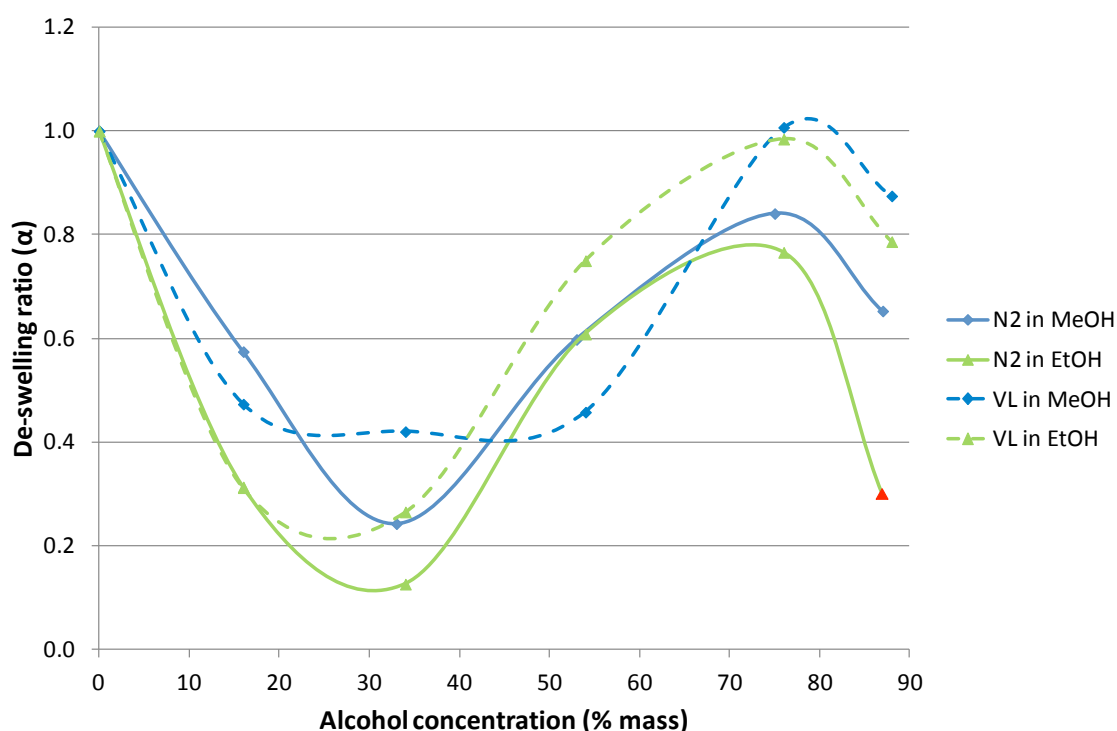
Figure 5.6 De-swelling ratios of N2 and VL microgel particles in aqueous MeOH and EtOH dispersants at 25 °C ▲ See explanation in text above Fig. 5.4.

Figure 5.6 compares the responses of both microgels to increasing concentrations of the two alcohols at 25 °C. It is clear that less MeOH was required to fully collapse VL (dotted blue line) than N2 (solid blue line). This may be explained by the fact that with more hydrophobic domains (due to the incorporation of 10 % of a more hydrophobic co-monomer) VL is less hydrophilic than N2 and therefore makes fewer hydrogen bonds with water and has an

increased capacity for hydrophobic interactions between its polymer chains. Together this may lead VL to collapse more rapidly than N2 in the presence of MeOH.

A similar trend is suggested in Fig. 5.6 for the two microgels in the aqueous EtOH dispersants: possibly slightly less EtOH is required to fully collapse VL (dotted green line) than to fully collapse N2 (solid green line). Figure 5.7 shows the actual particle D_H values from which the α values in Fig. 5.6 were calculated and here the trend for VL particles to reach full collapse at a lower percentage mass of MeOH or EtOH than the N2 particles is much more distinct.

The D_H values in Fig. 5.7 also indicate that the particle size of both microgels is more substantially reduced in EtOH (green lines) than in MeOH (blue lines). This could be because the longer-chain EtOH molecules require a greater number of water molecules than MeOH in order to form stable clathrate structures and therefore draw water molecules from the microgel particles more effectively than MeOH, resulting in a greater degree of collapse. The data in Figures 5.6 (α values) and 5.7 (D_H values) show broad agreement, in that both solvents cause a more substantial reduction in the size of N2 than for VL.
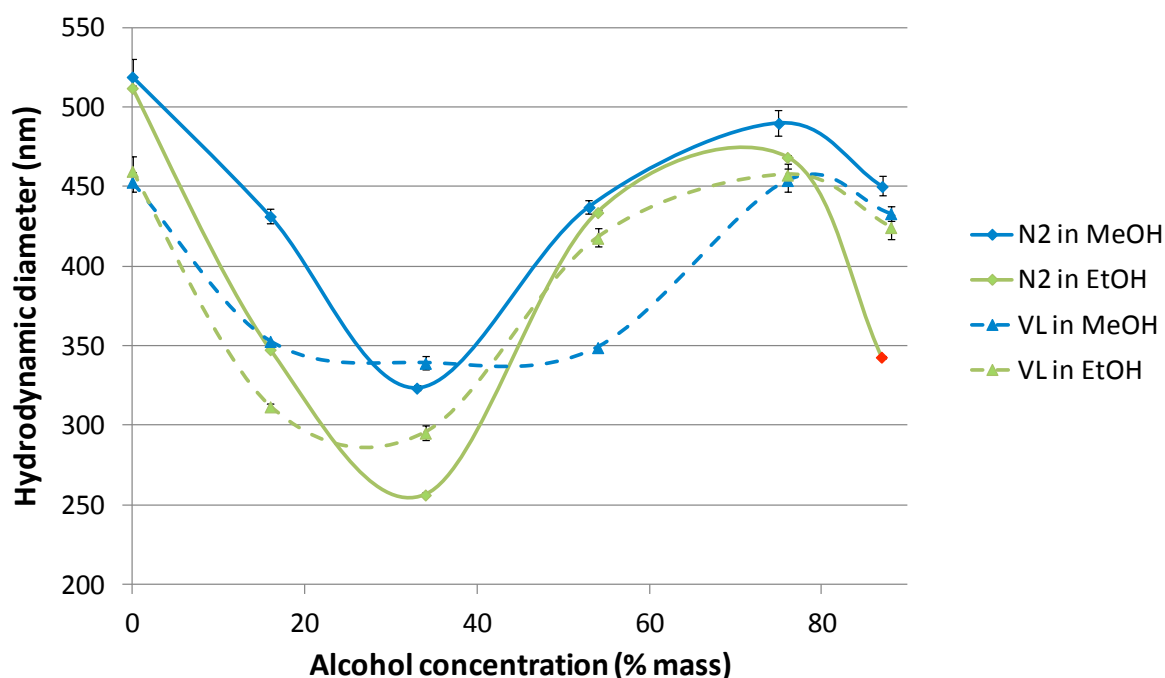
Figure 5.7 D_H **of N2 and VL microgel particles in aqueous MeOH and EtOH dispersants at 25 °C (± 1 s.d.)** ▲ See explanation in text above Fig. 5.4.

The possibly stronger influence of the presence of MeOH and EtOH on the onset of de-swelling of the hydrophobically modified VL compared to N2 could be explained by the balance of hydrophobic/hydrophobic regions in the two microgels. As VL contains 10 % less NIPAM than N2, it could be concluded that the proportion of hydrophilic domains available for hydrogen bonding with solvent molecules is also reduced by the order of 10 %. As a consequence, the disruption of hydrogen bonding (due to the withdrawal of water molecules to form clathrate structures around the added alcohol molecules) could proceed more rapidly for VL than for N2. Hence, a smaller volume of alcohol is required to withdraw all the interstitial water within VL compared to N2, which contains a greater number of water molecules. This is supported by the fact that N2 has a larger D_H in water than VL (see Fig. 5.7). Furthermore, the VL contains approximately 10 % more hydrophobic domains available to participate in hydrophobic interactions, which may contribute to the collapse at lower percentage mass alcohol than seen for N2.

The observation that the magnitude of de-swelling was greater for N2 than VL appears counter to the previous discussion on first consideration; if a smaller capacity for hydrogen bonding and a greater capacity for hydrophobic interactions (as in the case of the hydrophobically modified VL compared to N2) enables maximum de-swelling to occur from lower concentrations of alcohol co-solvent, then how can the more hydrophilic N2 achieve a greater extent of de-swelling? As already mentioned, it is likely that the N2 particles contain a greater number (and therefore volume) of water molecules. Although it takes a greater quantity of alcohol co-solvent to withdraw fully the water molecules from the N2 particles and cause full collapse (*i.e.* full collapse is reached from a higher percentage mass alcohol), the relative change in size (and therefore volume) of the N2 particles is greater than that of the VL particles. Hence the maximum extent of de-swelling observed is greater for N2.

The onset of re-entrant swelling for both microgels appears to begin at lower concentrations of EtOH (green lines) than MeOH (blue lines), particularly for VL (Fig. 5.6). This makes sense when considered in the light of the fact that the maximum de-swelling tends to be seen at lower concentrations of EtOH than MeOH for both microgels and hence re-entrant swelling in EtOH dispersants could reasonably be expected to commence at lower percentage mass alcohol. As the clathrate structures around the longer chain EtOH are more readily disrupted than around MeOH[6] (which is more polar, with a higher dielectric

constant and therefore is more likely to interact strongly with the water molecules), the water (and EtOH) molecules are freed and available to contribute to re-entrant swelling[1] at a lower percentage mass.

The balance of polarities between the two alcohols and the relative hydrophilic/hydrophobic balance of the two microgel particles may be influential. For example, MeOH ($\varepsilon = 31.50$) is more polar than EtOH ($\varepsilon = 24.3$), whilst N2 is considered more hydrophilic than VL, which is considered to have a more hydrophobic nature. The more polar MeOH could therefore be expected to have a greater impact upon the microgel with the larger capacity for hydrogen bonding, *i.e.* N2. Conversely, the less polar and more hydrophobic EtOH might be expected to have greater impact on the microgel with the more hydrophobic nature, *i.e.* VL. Indeed, MeOH induced de-swelling of N2 appears greater than the MeOH induced de-swelling of VL (Fig. 5.6). However, the EtOH induced de-swelling is also slightly greater in N2 than VL. This may be due to the fact that although EtOH has a longer carbon chain and therefore is less polar than MeOH, the difference is subtle. Further investigation of a broader range of alcohols may help elucidate the reasons behind these observations.

Interestingly, on re-entrant swelling, VL reached substantially higher α values than N2, with the VL re-swelling to sizes equivalent to those measured in pure water, whilst N2 only reached a maximum of 84 % of its D_H in pure water. This could be an indication that the additional hydrophobic domains in VL permit not only re-solvation with the water molecules but also an increased uptake of alcohol molecules compared to N2. Further work is required to determine whether this is the mechanism.

Finally, for both microgels in both dispersants from around 76 % mass alcohol, a second, smaller de-swelling event was observed. This could be due to the limited number of water molecules available at the higher alcohol concentrations, where the competition between the microgel particles and alcohol molecules for the water molecules (already observed at the lower alcohol concentrations) could increase once more. With the alcohol molecules exerting a greater pull on the water molecules, the microgel particles release the water molecules once more and the polymer chains again collapse. This type of second period of de-swelling has been observed in literature, *e.g.* by Crowther and Vincent[1] (Fig. 1.11, page 25).

It was clear from the results above that, as anticipated from the literature,[6,15] de-swelling, re-entrant swelling and co-non-solvency result from a fine balance of polymer-polymer, polymer-solvent and solvent-solvent interactions. For example, N2 can be considered more hydrophilic but less hydrophobic than VL, and consequently is more likely to hydrogen bond but less likely to participate in hydrophobic interactions. The inclusion of a more hydrophobic co-monomer such as VL obviously alters the co-non-solvency response of the particles. In order to clarify the findings, a more detailed investigation of the co-non-solvency behaviour of the two microgels was conducted and is described below.

5.4.2.2 Second set of measurements of N2 and VL in MeOH, EtOH and 2-PrOH at 25 and 50 °C

In this second investigation, the N2 and VL microgels were again tested (second batch, Appendix F) but this time the variation in D_H was measured as a function concentration of three short-chain alcohols: MeOH, EtOH and 2-PrOH. D_H measurements were taken over a more detailed range of percentage mass alcohol values and this time above (50 °C) and below (25 °C) the VPTT of the particles. Finally, the method was refined in an attempt to obtain more accurate and detailed results, for example by fully automating the heating and equilibration to temperature processes.
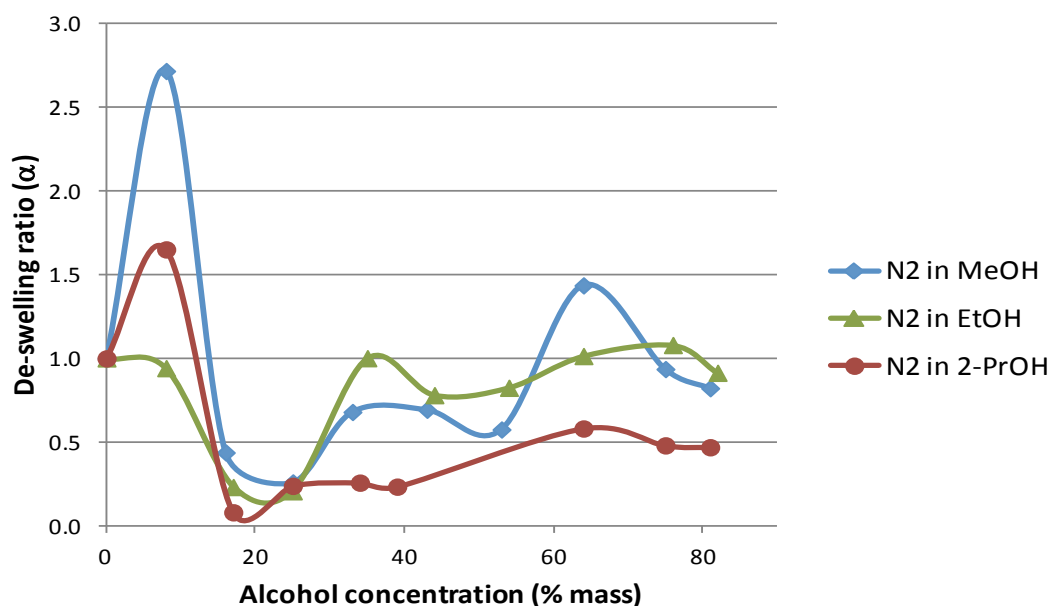
Figure 5.8 De-swelling ratios of N2 microgel particles in aqueous MeOH, EtOH and 2-PrOH dispersants at 25 °C

As in the previous investigation, de-swelling ratios were calculated from the 25 °C D_H data and plotted against percentage mass alcohol. Figure 5.8 shows the de-swelling ratios of N2 in aqueous dispersions of the three alcohols at 25 °C. It is immediately apparent that the results were far more variable and although de-swelling and re-entrant swelling were observed, previously unseen features had also emerged, *e.g.* the initial increase in de-swelling ratio observed below 8 % mass alcohol.

As a first step to determine whether the data were comparable to the results of the previous investigation, the data in Fig. 5.8 were re-plotted just showing the same limited number of percentage mass alcohol data points as collected in the previous experiment (Fig. 5.4). Figure 5.9 shows the re-plotted data. Comparison with Fig. 5.4 indicates that the data are broadly similar, showing de-swelling of the N2 particles at low percentage mass alcohol, re-entrant swelling at higher percentage mass alcohol and a greater maximum extent of de-swelling in MeOH than in EtOH. It was therefore concluded that despite the apparent variations, results from the revised method were showing reproducible evidence of the co-non-solvency behaviour of microgel particles in the presence of short-chain alcohols.
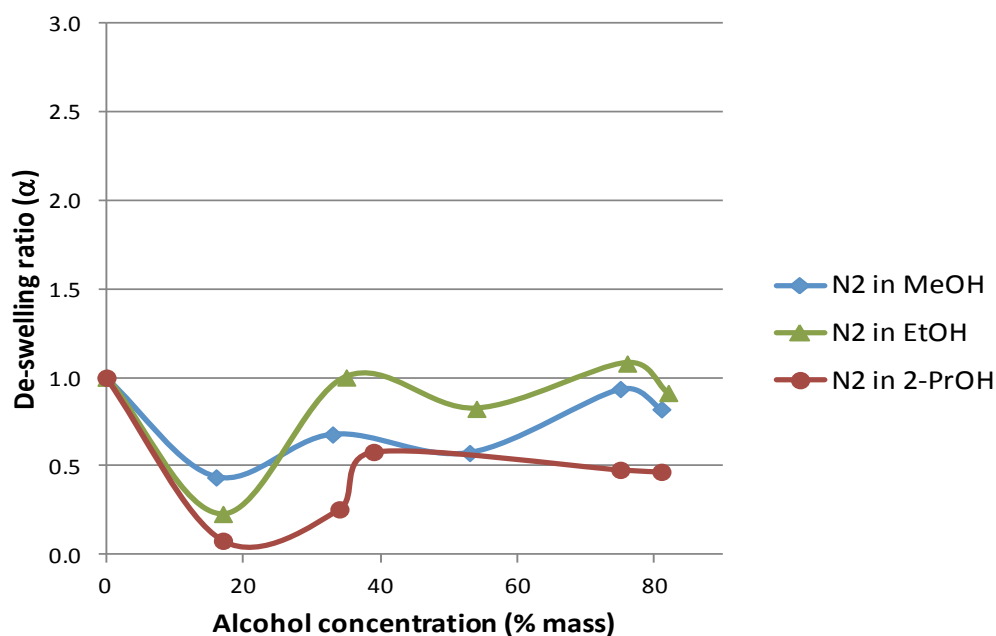
Figure 5.9 De-swelling ratios of N2 microgel particles in aqueous MeOH, EtOH and 2-PrOH dispersants at 25 °C (limited number of data points)

The original D_H data were also plotted against percentage mass alcohol to check whether the trends were clearer in that format (Fig. 5.10). As with the de-swelling ratio plots, the original D_H data also clearly show evidence of the de-swelling and re-entrant swelling behaviour of the microgel particles that is comparable with the initial data and the literature. The full range of percentage mass alcohol data points are presented in the form of de-swelling ratios from herein.
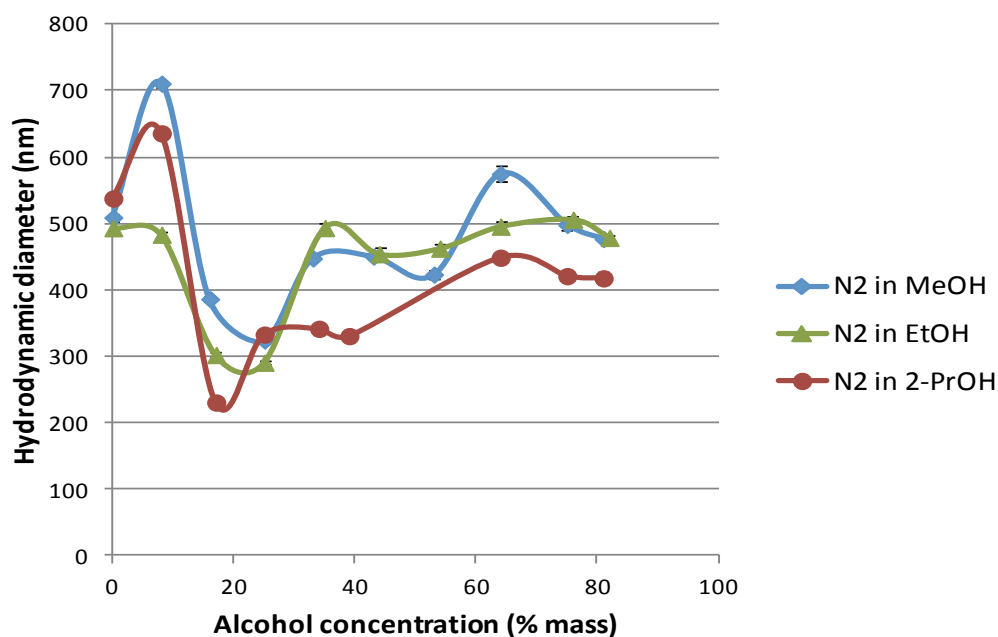
Figure 5.10 D_H values of N2 microgel particles in aqueous MeOH, EtOH and 2-PrOH dispersants at 25 °C (± 1 s.d.)

Comparison of the change in de-swelling ratios of N2 in Fig. 5.8 with the VL in Fig. 5.11 confirms that both microgels de-swell at low alcohol concentrations and undergo re-entrant swelling at higher alcohol concentrations, with a second phase of de-swelling occurring at the highest alcohol concentrations. These results broadly reproduce the findings of the initial study. However, there are clear differences. The extent of de-swelling and re-entrant swelling is generally greater for N2, especially in MeOH and EtOH. The VL curves are broader and flatter than N2, and for both microgels 2-PrOH appears to cause the greatest de-swelling and the least amount of re-entrant swelling.

Both microgels appear to reach their maximum extent of de-swelling (smallest α values) around 16–25 % mass alcohol. However, the N2 particles exhibited an initial swelling prior to that, in MeOH and EtOH particularly, around 0–16 % mass alcohol. The VL particles did

180

not exhibit an initial swelling. However, it is possible that, as in the previous experiment, the VL particles respond to even lower concentrations of alcohol, and therefore that an initial swelling could have occurred between 0–8 % mass alcohol, which was not detected due to the data intervals used. However, whether the VL particles do or do not exhibit such initial swelling, the data in Figures 5.8 and 5.11 suggest that VL begins to de-swell at lower alcohol concentrations than N2. Once again, this could be attributed to a lower capacity for hydrogen bonding in the VL particles, which results in fewer polymer-solvent interactions that are quicker to be disrupted upon increasing alcohol concentration. Measuring D_H at even smaller intervals would help clarify the position.
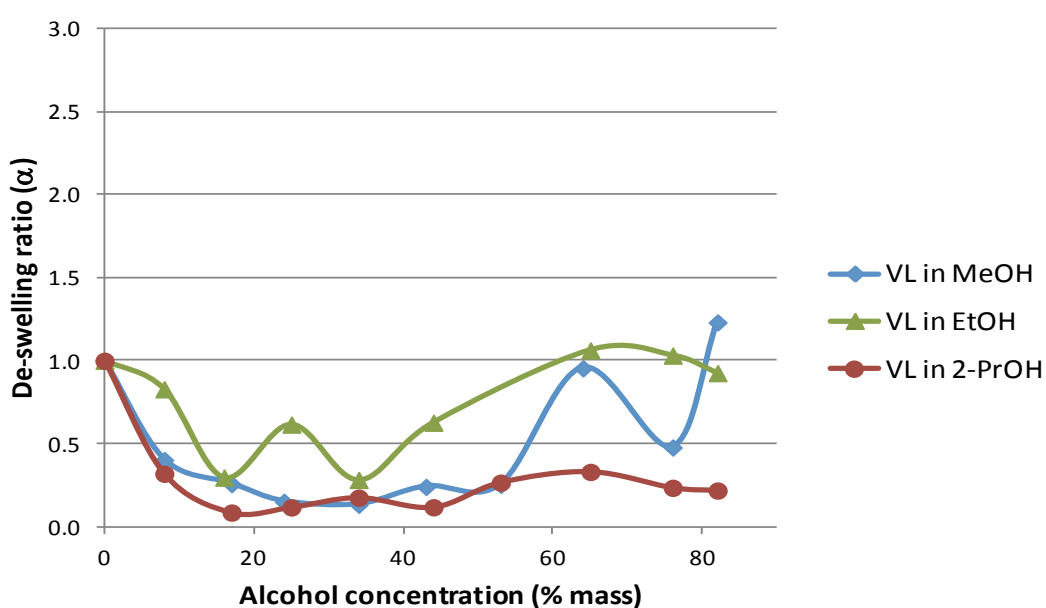
Figure 5.11 De-swelling ratios of VL microgel particles in aqueous MeOH, EtOH and 2-PrOH dispersants at 25 °C

The unusual initial increases in de-swelling ratio (*i.e.* $\alpha > 1.0$) observed for N2 were not anticipated from the literature. The initial swelling was greatest in MeOH, followed by 2-PrOH and almost absent for EtOH (MeOH > 2-PrOH > EtOH). It is possible that this response is related to the dielectric constant or polarity of the solvents. For example, MeOH with its single methyl group is the most polar of the three solvents. When MeOH is first added to the dispersant at low percentage mass, water is in excess in the system and there is no need for water to be removed from the particle interior for clathrate formation around the MeOH molecules. Some MeOH molecules may enter the interior of the microgel particles, either hydrogen bonding to the amide groups in the polymer chains due to its polar nature,

or entering into more hydrophobic interactions with the hydrophobic regions of the poly(NIPAM) chains due to its relatively less polar nature than the majority of the solvent (*i.e.* water). As a consequence, the initial swelling observed may be due to the uptake of MeOH by the microgel particles when water is greatly in excess in the dispersant.

In contrast, 2-PrOH has a longer carbon chain and therefore is less polar and more strongly hydrophobic than MeOH. Again, at low percentage mass 2-PrOH, when water is in excess, the microgel particles may take up some 2-PrOH from the bulk phase, leading to the initial swelling. However, due to the longer alcohol chain length, the 2-PrOH has a greater requirement for water molecules for clathrate formation and therefore may disrupt the hydrogen bonding within the particle more readily and lead to more rapid de-swelling than MeOH. Finally, EtOH is intermediate between MeOH and 2-PrOH in terms of hydrophobicity and polarity, resulting in less (no) initial EtOH uptake swelling, and a maximum de-swelling somewhere between that achieved by MeOH and EtOH.

There is a clear overall difference between the effect of the three alcohols upon the two microgels. 2-PrOH appears to have the greatest effect, causing the greatest extent of de-swelling (indicated by the smallest α values), the least amount of re-entrant swelling and the smallest magnitude of second phase de-swelling. The effect of the least polar alcohol, 2-PrOH, appears greater upon VL, *i.e.* the more hydrophobic microgel is affected more substantially than the less hydrophobic (N2) microgel, *i.e.* 2-PrOH de-swells N2 and VL to a similar extent, but N2 is able to re-swell more at higher 2-PrOH concentrations than VL.

The effects of MeOH and EtOH are less clear cut. In the presence of MeOH, the most polar alcohol, both microgels show higher maximum swelling values than in EtOH. However, it is not possible to state that the magnitude of swelling/de-swelling response of the particles correlates with alcohol chain length or polarity – in this case judged by dielectric constant, where dielectric constant H_2O > MeOH > EtOH > 2-PrOH (Table 5.1). In the case of VL, for example, at low alcohol concentrations the response of the particles to MeOH and 2-PrOH is fairly similar but once re-entrant swelling has commenced, the response in MeOH appears closer to that in EtOH. The fact that MeOH and EtOH seem relatively similar in influence compared to 2-PrOH may be related to the structure of the molecules, where MeOH and EtOH have the polar –OH group at a terminal end of the carbon chain and 2-PrOH has the –OH group in the middle of the carbon chain, adopting a more branched

structure. This may help explain why neither N2 or VL recovered their original sizes upon re-entrant swelling in 2-PrOH: perhaps the larger, more branched 2-PrOH is less likely either to release its clathrate water molecules or is less likely to participate in re-solvation of the microgel interiors during re-entrant swelling.

For both microgels in all three solvent combinations, the maximum re-entrant swelling appears to be reached around 64–65 % mass alcohol. In MeOH and EtOH, both N2 and VL re-swell to at least close to the starting value of $\alpha = 1.0$, if not higher. However, in 2-PrOH, neither microgel ever recovers: N2 reaches approximately $\alpha = 0.6$, whilst VL reaches only approximately $\alpha = 0.3$. This is evidence that the polarity of the alcohol itself is significant, with lower polarity (less hydrophilic) alcohols causing greater and more sustained collapse than higher polarity (more hydrophilic) alcohols. It also indicates that the nature of the microgel influences its response to alcohols of different polarity, with the hydrophobically modified VL tending to de-swell more and in a more sustained manner than the more hydrophilic N2. The broader, flatter curves associated with VL suggest that re-entrant swelling may commence sooner for N2 (from around 24–25 % mass) than for VL (around 53–54 % mass). However, the alcohol concentration at which maximum re-entrant swelling is achieved was roughly the same in both microgels and in all three alcohols, at around 60–70 % mass.

The next step in the investigation was to analyse the de-swelling ratios for both microgels in the three solvents at 50 °C, *i.e.* above the VPTT. Figure 5.12 shows the data for N2 and Fig. 5.13 shows the data for VL. The de-swelling ratio at 50 °C is also calculated using Equation 1.8, *i.e.* $\alpha = (d/d_0)^3$ and the D_H at 0 % mass alcohol at 25 °C as the fully swollen diameter (d_0) and the measured D_H at different alcohol concentrations at 50 °C as d. This enabled comparison of the relative extent of de-swelling and re-entrant swelling above and below the VPTT. If α values are the same at 25 and 50 °C, this indicates that the sizes from which the α values are calculated are the same at both temperatures.

As expected at temperatures above the VPTT, both microgels were already in the collapsed state and therefore no de-swelling was observed for either microgel at 50 °C at low percentage mass alcohol. However, re-entrant swelling occurred for both microgels in all three solvents, as did some final de-swelling at the highest percentage mass alcohol. The key difference between the results at 25 °C and 50 °C was that the magnitude of the re-

entrant swelling response was much larger at 50 °C, particularly for MeOH, with $\alpha > 2$ for both microgels compared to $\alpha < 1.25$ at 25 °C.
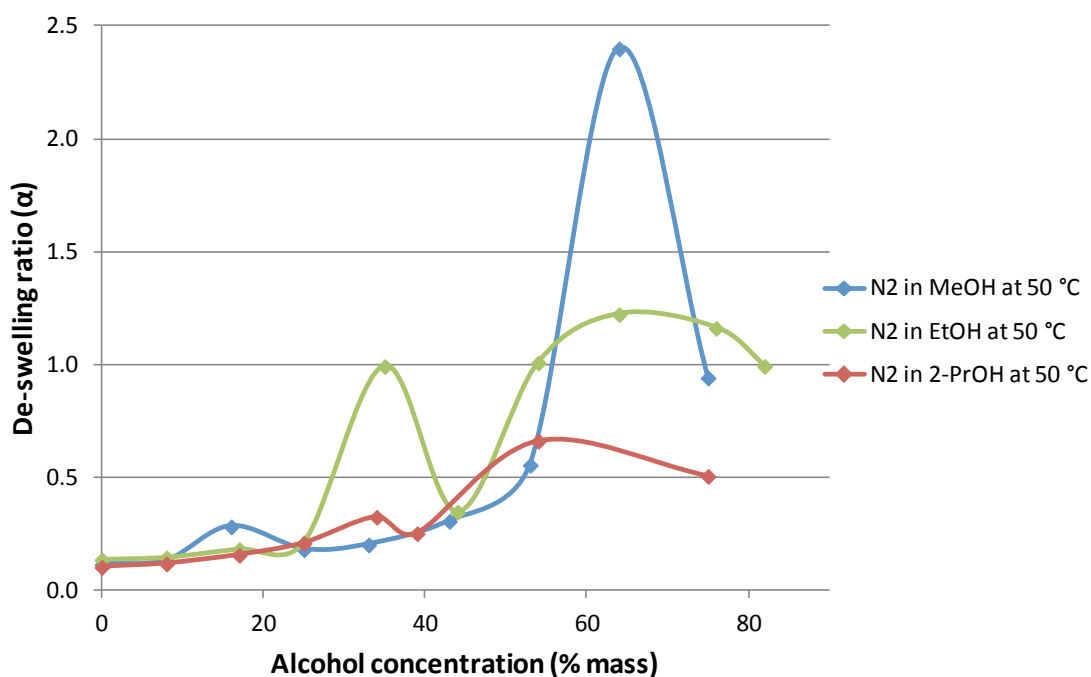
Figure 5.12 De-swelling ratios of N2 microgel particles in aqueous MeOH, EtOH and 2-PrOH dispersants at 50 °C
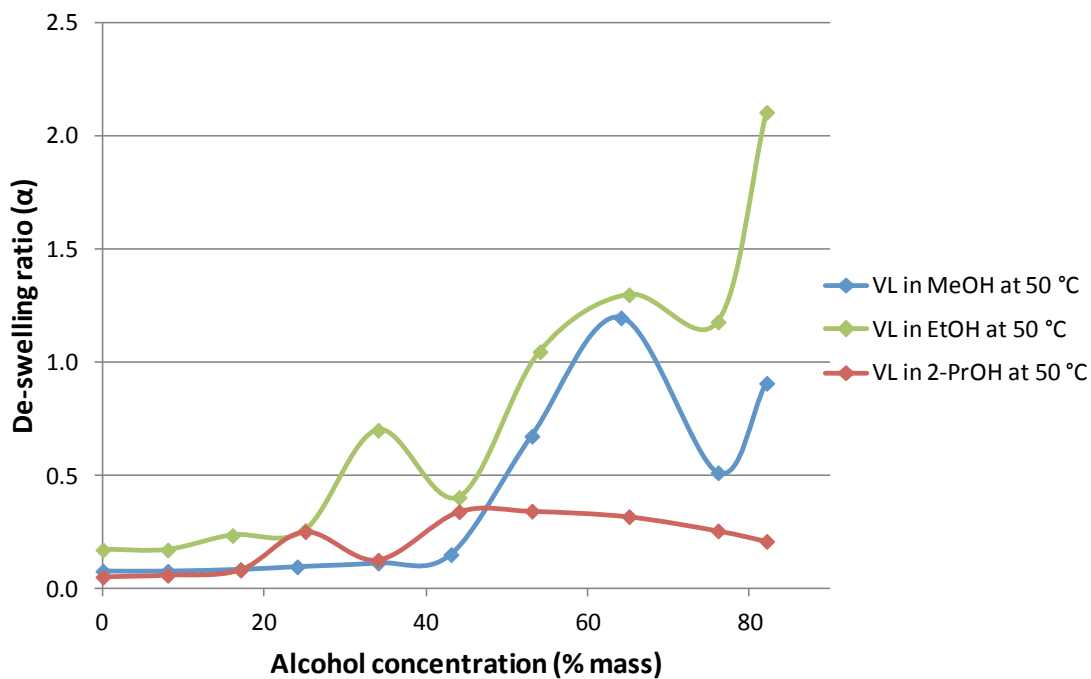
Figure 5.13 De-swelling ratios of VL microgel particles in aqueous MeOH, EtOH and 2-PrOH dispersants at 50 °C

The correlation between alcohol chain length and response of the microgels was clearer at 50 °C, with the extent of re-entrant swelling being greatest in MeOH > EtOH > 2-PrOH for N2. For VL, the order was EtOH > MeOH > 2-PrOH, but once again EtOH and MeOH were more similar in influence than to 2-PrOH. The percentage mass alcohol at onset of re-entrant swelling also showed a possible correlation with chain length, with the percentage mass alcohol required tending to decrease as the chain length increased, *i.e.* a greater percentage mass MeOH was required than of EtOH, and in turn of 2-PrOH (MeOH > EtOH > 2-PrOH).

Finally, to facilitate comparison of the response of the microgels to the individual solvents at the two temperatures, Figures 5.14, 5.15 and 5.16 show the de-swelling ratios of N2 and VL at 25 °C and 50 °C in MeOH, EtOH and 2-PrOH respectively. The key observation from this comparison is that at relatively low volume fractions, the α values are larger for the 25 °C data than 50 °C, *i.e.* the particles, both N2 and VL are more swollen at 25 °C. This is entirely as expected, as temperature sensitive poly(NIPAM)-based microgel particles tend to be swollen below the VPTT and collapsed above the VPTT, so the particles will be collapsed in water at 50 °C and more swollen at 25 deg. Interestingly, however, at higher percentage mass alcohol, this trend reverses with the α values becoming greater at 50 °C than at 25 °C, *i.e.* when re-entrant swelling recommences, the 50 °C particles re-swell to a greater extent than the 25 °C particles, and often to a magnitude substantially greater than the original 25 °C swollen value in water.

This indicates that it is possible to override the temperature-driven collapse of microgel particles above the VPTT by adding alcohol co-solvent. Furthermore, the concentration of alcohol required to overcome the temperature-driven collapse decreases as the chain length of the alcohol increases. For example, Fig. 5.14 shows that the α values at 50 °C start to exceed the 25 °C α values from approximately 54 % mass MeOH. The same cross-over occurs at around 34–35 % EtOH (Fig. 5.15) and around just 17 % mass 2-PrOH. Therefore, as the chain length of the alcohol co-solvent increases, the amount required to overcome the effect of temperature decreases substantially in the order MeOH > EtOH > 2-PrOH. However, as previously mentioned, as the chain length increases, the overall magnitude of de-swelling and re-entrant swelling tends to decrease.
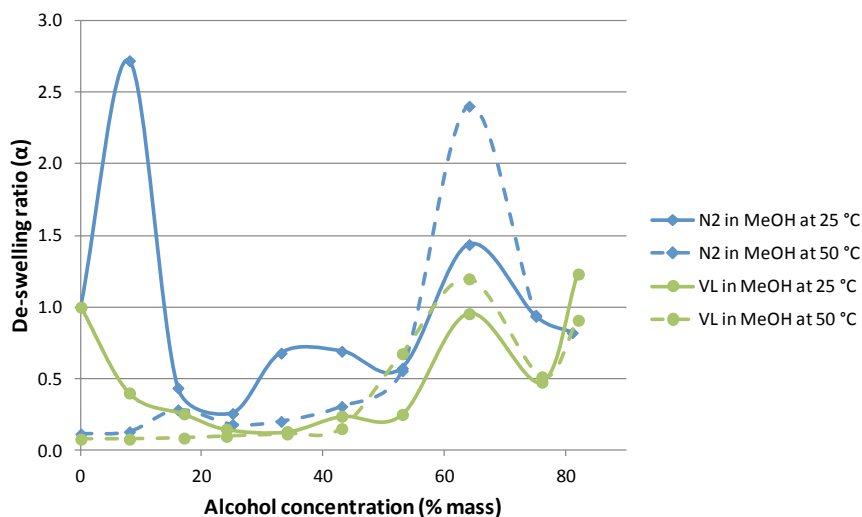
Figure 5.14 De-swelling of N2 and VL in aqueous MeOH dispersants at 25 °C and 50 °C
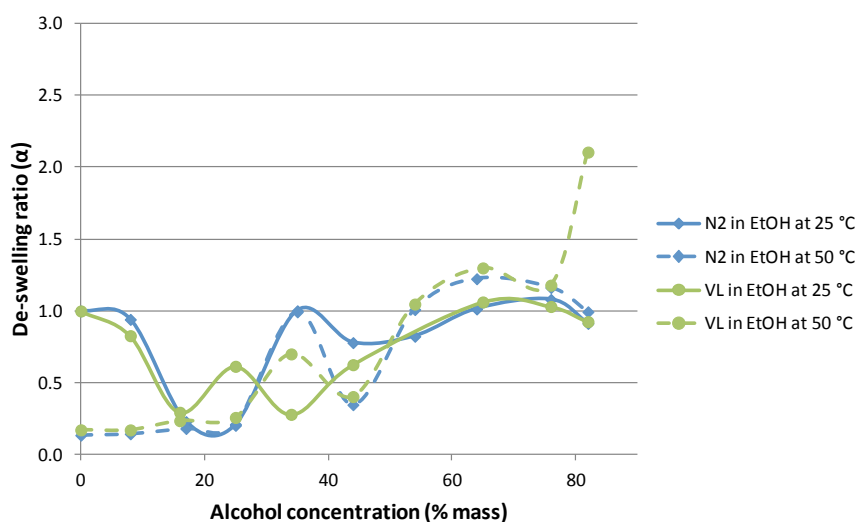
Figure 5.15 De-swelling of N2 and VL in aqueous EtOH dispersants at 25 °C and 50 °C
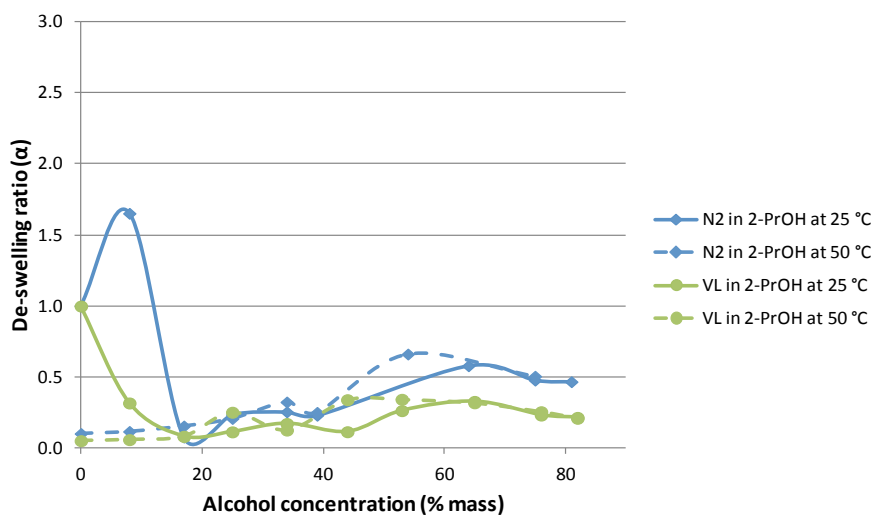
Figure 5.16 De-swelling of N2 and VL in aqueous 2-PrOH dispersants at 25 °C and 50 °C

The differences between the response of N2 and VL to the changing temperatures and alcohols types and concentrations, are not huge. However, the particles do appear to behave most similarly in EtOH, rather than MeOH or 2-PrOH. The intermediate relative polarity of EtOH may account for the similar responses observed for N2 and VL.

5.5   Summary of results

Incorporation of a hydrophobic co-monomer into a poly(NIPAM) microgel has an influence upon its alcohol-induced de-swelling and re-entrant swelling behaviour. Although the hydrophobically modified VL exhibited behaviour similar to that described for poly(NIPAM) in the literature, some differences were observed, *e.g.* a broader, flatter transition between the de-swelling and re-entrant swelling phases, and slightly different responses to the three short-chain alcohols with which N2 and VL were tested. A second period of de-swelling (following the re-entrant swelling) was frequently observed for both microgels and an initial swelling prior to de-swelling was observed for N2 that has not previously been reported in the literature.

The swelling behaviour of the microgels was studied above and below the VPTT. Interestingly it appears that the temperature-driven volume collapse characteristic of poly(NIPAM)-based microgels can be overcome at temperatures above the VPTT, *i.e.* collapsed N2 and VL particles at 50 °C can be induced to re-swell by the addition of alcohol co-solvents. The concentration of alcohol required to achieve this re-swelling decreases with alcohol chain length, as does the magnitude of the response. These behaviours have been discussed in terms of the relative hydrophobicity of the microgel particles N2 and VL, and the relative polarities of the aqueous MeOH, EtOH and 2-PrOH dispersants.

These findings show that the alcohol-induced swelling behaviour of poly(NIPAM)-based microgels can be influenced by hydrophobic modification of the particles, which appears to alter the extent and manner in which the particles interact with more hydrophobic solvents. Furthermore, alcohol co-solvents can be used to induce the re-swelling of collapsed particles above the VPTT. This may prove useful in developing novel formulations for applications that require a trigger for swelling above the VPTT, particularly when increased interactions with hydrophobic materials might be desirable.

5.6   References

[1] Crowther, H. M., Vincent, V. (1998) *Colloid & Polymer Science*, **276**, 46–51.

[2] Åkerlöf, G. (1932) *Journal of the American Chemical Society*, **54**(11), 4125–4139.

[3] Lide, D. R. (Ed) (1992) *CRC Handbook of Chemistry and Physics* (73rd Ed). Boca Raton: CRC Press.

[4] Malvern (2008) *Frequently Asked Question: Is it alright to estimate the solvent viscosity?* Malvern: Malvern Instruments. Available from Malvern Dispersion Technology Software version 5.10 Malvern Support Library.

[5] Malvern (2008) *Help Topic: Dispersant properties - advice?* Malvern: Malvern Instruments. Available from Malvern Dispersion Technology Software version 5.10 Help Topics.

[6] Bellingham + Stanley (2009) *Technical Bulleting 2002: Refractometers – What are they? What do they do? What are they used for?* Tunbridge Wells: Bellingham + Stanley.

[7] Herráez, J. V., Belda, R. (2006) *Journal of Solution Chemistry*, **35**, 1315–1328.

[8] Chang, R. (2000) *Physical Chemistry for the Chemical and Biological Sciences.* Sausalito: University Science Books.

[9] Yilmaz, H. (2002) *Turkish Journal of Physics*, **26**, 243–246.

[10] Onori, G. (1989) *Chemical Physics Letters*, **153**(3), 213–216. *In:* Crowther, H. M., Vincent, V. (1998) *Colloid & Polymer Science*, **276**, 46–51.

[11] Zhu, P. W., Napper, D. H. (1996) *Journal of Colloid and Interface Science*, **177**, 343–352.

[12] Zhang, J. and Pelton, R. (1999) *Colloid Surface*, **156**, 111-122.

[13] Soper, A. K. and Finney, J. L. (1993) *Physical Review Letters*, **71**, 4346–4349.

[14] Saunders, B. R., Crowther, H. M., Vincent, B. (1997) *Macromolecules*, **30**, 482–487.

[15] Pelton, R. (2000) *Advances in Colloid and Interface Science*, **85**, 1–33.

INVESTIGATION OF THE HETEROFLOCCULATION OF MIXED-CHARGE POLY(NIPAM) MICROGEL SYSTEMS

6.1   Introduction

The work described in previous chapters has been concerned with the behaviour of microgels from several perspectives: in aqueous dispersion, at air-water interfaces and in the presence of alcoholic co-solvents. The focus has been upon stable dispersions of hydrophobically modified microgels and the effect of varying dispersion conditions upon the particle properties and behaviour. The aim of this final experimental chapter was to study the aggregation behaviour of microgel dispersions, *i.e.* how the particles behave when they encounter each other and how these interactions can be manipulated. A great deal is known about colloidal stability and its control, but less is understood about the controlled aggregation of microgel particles, particularly mixtures of microgel particles of opposite charges.

In this study the aggregation behaviour of poly(NIPAM) microgels with different surface charge groups has been systematically investigated, with a view to increasing understanding of how the aggregation behaviour of individual and mixed-charged systems can be controlled. It is anticipated that this may aid the future development of new formulations useful in areas such as petrochemicals and personal care products.

It is clear from the existing wide-ranging literature on microgel particles and the results presented so far in this thesis that variations in dispersion conditions such as temperature, pH and solvent nature have significant impact upon the physico-chemical properties of the particles, including size, electrophoretic mobility and volume phase transition temperature (VPTT). As described in Section 1.2.6, a number of studies have investigated how changes in environmental conditions can also be used to control the stability of microgel dispersions and microgels mixed with

other colloid types (of opposite charge). However, little has been published about the control of aggregation of mixtures of oppositely charged microgels.

This phenomenon is the focus of this chapter. Three simple poly(NIPAM) microgels were prepared under identical synthesis conditions but with the variation of one single component: the initiator. This resulted in particles that varied predominantly only by surface charge group type, which were used to study how their stability, both alone and in mixtures of oppositely charged microgels, can be manipulated.

6.2   Materials and methods

6.2.1 Materials

The preparation of the three poly(NIPAM) microgels studied is described in Section 2.2.2.2 and their basic physico-chemical characteristics are reported in Section 3.3.2. The monomer (NIPAM), cross-linker (*N,N′*-methylenebisacrylamide, MBA) and synthesis conditions employed to prepare the microgels were identical. However, a different initiator was used in each case to vary the charged group expressed on the surface of the particles. Details of the two anionic and one cationic microgel, and the initiators from which they were prepared are summarized in Table 6.1. The initiator structures are shown in Table 2.1.

Table 6.1 Poly(NIPAM) microgels and initiators used in their preparation

Microgel[*]	Initiator	Charged group[†]
P-SO_3^- (N4)	Di-potassium peroxidisulphate (KPS)	SO_3H/SO_3^-
P-COO^- (N5)	4,4′-Azobis(4-cyanovaleric acid) (CVA)	$COOH/COO^-$
P-NH_3^+ (N6)	2,2′-Azobis(2-methylpropionamidine) dihydrochloride (MPA)	NH_3^+/NH_2

[*] For convenience, N4, N5 and N6 have been renamed in this chapter to indicate the charged group on the surface of each poly(NIPAM) dispersion, where P- represents poly(NIPAM). [†] The extent of ionization of the charged group is influenced by the dispersion pH, *i.e.* the form of the dominant species depends on whether the pH is above or below the pK_a of the charged group.

The behaviour of microgels P-SO_3^- (N4), P-COO^- (N5) and P-NH_3^+ (N6) was studied in the presence of three electrolytes: NaCl (Fisher, S/3120/53, Lot 0570876), $MgCl_2$ (Fisher $MgCl_2$, M10550153, Lot 0817452) and $LaCl_3$ (Aldrich, 31821, Lot SZB82490).

6.2.2 Characterization of poly(NIPAM) microgels

6.2.2.1 Particle size, electrophoretic mobility and VPTT

The basic physico-chemical characteristics of the microgels were measured as described in Sections 3.2.3, 3.2.4 and 3.2.5.

6.2.2.2 Particle electrophoretic mobility as a function of dispersion pH

The influence of dispersion pH upon particle electrophoretic mobility was investigated using the Malvern Zetasizer Nano ZS and MPT-2 autotitrator. Samples of each microgel were diluted 1:4 with 0.1 mM NaCl and placed by syringe into a folded capillary cell (DTS1060C). The average of five electrophoretic mobility measurements was automatically taken at pH increments of 0.5 ± 0.2 from pH 3–10, at a constant temperature of 25 °C. The autotitrator was programmed to adjust the pH using standard solutions of NaOH and HCl.

6.2.3 VPTT of microgels in electrolytes

The variation in turbidity of each microgel as a function of temperature was measured as described in Section 3.2.4. However, this time the microgels were diluted with electrolyte solution rather than distilled water. The VPTT of each microgel was determined in the presence of 0.1 mM and 1.0 mM NaCl, $MgCl_2$ and $LaCl_3$.

6.2.4 Flocculation of individual microgels

6.2.4.1 Flocculation in electrolytes

In order to determine the effect of the presence of electrolyte ions of different valencies upon the size and flocculation behaviour of each individual microgel, the hydrodynamic diameter (D_H) of the particles as a function of electrolyte concentration (0–0.9 M) was studied. Samples of P-SO_3^-, P-COO^- and P-NH_3^+ were prepared at the following NaCl, $MgCl_2$ and $LaCl_3$ concentrations: 0, 0.1, 1, 10 and 100 mM. Each sample contained an equal volume of microgel and therefore an approximately equal number of microgel particles.

Three 1 mL aliquots of each sample were transferred into disposable plastic cuvettes with lids. One set of samples was kept at room temperature (approximately 21 °C),

another was refrigerated at 6 °C and another was placed in an oven at 50 °C. Once equilibrated to temperature, three D_H measurements of the particles in each sample were taken at the appropriate temperature using the Malvern Zetasizer Nano ZS, with dispersant characteristics automatically calculated by the Complex Solvent Builder within the instrument software. Unfortunately, this was not available for $LaCl_3$ so the $MgCl_2$ dispersant parameters were used for the $LaCl_3$ samples. This approach was justified by the fact that the aim of the experiment was to measure the relative change in particle size as a function of concentration, not to determine absolute sizes, and recalculation of the data using alternative dispersant parameters showed that the variation in dispersant characteristics had little influence upon the results.

6.2.4.2 Investigation of floc redispersion upon cooling

Having determined the concentration of flocculation onset of the three microgels in the different electrolytes (Section 6.2.4.1), an investigation was made of whether flocculated particles would redisperse upon cooling. A portion of P-SO_3^- dispersion was diluted 1:4 with $MgCl_2$ solution to produce a sample of P-SO_3^- particles in a 10 mM $MgCl_2$ dispersant, which was placed in a glass cell. The Malvern Zetasizer Nano ZS was used to measure the D_H at 5, 25 and 50 °C (five repeat measurements at each temperature, which were each the average of three measurements). The sample was then cooled back to 25 °C and re-measured. As some sedimentation of flocs had occurred by this stage, the sample cell was then gently inverted five times and additional D_H measurements were taken at intervals for at least 24 hours. The process was repeated for P-SO_3^- in 10 mM NaCl.

6.2.4.3 Scanning electron microscope images of flocculated dispersions

Scanning electron micrographs of examples of flocculated P-SO_3^-, P-COO^- and P-NH_3^+ particles in NaCl were obtained with a Cambridge Stereoscan S-360 scanning electron microscope (SEM), using the technique described in Section 3.2.6.

6.2.5 Stability of mixed-charge microgel systems

Having determined the characteristics and flocculation behaviour of the individual P-SO_3^-, P-COO^- and P-NH_3^+ dispersions, the stability and/or heteroflocculation behaviour of mixed systems was investigated. Oppositely charged particles were

combined under different dispersant conditions so that the response of the particles to changes in dispersion characteristics (*e.g.* pH, temperature, ionic strength and net charge) could be studied and related to particle interactions taking place.

6.2.5.1 Exploratory visual evaluations of mixed-system stability

Visual investigation A

Initial visual evaluations of the stability of the mixed systems under different solvent conditions were undertaken. In the first investigation (A), the ratio of anionic to cationic microgel particles was varied, as was dispersion temperature and pH. Samples were prepared as detailed in Table 6.2. Three identical sets of each of the six combinations were prepared at room temperature and visual observations of stability were recorded ($t = 0$).[2] One set (i) was kept at room temperature (approximately 25 °C), a second set (ii) was cooled on ice (approximately 6 °C) and the third set (iii) was heated to 50 °C in a Lite Scientific Raven Oven. After 30 minutes at under these conditions, the stability was again noted ($t \approx 30$ min). The samples were then allowed to cool back to room temperature and the stability was noted ($t \approx 60$ min).

Table 6.2 Composition of mixed-charge samples for visual investigation A

Sample type	Anionic microgel	Cationic microgel	Ratio anionic:cationic microgel volumes
1	P-SO_3^-	P-NH_3^+	10:1
2	P-SO_3^-	P-NH_3^+	1:1
3	P-SO_3^-	P-NH_3^+	1:10
4	P-COO^-	P-NH_3^+	10:1
5	P-COO^-	P-NH_3^+	1:1
6	P-COO^-	P-NH_3^+	1:10

In order to assess of the influence of pH upon dispersion stability, the pH of the (ii) samples was increased above pH 8 with a drop of 0.1 M NaOH, the pH of the (iii) samples was decreased to below pH 8 with a drop of 0.1 M HCl, whilst the (i) samples were left unadjusted. All the samples were gently inverted and a stability observation was made at $t \approx 90$ min. The (ii) and (iii) samples were then re-heated to 50 °C whilst the (i) samples were left at room temperature and after 30 mins another observation was made ($t \approx 120$ min). Finally, all the samples were left at room

---

[2] In this exploratory experiment, the P-SO_3^- dispersion used was N2 (see Chapter 2), whilst the P-COO^- and P-NH_3^+ samples were equivalent samples previously prepared by Dr Jabeen Teymour. In the later, more formal investigation, the P-SO_3^- (N4), P-COO^- (N5) and P-NH_3^+ (N6) dispersions were used.

temperature overnight (observation at $t \approx 24$ hours), then refrigerated at 6 °C for a further 24 hours (observation at $t \approx 48$ hours).

Visual investigation B

A second visual investigation (B) was undertaken to determine whether the results from investigation A were repeatable and to study the added influence of electrolyte. Mixtures of P-COO$^-$ (carboxylic acid surface groups) and P-NH$_3^+$ (amine surface groups)[3] were prepared in a similar manner to investigation A but incorporating NaCl at final concentrations of 1 mM or 10 mM. Three identical sets of each of the nine combinations were prepared (Table 6.3). One set (a) was adjusted to pH ≤ 3 with 0.1 M HCl, one set (b) was adjusted to pH ≥ 8 with 0.1 M NaOH and the final set (c) was left unadjusted. Each sample in these three sets was sub-divided into three portions, of which one was left at room temperature, one was refrigerated at 6 °C and one was heated to 50 °C in the oven.

Table 6.3 Composition of mixed-charge samples for visual investigation B

Sample type	Ratio of P-COO$^-$/P-NH$_3^+$	[NaCl] (mM)
1	10:1	0
2	10:1	1
3	10:1	10
4	1:1	0
5	1:1	1
6	1:1	10
7	1:10	0
8	1:10	1
9	1:10	10

6.2.5.2 Investigation of stability of mixed-microgel systems using UV-visible spectrophotometry to measure *n*-values

Based upon the initial findings from the exploratory investigations, samples of cationic P-NH$_3^+$ mixed with anionic P-SO$_3^-$ or P-COO$^-$ were prepared with dispersion conditions that systematically varied the relative proportions of anionic:cationic charge, electrolyte type, electrolyte concentration, dispersion pH and temperature.

---

[3] In this second exploratory experiment, the P-COO$^-$ and P-NH$_3^+$ samples were equivalent samples previously prepared by Dr Jabeen Teymour. In the later, more formal investigation, the P-COO$^-$ (N5) and P-NH$_3^+$ (N6) dispersions were used.

The flocculation behaviour of the mixtures was monitored visually and by measurement of the *n*-value using an HP UV 8453 diode array spectrophotometer.

In each mixture, the total volume of microgel particles was kept constant at 2ml in a 10 mL total dispersion volume. The first step was to mix the anionic (P-SO$_3^-$ or P-COO$^-$) microgel with the cationic P-NH$_3^+$ in the correct proportions to obtain the required ratios of charged microgel particles, *i.e.* 10:1 (excess anionic), 1:1 (equal charges) or 1:10 (excess cationic). Then 1 mL of the appropriate concentration of electrolyte was added and the dispersion was made up to 9 mL with distilled water. Following mixing, it was divided into two 4.5 mL portions. One of the portions was adjusted to pH 3 using a small quantity of 0.1 M HCl and the other was adjusted to pH 8 using 0.1 M NaOH. The quantity of acid or base used to adjust the pH was noted so that each sample could finally be made up accurately to the total 5 mL.

For example, to prepare the 10:1 P-SO$_3^-$/P-NH$_3^+$ mixture in 100 mM NaCl, 1.82 mL P-SO$_3^-$ was added to 0.18 mL P-NH$_3^+$, to which 1 mL 1.0 M NaCl was added before the dispersion was made up to 9 mL with distilled water. This was split into equal 4.5 mL portions, one of which was adjusted to pH 3 and the other was adjusted to pH 8, before both were accurately made up to 5 mL. In summary, the mixtures were prepared:

- for two microgel combinations (P-SO$_3^-$/P-NH$_3^+$ and P-COO$^-$/P-NH$_3^+$);
- at three anionic:cationic microgel charge ratios (10:1, 1:1 and 1:10);
- at two pH values (3 and 8);
- at four electrolyte concentrations (0, 1, 10 and 100 mM);
- for three types of electrolyte (NaCl, MgCl$_2$ and LaCl$_3$).

The NaCl samples were prepared first. A 1 mL aliquot of each mixture was placed in a plastic cuvette with lid and left at 25 °C for 1 hour, after which the UV-visible absorbance was measured and visual observations of dispersion stability were recorded. The samples were then refrigerated for approximately 1 hour, before UV-visible measurements and observations were repeated. The samples were then placed in the oven at 50 °C for approximately 1 hour before final measurements and observations were taken.

This process was repeated for the MgCl$_2$ samples, which were measured after an additional 24 hours at 25 °C. Digital images of the samples were taken. The process was then repeated for the LaCl$_3$ samples, which were studied even longer, with the samples measured at 24 hours, then immediately following gentle inversion, then after at least one further 24 hour period at room temperature. The *n*-values were calculated from the UV-visible measurements as described in Equation 1.15.

6.3 Results and discussion

6.3.1 Characterization of poly(NIPAM) microgels

6.3.1.1 Particle size, electrophoretic mobility and VPTT

The hydrodynamic diameter (D_H) of *P*-SO$_3^-$, *P*-COO$^-$ and *P*-NH$_3^+$ in water as a function of temperature is shown in Fig. 6.1. All three microgels undergo a volume phase transition at approximately 34 °C (the VPTT), swelling below the VPTT and collapsing above the VPTT. The data is discussed in more detail in the Section 3.3.2, where spectroscopic measurements of particle VPTT and laser Doppler velocimetry measurements of electrophoretic mobility are also presented. For convenience, the data is summarized in Table 6.4.

The data clearly indicates differences between the three microgels. In terms of particle size, the main observations were that the D_H of all three microgels decreases substantially with temperature, with *P*-SO$_3^-$ substantially larger throughout than the similarly-sized *P*-COO$^-$ and *P*-NH$_3^+$. The variation in D_H was greater below the VPTT than above it and there was little difference in overall de-swelling ratios (α) between the microgels (5–50 °C), with all three decreasing in volume by approximately 90 %.

As the synthesis conditions for all three microgels were identical apart from the type of initiator used, the differences in D_H and α values are likely to result from the differences in surface charge group introduced by each initiator. As discussed in Section 3.3.4.4, not only does each microgel carry a different charge type but there are also differences in the size and structure of the R groups to which the charged groups are attached, which may influence the extent to which the particles swell or collapse.
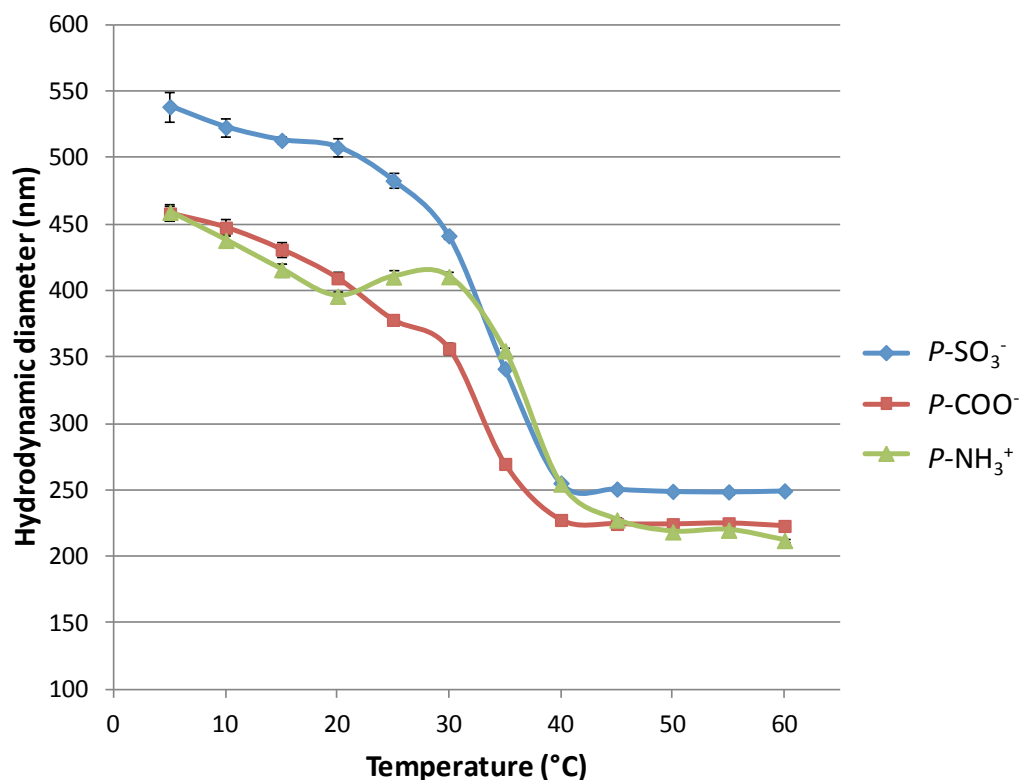
Figure 6.1 D_H **of** *P*-**SO₃⁻**, *P*-**COO⁻ and** *P*-**NH₃⁺ particles in water as a function of temperature (5 °C intervals) (± 1 s.d.).** *P*- stands for poly(NIPAM).

Table 6.4 Physico-chemical properties of *P*-**SO₃⁻**, *P*-**COO⁻ and** *P*-**NH₃⁺ particles**

Poly(NIPAM) microgel		*P*-SO₃⁻ (N4)	*P*-COO⁻ (N5)	*P*-NH₃⁺ (N6)
Initiator		KPS	CVA	MPA
pH of stock dispersion		7	7	8
Charged group on surface at stock pH		SO₃⁻	COO⁻	NH₃⁺
Approximate pK_a of surface group[1]		2	4.5	10
VPTT (°C)		34	34	34
D_H ± 1 s.d. (nm)	5 °C	539 ± 12	458 ± 6	459 ± 6
	25 °C	483 ± 6	378 ± 3	410 ± 5
	50 °C	249 ± 1	224 ± 1	218 ± 1
De-swelling ratio (α)†	5–25 °C	0.72	0.56	0.71
	25–50 °C	0.14	0.21	0.15
	5–50 °C	0.10	0.12	0.11
EM ± 1 s.d. (10^{-8} m²s⁻¹V⁻¹)	5 °C	-0.66 ± 0.01	-0.91 ± 0.01	+0.39 ± 0.01
	25 °C	-1.11 ± 0.02	-1.43 ± 0.03	+0.62 ± 0.02
	50 °C	-4.05	-3.99 ± 0.04	+3.75 ± 0.09
Theoretical no. of particles in dispersion††		6.8×10^{14}	9.4×10^{14}	1.0×10^{15}
Theoretical no. radical groups per particle††		3.3×10^6	2.3×10^6	2.2×10^6

† $\alpha = (d/d_0)^3$, where d = collapsed diameter relative to d_0 = swollen diameter for specified temperature range. †† Calculated using NIPAM monomer density = 1.09 g/cm³ from Ref. [2] based on particle D_H at 50 °C (Appendix G).

The magnitude of the surface charge density (electrophoretic mobility) increased substantially for all three particles above the VPTT, corresponding to the reduction in particle size (and thus surface area). However, the magnitude of the charge density varied between the particles, with P-COO$^-$ > P-SO$_3^-$ > P-NH$_3^+$ below the VPTT and more similar values above the VPTT (as was the case for D_H measurements). The anionic particles (P-SO$_3^-$ and P-COO$^-$) were more strongly charged than the cationic P-NH$_3^+$, particularly below the VPTT, and P-COO$^-$ with carboxylic acid groups tended to be more strongly charged than P-SO$_3^-$ with sulphate groups.

These differences may be related to the extent of ionization of the charged groups and the water molecules in the bulk solvent. As shown in Table 6.4 the stock dispersions were within pH 7–8, which, according to the pK$_a$ values, suggests that all the charged groups were predominantly ionized. The electrophoretic mobility values in Table 6.4 represent the net charge of the particles at the time of measurement. At any given pH, not all charged groups are in the same ionization state because an equilibrium exists, where, for example:

$$R - COOH \rightleftharpoons R - COO^- + H^+$$
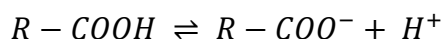
[Equation 6.1]

Therefore it is possible that not all carboxylate groups on the P-COO$^-$ particle surfaces will be ionized: some will be protonated (–COOH) whilst others will be deprotonated (–COO$^-$). Only the ionized species contribute to the electrophoretic mobility.

This could help explain why the magnitude of the P-NH$_3^+$ electrophoretic mobility values were substantially smaller than those for P-SO$_3^-$ and P-COO$^-$. With a pK$_a$ of approximately 10, the majority of the P-NH$_3^+$ amine groups are likely to be protonated (-NH$_3^+$) at the stock dispersion pH of 8. However, because the dispersion pH is approaching the pK$_a$, some of the groups may already be in the deprotonated, uncharged –NH$_2$ form and therefore would not contribute to the electrophoretic mobility of the particles. The pH values of the P-SO$_3^-$ and P-COO$^-$ dispersions were substantially above the pK$_a$ values and therefore the majority of the respective sulphate and carboxylate groups were likely to be ionized.

6.3.1.2 Influence of pH upon surface charge

In order to obtain a clearer understanding of the influence of ionization upon particle surface charge, the electrophoretic mobility was measured as a function of dispersion pH from approximately pH 3–10 (Fig. 6.2).
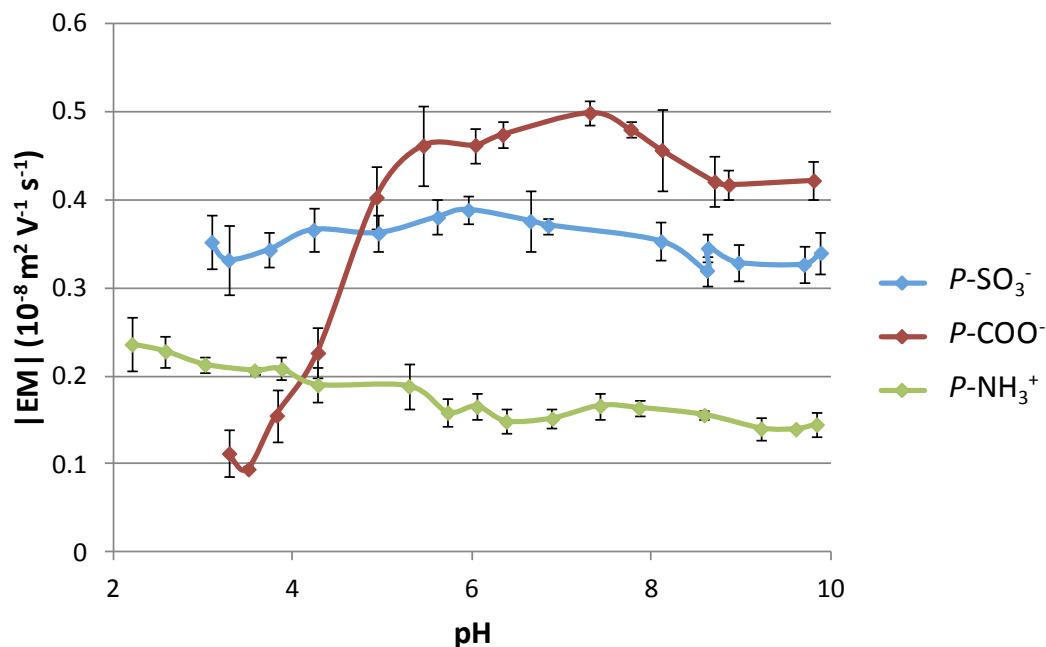
Figure 6.2 Magnitude of electrophoretic mobility of *P*-SO$_3^-$, *P*-COO$^-$ and *P*-NH$_3^+$ particles in 0.1 mM NaCl as a function of pH at 25 °C (± 1 s.d)

For the sulphate groups on *P*-SO$_3^-$, all the measurements were taken above the pK$_a \approx 2$, so the majority of the groups would be deprotonated throughout (-SO$_3^-$) and therefore, as expected, little change was observed with increasing pH. With pK$_a \approx 10$, the amine groups on *P*-NH$_3^+$ were predominantly protonated (-NH$_3^+$) throughout so, as expected, just a slight decrease in electrophoretic mobility was observed as the particles approached their pK$_a$ and therefore the proportion of deprotonated (-NH$_2$) groups increased. However, with pK$_a \approx 4.5$, the carboxylate groups on *P*-COO$^-$ switched from the protonated (-COOH) to deprotonated (-COO$^-$) form as the pH increased and consequently a substantial increase in the magnitude of electrophoretic mobility was observed as the pH and relative proportion of deprotonated groups increased.

6.3.2 VPTT of microgels in electrolytes

The potential influence of the three electrolytes of increasing cationic valency upon the VPTT of the P-SO_3^- microgels was investigated by monitoring the change in turbidity of the dispersions in the presence of 0.1 mM and 1.0 mM electrolyte. A summary of the VPTT values is given in Table 6.5. In this form the data suggests that the electrolytes make virtually no difference to the VPTT of P-SO_3^- at either concentration, although it is possible that 1.0 mM $LaCl_3$ does cause a small reduction in VPTT. If the full transmittance data (5–60 °C) for each system is plotted (data not shown) the curves are virtually superimposable upon one another.

Table 6.5 VPTT of P-SO_3^- in presence of NaCl, $MgCl_2$ and $LaCl_3$

Electrolyte	0.1 mM	1.0 mM
None (H_2O only)	35.0	35.0
NaCl	35.3	35.0
$MgCl_2$	35.5	35.4
$LaCl_3$	35.2	34.4

However, to determine whether any further information is contained within the data, the measurements for the P-SO_3^- particles in electrolyte solution were normalized against the data for the P-SO_3^- particles in water only, *i.e.* the values for the samples containing microgel, water and electrolyte were divided by the values for the sample containing microgel and water only. Figure 6.3 shows the plots of the normalized transmittance as a function of temperature.

In this format, the data clearly shows different responses to the three electrolytes from around the VPTT (approximately 35 °C), with the magnitude of the effect increasing with cation valency, *i.e.* $Na^+ < Mg^{2+} < La^{3+}$. A marked increase in the response was also observed as the concentration of the electrolytes increased, *i.e.* the response to 0.1 mM electrolyte was less than to 1.0 mM electrolyte. Higher concentrations were not tested because of the likelihood of inducing flocculation (see next section).

The data shows that dispersion turbidity increased (*i.e.* decreased transmittance) as the ion valency increased. The VPTT was virtually unaffected, *i.e.* the swelling behaviour of the particles was not affected. Instead, the variations apparent in Fig. 6.3 indicate that the extent to which P-SO_3^- is solvated varies between the

different electrolytes and concentrations. This may reflect increased competition between particles and electrolyte ions for the water molecules as both the ion valency and ion concentration increases.
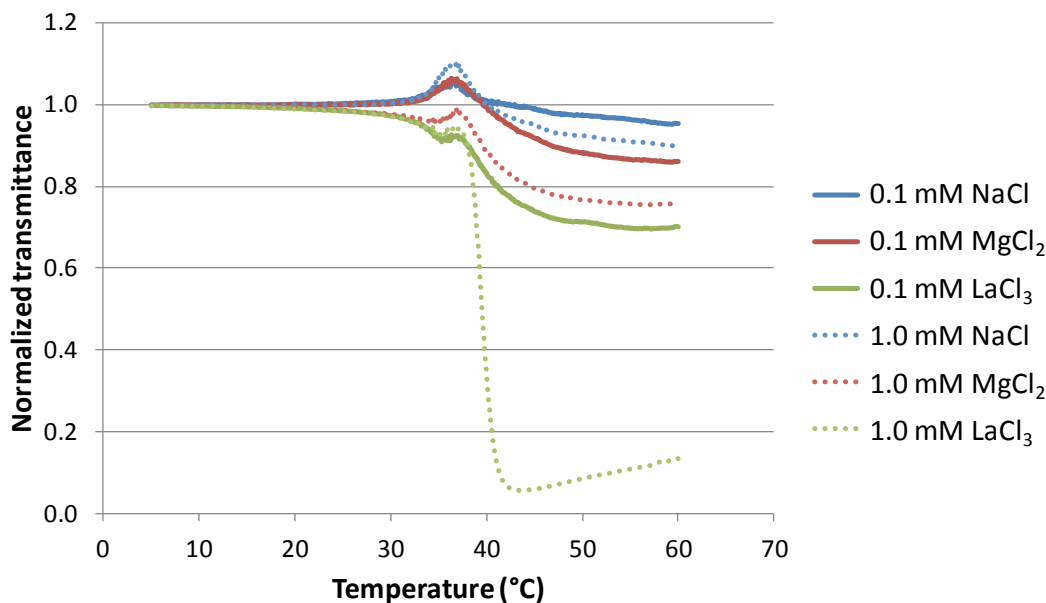
Figure 6.3   Normalized transmittance of *P*-SO₃⁻ dispersions in the presence of NaCl, MgCl₂ or LaCl₃ as a function of temperature

6.3.3 *Flocculation of microgels in electrolytes*

The influence of adding electrolyte of increasing valencies to the three microgel dispersions was investigated using dynamic light scattering (DLS) to study both the effect of the electrolytes upon stable particle sizes and the extent to which they cause flocculation of the particles. As described in Section 1.2.3.4, the double layer thickness (Debye length, $1/\kappa$) of a particle in dispersion is strongly influenced by the ionic strength of the dispersant. Changes in the concentration or valency of the electrolyte alter the ionic strength, which in turn influences the value of κ (see Equations 1.1–1.3); increased ion concentration or valency therefore lead to a reduction in the double layer thickness ($1/\kappa$). The D_H was measured as a function of electrolyte concentration at temperatures above and below the VPTT of the particles to investigate the effect of increasing cation valency upon microgel size and flocculation behaviour.

6.3.3.1 Influence of electrolyte on D_H of dispersed microgel particles

Firstly, the effect of the electrolytes upon the D_H of stable microgel dispersions was measured. Figures 6.4, 6.5 and 6.6 show the D_H of P-SO_3^-, P-COO^- and P-NH_3^+ particles respectively as a function of NaCl, $MgCl_2$ and $LaCl_3$ concentration at 25 °C. Figure 6.4 shows that in general, the size of P-SO_3^- decreases with increasing electrolyte concentration. This was anticipated as several authors have reported such behaviour for poly(NIPAM) and more hydrophilic poly(NIPAM) co-polymer microgels.[3,4,5] The reduction can be ascribed to the decrease of the double layer thickness resulting from the increasing in electrolyte concentration.

There was also a difference in the effect of the electrolytes, with P-SO_3^- smaller in NaCl than in $MgCl_2$ or $LaCl_3$. This is unexpected in that the higher valency Mg^{2+} and La^{3+} ions should in theory cause greater reductions in double layer thickness and thereby reduce particle D_H to a greater extent.[6,7] However, the results do suggest that increasing electrolyte concentration of any type makes the solution a poorer solvent for P-SO_3^- particles. Furthermore, it suggests that NaCl is a poorer solvent for P-SO_3^- than $MgCl_2$ or $LaCl_3$ (which have similar effects upon D_H). In fact, the higher valency electrolytes do have a greater effect but not in terms of decreasing particle size; conversely as electrolyte valency increases, the solvent becomes better (provides more hydrogen bonding opportunities) for the particles and swelling is observed.

The hydrated effective diameters of the cations are reported in Table 6.6, which shows that the hydrated Mg^{2+} (800 pm) and La^{3+} (900 pm) ions are similar in size, approximately double that of the hydrated Na^+ ion (450 pm). It is possible that the thicker hydrated layers associated with Mg^{2+} and La^{3+} screen the charged ions more effectively than the narrower hydrated layer around the Na^+ ions, permitting the lower valency Na^+ to have a greater effect upon the electric double layer of the microgels than the higher valency Mg^{2+} and La^{3+}.

Similar were observed for P-COO^-, with slight increases in D_H observed at the higher electrolyte concentrations (Fig. 6.5). Once again, NaCl reduced D_H to a greater extent than $MgCl_2$ and $LaCl_3$. However, more variation was observed for P-NH_3^+ (Fig. 6.6). This is further evidence that the nature of the charged surface groups is significant to the overall size and swelling behaviour of poly(NIPAM) particles.
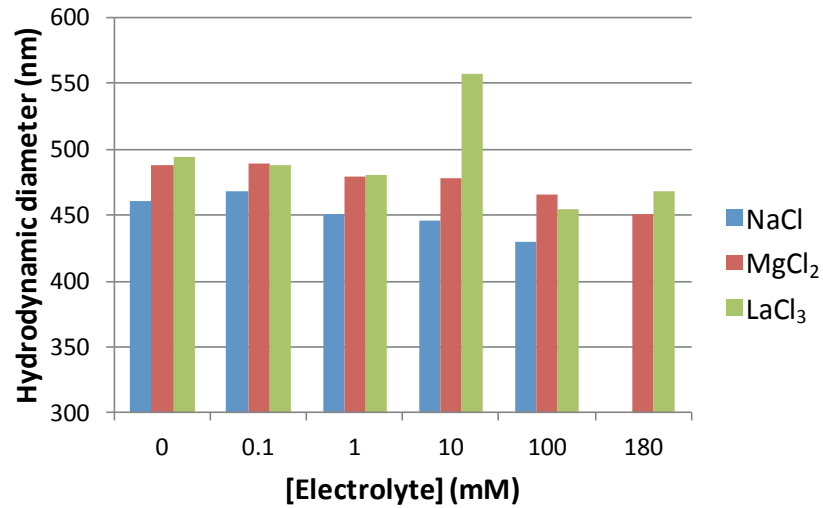
Figure 6.4 D_H of dispersed *P*-SO_3^- particles at 25 °C in NaCl, $MgCl_2$ and $LaCl_3$
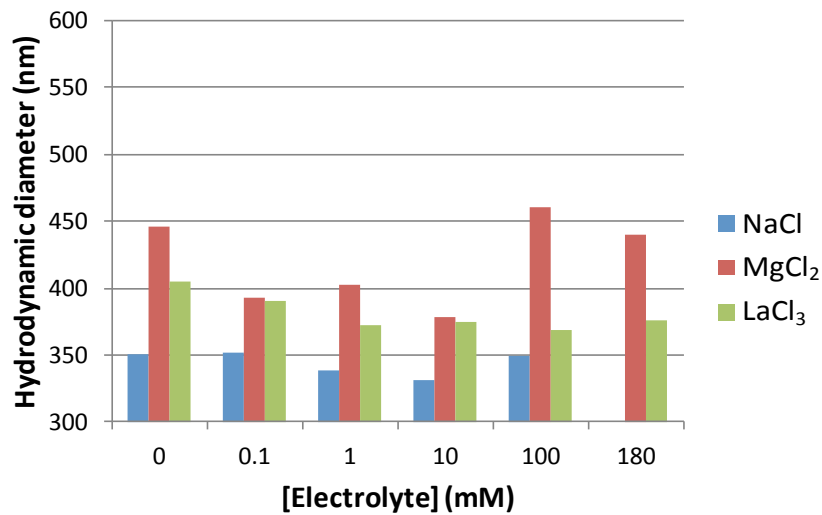
Figure 6.5 D_H of dispersed *P*-COO^- particles at 25 °C in NaCl, $MgCl_2$ and $LaCl_3$
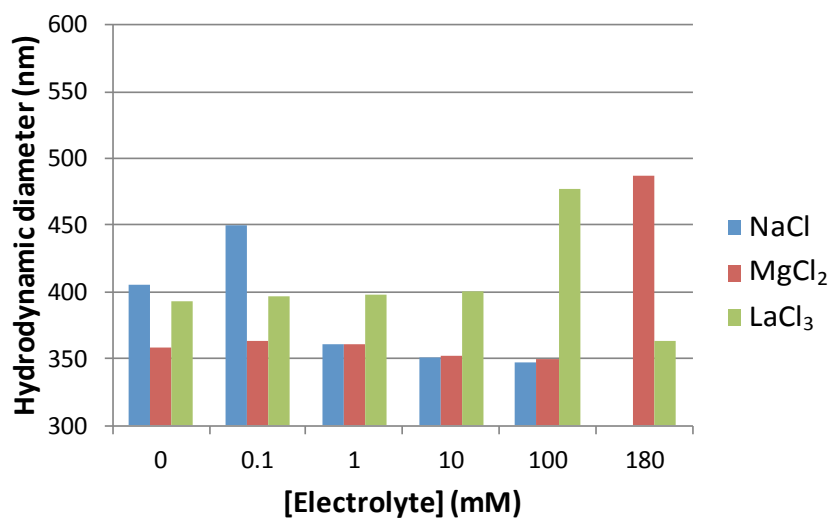
Figure 6.6 D_H of dispersed *P*-NH_3^+ particles at 25 °C in NaCl, $MgCl_2$ and $LaCl_3$

Table 6.6 Electrolyte ion diameters

Ion	Cl^-	Na^+	Mg^{2+}	La^{3+}
Unhydrated effective diameter (pm)	190	100	90	200
Hydrated effective diameter (pm)	300	450	800	900

Data from Ref. [8].

In order to investigate the influence of temperature and particle conformation upon these trends, further measurements were made at 6 and 50 °C, to see what effect, if any, cooling or heating the systems might have. The results for P-SO_3^- in NaCl at 6, 25 and 50 °C are summarized in Fig. 6.7, whilst the plots of the full results for P-SO_3^-, P-COO^- and P-NH_3^+ at 6 and 50 °C in all three electrolytes are given in Appendix H.
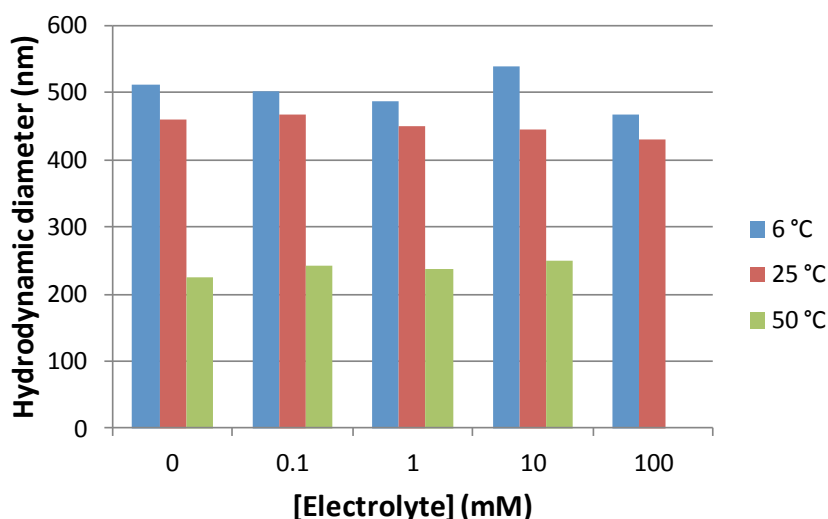
Figure 6.7 D_H of dispersed P-SO_3^- particles at 6, 25 and 50 °C in NaCl

As expected, the trends observed for D_H in water as a function of temperature (Table 4.3) were replicated in the presence of NaCl, *i.e.* D_H was substantially reduced above the VPTT and additional swelling of the particles was observed on cooling the dispersion from 25 to 6 °C. The data in Appendix H indicates that, as with the 25 °C data, at 6 °C there was a general tendency for D_H to decrease with increasing concentration of all three electrolytes. At 50 °C the variation between the different electrolytes, different particles and with increasing concentration was much less, as would be expected for the collapsed particles of more uniform size. In the collapsed conformation above the VPTT the surface charge density is much greater and therefore the particle diameter is likely to be less influenced by low electrolyte concentrations.

In summary, the three poly(NIPAM) microgels with different charged surface groups respond slightly differently to electrolytes of increasing cation valency. This effect appears to be related to the extent to which the different electrolyte solutions solvate the particles. This in turn may be at least partly determined by the thickness of the hydrated layers surrounding the cations, where Na^+ ions with a relatively thinner hydrated layer (350 pm) appear to have greater influence upon the particle D_H than the higher valency ions ($Mg^{2+} = 710$ pm and $La^{3+} = 700$ pm) which have thicker hydrated diameters (Table 6.6).

6.3.3.2 Determination of the critical flocculation concentration

As described in Section 1.2.6, when dispersed particles collide, if they remain in contact afterwards they aggregate and may precipitate out of dispersion.[9] Permanent aggregation is known as coagulation, whilst temporary (reversible) aggregation is known as flocculation.[9] Studies such as those by Snowden and Vincent[10] and Rasmussen and Vincent[11,12] showed that the aggregation of poly(NIPAM) microgels in the presence of NaCl was reversible, *i.e.* flocculation.

Furthermore, the nature of the electrolyte (cation and anion) has been shown to be significant.[13,14] It was therefore anticipated that the P-SO$_3^-$, P-COO$^-$ and P-NH$_3^+$ microgels in this study were each likely to exhibit flocculation at a specific critical flocculation concentration (CFC) of NaCl, MgCl$_2$ and LaCl$_3$. The D_H of each dispersion was therefore monitored as a function of electrolyte concentration at 6, 25 and 50 °C. The results for P-SO$_3^-$ at these temperatures are shown in Figures 6.8, 6.9 and 6.10.

At 6 °C, no flocculation of the P-SO$_3^-$ particles was observed (Fig. 6.8). At 25 °C, as previously noted, the particles were slightly smaller, in agreement with data for particle size in water (Table 4.3). Flocculation was observed for particles in 0.9 M NaCl.
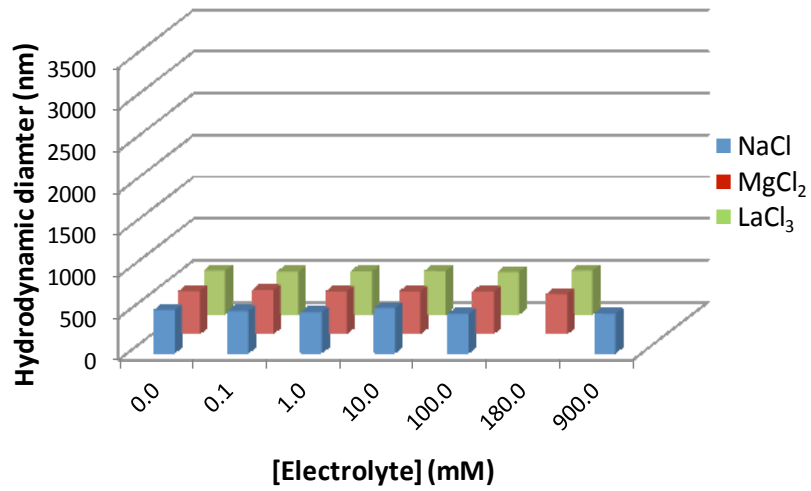
Figure 6.8 *P*-SO$_3^-$ particle *D*$_H$ as a function of electrolyte concentration at 6 °C
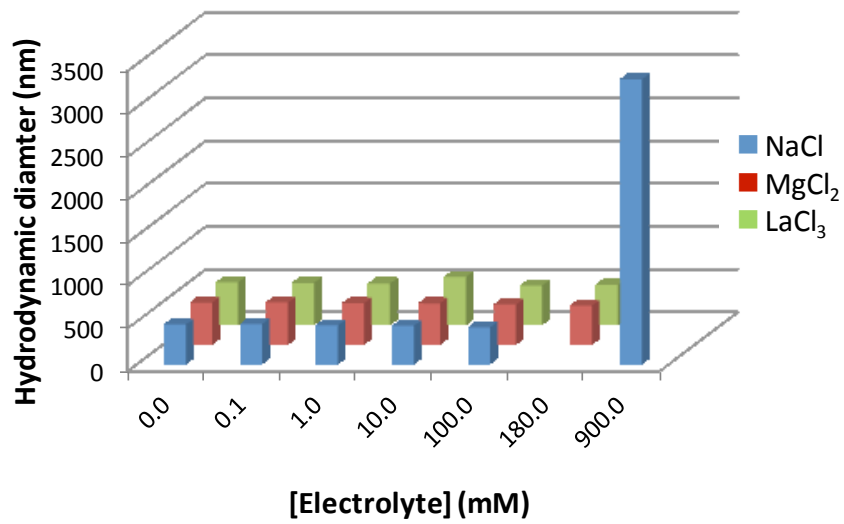
Figure 6.9 *P*-SO$_3^-$ particle *D*$_H$ as a function of electrolyte concentration at 25 °C
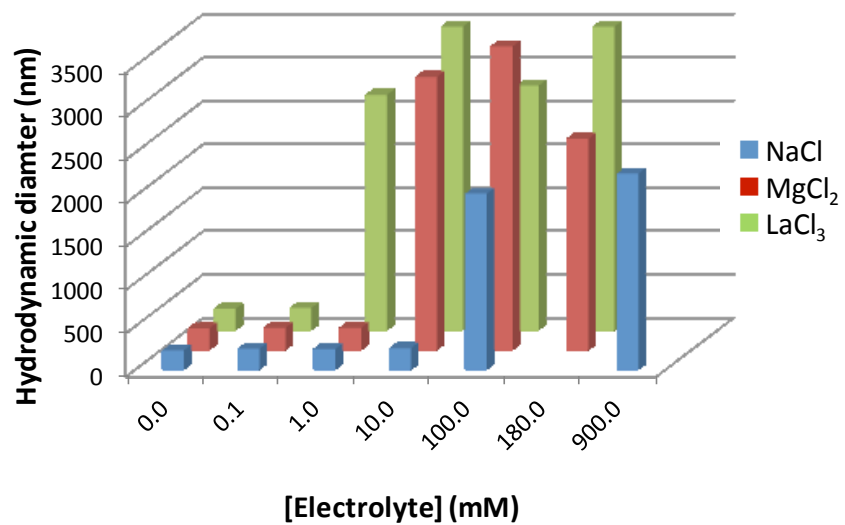
Figure 6.10 *P*-SO$_3^-$ particle *D*$_H$ as a function of electrolyte concentration at 50 °C

At 50 °C, however, far more P-SO$_3^-$ flocculation was observed. Flocculation occurred above the VPTT in all three electrolytes, with the amount of electrolyte required to induce flocculation decreasing as the valency of the cation increased. For example, P-SO$_3^-$ flocculated in 100 mM NaCl, compared to just 10 mM MgCl$_2$ and only 1 mM LaCl$_3$. The experiment was repeated for the other two microgels and the results are summarized in Table 6.7.

Table 6.7 Critical flocculation concentrations of P-SO$_3^-$, P-COO$^-$ and P-NH$_3^+$ microgels in NaCl, MgCl$_2$ and LaCl$_3$ at 6, 25 and 50 °C (from 0–180 mM)

Microgel	NaCl (mM)			MgCl$_2$ (mM)			LaCl$_3$ (mM)		
	6 °C	25 °C	50 °C	6 °C	25 °C	50 °C	6 °C	25 °C	50 °C
P-SO$_3^-$	–	–	100	–	–	10	–	–	1
P-COO$^-$	–	–	100	–	–	10	–	–	10
P-NH$_3^+$	–	–	100	–	–	10	–	–	1

In NaCl, MgCl$_2$ and LaCl$_3$ no flocculation was observed from 0–180 mM electrolyte at 6 or 25 °C. However, flocculation was observed for all three microgels at 50 °C in all three electrolytes. Below the VPTT, the stability of aqueous microgel dispersions is maintained by repulsive electrostatic interactions[15] and steric stabilization[16,17] which oppose the attractive long-range van der Waals forces that result from temporary or induced dipoles.[7,9] Above the VPTT, as evident in Table 6.4, the charge density of the particles increases substantially, increasing electrostatic repulsion between the particles.

In theory, this makes the dispersion more stable to flocculation but as steric stabilization is lost above the VPTT due to collapse of the "hairy layer", if the electrostatic repulsion is screened in some way, *e.g.* by addition of counter-ions, the forces opposing flocculation may be overcome by the now even stronger van der Waals attractions.[18,19] This explains why over this concentration range flocculation was only seen at 50 °C – below the VPTT is likely that the steric stabilization from the "hairy layer" was sufficient to maintain dispersion stability even when electrostatic repulsions were reduced by the addition of higher concentrations of electrolyte. The results suggest that cooling from 25 to 5 °C may enhance resistance to flocculation.

Overall, the CFC of all the microgels decreased as the valency of the electrolyte cation increased, *i.e.* the concentration of NaCl required to induce flocculation was larger than in MgCl$_2$, which in turn was larger than in LaCl$_3$. This is in accordance

with theory, where an ion of greater valency will decrease the double layer thickness by a greater extent, therefore decreasing the electrostatic repulsion between the particles and increasing the likelihood of flocculation occurring. There was almost no difference in the way the microgels responded to the electrolytes, with the same CFC values found in each electrolyte, apart from P-COO$^-$, which had a CFC of 10 mM LaCl$_3$ compared to a CFC of 1 mM LaCl$_3$ for P-SO$_3^-$ and P-NH$_3^+$.

It appears that the higher the cation valency and size, the more effectively the surface charge is screened above the VPTT, resulting in a lower CFC. This is as anticipated from the Shultze-Hardy rule (Equation 1.10), which states that the critical coagulation concentration (comparable to the CFC) is inversely proportional to the ion valency.[7] Charged surfaces preferentially adsorb counter-ions, particularly those with a high charge number.[12] The decrease in CFC also correlates with the effective hydrated diameters of the cations (Table 6.6), with the far larger Mg^{2+} and La^{3+} having greater effect than the smaller Na$^+$.

However, these effects appear to be opposite to those observed for the influence of the cations upon D_H prior to flocculation onset, where NaCl generally reduced D_H to a greater extent than MgCl$_2$ and LaCl$_3$ (Section 6.3.4.1). This may highlight a difference between the mechanisms at play. The reduction in particle size prior to flocculation appears to be related to differences in the extent to which the three electrolytes solvate the particles, with NaCl solutions generally providing solvent conditions that are least effective at hydrating and swelling the particles. Conversely, the onset of flocculation appears to be related to the charge of the cations, with the higher valency cations having the greater effect, by more effectively screening the electrostatic repulsion between the particles. However, the two mechanisms are closely related, *e.g.* the "stronger", larger Mg^{2+} and La^{3+} attract more water molecules giving them thicker effective hydrated diameters, which screen them more effectively from the microgel particles, giving them less influence upon the solvation of the particles.

The relatively insubstantial differences in response between the anionic (P-SO$_3^-$ and P-COO$^-$) particles compared to the cationic (P-NH$_3^+$) particles is also noteworthy. The CFCs for each particle type were almost entirely the same in each electrolyte, irrespective of the microgel surface charge. Determination of more precise CFC

values in each electrolyte might highlight more subtle differences between the particles but on the basis of these results, it appears that particle surface charge type (*i.e.* anionic or cationic) does not substantially alter the CFC in any given electrolyte. The anionic particles (*P*-SO$_3^-$ and *P*-COO$^-$) attract cationic counter-ions (Na$^+$, Mg^{2+}, La^{3+}) but the cationic *P*-NH$_3^+$ will attract anionic counter-ions (Cl$^-$ in each case). If dramatically different CFC values had been obtained for the cationic *P*-NH$_3^+$, it would suggest that the cations are primarily responsible for causing flocculation. However, as the CFC was the same for the cationic *P*-NH$_3^+$ it suggests that the Cl$^-$ ions must also be influential.

Consideration of the stoichiometry shows that complete dissociation of an equal concentration of each electrolyte molecule would yield a different number of moles of Cl$^-$ ions, *i.e.* NaCl would yield one mole of Cl$^-$ ions, whilst MgCl$_2$ would yield 2 moles of Cl$^-$ and LaCl$_3$ would yield 3 moles of Cl$^-$. As the CFC for *P*-NH$_3^+$ also decreases in the order NaCl > MgCl$_2$ > LaCl$_3$, this suggest that it may be the increasing concentration of Cl$^-$ ions that is responsible for lowering the CFC, whereas for anionic *P*-SO$_3^-$ and *P*-COO$^-$ it appears to be the increasing valency of the cations that is responsible (the relative number of moles of each cation is the same in each case).

6.3.3.3 Investigation of redispersion of flocculated particles upon cooling

The next step was to confirm whether the observed flocculation was truly reversible and, if so, whether the flocculated particles redispersed completely. Dispersion-flocculation-redispersion cycles for poly(NIPAM) in NaCl that can be repeated many times have been reported[10] so it was anticipated that the flocculated particles in this study would redisperse upon cooling. DLS was used to monitor changes in dispersion particle size after flocculation induced by heating above the VPTT.

Figure 6.11 shows the variation in particle size of *P*-SO$_3^-$ particles dispersed in 0.8 M NaCl. The initial particle size prior to heating was 295 nm. The dramatic increase in reported particle size upon heating (more than 6 μm) indicates that flocculation had occurred. As the dispersion cooled, the reported particle size decreased with time. However, when the cooled dispersion size stabilized (after approximately 55 hours), the reported size was approximately 1 μm, substantially greater than the original particle size of 295 nm prior to heating. This suggests that the previously flocculated

particles do not completely redisperse upon cooling, instead they may remain as dimer or trimer units. The average particle size of 900 nm at 67 hours is roughly three times that of the original size prior to flocculation, which supports the idea of trimer formation. At around 1 μm diameter even the trimers could be colloidally stable. The smallest redispersed size of 415 nm was measured at around 50 hours.
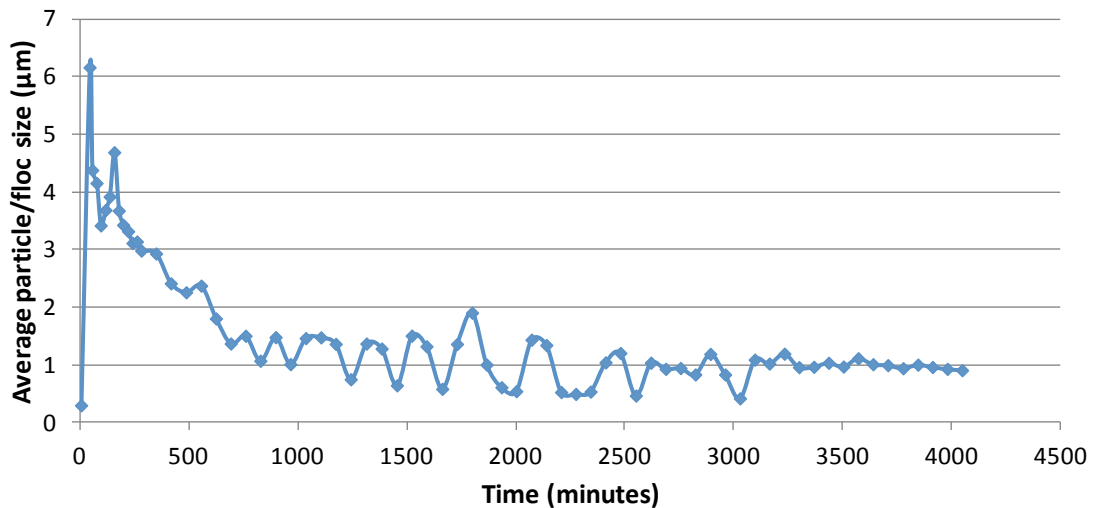
Figure 6.11 Change in average particle/floc size of *P*-SO$_3^-$ in 0.8 M NaCl through a heating and cooling cycle, as a function of time

First data point represents dispersed particle size at 25 °C prior to heating; second data point represents size of flocs at 50 °C; third data point shows average size on cooling to 25 °C; forth data point onwards show average floc/particle size at 25 °C (following gentle inversion of cuvette) over time.
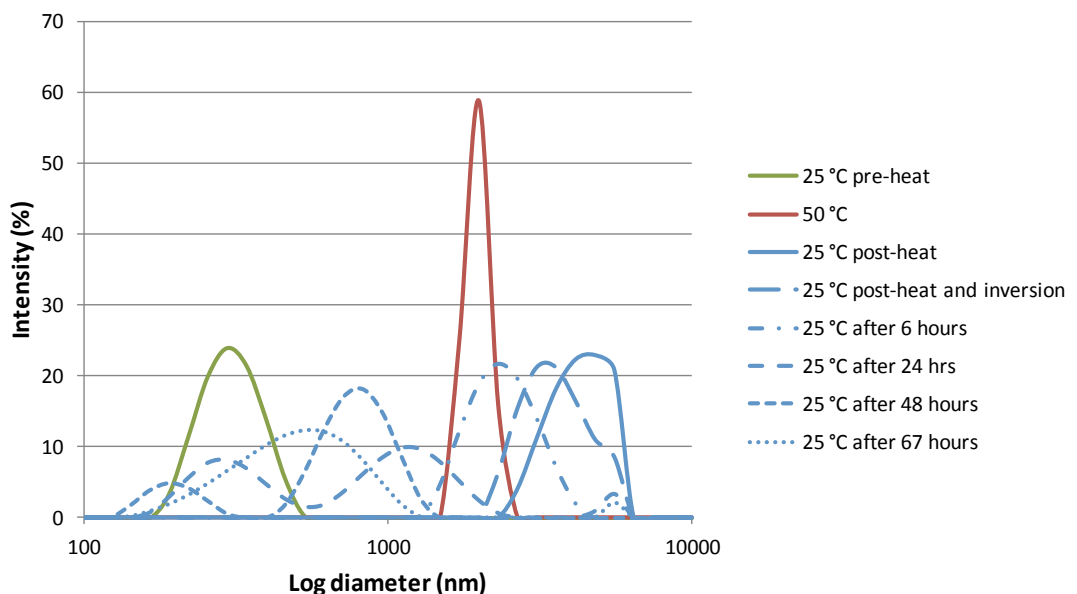
Figure 6.12 Changes in intensity size distribution of *P*-SO$_3^-$ in 0.8 M NaCl as a function of time

The particle sizes reported by DLS are the average of the particle size distribution at a given time or temperature. Therefore the measurement at any given time reflects the average of a range of particles, which likely include single particles, dimers, trimers and even larger aggregates of particles. To investigate this further, the particle size intensity distributions at key points were plotted in Fig. 6.12.

The green monomodal curve represents the particle size distribution at 25 °C prior to heating. Upon heating, the average size increases dramatically (red curve), indicating the presence of large aggregates and the single peak indicates that all the particles have aggregated – there are no separate smaller particles/aggregates. The solid blue curve shows the distribution after cooling, which is still a single peak but the average aggregate size is even larger. However, as the dispersion cools further and after the sample was gently inverted to redisperse the sediment (blue dashed curves, where dashes get smaller as time increases) the distribution peaks shift to the left and become multimodal. This indicates that the aggregates were redispersing, *i.e.* the particles were flocculated rather than coagulated. The multimodal peaks reflect the fact that whilst some particles have redispersed, others remain aggregated. The final distribution (small dotted blue line) at 67 hours indicates that whilst the majority of the particles have redispersed, the average size is still substantially larger than the original particle size, suggesting the existence of dimers or other multiples of particles.
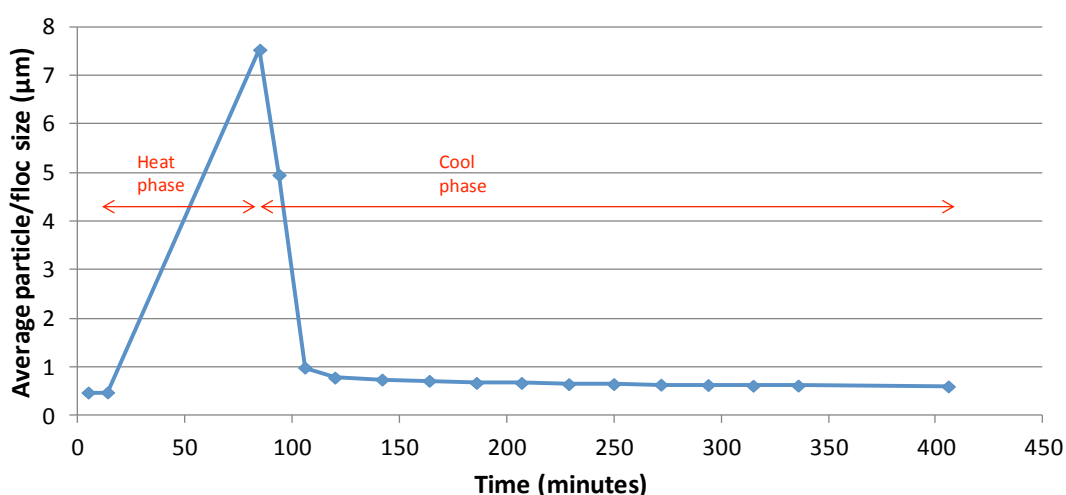
Figure 6.13 Change in average particle/floc size of *P*-SO$_3^-$ in 0.8 M MgCl$_2$ through a heating and cooling cycle, as a function of time

The experiment was repeated for *P*-SO$_3^-$ in 0.8 M MgCl$_2$ over a shorter period to check that the phenomenon was not limited to NaCl (Fig. 6.13). A similar trend was observed, with particle size increasing from 469 nm at 25 °C to flocs of more than 7.5 µm at 50 °C, which gradually redispersed to an average of around 600 nm on cooling. At around double the initial particle size, it suggests dimers remained after redispersion. Once again, the intensity size distributions at key points were contrasted (Fig. 6.14), showing similar trends to those observed for *P*-SO$_3^-$ in 0.8 M NaCl.
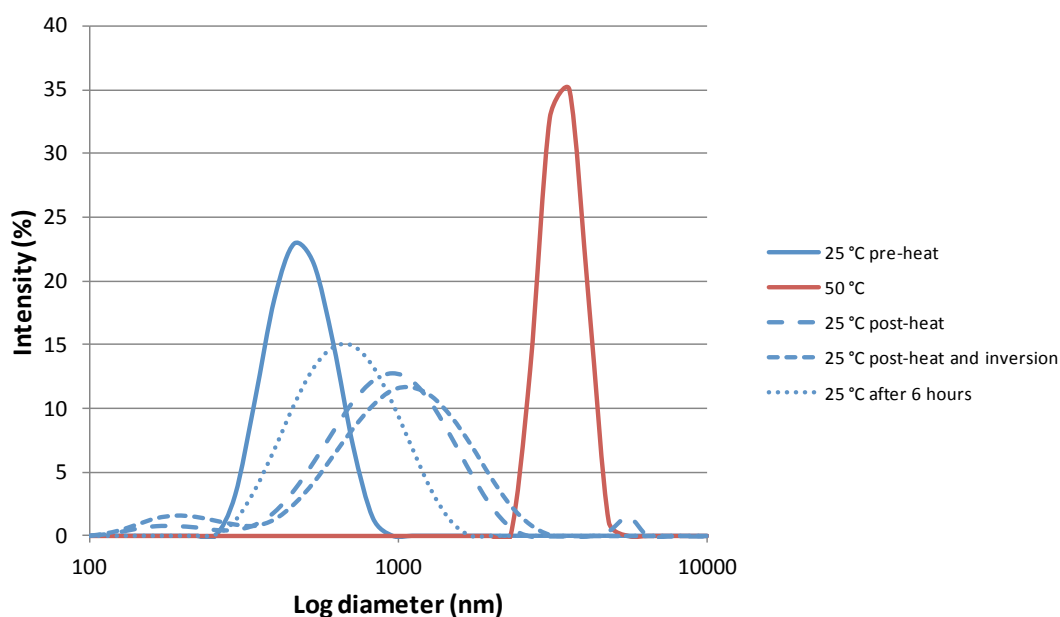
Figure 6.14 Changes in intensity size distribution of *P*-SO$_3^-$ in 0.8 M MgCl$_2$ as a function of time

The results suggest that although the microgel particles do redisperse following flocculation, the dispersion may not be complete when left simply to the cooling process and gentle inversion of the sample. More substantial energy input into the system, *e.g.* shaking or sonication of the sample, might result in more complete re-dispersion. The results also suggest that cooling a sample may enhance resistance to flocculation.

6.3.3.4 Scanning electron micrographs of flocculated particles

The occurrence of aggregated particles in the presence of NaCl was confirmed by SEM. Figure 6.15 shows micrographs of flocculated regions of all three microgels. Although dispersed particles are apparent in (a), (b) and (c), clear regions of

aggregated particles are also visible. The image (d) shows the *P*-COO⁻ sample from (b) at a lower magnification.

(a) *P*-SO₃⁻ in 0.9 M NaCl

(b) *P*-COO⁻ in 0.9 M NaCl

(c) *P*-NH₃⁺ in 0.9 M NaCl

(d) *P*-COO⁻ in 0.9 M NaCl
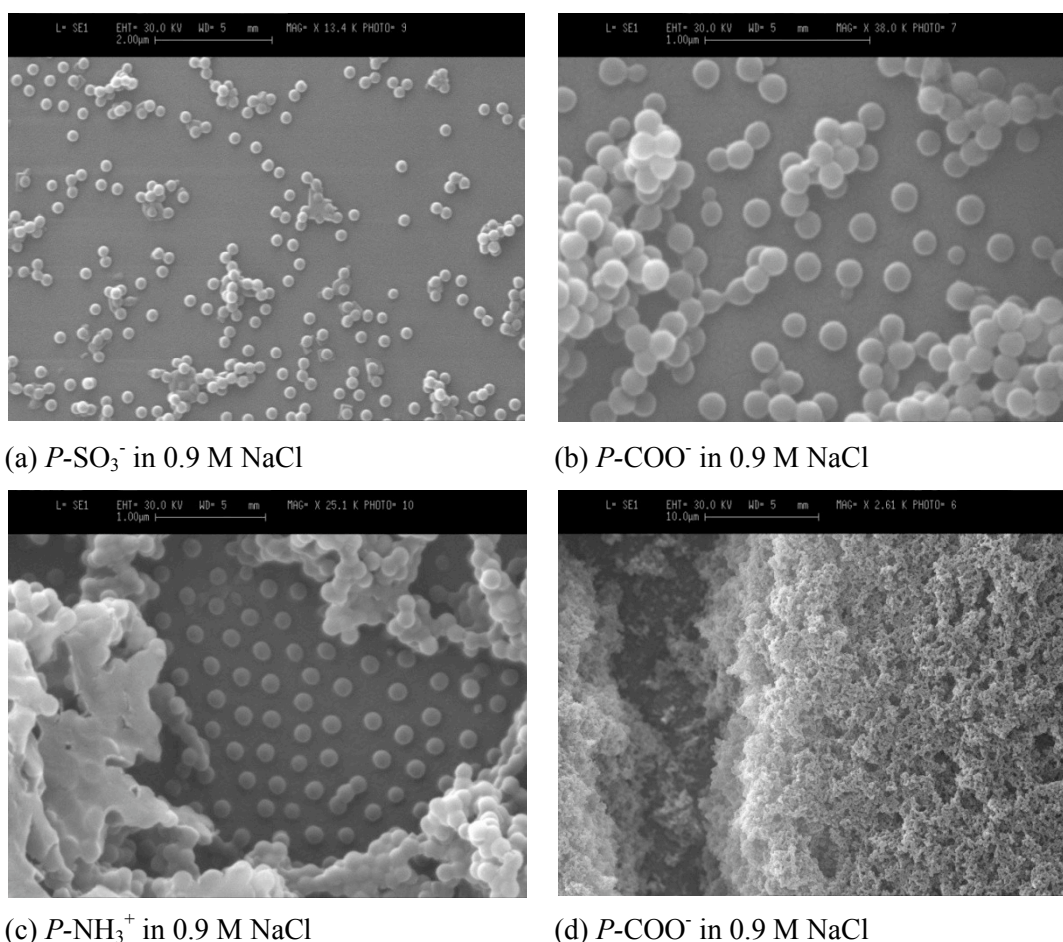
Figure 6.15 Scanning electron micrographs of *P*-SO₃⁻, *P*-COO⁻ and *P*-NH₃⁺ particles flocculated by 0.9 M NaCl

6.3.4 Heteroflocculation of mixed-charge poly(NIPAM) systems

Having determined the basic physico-chemical characteristics and flocculation behaviour of the poly(NIPAM) microgels *P*-SO₃⁻, *P*-COO⁻ and *P*-NH₃⁺, the next step was to investigate the heteroflocculation behaviour of mixtures of these anionic and cationic particles under a range of different conditions.

6.3.4.1 Exploratory visual evaluations of mixed-system stability

The objective of the initial visual evaluations was to explore the influence of variations in conditions such as temperature and pH upon microgel mixture stability, then to use the information to develop a more quantitative study of heteroflocculation.

213

Investigation A

The results from visual investigation A are shown in Table 6.8. The samples kept at room temperature without any pH adjustments (i) were almost all stable throughout. Flocculation was only observed for the 1:1 samples (P-SO$_3^-$/P-NH$_3^+$ and P-COO$^-$/ P-NH$_3^+$) when the samples were left undisturbed for approximately 24 hours (at room temperature and at 6 °C). This suggests that the approximately equal anionic:cationic charges cancelled one another out, giving the dispersion a zero net charge and promoting aggregation of the particles.

The second set of samples (ii), which were cooled to approximately 6 °C, initially behaved in the same manner as the room temperature samples (i), suggesting that cooling the samples did not promote flocculation. However, once returned to room temperature and adjusted to pH > 8, certain samples appeared more susceptible to flocculation, especially the 1:1 samples (P-SO$_3^-$/P-NH$_3^+$ and P-COO$^-$/P-NH$_3^+$). The 1:1 P-SO$_3^-$/P-NH$_3^+$ samples in particular exhibited greater flocculation. This suggests that increasing the pH alters the net charge of the dispersion, possibly by deprotonating a larger proportion of the P-NH$_3^+$ amine groups, reducing their contribution to electrostatic repulsion and encouraging aggregation. This is supported by the observation that the 10:1 P-COO$^-$/P-NH$_3^+$ sample, with excess anionic charge became less stable at 50 °C when the pH was greater than 8 and therefore a greater proportion of amine groups would have been in the neutral NH$_2$ form.

The results for the samples heated to 50 °C (iii) indicate that heating the samples enhances the likelihood of flocculation, particularly for the 1:1 samples. However, cooling the samples allowed the particles to redisperse, suggesting that cooling may enhance flocculation resistance. Reducing the pH below 8 at room temperature did not alter stability but flocculation was once again observed when the samples were heated to 50 °C. The 1:1 samples, particularly P-SO$_3^-$/P-NH$_3^+$, were most susceptible, but the excess anionic samples (10:1) were also flocculated at $t \approx 24$ hours. This suggests that lowering the pH may be increasing the proportion of protonated forms of the sulphate (P-SO$_3^-$) and carboxylic (P-COO$^-$) groups, reducing the overall anionic contribution to the dispersion net charge and encouraging flocculation.

Table 6.8 Stability observation results from visual investigation A

(i) Samples kept at room temperature with unadjusted pH

Likely surface charges: $P\text{-}SO_3^- = SO_3^-$, $P\text{-}COO^- = COO^-$, $P\text{-}NH_3^+ = NH_3^+$

Time (t)	Observation conditions	10:1 $P\text{-}SO_3^-$/ $P\text{-}NH_3^+$	1:1 $P\text{-}SO_3^-$/ $P\text{-}NH_3^+$	1:10 $P\text{-}SO_3^-$/ $P\text{-}NH_3^+$	10:1 $P\text{-}COO^-$/ $P\text{-}NH_3^+$	1:1 $P\text{-}COO^-$/ $P\text{-}NH_3^+$	1:10 $P\text{-}COO^-$/ $P\text{-}NH_3^+$
0 min	After preparation	S	S	S	S	S	S
30 min	No change	S	S	S	S	S	S
60 min	No change	S	S	S	S	S	S
90 min	After inversion	S	S	S	S	S	S
120 min	No change	S	S	S	S	S	S
24 hr	No change	S	F	S	S	F	S
24 hr	After inversion	S	S	S	S	S	S
48 hr	After 24 hr at 6 °C	S	F	S	S	F	S

(ii) Samples cooled to 6 °C then later adjusted to pH > 8 and reheated then re-cooled

Likely surface charges at pH > 8: $P\text{-}SO_3^- = SO_3^-$, $P\text{-}COO^- = COO^-$, $P\text{-}NH_3^+ = NH_3^+/NH_2$

Time (t)	Observation conditions	10:1 $P\text{-}SO_3^-$/ $P\text{-}NH_3^+$	1:1 $P\text{-}SO_3^-$/ $P\text{-}NH_3^+$	1:10 $P\text{-}SO_3^-$/ $P\text{-}NH_3^+$	10:1 $P\text{-}COO^-$/ $P\text{-}NH_3^+$	1:1 $P\text{-}COO^-$/ $P\text{-}NH_3^+$	1:10 $P\text{-}COO^-$/ $P\text{-}NH_3^+$
0 min	After preparation	S	S	S	S	S	S
30 min	After 30 min at 6 °C	S	S	S	S	S	S
60 min	After 30 min at RT	S	S	S	S	S	S
90 min	pH >8 at RT	S	S	S	S	S	S
120 min	After 30 min at 50 °C	S	F	S	F	F	S
24 hr	After 22 hr at RT	S	FF	S	S	F	S
24 hr	After inversion	S	F	S	S	S	S
48 hr	After 24 hr at 6 °C	S	F	S	S	F	S

S = stable dispersion; SF = slightly flocculated; F = flocculated; FF = very flocculated; *P-* = poly(NIPAM).

Table 6.8 Continued...

(iii) Samples heated to 50 °C then later adjusted to pH < 8 and reheated then re-cooled

Likely surface charges at pH < 8: $P\text{-}SO_3^- = SO_3^-$, $P\text{-}COO^- = COOH/COO^-$, $P\text{-}NH_3^+ = NH_3^+$

Time (t)	Observation conditions	10:1 $P\text{-}SO_3^-/$ $P\text{-}NH_3^+$	1:1 $P\text{-}SO_3^-/$ $P\text{-}NH_3^+$	1:10 $P\text{-}SO_3^-/$ $P\text{-}NH_3^+$	10:1 $P\text{-}COO^-/$ $P\text{-}NH_3^+$	1:1 $P\text{-}COO^-/$ $P\text{-}NH_3^+$	1:10 $P\text{-}COO^-/$ $P\text{-}NH_3^+$
0 min	After preparation	S	SF	S	S	SF	S
30 min	After 30 min at 50 °C	S	F	S	S	F	S
60 min	After 30 min at RT	S	S	S	S	S	S
90 min	pH <8 at RT	S	S	S	S	S	S
120 min	After 30 min at 50 °C	S	F	S	S	SF	S
24 hr	After 22 hr at RT	F	F	S	SF	SF	S
24 hr	After inversion	S	S	S	S	S	S
48 hr	After 24 hr at 6 °C	S	F	S	S	SF	S

S = stable dispersion; SF = slightly flocculated; F = flocculated; FF = very flocculated; *P-* = poly(NIPAM).

The results of investigation A therefore suggest that the incidence and extent of heteroflocculation of mixed poly(NIPAM) microgel systems is influenced by the ratio of anionic:cationic surface charges, temperature and pH.

Investigation B

Investigation B aimed to determine if the results were reproducible and introduce influences of electrolyte type and concentration. The results are shown in Table 6.9. The 0 mM results were broadly similar to investigation A in that the 1:1 mixtures were more susceptible to flocculation than the excess anionic or cationic mixtures, heating above the VPTT promoted flocculation and temperatures below the VPTT appeared to enhance flocculation resistance (apart from the unadjusted pH 1:1 mixtures, which were also flocculated below the VPTT).

Some differences were observed: unlike investigation A, increasing or decreasing the dispersion pH appeared to reduce the extent of flocculation. The differences may be attributed to variations in the methods and were investigated further in the following more quantitative experiment.

Table 6.9 Stability observation results from visual investigation B

(a) Sample pH ≤ 3 (Likely surface charges: *P*-COO⁻ = COOH, *P*-NH₃⁺ = NH₃⁺)

[NaCl] (mM)	0			1			10		
Ratio *P*-COO⁻/*P*-NH₃⁺	10:1	1:1	1:10	10:1	1:1	1:10	10:1	1:1	1:10
6 °C	S	S	S	S	S	S	S	S	S
~ 25 °C	S	S	S	S	S	S	S	S	S
50 °C	F	S	S	F	F	S	F	F	SF

(b) Sample pH unadjusted (Likely surface charges: *P*-COO⁻ = COO⁻, *P*-NH₃⁺ = NH₃⁺)

[NaCl] (mM)	0			1			10		
Ratio *P*-COO⁻/*P*-NH₃⁺	10:1	1:1	1:10	10:1	1:1	1:10	10:1	1:1	1:10
6 °C	S	F	S	S	F	S	S	S	S
~ 25 °C	S	F	S	S	F	S	S	S	S
50 °C	SF	F	SF	S	F	S	S	F	SF

(c) Sample pH ≥ 8 (Likely surface charges: *P*-COO⁻ = COO⁻, *P*-NH₃⁺ = NH₃⁺/NH₂)

[NaCl] (mM)	0			1			10		
Ratio *P*-COO⁻/*P*-NH₃⁺	10:1	1:1	1:10	10:1	1:1	1:10	10:1	1:1	1:10
6 °C	S	S	S	S	S	S	S	S	S
~ 25 °C	S	S	S	S	S	S	S	S	S
50 °C	S	F	S*	F	F	F	F	F	F

S = stable dispersion; S* = totally clear dispersion so possibly anomalous result; SF = slightly flocculated; F = flocculated; FF = very flocculated; *P*- = poly(NIPAM).

In general, increasing the electrolyte concentration appeared to increase the occurrence of flocculation at each pH at 50 °C, with the unadjusted pH 1:1 mixtures also flocculated below the VPTT in 1 mM NaCl. However, the same mixtures in 10 mM NaCl were stable below the VPTT, suggesting that certain electrolyte concentrations may actually enhance stability to flocculation. In general, the mixtures at pH ≥ 8 (*P*-COO⁻ = COO⁻ and *P*-NH₃⁺ = mostly NH₂) were more susceptible to flocculation above the VPTT than the unadjusted (*P*-COO⁻ = COO⁻ and *P*-NH₃⁺ = NH₃⁺) and pH ≤ 3 (*P*-COO⁻ = COOH and *P*-NH₃⁺ = NH₃⁺) samples. Deprotonation of *P*-NH₃⁺ amine groups above pH 8 therefore may be more significant to destabilization of the mixtures than the species of the carboxylate group (COO⁻ or COOH) on *P*-COO⁻.

6.3.4.2   Investigation of stability of mixed-microgel systems using UV-visible spectrophotometry to measure *n*-values

In order to investigate the findings of the initial study more thoroughly, visual inspections and more quantitative measurements of the stability of mixed-charge microgel systems based on *n*-value were made at different temperatures, pH, charge ratios, electrolyte types and concentrations. Table 6.10 shows the *n*-values of $P\text{-}SO_3^-/$ $P\text{-}NH_3^+$ and $P\text{-}COO^-/P\text{-}NH_3^+$ mixtures in the presence of increasing NaCl. The type of microgel mixture and dispersion pH are detailed along the top of the table, as are the three temperatures at which the mixtures were tested. The relative proportions of anionic:cationic microgels are shown on the left hand side.

The figures in the body of the table are the *n*-values. However, for simplicity the colours denote, according to the *n*-values, whether a system was stable and dispersed (green) or flocculated (red). The limit of $n = 2$ described by Hall *et al.*[18] was used to determine whether a given mixture was stable or flocculated, *i.e.* $0 < n < 2$ for flocculated and $2 < n < 4$ for stable. The suitability of this limit is discussed below.

A large amount of information is contained within Table 6.10. However, it is clear just from a glance at the colours that some trends are apparent. For example, red cells occur mainly in the 50 °C columns, indicating that flocculation is more likely to occur above the particle VPTTs. This is expected because below the VPTT steric repulsion resulting from the overlap of the "hairy" polymer chains extending out into the bulk solvent counterbalances the electrostatic attraction between the anionic and cationic particles. However, above the VPTT, steric repulsion no longer occurs and, due to the particle collapse, the surface charge density is increased substantially, further enhancing electrostatic attraction and encouraging flocculation.

In addition, simply by counting the proportion of red:green cells for each charge ratio group, it becomes clear that the mixtures with equal proportions of anionic and cationic particles (1:1, middle rows) tend display the most flocculation, whilst the excess cationic mixtures (10:1, bottom rows) tend to be the most stable, particularly below the VPTT. Again, this is as expected because if there are an equal number of oppositely charged particles (1:1), the electrostatic attraction between them will encourage flocculation, but if one charged species is in excess (1:10 or 10:1), stable

particles will remain in dispersion even when the minority species has entirely flocculated. The superficial analysis of the data in Table 6.10 also suggests a difference in the extent of flocculation according to dispersion pH.

Table 6.10 Extent of flocculation of mixed-charge systems in the presence of NaCl

Microgel ratio	NaCl (mM)	P-SO_3^-/P-NH_3^+ at pH 8			P-SO_3^-/P-NH_3^+ at pH 3		
		6 °C	25 °C	50 °C	6 °C	25 °C	50 °C
Excess anionic charges (10:1)	0	1.81	1.77	0.91	2.49	2.36	0.65
	1	2.43	2.40	0.58	2.55	2.57	0.75
	10	2.57	2.55	1.01	2.47	2.56	0.88
	100	2.53	2.55	0.27	2.47	2.53	0.08
Equal charges (1:1)	0	0.42	0.40	1.74	2.32	1.56	1.16
	1	2.22	1.87	1.34	2.61	2.54	0.09
	10	2.67	2.57	0.00	2.48	2.56	0.01
	100	2.55	2.56	0.02	2.50	2.55	0.00
Excess cationic charges (10:1)	0	2.28	2.26	2.08	2.53	2.42	1.87
	1	2.51	2.40	1.66	2.66	2.56	1.62
	10	2.68	2.60	1.64	2.54	2.62	1.71
	100	2.63	2.60	0.00	2.57	2.55	0.00

Microgel ratio	NaCl (mM)	P-COO^-/P-NH_3^+ at pH 8			P-COO^-/P-NH_3^+ at pH 3		
		6 °C	25 °C	50 °C	6 °C	25 °C	50 °C
Excess anionic charges (10:1)	0	1.88	1.86	0.65	2.60	2.57	0.00
	1	2.55	2.44	0.43	2.63	2.61	0.00
	10	2.70	2.58	1.17	x	2.61	0.05
	100	2.54	2.59	0.19	2.56	2.58	0.00
Equal charges (1:1)	0	0.44	0.43	0.73	2.57	2.63	0.00
	1	2.27	2.12	1.04	2.65	2.57	0.00
	10	2.72	2.58	0.04	x	2.63	0.00
	100	2.60	2.58	0.04	2.52	2.59	0.00
Excess cationic charges (10:1)	0	2.18	2.15	2.00	2.57	2.58	2.40
	1	2.53	2.41	1.89	2.68	2.57	2.25
	10	2.75	2.53	1.84	x	2.57	1.67
	100	2.61	2.53	0.00	2.50	2.56	0.00

Unstable (0 < n < 2)   Stable (2 < n < 4)   x Missing data

On boundary between stable and flocculated (1.95 < n < 2.05)

In order to ascertain more detail, each "group" of samples can be analysed in a systematic way, looking first at the stability of the particles in water at room temperature and then determining the effect of increasing or decreasing temperature,

changing the pH (by comparison with a neighbouring group) or increasing electrolyte concentration. For example, $P\text{-}SO_3^-/P\text{-}NH_3^+$ in water at pH 3 and 25 °C is stable ($n = 2.36$). If the temperature is lowered, the dispersion becomes very slightly more stable ($n = 2.49$), however, if the temperature is raised above the VPTT, flocculation is observed ($n = 0.65$). If the pH is increased, the dispersion flocculates above and below the VPTT, but at pH 3, the dispersion is stable below the VPTT. Finally, if the electrolyte concentration is raised at pH 3 the dispersions remain stable below the VPTT and flocculated above the VPTT. However, at pH 8, increasing the electrolyte stabilizes the dispersions below the VPTT, suggesting that under these conditions the presence of NaCl may enhance flocculation resistance, possibly by screening some of the surface charge and reducing electrostatic attraction between the particles. As steric repulsion is also present below the VPTT, the combined effect is sufficient to maintain a stable dispersion but this is disrupted when the temperature is increased above the VPTT and steric stabilization is lost.

If this systematic approach is followed with each of the six mixture groups in Table 6.10 (*i.e.* the $P\text{-}SO_3^-/P\text{-}NH_3^+$ and $P\text{-}COO^-/P\text{-}NH_3^+$ mixtures at each of the three charge ratios), then some general trends for the behaviour of mixed-charge dispersions in the presence of NaCl become apparent.

- Temperature shows the clearest influence, with *n*-values indicating flocculation of almost all mixtures at 50 °C. This must be related to the volume phase transition, where in the collapsed state above the VPTT, steric stabilization is lost and electrostatic attraction is greater due to the increased electrophoretic mobility (and charge density). In addition, above the VPTT, the difference in anionic and cationic particle sizes is less, which in turn reduces the likelihood of formation of the stable hetero-macrocomplexes observed by Hall *et al.*, which are most likely when substantially smaller cationic particles surround a larger anionic particle.[18]

- Below the VPTT, stability tended to be greatest for the anionic:cationic particle ratios in the order 1:10 > 1:1 > 10:1. Above the VPTT, although the majority of mixtures were flocculated, the *n*-values of the 1:10 mixtures tend to be greater than the 1:1 and 10:1 mixtures, again suggesting greater stability.

- The greatest degree of flocculation tended to be observed for particle mixtures in water alone (*i.e.* 0 mM for 10:1 and 1:1).

- The addition of NaCl tended to increase stability (increased *n*-value) below the VPTT, particularly at pH 8. It is likely that the electrolyte ions screened the surface charges, reducing the electrostatic attraction between the anionic and cationic particles and thereby enhancing resistance to flocculation (supported by the presence of steric stabilization).

- However, above the VPTT, the addition of NaCl tended to decrease the *n*-value, *i.e.* increase the extent of flocculation.

- The reduction of pH (to 3) for both the P-SO$_3^-$/P-NH$_3^+$ and P-COO$^-$/P-NH$_3^+$ mixtures tended to increase stability at all electrolyte concentrations below the VPTT. However, above the VPTT, the reduction in pH tended to dramatically reduce stability (*n*-value decreased) for the 10:1 and 1:1 P-COO$^-$/P-NH$_3^+$ mixtures. At pH 3 the P-COO$^-$ surface groups adopt the protonated –COOH form, which, although reducing electrostatic attraction with the still charged P-NH$_3^+$, reduces any potential electrostatic repulsion between the –COO$^-$ groups that may have contributed to dispersion stability at pH 8.

The greatest influence upon stability appears to be temperature, which is unsurprising given the dramatic conformational changes that occur through the VPTT, accompanied by substantial changes in charge density and the loss of steric stabilization above the VPTT. The data suggest that subtle tuning of dispersion stability, particularly below the VPTT could be achieved through manipulation of dispersion pH and ionic strength. Changes in electrolyte concentration alter the extent of electrostatic interactions by screening of the charged surface groups, whilst pH adjustments can be used to alter electrostatic interactions by influencing the ionization state of the surface groups. A summary of the likely forms of the charged groups at the two pH values is given in Table 6.11.

At pH 8 both P-SO$_3^-$ and P-COO$^-$ carry ionized charges, so P-SO$_3^-$/P-NH$_3^+$ and P-COO$^-$/P-NH$_3^+$ could be considered roughly equivalent in terms of net charge. However, at pH 3, the protonated carboxyl groups on P-COO$^-$ result in the -COOH/-NH$_3^+$ mixture having different net charge to the -SO$_3^-$/-NH$_3^+$ mixture due to the still ionized sulphate groups on P-SO$_3^-$. Although the relative ratio of the anionic:cationic particles will of course also be influential in determining the overall net charge of the dispersion, this comparison suggests that the greater charge difference

between the P-SO$_3^-$/P-NH$_3^+$ and P-COO$^-$/P-NH$_3^+$ mixtures at pH 3 may mean that more marked differences are apparent between the P-SO$_3^-$ and P-COO$^-$ mixtures at pH 3 than at pH 8.

Table 6.11 Likely surface charge group species at pH 3 and pH 8

	P-SO$_3^-$ (N4)	P-NH$_3^+$ (N6)	P-COO$^-$ (N5)
Surface group	sulphate	amine	carboxyl
Approximate pK$_a$	2	10	4.5
Dominant species at pH 3	SO$_3^-$ but [SO$_3$H] greater than at pH 8	NH$_3^+$	COOH
Dominant species at pH 8	SO$_3^-$	NH$_3^+$ but [NH$_2$] greater than at pH 3	COO$^-$

A basic comparison of n-values at pH 8 show that the P-SO$_3^-$ and P-COO$^-$ mixtures display very similar extents of flocculation, above and below the VPTT. Below the VPTT at pH 3, the situation is similar, with the P-COO$^-$ mixtures (with protonated COOH groups) very slightly more stable than the P-SO$_3^-$ mixtures (with mostly deprotonated SO$_3^-$ groups). However, above the VPTT at pH 3, the difference between the two is much greater, with the P-COO$^-$ (-COOH) being far less stable than the P-SO$_3^-$ mixtures (according to the n-values) at 10:1 and 1:1 ratios. These observations are as anticipated from the previous paragraph. The P-SO$_3^-$ and P-COO$^-$ mixtures behave very similarly at pH 8 when their net dispersion charges are close, but more differences are apparent at pH 3, when the net charges differ more substantially, particularly above the VPTT, when stability relies upon electrostatic repulsion only (steric stabilization is lost).

In order to investigate the repeatability of these phenomena and to look in more detail at the influence of electrolyte cation valency, the stability of the mixtures in MgCl$_2$ and LaCl$_3$ was studied. This also permitted observations and measurements to be carried out over longer timescales and enabled investigation of the effect of inverting a sample after it had been flocculated by heating. Furthermore, specific comparisons of visual observations and n-value measurements were made. Table 6.12 shows the n-value measurements for the mixtures in MgCl$_2$; the green colour coding indicates stable mixtures ($n > 2$) and the red indicates flocculated mixtures ($n < 2$).

Table 6.12 *n*-values of *P*-SO₃⁻/*P*-NH₃⁺ and *P*-COO⁻/*P*-NH₃⁺ mixtures in MgCl₂

P-SO₃⁻/*P*-NH₃⁺ at pH 8						*P*-SO₃⁻/*P*-NH₃⁺ at pH 3					
Microgel ratio	MgCl₂ (mM)	25 °C	5 °C	50 °C	24 hr 25 °C	Microgel ratio	MgCl₂ (mM)	25 °C	5 °C	50 °C	24 hr 25 °C
Excess anionic charges (10:1)	0	1.73	1.85	1.01	2.31	Excess anionic charges (10:1)	0	2.56	2.78	0.98	2.57
	1	2.57	2.52	0.87	2.52		1	1.58	1.49	0.74	2.56
	10	2.57	x	0.26	2.64		10	2.58	x	0.21	2.55
	100	1.56	1.97	0.00	2.69		100	2.57	2.38	0.00	3.46
Equal charges (1:1)	0	0.97	1.10	2.04	0.49	Equal charges (1:1)	0	2.57	2.54	0.13	2.50
	1	2.59	2.54	0.09	1.56		1	2.59	2.54	0.10	2.48
	10	2.62	2.54	0.00	1.28		10	2.61	2.55	0.00	2.44
	100	2.61	2.57	0.00	0.89		100	2.61	2.56	0.00	4.21
Excess cationic charges (1:10)	0	1.99	2.37	2.13	2.43	Excess cationic charges (1:10)	0	2.59	3.19	1.87	2.60
	1	2.58	2.55	1.73	2.47		1	2.59	2.56	1.84	2.61
	10	2.60	2.58	0.05	2.30		10	2.58	2.54	0.00	2.53
	100	2.61	2.58	0.00	0.60		100	2.56	2.58	0.00	2.98

P-COO⁻/*P*-NH₃⁺ at pH 8						*P*-COO⁻/*P*-NH₃⁺ at pH 3					
Microgel ratio	MgCl₂ (mM)	25 °C	5 °C	50 °C	24 hr 25 °C	Microgel ratio	MgCl₂ (mM)	25 °C	5 °C	50 °C	24 hr 25 °C
Excess anionic charges (10:1)	0	1.83	1.95	1.18	2.04	Excess anionic charges (10:1)	0	2.61	2.80	0.21	2.56
	1	2.61	2.58	0.34	2.60		1	2.56	2.58	0.00	2.57
	10	2.62	1.62	0.21	2.63		10	2.62	1.42	0.20	0.80
	100	2.60	2.35	0.00	3.30		100	2.61	2.41	0.00	3.28
Equal charges (1:1)	0	1.14	1.30	1.79	0.95	Equal charges (1:1)	0	2.60	2.57	0.16	2.58
	1	2.60	2.56	0.23	2.47		1	2.61	2.57	0.00	2.58
	10	2.64	2.56	0.00	2.31		10	2.64	2.58	0.13	2.54
	100	2.62	2.61	0.00	3.97		100	2.63	2.59	0.00	3.15
Excess cationic charges (1:10)	0	2.58	3.24	2.17	2.65	Excess cationic charges (1:10)	0	2.01	2.32	1.87	2.31
	1	2.59	2.54	1.97	2.61		1	2.57	2.56	1.87	2.62
	10	2.60	2.58	0.00	2.60		10	2.59	2.57	0.18	0.34
	100	2.61	2.59	0.00	3.25		100	2.61	2.59	0.00	3.31

■ Unstable (0 < n < 2)   ■ Stable (2 < n < 4)   x Missing data

■ On boundary between stable and flocculated (1.95 < n < 2.05)

The same systematic approach was applied to the MgCl₂ *n*-value data in Table 6.12. Many of the general trends observed for mixtures in NaCl were also apparent for the MgCl₂ mixtures, but some differences and additional patterns were observed:

- Temperature (and its effect it has upon particle size and electrophoretic mobility) was once again the most influential variable, with almost all mixtures flocculated at 50 °C.

- There was substantial evidence that flocculated dispersions at 50 °C would redisperse on cooling back to room temperature. The 1:1 P-SO$_3^-$/P-NH$_3^+$ at pH 8 and all MgCl$_2$ concentrations was an exception; it remained flocculated after 24 hours although the increase in n-values over this time suggests that the particles might be redispersing. (N.B. See also discussion below on relationship between n-value and visual observations.)

- Below the VPTT, stability tended to be greatest for 1:10 excess cationic particle mixtures, with less difference between the more flocculated 10:1 and 1:1.

- Below the VPTT, the pH 8 P-SO$_3^-$ and P-NH$_3^+$ again tended to be more flocculated in water than in the presence of MgCl$_2$, but the pH 3 mixtures were more stable in water and slightly more susceptible to flocculation in MgCl$_2$ than NaCl. The divalent Mg^{2+} cation may encourage flocculation more readily than the monovalent Na$^+$. However, at either pH, increasing MgCl$_2$ concentration below the VPTT again tended to increase stability, *i.e.* enhance flocculation resistance.

- Above the VPTT, the decreasing n-values indicated that, as for NaCl, the extent of flocculation increased with increasing MgCl$_2$ concentration.

- The pH reduction from 8 to 3 tended to slightly increase stability, particularly in water, although the n-values were fairly similar at the two pH values. Once again, the deionization of P-COO$^-$ on moving from COO$^-$ at pH 8 to COOH at pH 3 appeared to increase stability. The fact that the P-SO$_3^-$ mixtures also tended to be more stable at pH 3 than pH 8, despite the fact that the sulphate groups remain ionized at both pH values, indicates how even small changes in the balance of ionized:deionized species are influential. At pH 3, more P-SO$_3^-$ groups will be protonated and deionized than at pH 8, whilst the opposite is true for the P-NH$_3^+$ groups, which although more protonated at pH 3, they are also more ionized, compared to pH 8, when a greater proportion are deprotonated. The extent of ionization of both the cationic and ionic surface charge groups is clearly influential, which may explain why the difference between the response of P-SO$_3^-$/P-NH$_3^+$ and the P-COO$^-$/P-NH$_3^+$ is perhaps not as great as expected.

- Slightly more flocculation appeared to occur in the MgCl$_2$ than in NaCl.

The MgCl$_2$ results were generally in good agreement with the findings for NaCl. In an attempt to correlate the n-values with the visual appearance of each sample, the MgCl$_2$ n-value results in Table 6.12 were compared with the visual observations in Table 6.13.

This comparison identified several discrepancies. For example, although the general trend of increased flocculation above the VPTT suggested by the *n*-values was also observed visually, in many cases the flocculation persisted visually after a further 24 hours at 25 °C, contradicting the stability suggested by corresponding *n*-values after 24 hours at 25 °C. Other examples include: the flocculation inferred from the *n*-values of 10:1 *P*-SO$_3^-$/*P*-NH$_3^+$ mixtures in water at 25, 5 and 50 °C at pH 8 (top left row in Table 6.12) compared to the visually stable mixtures in Table 6.13; and the highly flocculated pellet of 1:1 *P*-SO$_3^-$/*P*-NH$_3^+$ at pH 8 and 50 °C in Table 6.13, compared to the *n*-value of 2.04 in Table 6.12 that suggests the sample is actually stable.

Several potential explanations for such discrepancies were considered. Firstly, it was possible that the $n = 2$ limit used to determine whether or not mixtures were stable, although derived from literature,[18] may not have been accurate for the systems under consideration. Hall *et al.*[18] selected this value on the basis of measured *n*-values for the individual dispersions (equivalent to the 0 mM electrolyte samples in this study) and *n*-values of the mixtures compared to their visual conditions. To assess the suitability of the $n = 2$ limit for this study, digital images of a range of flocculated and stable dispersions were obtained (Table 6.14). It was clear from the images that flocculation took various forms, *e.g.* flocs could be tiny and appear relatively dispersed throughout the dispersant medium (Table 6.14.C), loosely sedimented (Table 6.14.G) or even tightly pelleted (Table 6.14.J). No simple correlation with *n*-value could be discerned and it was therefore not possible to determine a precise *n*-value boundary for these systems.

It rapidly became clear that the discrepancies between the *n*-value and visual results were due to experimental differences. Each *n*-value and visual observation relates to the same sample at the same point in time but the perspectives from which they are determined vary substantially. For example, the visual observations, although qualitative, encompass the entire sample cuvette and in the majority of cases, including those shown in Table 6.14, it was simple to determine whether the entire sample should be categorized as stable or flocculated. However, the quantitative *n*-value measurements relate only to that portion of the sample through which the incident light passes. In the case of a fully dispersed sample (*e.g.* A or B in Table 6.14), the *n*-value measurement is representative of the state of the dispersion throughout the entire cuvette. However, when flocculation and/or sedimentation has occurred, the measurement may not be as representative.

Table 6.13 Visual observations of stability of *P*-SO$_3^-$/*P*-NH$_3^+$ and *P*-COO$^-$/*P*-NH$_3^+$ mixtures in MgCl$_2$

P-SO$_3^-$/P-NH$_3^+$ at pH 8					
Microgel ratio	MgCl$_2$ (mM)	25 °C	5 °C	50 °C	24 hr 25 °C
Excess anionic charges (10:1)	0	S	x	S	SF
	1	S	x	S	S
	10	S	x	F	F
	100	S	x	F	F
Equal charges (1:1)	0	F	F	FP	F
	1	S	S	F	F
	10	S	S	F	F
	100	S	S	F	F
Excess cationic charges (1:10)	0	S	S	S	S
	1	S	S	S	S
	10	S	S	F	F
	100	S	S	F	F

P-SO$_3^-$/P-NH$_3^+$ at pH 3					
Microgel ratio	MgCl$_2$ (mM)	25 °C	5 °C	50 °C	24 hr 25 °C
Excess anionic charges (10:1)	0	S	x	S	S
	1	S	x	S	S
	10	S	x	F	F
	100	S	x	F	F
Equal charges (1:1)	0	S	S	F	F
	1	S	S	F	F
	10	S	S	F	F
	100	S	S	F	F
Excess cationic charges (1:10)	0	S	S	S	S
	1	S	S	S	S
	10	S	S	F	F
	100	S	S	F	F

P-COO$^-$/P-NH$_3^+$ at pH 8					
Microgel ratio	MgCl$_2$ (mM)	25 °C	5 °C	50 °C	24 hr 25 °C
Excess anionic charges (10:1)	0	S	x	S	SF
	1	S	x	S	S
	10	S	x	F	F
	100	S	x	F	F
Equal charges (1:1)	0	F	F	FP	F
	1	S	S	F	F
	10	S	S	F	F
	100	S	S	F	F
Excess cationic charges (1:10)	0	S	S	S	S
	1	S	S	S	S
	10	S	S	F	F
	100	S	S	F	F

P-COO$^-$/P-NH$_3^+$ at pH 3					
Microgel ratio	MgCl$_2$ (mM)	25 °C	5 °C	50 °C	24 hr 25 °C
Excess anionic charges (10:1)	0	S	x	F	F
	1	S	x	F	F
	10	S	x	F	F
	100	S	x	F	F
Equal charges (1:1)	0	S	S	S	S
	1	S	S	S	S
	10	S	S	F	F
	100	S	S	F	F
Excess cationic charges (1:10)	0	S	S	S	S
	1	S	S	S	S
	10	S	S	F	S
	100	S	S	F	F

S	Stable	SF	Slight floccuation	F	Flocculated	FP	Flocculated pellet	x	Missing data

Take for example, the densely sedimented floc F in Table 6.14. The dispersant above the sediment is visually entirely clear and as the incident light passes through the cuvette, it is likely to encounter predominantly only clear dispersion, missing the sedimented floc at the base of the cuvette and resulting in an *n*-value that indicates the presence of a stable dispersion.   However, the differences may be even more complex.   For example, sample 6.14.J appears visually far more flocculated than sample 6.14.F. However, the dispersant medium is more turbid in sample J, which would result in *n*-values that may indicate that sample J is more flocculated than sample F, but, in fact, the visual clarity of

the dispersant in sample F indicates that a greater proportion of the particles have flocculated and sedimented out of dispersion than in sample J.

Table 6.14 Examples of stable and flocculated/sedimented dispersions

A	B	C	D	E
Stable dispersion below VPTT	Stable dispersion above VPTT	Tiny dispersed flocs	Small loose dispersed flocs	Slightly sedimented floc
F	**G**	**H**	**I**	**J**
Densely sedimented floc	Loosely sedimented floc	Tight, sticky floc	Loose sticky floc	Pelleted floc

It is clearly a complex situation but it does begin to explain some of the discrepancies noted above. For example, the image of sample F in Table 6.14 corresponds to the visual highly flocculated pellet observation (FP) in Table 6.13 (1:1 P-SO$_3^-$/P-NH$_3^+$ in 0 mM MgCl$_2$ at pH 8 and 50 °C) and the just stable n = 2.04 in Table 6.12. The previous paragraph clarifies how conflicting n-value and visual observations can indeed apply to the same sample.

Another example relates to the apparent trend in stability based on n-values for MgCl$_2$ described above (Table 6.12), where mixtures flocculated at 50 °C appeared redispersed after cooling back to room temperature for 24 hours. The visual observations (Table 6.13) indicate that very few mixtures were redispersed after 24 hours (generally only 1:1 mixtures at low MgCl$_2$ concentrations). This suggests that

sedimentation of the flocculated particles continues over longer timescales and because the sedimented flocs accumulate at the bottom of the cuvettes, they are potentially less dominant in the UV-visible measurements. Depending on the nature of the floc, the *n*-values therefore suggest that the mixtures become more dispersed because they predominantly relate only to the any particles remaining in the path of the incident light. The visual observations also suggest that the flocculation increases with increasing $MgCl_2$ concentration, which may be evidence that the bivalent Mg^{2+} cations promote flocculation and sedimentation by forming bridges between like-charged microgel particles, as well as screening charges that would otherwise result in stabilizing electrostatic repulsion (as well as screening electrostatic attraction between oppositely charged particles).

The discrepancies between the two data sets identified a further dilemma: whether or not a sample of flocculated particles that had sedimented to the base of a cuvette should be gently inverted in order to distribute the flocculated particles throughout the cuvette and back into the path of the incident light. Whilst gentle inversion might surmount the issue of bypassing flocculated particles that had sedimented, it also ran the risk of breaking up the flocs and introducing further error into the measurements. The effect of gentle inversion was studied in the $LaCl_3$ measurements (see below).

The benefit of quantitative measurement of the extent of flocculation is clear but the results of this study suggest that *n*-value alone is not sufficient to judge the stability of mixed-microgel systems, particularly when the turbidity of a sample is being monitored over long periods. The colloidal phase-coexistence[20] (*i.e.* the presence of both dispersed and flocculated and possibly sedimented particles) makes qualitative measurement difficult. In its current form, the *n*-values possibly provide more of a measure of the extent of sedimentation. Further work is required to reconcile *n*-value measurements with visual observations and develop a more refined system for measuring the extent of microgel particle flocculation. It is also a timely reminder of the value of the visual inspection of results and the importance of comparing them with quantitative measurements from an instrument, rather than simply assuming the data encompass the complete picture.

Finally, the *n*-values and visual observations for LaCl$_3$ are shown in Tables 6.15 and 6.16, respectively. Before considering the general trends, it is worth noting that similar discrepancies between the data sets were once again apparent. For example, the *n*-values suggest that having flocculated at 50 °C, most mixtures began to redisperse after 24 hours at room temperature. However, the visual observations indicate little difference after 24 hours. Furthermore, the *n*-values for the *P*-SO$_3^-$/*P*-NH$_3^+$ and *P*-COO$^-$/*P*-NH$_3^+$ mixtures at pH 8 indicate that inverting the mixtures tended to increase the extent of flocculation (decreased *n*-values), but the visual observations indicate the opposite, *i.e.* that inversion increased stability/redispersion. In addition, the *n*-value data suggests that the pH 3 mixtures behaved very differently after inversion compared to the pH 8 mixtures, with no real difference in *n*-value recorded, but the visual observations suggest no such difference between the two pH values. This tends to confirm the need to develop a method to reconcile the results obtained from the two techniques.

From the two sets of data for LaCl$_3$ the following general trends were apparent.

- Heating above the VPTT was once again the dominant effect, with almost all mixtures flocculated at 50 °C. Only the excess cationic 1:10 mixtures of both *P*-SO$_3^-$/*P*-NH$_3^+$ and *P*-COO$^-$/*P*-NH$_3^+$ appeared to resist flocculation at low LaCl$_3$ concentrations at both pH 3 and pH 8.

- Both the *n*-value data and visual observations indicate that the mixtures were more stable at pH 3 than pH 8.

- The *n*-value data suggested that redispersion occurred with time, but the visual observations indicate that redispersion only occurs after inversion and then, only the pH 3 mixtures remain dispersed – the pH 8 mixtures re-flocculate.

- According to the *n*-values, the 1:10 mixtures were the most stable. The visual observations confirm this for mixtures at pH 3 but suggest the opposite situation is true at pH 8.

- Below the VPTT, increasing LaCl$_3$ concentration appears to very slightly increase stability according to the *n*-values, but the visual observations suggest that at pH 3, increasing LaCl$_3$ promotes flocculation. Once again, these differences are likely to be the result of the *n*-value measurement method.

Table 6.15 *n*-value measurements of *P*-SO₃⁻/*P*-NH₃⁺ and *P*-COO⁻/*P*-NH₃⁺ in LaCl₃

P-SO₃⁻/*P*-NH₃⁺ at pH 3

Microgel ratio	LaCl₃ (mM)	25 °C	5 °C	50 °C	24 hr 25 °C	Shake	24 hr post shake
Excess anionic charges (10:1)	0	2.57	2.53	1.00	2.51	2.52	2.53
	1	2.57	2.53	0.30	2.55	2.57	2.56
	10	2.59	2.52	0.00	2.60	2.56	2.55
	100	2.60	2.55	0.00	3.00	2.59	2.56
Equal charges (1:1)	0	2.59	2.54	0.36	2.62	2.58	2.56
	1	2.60	2.54	0.32	2.61	2.57	2.59
	10	2.59	4.27	0.12	2.85	2.58	2.57
	100	2.58	2.51	0.00	2.61	2.56	2.57
Excess cationic charges (1:10)	0	2.59	2.57	1.92	2.62	2.60	2.61
	1	2.59	2.58	1.88	2.36	2.59	2.59
	10	2.61	2.56	0.06	2.66	2.60	2.61
	100	2.60	2.57	0.00	2.56	2.56	2.56

P-COO⁻/*P*-NH₃⁺ at pH 3

Microgel ratio	LaCl₃ (mM)	25 °C	5 °C	50 °C	24 hr 25 °C	Shake	24 hr post shake
Excess anionic charges (10:1)	0	2.59	2.59	0.26	2.67	2.62	2.62
	1	2.64	2.56	0.19	2.60	2.61	2.62
	10	2.60	2.58	0.00	2.52	2.62	2.61
	100	2.61	2.61	0.01	2.85	2.62	2.60
Equal charges (1:1)	0	2.61	1.92	0.02	2.62	2.61	2.61
	1	2.62	1.05	0.00	2.61	2.60	2.59
	10	2.62	2.94	0.27	1.27	2.60	2.62
	100	2.60	2.29	0.00	2.55	2.60	2.61
Excess cationic charges (1:10)	0	2.59	2.57	2.14	2.61	2.59	2.61
	1	2.60	2.57	2.02	2.61	2.61	2.62
	10	2.62	2.59	0.13	2.47	2.57	2.59
	100	2.60	2.56	0.00	2.56	2.57	2.60

P-SO₃⁻/*P*-NH₃⁺ at pH 8

Microgel ratio	LaCl₃ (mM)	25 °C	5 °C	50 °C	24 hr 25 °C	Shake	24 hr post shake
Excess anionic charges (10:1)	0	1.81	1.88	1.22	2.28	1.71	2.33
	1	2.31	2.31	0.33	1.97	1.24	2.11
	10	1.95	1.96	0.00	0.88	0.95	2.22
	100	2.56	2.55	0.55	1.45	1.13	2.20
Equal charges (1:1)	0	0.98	1.08	1.79	1.09	0.39	0.90
	1	2.33	2.31	0.22	1.98	1.70	2.14
	10	1.98	6.99	0.05	2.69	1.25	2.50
	100	2.55	2.42	0.45	1.67	1.02	2.57
Excess cationic charges (1:10)	0	2.32	2.33	2.16	2.43	2.32	2.47
	1	2.46	2.50	3.07	2.59	2.07	2.59
	10	2.45	2.47	0.25	2.65	1.99	2.60
	100	2.54	2.49	0.00	3.48	1.75	2.52

P-COO⁻/*P*-NH₃⁺ at pH 8

Microgel ratio	LaCl₃ (mM)	25 °C	5 °C	50 °C	24 hr 25 °C	Shake	24 hr post shake
Excess anionic charges (10:1)	0	1.92	1.94	1.25	2.33	1.82	2.38
	1	2.33	1.72	0.14	2.22	1.91	2.11
	10	1.72	1.69	0.00	2.03	0.69	2.13
	100	2.11	1.84	0.19	2.52	1.70	2.54
Equal charges (1:1)	0	1.10	0.36	0.25	0.26	0.20	0.84
	1	2.12	1.76	0.17	2.10	1.62	2.21
	10	2.10	4.00	0.30	2.53	1.13	2.52
	100	1.88	1.63	0.13	2.10	1.35	2.40
Excess cationic charges (1:10)	0	2.18	2.05	2.05	2.39	2.15	2.48
	1	2.48	2.52	3.11	2.61	2.14	2.59
	10	2.49	2.52	0.19	x	1.81	2.59
	100	2.39	2.26	0.00	2.49	1.53	2.58

Legend:
- Unstable (0 < n < 2)
- Stable (2 < n < 4)
- On boundary between stable and flocculated (1.95 < n < 2.05)
- x Missing data

Table 6.16 Visual observations of *P*-SO$_3^-$/*P*-NH$_3^+$ and *P*-COO$^-$/*P*-NH$_3^+$ in LaCl$_3$

P-SO$_3^-$/*P*-NH$_3^+$ at pH 3

Microgel ratio	LaCl$_3$ (mM)	25 °C	5 °C	50 °C	24 hr 25 °C	Shake	24 hr post shake
Excess anionic charges (10:1)	0	S	S	S	S	S	S
	1	S	S	F	F	S	S
	10	S	S	F	F	S	S
	100	S	S	F	F	S	S
Equal charges (1:1)	0	S	S	F	F	S	S
	1	S	S	F	F	S	S
	10	S	S	F	F	S	S
	100	S	S	F	F	SF	S
Excess cationic charges (1:10)	0	S	S	S	S	S	S
	1	S	S	S	S	S	S
	10	S	S	F	F	S	S
	100	S	S	F	F	S	S

P-COO$^-$/*P*-NH$_3^+$ at pH 3

Microgel ratio	LaCl$_3$ (mM)	25 °C	5 °C	50 °C	24 hr 25 °C	Shake	24 hr post shake
Excess anionic charges (10:1)	0	S	S	F	F	S	S
	1	S	S	F	F	S	S
	10	S	S	F	F	S	S
	100	S	S	F	F	S	S
Equal charges (1:1)	0	S	S	S	S	S	S
	1	S	S	S	S	S	S
	10	S	S	F	F	S	S
	100	S	S	F	F	S	S
Excess cationic charges (1:10)	0	S	S	S	S	S	S
	1	S	S	S	S	S	S
	10	S	S	F	F	S	S
	100	S	S	F	F	S	S

P-SO$_3^-$/*P*-NH$_3^+$ at pH 8

Microgel ratio	LaCl$_3$ (mM)	25 °C	5 °C	50 °C	24 hr 25 °C	Shake	24 hr post shake
Excess anionic charges (10:1)	0	S	S	S	SF	S	sF
	1	S	S	F	F	S	F
	10	F	S	F	F	S	F
	100	S	S	F	F	S	F
Equal charges (1:1)	0	F	F	FP	F	F	F
	1	S	S	SF	SF	S	F
	10	F	F	F	F	SF	F
	100	S	S	F	F	S	F
Excess cationic charges (1:10)	0	S	S	S	S	S	S
	1	SF	F	SF	SF	S	SF
	10	SF	F	F	F	S	SF
	100	F	F	F	F	S	F

P-COO$^-$/*P*-NH$_3^+$ at pH 8

Microgel ratio	LaCl$_3$ (mM)	25 °C	5 °C	50 °C	24 hr 25 °C	Shake	24 hr post shake
Excess anionic charges (10:1)	0	S	S	S	SF	S	sF
	1	S	S	F	F	S	F
	10	F	F	F	F	S	F
	100	S	SF	F	F	S	sF
Equal charges (1:1)	0	F	F	FP	F	SF	F
	1	S	S	SF	SF	S	F
	10	F	F	F	F	SF	F
	100	S	S	F	F	S	F
Excess cationic charges (1:10)	0	S	F	S	S	S	S
	1	SF	F	SF	SF	SF	SF
	10	F	F	F	F	S	F
	100	F	F	F	F	S	F

Legend: S Stable | SF Slight flocculation | F Flocculated | FP Flocculated pellet | x Missing data

Table 6.17 Comparison of flocculation frequency at 5, 25 and 50 °C

Cation	Anionic/cationic ratio	0 mM PSO$_3^-$/PNH$_3^+$ pH 8	0 mM PSO$_3^-$/PNH$_3^+$ pH 3	0 mM PCOO$^-$/PNH$_3^+$ pH 8	0 mM PCOO$^-$/PNH$_3^+$ pH 3	1 mM PSO$_3^-$/PNH$_3^+$ pH 8	1 mM PSO$_3^-$/PNH$_3^+$ pH 3	1 mM PCOO$^-$/PNH$_3^+$ pH 8	1 mM PCOO$^-$/PNH$_3^+$ pH 3	10 mM PSO$_3^-$/PNH$_3^+$ pH 8	10 mM PSO$_3^-$/PNH$_3^+$ pH 3	10 mM PCOO$^-$/PNH$_3^+$ pH 8	10 mM PCOO$^-$/PNH$_3^+$ pH 3	100 mM PSO$_3^-$/PNH$_3^+$ pH 8	100 mM PSO$_3^-$/PNH$_3^+$ pH 3	100 mM PCOO$^-$/PNH$_3^+$ pH 8	100 mM PCOO$^-$/PNH$_3^+$ pH 3
Na$^+$	10:1	3	1	3	1	1	1	1	1	1	1	1	1	1	1	1	1
Na$^+$	1:1	3	2	3	1	2	1	1	1	1	1	1	1	1	1	1	1
Na$^+$	1:10	0	1	0	0	0	1	1	0	1	1	1	1	1	1	1	1
Mg^{2+}	10:1	3	1	3	1	1	3	1	1	1	1	2	2	3	1	1	1
Mg^{2+}	1:1	2	1	3	1	1	1	1	1	1	1	1	1	1	1	1	1
Mg^{2+}	1:10	1	1	0	1	1	1	1	1	1	1	1	1	1	1	1	1
La^{3+}	10:1	3	1	3	1	1	1	2	1	3	1	3	1	1	1	2	1
La^{3+}	1:1	3	1	3	2	1	1	2	2	2	1	1	1	1	1	3	1
La^{3+}	1:10	0	1	0	0	0	1	0	0	1	1	1	1	1	1	1	1

Cation	Anionic/cationic ratio	0 mM PSO$_3^-$/PNH$_3^+$ pH 8	0 mM PSO$_3^-$/PNH$_3^+$ pH 3	0 mM PCOO$^-$/PNH$_3^+$ pH 8	0 mM PCOO$^-$/PNH$_3^+$ pH 3	1 mM PSO$_3^-$/PNH$_3^+$ pH 8	1 mM PSO$_3^-$/PNH$_3^+$ pH 3	1 mM PCOO$^-$/PNH$_3^+$ pH 8	1 mM PCOO$^-$/PNH$_3^+$ pH 3	10 mM PSO$_3^-$/PNH$_3^+$ pH 8	10 mM PSO$_3^-$/PNH$_3^+$ pH 3	10 mM PCOO$^-$/PNH$_3^+$ pH 8	10 mM PCOO$^-$/PNH$_3^+$ pH 3	100 mM PSO$_3^-$/PNH$_3^+$ pH 8	100 mM PSO$_3^-$/PNH$_3^+$ pH 3	100 mM PCOO$^-$/PNH$_3^+$ pH 8	100 mM PCOO$^-$/PNH$_3^+$ pH 3
Na$^+$	10:1	3	1	3	1	1	1	1	1	1	1	1	1	1	1	1	1
Mg^{2+}	10:1	3	1	3	1	1	3	1	1	1	1	2	2	3	1	1	1
La^{3+}	10:1	3	1	3	1	1	1	2	1	3	1	3	1	1	1	2	1
Na$^+$	1:1	3	2	3	1	2	1	1	1	1	1	1	1	1	1	1	1
Mg^{2+}	1:1	2	1	3	1	1	1	1	1	1	1	1	1	1	1	1	1
La^{3+}	1:1	3	1	3	2	1	1	2	2	2	1	1	1	1	1	3	1
Na$^+$	1:10	0	1	0	0	0	1	1	0	1	1	1	1	1	1	1	1
Mg^{2+}	1:10	1	1	0	1	1	1	1	1	1	1	1	1	1	1	1	1
La^{3+}	1:10	0	1	0	0	0	1	0	0	1	1	1	1	1	1	1	1

= 0 or 1 = more stable than flocculated

= 3 or 4 = more flocculated than stable

= intermediate

In order to compare the overall responses of each of the anionic/cationic particle mixtures to the three electrolytes, a simple comparison of the numerical incidence of flocculation under each set of conditions was made. Table 6.17 summarizes the frequency of flocculation of each set of mixtures at 5, 25 and 50 °C. For example, in Table 6.10, the 10:1 mixture of P-SO$_3^-$/P-NH$_3^+$ in NaCl at pH 8 (top row, first three columns on far left) was flocculated at all three temperatures; therefore in Table 6.17, the same 10:1 mixture of P-SO$_3^-$/P-NH$_3^+$ in NaCl at pH 8 (top row, far left column) shows a number three, indicating that the mixture was flocculated at all three temperatures (and colour coded red). Mixtures that were flocculated at none or only one of three temperatures are colour coded green.

The top half of Table 6.17 indicates that the samples tended to be more flocculated in water than in the presence of any of the electrolytes. It also suggests that there was very little difference either between the two combinations of anionic/cationic particles (*i.e.* between P-SO$_3^-$/P-NH$_3^+$ or P-COO$^-$/P-NH$_3^+$) or between the response to the two pH values. It also shows that the incidence of flocculation increases as the cation valency increases, as anticipated from theory. The lower half of the table, which is grouped by anionic:cationic ratio, clearly shows that the excess cationic (1:10) mixtures were more stable than the 1:1 or 10:1 mixtures, which are more similar in behaviour. These conclusions are broadly in agreement with the previous findings.

Although there are some ambiguities and unexpected results in the studies of the mixed-charge dispersions, particularly the discrepancies between the *n*-value and visual results, it is clear that the stability of the systems can be manipulated by subtle changes in dispersion conditions. Whilst this is particularly clear below the VPTT, where the swollen particles are more resistant to flocculation, it is also apparent from the *n*-values that changes in pH, electrolyte and surface charge group can also influence the stability of mixtures above the VPTT.

Mixtures with excess cationic particles (1:10) were particularly robust to flocculation, in agreement with the reports in the literature.[9,18] In these mixtures, in addition to the electrostatic repulsion between the excess cationic particles themselves, there is also evidence that they surround typically larger anionic particles, reversing the net charge of the complex and resulting in a stable dispersion. Although no evidence of

such particles was observed from the limited SEM undertaken in this study, it is possible that such hetero-macrocomplexes may account for the greater stability observed in the 1:10 mixtures. Additional investigation with SEM may result in conformation of their existence.

6.4 Summary

The dispersion temperature and ratio of anionic:cationic particles appear to be the most significant variables in determining the stability of a mixture. However, the dispersion pH is also very influential, by controlling the extent of ionization of surface charge groups. This can be further influenced by changes in electrolyte concentration and cation valency, which may either promote or prevent flocculation. Through careful selection of dispersion and microgel characteristics, it is therefore possible to prepare mixtures of anionic and cationic poly(NIPAM) microgel particles that reversibly flocculate under specific conditions.

6.5 References

[1] Atkins, P. W. (1994) *Atkins' Physical Chemistry* (5th Edition). Oxford: Oxford University Press.

[2] Chiklis, C. K., Grasshof, J. M. (1970) *Journal of Polymer Science, Part A-2*, **8**, 1617–1626. *In*: Meunier, F., Elaïssari, A., Pichot, C. (1995) *Polymers for Advanced Technologies*, B6B, 489–496.

[3] Snowden, M. J., Chowdhry, B. Z., Vincent, B., Morris, G.E. (1996) *Journal of the Chemical Society, Faraday Transactions*, **92**(24), 5013–5016.

[4] Garner, B.W., Cai, T., Hu, Z., Neogi, A. (2008) *Optics Express*, **16**(24), 19410–19418.

[5] Daly, E., Saunders, B.R. (2000) *Physical Chemistry Chemical Physics*, **2**, 3187–3193.

[6] Shaw, D.J. (1992) *Introduction to Colloid and Surface Chemistry* (4th Edition). Oxford: Butterworth Heinemann.

[7] Eastman, J. (2005) 'Colloid Stability'. *In*: Cosgrove, T. (Ed) *Colloid Science: Principles, Methods and Applications*. Oxford: Blackwell, pp36–49.

[8] Keilland, J. (1937) *Journal of the American Chemical Society*, **59**, 1675-1678.

[9] Islam, A. M., Chowdhry, B. Z., Snowden, M. J. (1995) *Advances in Colloid Interface Science*, **62**, 109–136.

[10] Snowden, M. J., Vincent, B. (1992) *Journal of the Chemical Society - Chemical Communications*, (16) 1103–1105.

[11] Rasmussen, M., Routh, A., Vincent, B. (2004) *Langmuir*, **20**(9), 3536–3542.

[12] Rasmussen, M., Vincent, B. (2004) *Reactive and Functional Polymers*, **58**, 203–211.

[13] Hou, Y., Yu, C., Liu, G., Ngai, T., Zhang, G. (2010) *Journal of Physical Chemistry B*, **114**(11), 3799–3803.

[14] Daly, E., Saunders, B. R. (2000) *Langmuir*, **16**(13), 5546–5552.

[15] Vincent, B. (2005) 'Introduction to Colloidal Dispersions'. *In*: Cosgrove, T. (Ed) *Colloid Science: Principles, Methods and Applications*. Oxford: Blackwell, pp 1–13.

[16] Meunier, F., Elaïssari, A., Pichot, C. (1995) *Polymers for Advanced Technologies*, **6**, 489–496.

[17] Wu, X., Pelton, R. H., Hamielec, A. E., Woods, D. R., McPhee, W. (1994) *Colloid & Polymer Science*, **272**, 467–477.

[18] Hall, R. J., Pinkrah, V. T., Chowdhry, B. Z., Snowden, M. J. (2004) *Colloids and Surfaces A: Physicochemical and Engineering Aspects*, **233**, 25–38.

[19] Islam, A. M., Chowdhry, B. Z., Snowden, M. J. (1995) *Journal of Physical Chemistry*, **99**, 14205–14206.

[20] Vincent, B., Saunders, B. (2011) 'Interactions and colloid stability of microgel particles'. *In:* Fernandez-Nieves, A., Wyss, H., Mattsson, J., Weitz, D. A. (Eds) *Microgel Suspensions: Fundamentals and Applications*. Weinheim: Wiley.

CONCLUSIONS AND FUTURE WORK

7.1   Conclusions

The objective of the work presented in this thesis was to prepare novel hydrophobically modified microgel particles by co-polymerization of N-*iso*propylacrylamide (NIPAM) with more hydrophobic co-monomers, and to investigate the impact such modifications have upon the physico-chemical properties and interfacial behaviour of the particles.   It is anticipated that the knowledge obtained from these investigations may support the future development of microgels with applications relating to more hydrophobic environments and materials.

7.1.1   *Synthesis of novel hydrophobically modified poly(NIPAM) co-polymer microgels*

A range of hydrophobically modified poly(NIPAM)-based microgels was prepared by co-polymerizing NIPAM with 10 % w/w total monomer of more hydrophobic vinyl co-monomers.   Nine novel anionic microgels were prepared, along with a selection of additional anionic and cationic poly(NIPAM)-based microgels that have been previously reported in the literature.   Several batches of homo-polymer poly(NIPAM) and a hydrophilically modified poly(NIPAM-*co*-methacrylic acid) were prepared, with which the hydrophobically modified microgels could be compared.   The initiator type and solvent:reagent ratio was also varied for some of the homo-polymer microgels so that the influence of synthesis conditions could be investigated.

7.1.2 *Characterization*

Key physico-chemical properties – particle size, electrophoretic mobility and VPTT – were determined for the homo-polymer and co-polymer microgels.   This was particularly important for the novel co-polymer microgels. All were found to display the thermosensitive volume phase transition typical of poly(NIPAM)-based particles. The VPTT was generally very similar for each microgel but the particle size varied considerably, as did the electrophoretic mobility.   Hydrophobic modification of

poly(NIPAM) microgels was found to have substantial influence upon particle size, which was also influenced by synthesis method, relative proportions of reagents and initiator type. Electrophoretic mobility was less influenced by hydrophobic modification but more so by initiator type.

The extent to which individual co-monomer characteristics such as size, structure, functional group and relative hydrophobicity influence the co-polymer microgel properties was investigated to determine whether particle characteristics can be predicted from co-monomer properties. Particle size appeared to be strongly influenced by co-monomer structure and composition, with incorporation of vinyl ether or vinyl silane co-monomers tending to increase particle size compared to homo-polymer poly(NIPAM), and vinyl ester co-monomers tending to decrease particle size. The co-monomers containing aromatic moieties tended to result in particles that exhibited properties substantially different to the other branched and linear co-monomer microgels, *e.g.* the VPTT and de-swelling ratios of V4TBB were significantly different to those of the other microgels. The co-monomer structure therefore appears to be influential.

Although no direct correlation between the particle properties and co-monomer characteristics such as logP (as an indicator of hydrophobicity) was found, some trends suggesting a link emerged. It was clear that a complex balance of influences takes place, with co-monomer structural differences appearing to be particularly significant. The data gathered on the particle physico-chemical properties provided a firm base of information from which to develop the following investigations.

7.1.3 Interfacial properties

The investigation found that the surface tension of water is substantially lowered in the presence of poly(NIPAM)-based microgel particles. Hydrophobic modification generally resulted in greater reductions in surface tension, which appeared to be influenced by a range of parameters including particle size, charge, conformation and co-monomer type. In addition, dispersion temperature and solvent quality were influential. The maximum reduction in surface tension achieved by the particles was comparable to that obtained using the surfactant sodium dodecyl sulphate (SDS) and was observed at far lower concentrations than SDS.

It was not possible to correlate surface tension measurements with individual particle or co-monomer characteristics, such as particle size or electrophoretic mobility, or relative co-monomer hydrophobicity (logP). Despite this, indications that particle size and charge are particularly influential were observed.

Although there is debate in the literature regarding whether particles are actually capable of lowering surface tension and consequently whether the findings of this study are actually the result of alternative mechanisms, these initial results strongly suggest that the microgel particles do influence surface tension. Further work is proposed to establish unequivocally whether microgel particles do lower surface tension and, if so, determine more precisely how microgel composition and properties influence their interfacial behaviour. It is anticipated that such information might aid the development of novel formulations with applications at interfaces with more hydrophobic materials.

7.1.4 Response to short-chain alcohol co-solvents

Hydrophobic modification of a poly(NIPAM) microgel by incorporation of a more hydrophobic co-monomer such as vinyl laurate influences the alcohol induced de-swelling and re-entrant swelling behaviour of the particle. The modification appears to alter the extent to which the particles interact with more hydrophobic co-solvents such as short-chain alcohols. Interestingly, it appears that the temperature-driven volume collapse characteristic of poly(NIPAM)-based microgels can be overcome at temperatures above the VPTT by the addition of alcohol, which induces re-swelling. The magnitude and onset of the response is strongly influenced by the alcohol chain length. These results may prove very useful in the development of formulations for applications requiring a trigger for inducing swelling above the VPTT, particularly in more hydrophobic environments.

7.1.5 Heteroflocculation

Three poly(NIPAM) microgels that varied predominantly only by surface charge group type were prepared (one cationic and two anionic dispersions). The basic physico-chemical properties of the microgels were determined and their stability, both alone and in mixtures of oppositely charged microgels, was studied under a wide

range of dispersion conditions, which varied by temperature, pH, electrolyte type, electrolyte concentration and relative proportions of anionic and cationic microgel particles.

The influence of temperature upon particle stability was clear, with both individual and mixed-charge dispersions more likely to display flocculation above the VPTT than below it. The presence of electrolyte also strongly effected dispersion stability. The stability of mixtures was often enhanced at low concentrations of electrolyte, whilst flocculation was promoted at high concentrations. A clear effect of electrolyte cation valency and concentration was detected, with an increase in flocculation observed in individual and mixed-charge dispersions observed with increasing valency ($Na^+ < Mg^{2+} < La^{3+}$) and/or concentration, due to the associated reduction in particle double layer thickness.

Dispersion pH was also influential upon particle mixtures, due to its role in altering the ionization state of the charge groups expressed on particle surfaces; this in turn adjusted the balance of charges within each dispersion and therefore altered the incidence of electrostatic repulsion or attraction that occurred. In addition, the balance of anionic and cationic particles within a mixture was strongly influential, with mixtures containing equal (1:1) proportions of oppositely charged particles tending to exhibit the most flocculation and mixtures of excess charge (10:1 or 1:10), especially excess cationic particles, showing the greatest resistance to flocculation.

It is clear that the stability of mixtures of anionic and cationic poly(NIPAM) microgel mixtures can be manipulated by subtle alterations in dispersion conditions. Through careful selection of dispersant and microgel characteristics, mixtures that reversibly flocculate under specific conditions can be prepared. This may be of value in applications that require the potential to reverse a flocculation under particular conditions, *e.g.* a microgel combination that will reversibly flocculate when environmental conditions pass specified thresholds, but will re-disperse if the conditions return to within the desired range. Such combinations could offer potential as a type of switch.

7.2   Future work

7.2.1 Synthesis and characterization

Although the potential influence of co-monomer characteristics upon the physico-chemical properties of the resultant co-polymer microgels was apparent from the characterization of the particles, it was not possible to quantify any direct relationships between the two. It is possible that the particular compositions of co-polymer microgels studied, *i.e.* 10 % co-monomer and 10 % cross-linker, were such that the particular influences of the added co-monomers were masked, either by the cross-linker or the 90% NIPAM. For example, the relatively high 10 % cross-linker might be sufficient to overcome any influence 10 % cross-linker might exert upon particle de-swelling. Alternatively, 10 % co-monomer may not be sufficient for the co-monomer influence to be apparent in the presence of 90 % NIPAM. It would therefore be informative to prepare a range of co-polymer microgels based upon the same co-monomers but at different co-monomer and cross-linker inclusion ratios, to determine whether the relationships between co-monomer characteristics and particle properties could be clarified.

Development of a method to assess the relative hydrophobicities of microgel particles as a whole rather than using the relative co-monomer hydrophobicity would also be valuable. Potential techniques might include using fluorophore dyes that could identify and quantify the proportion of more hydrophobic regions within the structure of a particle. Alternatively, small angle neutron scattering has been used to confirm the location of hydrophobic co-monomers[1] whilst solid state Raman and NMR spectroscopy have been used to confirm and semi-quantitatively measure the percentage incorporation of co-monomers.[2] Collectively, it might be possible to use such techniques to build a picture of the relative extent of hydrophobicity of different co-polymer microgels.

Another option would be to try to measure the particle hydrophobicity more directly, *e.g.* by determining the specific contact angle made by each co-polymer microgel at specific interfaces.   Direct measurement of the contact angle would require analysis/imaging of the particles in situ at the interface, *e.g.* by atomic force microscopy or cryo-electron microscopy. If the particles could be secured uniformly

across a surface, the contact angle made with the particle layer by drops of different hydrophobic solvents could be measured. Less direct alternatives might include preparing a series of microgels of increasing hydrophobic co-monomer content and measuring the effect upon the surface tension of water (see also discussion of future work regarding interfacial properties below). Whichever route might prove successful, more detailed knowledge and understanding of the relative hydrophobicities of microgel particles may help elucidate the dependence of microgel properties upon co-monomer characteristics.

7.2.2 *Interfacial properties*

In order to determine unequivocally whether microgel particles do lower the surface tension of water, several relatively simple experiments would be informative. For example, pendant drop-shape analysis would permit the measurement of dispersion surface tension without the use of a probe, thereby removing the potential for contaminants attached to the Wilhelmy plate interfering with the results. In addition, centrifugation of the microgel dispersion to obtain a particle-free supernatant, followed by surface tension measurements of the supernatant, should make it possible to determine whether it is the microgel particles or some other dispersion component that drives the surface tension reduction.

Further investigation of the relationship between microgel composition and interfacial properties could be based upon measurements of the effects of the range of co-polymer microgels based upon the same co-monomers but with different proportions of co-monomer and cross-linker as mentioned above (Section 7.2.1). In addition, drop volume tensiometry could be used to evaluate the behaviour of the particles at oil-water interfaces, which would provide additional information useful to developing formulations suitable for applications in more hydrophobic environments.

7.2.3 *Response to short-chain alcohol co-solvents*

Having established that hydrophobic modification of poly(NIPAM) with vinyl laurate co-monomer alters the response of the microgel particles to the presence of short-chain alcohol co-solvents, it would be informative to study a wider range of hydrophobically modified particles. This would facilitate determination of any

correlations between the type or scale of hydrophobic modification (*e.g.* which co-monomer and at which inclusion ratio) and the observed re-entrant swelling behaviour. Observations at smaller alcohol intervals would permit more detailed study of the potential trends identified in this study, whilst measurements over a range of temperatures would provide more information about how the temperature-driven collapse can be overcome by alcohol addition.

7.2.4 Heteroflocculation

This study focussed on manipulating the reversible flocculation of anionic and cationic poly(NIPAM) microgels. The next step would be to introduce some of the novel hydrophobically modified microgels prepared in this study, to determine whether such modifications offer an additional level of control over dispersion stability. This could be of particular interest when considering potential applications relating to more hydrophobic environments and materials. It would also be interesting to look in more detail at the influence of electrolyte anions of increasing valency.

Further work to reconcile instrumental measurements based on *n*-values with visual assessments of dispersion stability would be valuable, in order that a more robust quantitative measurement system could be developed for studying the stability of colloidal systems such as these.

7.3   References

[1] Gracia, L. (2007) *Co-polymer microgels: contemporary physico-chemical, structural and analytical investigations*. Thesis (Ph.D.). University of Greenwich, London.

[2] Nur, H., Cornelius, V. J., Benée, L. S., Mitchell, J. C., Day, I. J., Snowden, M. J. (2009) *Analyst*, **134**, 1366–1372.

APPENDIX A

Monomer and co-monomer predicted logP values

Data predicted by ACD/Labs and obtained from ChemSpider [Accessed 02/12/11].

Chemical	ChemSpider reference
NIPAM	http://www.chemspider.com/Chemical-Structure.15774.html
MBA	http://www.chemspider.com/Chemical-Structure.7750.html
KPS	http://www.chemspider.com/Chemical-Structure.22821.html
CVA	http://www.chemspider.com/Chemical-Structure.83896.html
MPA	http://www.chemspider.com/Chemical-Structure.68821.html
DVE	http://www.chemspider.com/Chemical-Structure.63023.html
TBVE	http://www.chemspider.com/Chemical-Structure.63406.html
TPVE	http://www.chemspider.com/Chemical-Structure.468368.html
VD	http://www.chemspider.com/Chemical-Structure.55971.html
VL	http://www.chemspider.com/Chemical-Structure.67621.html
VS	http://www.chemspider.com/Chemical-Structure.59467.html
V4TBB	http://www.chemspider.com/Chemical-Structure.76625.html
TMVS	http://www.chemspider.com/Chemical-Structure.71433.html
VTMOS	http://www.chemspider.com/Chemical-Structure.68503.html
TPVS	http://www.chemspider.com/Chemical-Structure.79165.html
MAA	http://www.chemspider.com/Chemical-Structure.3951.html

APPENDIX B

Co-monomer properties and mole fractions present in co-polymer microgels

Co-monomer	LogP[*]	RMM	Molar volume[*] (cm^3)	Mole fraction in microgel
DVE	6.35	212.37	261	0.06
TBVE	1.74	100.16	129	0.09
TPVE	2.27	114.19	146	0.08
VD	4.98	198.3	225	0.06
VL	6.04	226.36	258	0.05
VS	9.23	310.51	357	−
V4TBB	3.94	204.26	206	0.06
TMVS	1.58	100.23	142	0.08
VTMOS	1.95	148.23	161	0.08
TPVS	7.02	286.44	274	0.04
MAA	0.57	86.09	84	0.06

[*] Predicted from ACDLabs in Chemspider (see Appendix A).

APPENDIX C

Predicted refractive index values of alcohol-water mixtures

Experimentally determined refractive index values of binary mixtures of water with MeOH, EtOH or 2-PrOH were used to interpolate predicted refractive index values for 0–100 % mass alcohol.

% mass alcohol	MeOH @ 25 °C	MeOH @ 50 °C	EtOH @ 25 °C	EtOH @ 50 °C	2-PrOH @ 25 °C	2-PrOH @ 50 °C
0	1.333	1.333	1.333	1.333	1.333	1.333
1	1.334	1.333	1.334	1.334	1.334	1.334
2	1.334	1.334	1.334	1.334	1.335	1.335
3	1.334	1.334	1.335	1.335	1.336	1.336
4	1.334	1.334	1.336	1.336	1.337	1.337
5	1.334	1.334	1.336	1.336	1.338	1.337
6	1.335	1.334	1.337	1.337	1.339	1.338
7	1.335	1.335	1.338	1.338	1.340	1.339
8	1.335	1.335	1.338	1.338	1.340	1.340
9	1.335	1.335	1.339	1.339	1.341	1.340
10	1.336	1.335	1.340	1.339	1.342	1.341
11	1.336	1.335	1.341	1.340	1.343	1.342
12	1.336	1.336	1.341	1.341	1.344	1.343
13	1.336	1.336	1.342	1.341	1.345	1.343
14	1.337	1.336	1.343	1.342	1.346	1.344
15	1.337	1.336	1.343	1.342	1.347	1.345
16	1.337	1.336	1.344	1.343	1.347	1.346
17	1.337	1.336	1.345	1.343	1.348	1.346
18	1.338	1.337	1.345	1.344	1.349	1.347
19	1.338	1.337	1.346	1.345	1.350	1.348
20	1.338	1.337	1.347	1.345	1.351	1.348
21	1.338	1.337	1.347	1.346	1.352	1.349
22	1.338	1.337	1.348	1.346	1.352	1.350
23	1.339	1.337	1.349	1.347	1.353	1.350
24	1.339	1.337	1.349	1.347	1.354	1.351
25	1.339	1.337	1.350	1.348	1.354	1.351
26	1.339	1.338	1.350	1.348	1.355	1.352
27	1.340	1.338	1.351	1.348	1.356	1.353
28	1.340	1.338	1.352	1.349	1.357	1.353
29	1.340	1.338	1.352	1.349	1.357	1.354
30	1.340	1.338	1.353	1.350	1.358	1.354
31	1.340	1.338	1.353	1.350	1.358	1.355

% mass alcohol	MeOH @ 25 °C	MeOH @ 50 °C	EtOH @ 25 °C	EtOH @ 50 °C	2-PrOH @ 25 °C	2-PrOH @ 50 °C
32	1.340	1.338	1.354	1.350	1.359	1.355
33	1.341	1.338	1.354	1.351	1.360	1.356
34	1.341	1.338	1.355	1.351	1.360	1.356
35	1.341	1.338	1.355	1.352	1.361	1.357
36	1.341	1.338	1.356	1.352	1.361	1.357
37	1.341	1.338	1.356	1.352	1.362	1.358
38	1.341	1.339	1.356	1.353	1.362	1.358
39	1.341	1.339	1.357	1.353	1.363	1.358
40	1.341	1.339	1.357	1.353	1.363	1.359
41	1.342	1.339	1.358	1.353	1.364	1.359
42	1.342	1.339	1.358	1.354	1.364	1.360
43	1.342	1.339	1.358	1.354	1.365	1.360
44	1.342	1.339	1.359	1.354	1.365	1.361
45	1.342	1.339	1.359	1.355	1.366	1.361
46	1.342	1.338	1.359	1.355	1.366	1.361
47	1.342	1.338	1.360	1.355	1.367	1.362
48	1.342	1.338	1.360	1.355	1.367	1.362
49	1.342	1.338	1.360	1.355	1.367	1.362
50	1.342	1.338	1.360	1.356	1.368	1.363
51	1.342	1.338	1.361	1.356	1.368	1.363
52	1.342	1.338	1.361	1.356	1.368	1.363
53	1.342	1.338	1.361	1.356	1.369	1.364
54	1.342	1.338	1.361	1.356	1.369	1.364
55	1.342	1.338	1.361	1.356	1.369	1.364
56	1.342	1.338	1.362	1.357	1.370	1.364
57	1.342	1.337	1.362	1.357	1.370	1.365
58	1.342	1.337	1.362	1.357	1.370	1.365
59	1.341	1.337	1.362	1.357	1.371	1.365
60	1.341	1.337	1.362	1.357	1.371	1.365
61	1.341	1.337	1.362	1.357	1.371	1.366
62	1.341	1.337	1.363	1.357	1.371	1.366
63	1.341	1.336	1.363	1.357	1.372	1.366
64	1.341	1.336	1.363	1.357	1.372	1.366
65	1.341	1.336	1.363	1.357	1.372	1.367
66	1.340	1.336	1.363	1.358	1.372	1.367
67	1.340	1.335	1.363	1.358	1.373	1.367
68	1.340	1.335	1.363	1.358	1.373	1.367
69	1.340	1.335	1.363	1.358	1.373	1.367
70	1.340	1.335	1.363	1.358	1.373	1.368
71	1.339	1.334	1.364	1.358	1.374	1.368
72	1.339	1.334	1.364	1.358	1.374	1.368
73	1.339	1.334	1.364	1.358	1.374	1.368
74	1.339	1.333	1.364	1.358	1.374	1.368
75	1.338	1.333	1.364	1.358	1.374	1.368

% mass alcohol	MeOH @ 25 °C	MeOH @ 50 °C	EtOH @ 25 °C	EtOH @ 50 °C	2-PrOH @ 25 °C	2-PrOH @ 50 °C
76	1.338	1.333	1.364	1.358	1.375	1.368
77	1.338	1.332	1.364	1.358	1.375	1.369
78	1.337	1.332	1.364	1.358	1.375	1.369
79	1.337	1.332	1.364	1.358	1.375	1.369
80	1.337	1.331	1.364	1.358	1.375	1.369
81	1.336	1.331	1.364	1.358	1.376	1.369
82	1.336	1.330	1.364	1.358	1.376	1.369
83	1.336	1.330	1.364	1.357	1.376	1.369
84	1.335	1.330	1.364	1.357	1.376	1.369
85	1.335	1.329	1.364	1.357	1.376	1.369
86	1.334	1.329	1.364	1.357	1.376	1.369
87	1.334	1.328	1.363	1.357	1.376	1.369
88	1.333	1.328	1.363	1.357	1.376	1.369
89	1.333	1.327	1.363	1.357	1.377	1.370
90	1.333	1.327	1.363	1.357	1.377	1.370
91	1.332	1.326	1.363	1.356	1.377	1.370
92	1.332	1.326	1.363	1.356	1.377	1.370
93	1.331	1.325	1.363	1.356	1.377	1.370
94	1.331	1.324	1.362	1.356	1.377	1.369
95	1.330	1.324	1.362	1.355	1.377	1.369
96	1.330	1.323	1.362	1.355	1.377	1.369
97	1.329	1.323	1.362	1.355	1.376	1.369
98	1.329	1.322	1.361	1.354	1.376	1.369
99	1.328	1.322	1.361	1.354	1.376	1.369
100	1.328	1.321	1.360	1.354	1.376	1.369

Trend lines used to calculate interpolated values

Aqueous alcohol mixture	Equation
MeOH @ 25 °C	$y = 1.33332 + 2.05471E\text{-}4x + 3.1636E\text{-}6x^2 - 9.45376E\text{-}8x^3 + 3.66669E\text{-}10x^4$
MeOH @ 50 °C	$y = 1.33325 + 1.93357E\text{-}4x + 1.48433E\text{-}7x^2 - 4.73362E\text{-}8x^3 + 1.41822E\text{-}10x^4$
EtOH @ 25 °C	$y = 1.33328 + 5.74254E\text{-}4\ x + 1.20352E\text{-}x^2 - 4.5255E\text{-}7x^3 + 4.92458E\text{-}9x^4 - 1.90583E\text{-}11x^5$
EtOH @ 50 °C	$y = 1.33324 + 6.07336E\text{-}4x + 2.62845E\text{-}6x^2 - 2.22351E\text{-}7x^3 + 2.66046E\text{-}9x^4 - 1.1028E\text{-}11x^5$
2-PrOH @ 25 °C	$y = 1.33324 + 8.81551E\text{-}4x + 5.01675E\text{-}6x^2 - 3.45613E\text{-}7x^3 + 4.21732E\text{-}9x^4 - 1.71649E\text{-}11x^5$
2-PrOH @ 50 °C	$y = 1.33325 + 8.30231E\text{-}4x - 2.38134E\text{-}6\ x^2 - 1.05981E\text{-}7x^3 + 1.42974E\text{-}9x^4 - 6.04435E\text{-}12x^5$

APPENDIX D

Dielectric constants of alcohol-water mixtures from literature

% mass alcohol	MeOH @ 25 °C	MeOH @ 50 °C	EtOH @ 25 °C	EtOH @ 50 °C	2-PrOH @ 25 °C	2-PrOH @ 50 °C
0	78.50	69.85	78.50	69.85	78.50	69.85
10	74.10	65.66	72.80	64.53	71.40	63.12
20	69.20	61.06	67.00	59.22	64.10	56.61
30	64.30	56.59	61.10	53.79	56.90	50.18
40	59.60	52.17	55.00	48.36	49.70	43.54
50	54.90	47.82	49.00	42.92	42.50	37.03
60	50.10	43.22	43.40	37.72	35.30	30.67
70	45.00	38.81	38.00	32.86	28.70	24.85
80	40.10	34.62	32.80	28.10	23.70	20.26
90	35.70	30.67	28.10	24.08	20.30	17.11
100	31.50	27.44	24.30	20.87	18.00	15.06
Source table in Ref. [1]	XII	II	XII	III	XII	V

Dielectric constants of alcohol-water mixtures interpolated from data from Ref. [1]

% mass alcohol	MeOH @ 25 °C	MeOH @ 50 °C	EtOH @ 25 °C	EtOH @ 50 °C	2-PrOH @ 25 °C	2-PrOH @ 50 °C
0	78.50	69.82	79.09	70.38	79.84	69.55
1	78.06	69.40	78.45	69.79	78.96	68.97
2	77.61	68.99	77.80	69.19	78.10	68.38
3	77.16	68.57	77.16	68.60	77.23	67.79
4	76.71	68.15	76.52	68.01	76.37	67.19
5	76.26	67.73	75.89	67.42	75.52	66.58
6	75.81	67.31	75.25	66.83	74.67	65.97
7	75.35	66.88	74.62	66.25	73.83	65.35
8	74.90	66.46	73.99	65.66	72.99	64.72
9	74.44	66.03	73.36	65.08	72.15	64.10
10	73.98	65.60	72.73	64.50	71.32	63.46
11	73.52	65.16	72.11	63.92	70.49	62.82
12	73.05	64.73	71.48	63.35	69.67	62.18
13	72.59	64.29	70.86	62.77	68.86	61.53
14	72.12	63.85	70.24	62.20	68.05	60.88
15	71.65	63.41	69.62	61.63	67.24	60.23
16	71.18	62.97	69.00	61.06	66.44	59.57
17	70.71	62.53	68.39	60.49	65.64	58.91
18	70.24	62.09	67.77	59.93	64.85	58.25
19	69.77	61.64	67.16	59.36	64.06	57.58
20	69.29	61.20	66.55	58.80	63.28	56.91
21	68.82	60.75	65.94	58.24	62.50	56.24

% mass alcohol	MeOH @ 25 °C	MeOH @ 50 °C	EtOH @ 25 °C	EtOH @ 50 °C	2-PrOH @ 25 °C	2-PrOH @ 50 °C
22	68.34	60.30	65.34	57.68	61.73	55.57
23	67.86	59.85	64.73	57.13	60.96	54.89
24	67.38	59.40	64.13	56.57	60.20	54.22
25	66.90	58.95	63.53	56.02	59.44	53.54
26	66.42	58.49	62.93	55.47	58.69	52.86
27	65.94	58.04	62.33	54.92	57.94	52.18
28	65.46	57.59	61.74	54.37	57.20	51.50
29	64.98	57.13	61.14	53.82	56.46	50.82
30	64.49	56.68	60.55	53.28	55.72	50.14
31	64.01	56.22	59.96	52.74	54.99	49.46
32	63.52	55.76	59.37	52.20	54.27	48.78
33	63.04	55.30	58.79	51.66	53.55	48.10
34	62.55	54.85	58.20	51.12	52.84	47.43
35	62.06	54.39	57.62	50.59	52.13	46.75
36	61.57	53.93	57.04	50.05	51.42	46.07
37	61.09	53.47	56.46	49.52	50.72	45.40
38	60.60	53.01	55.88	48.99	50.02	44.73
39	60.11	52.55	55.31	48.47	49.33	44.06
40	59.62	52.10	54.73	47.94	48.65	43.39
41	59.13	51.64	54.16	47.41	47.96	42.73
42	58.64	51.18	53.59	46.89	47.29	42.07
43	58.15	50.72	53.02	46.37	46.62	41.41
44	57.66	50.26	52.46	45.85	45.95	40.75
45	57.17	49.80	51.89	45.34	45.29	40.10
46	56.68	49.34	51.33	44.82	44.63	39.45
47	56.19	48.89	50.77	44.31	43.98	38.81
48	55.69	48.43	50.21	43.80	43.33	38.17
49	55.20	47.97	49.65	43.29	42.69	37.53
50	54.71	47.52	49.10	42.78	42.05	36.90
51	54.22	47.06	48.54	42.27	41.41	36.28
52	53.73	46.60	47.99	41.77	40.79	35.66
53	53.24	46.15	47.44	41.26	40.16	35.04
54	52.75	45.70	46.89	40.76	39.54	34.43
55	52.26	45.24	46.34	40.27	38.93	33.83
56	51.77	44.79	45.80	39.77	38.32	33.23
57	51.28	44.34	45.25	39.27	37.72	32.64
58	50.79	43.89	44.71	38.78	37.12	32.06
59	50.30	43.44	44.17	38.29	36.52	31.48
60	49.82	43.00	43.64	37.80	35.93	30.91
61	49.33	42.55	43.10	37.31	35.34	30.35
62	48.84	42.10	42.57	36.82	34.76	29.80
63	48.36	41.66	42.03	36.34	34.19	29.25
64	47.87	41.22	41.50	35.86	33.62	28.71
65	47.39	40.78	40.97	35.37	33.05	28.18
66	46.90	40.34	40.45	34.89	32.49	27.66
67	46.42	39.90	39.92	34.42	31.93	27.15

% mass alcohol	MeOH @ 25 °C	MeOH @ 50 °C	EtOH @ 25 °C	EtOH @ 50 °C	2-PrOH @ 25 °C	2-PrOH @ 50 °C
68	45.94	39.46	39.40	33.94	31.38	26.64
69	45.45	39.03	38.88	33.47	30.83	26.15
70	44.97	38.60	38.36	33.00	30.29	25.66
71	44.49	38.16	37.84	32.53	29.75	25.19
72	44.01	37.73	37.32	32.06	29.22	24.72
73	43.54	37.31	36.81	31.59	28.69	24.27
74	43.06	36.88	36.30	31.13	28.17	23.82
75	42.58	36.46	35.79	30.66	27.65	23.39
76	42.11	36.04	35.28	30.20	27.14	22.97
77	41.64	35.62	34.77	29.74	26.63	22.56
78	41.16	35.20	34.26	29.28	26.13	22.16
79	40.69	34.79	33.76	28.83	25.63	21.77
80	40.22	34.38	33.26	28.38	25.13	21.39
81	39.75	33.97	32.76	27.92	24.64	21.03
82	39.29	33.56	32.26	27.47	24.16	20.68
83	38.82	33.15	31.76	27.02	23.68	20.34
84	38.36	32.75	31.27	26.58	23.21	20.01
85	37.90	32.35	30.78	26.13	22.74	19.70
86	37.44	31.95	30.29	25.69	22.27	19.40
87	36.98	31.56	29.80	25.25	21.81	19.11
88	36.52	31.17	29.31	24.81	21.35	18.84
89	36.06	30.78	28.82	24.37	20.90	18.59
90	35.61	30.40	28.34	23.93	20.46	18.34
91	35.16	30.01	27.86	23.50	20.01	18.11
92	34.71	29.63	27.38	23.07	19.58	17.90
93	34.26	29.26	26.90	22.64	19.15	17.70
94	33.81	28.88	26.42	22.21	18.72	17.52
95	33.37	28.51	25.95	21.78	18.30	17.35
96	32.92	28.15	25.47	21.36	17.88	17.20
97	32.48	27.78	25.00	20.93	17.47	17.06
98	32.04	27.42	24.53	20.51	17.06	16.94
99	31.61	27.07	24.07	20.09	16.66	16.84
100	31.17	26.72	23.60	19.67	16.26	16.75

Trend lines used to calculate values

Aqueous alcohol mixture	Equation
MeOH @ 25 °C	$y = 7E\text{-}06x^3 - 0.001x^2 - 0.4433x + 78.503$
MeOH @ 50 °C	$y = 1E\text{-}05x^3 - 0.0012x^2 - 0.411x + 69.815$
EtOH @ 25 °C	$y = 0.0009x^2 - 0.6449x + 79.09$
EtOH @ 50 °C	$y = 0.0009x^2 - 0.5971x + 70.383$
2-PrOH @ 25 °C	$y = 0.0024x^2 - 0.8758x + 79.838$
2-PrOH @ 50 °C	$y = 4E\text{-}05x^3 - 0.0035x^2 - 0.578x + 69.552$

[1] Åkerlöf, G. (1932) *Journal of the American Chemical Society*, **54**(11), 4125–4139.

APPENDIX E

Predicted viscosity values of alcohol-water mixtures, back-calculated from dynamic light scattering measurements using latex doping

% mass alcohol	MeOH @ 25 °C	MeOH @ 50 °C	EtOH @ 25 °C	EtOH @ 50 °C	2-PrOH @ 25 °C	2-PrOH @ 50 °C
0	0.8923	0.5527	0.8760	0.5446	0.8824	0.5468
1	0.9120	0.5609	0.9108	0.5627	0.9201	0.5674
2	0.9326	0.5694	0.9465	0.5799	0.9599	0.5868
3	0.9542	0.5783	0.9831	0.5964	1.0017	0.6053
4	0.9764	0.5874	1.0206	0.6122	1.0452	0.6230
5	0.9992	0.5967	1.0588	0.6275	1.0903	0.6400
6	1.0224	0.6062	1.0978	0.6423	1.1368	0.6565
7	1.0459	0.6158	1.1373	0.6567	1.1845	0.6726
8	1.0696	0.6254	1.1773	0.6708	1.2332	0.6885
9	1.0934	0.6351	1.2178	0.6847	1.2828	0.7041
10	1.1171	0.6447	1.2586	0.6983	1.3331	0.7196
11	1.1407	0.6542	1.2996	0.7118	1.3838	0.7351
12	1.1641	0.6636	1.3408	0.7251	1.4350	0.7505
13	1.1872	0.6729	1.3820	0.7383	1.4864	0.7660
14	1.2099	0.6820	1.4230	0.7515	1.5378	0.7816
15	1.2320	0.6909	1.4639	0.7645	1.5892	0.7972
16	1.2536	0.6995	1.5045	0.7774	1.6405	0.8129
17	1.2746	0.7079	1.5447	0.7903	1.6914	0.8287
18	1.2949	0.7160	1.5843	0.8030	1.7419	0.8446
19	1.3144	0.7238	1.6234	0.8157	1.7919	0.8606
20	1.3331	0.7313	1.6617	0.8282	1.8412	0.8767
21	1.3509	0.7385	1.6992	0.8407	1.8899	0.8928
22	1.3678	0.7453	1.7358	0.8529	1.9377	0.9090
23	1.3838	0.7518	1.7713	0.8650	1.9847	0.9252
24	1.3988	0.7579	1.8058	0.8769	2.0307	0.9414
25	1.4127	0.7637	1.8391	0.8886	2.0758	0.9576
26	1.4257	0.7690	1.8712	0.9001	2.1197	0.9737
27	1.4375	0.7740	1.9020	0.9113	2.1626	0.9897
28	1.4483	0.7786	1.9313	0.9222	2.2043	1.0056
29	1.4580	0.7828	1.9592	0.9328	2.2448	1.0214
30	1.4666	0.7866	1.9857	0.9431	2.2841	1.0370
31	1.4740	0.7900	2.0105	0.9530	2.3221	1.0524
32	1.4804	0.7930	2.0338	0.9625	2.3590	1.0675
33	1.4857	0.7957	2.0554	0.9717	2.3945	1.0825
34	1.4899	0.7980	2.0754	0.9804	2.4289	1.0971
35	1.4930	0.7999	2.0938	0.9886	2.4619	1.1115
36	1.4950	0.8014	2.1104	0.9965	2.4938	1.1256
37	1.4960	0.8026	2.1253	1.0038	2.5244	1.1393
38	1.4960	0.8034	2.1385	1.0106	2.5539	1.1527
39	1.4949	0.8039	2.1501	1.0170	2.5822	1.1658
40	1.4929	0.8041	2.1599	1.0228	2.6093	1.1785

% mass alcohol	MeOH @ 25 °C	MeOH @ 50 °C	EtOH @ 25 °C	EtOH @ 50 °C	2-PrOH @ 25 °C	2-PrOH @ 50 °C
41	1.4900	0.8039	2.1681	1.0282	2.6354	1.1909
42	1.4861	0.8035	2.1747	1.0330	2.6604	1.2029
43	1.4814	0.8027	2.1796	1.0374	2.6844	1.2146
44	1.4758	0.8017	2.1830	1.0412	2.7074	1.2259
45	1.4695	0.8003	2.1848	1.0445	2.7295	1.2369
46	1.4624	0.7988	2.1852	1.0473	2.7508	1.2476
47	1.4545	0.7969	2.1841	1.0497	2.7712	1.2580
48	1.4460	0.7949	2.1817	1.0515	2.7909	1.2682
49	1.4369	0.7926	2.1780	1.0529	2.8099	1.2780
50	1.4272	0.7900	2.1730	1.0539	2.8283	1.2876
51	1.4170	0.7873	2.1669	1.0544	2.8461	1.2971
52	1.4062	0.7844	2.1597	1.0546	2.8634	1.3063
53	1.3951	0.7813	2.1515	1.0543	2.8801	1.3154
54	1.3835	0.7781	2.1424	1.0537	2.8965	1.3243
55	1.3716	0.7747	2.1324	1.0528	2.9125	1.3332
56	1.3594	0.7711	2.1217	1.0516	2.9282	1.3419
57	1.3469	0.7675	2.1102	1.0501	2.9436	1.3507
58	1.3343	0.7636	2.0983	1.0484	2.9588	1.3594
59	1.3214	0.7597	2.0858	1.0465	2.9737	1.3682
60	1.3084	0.7557	2.0728	1.0443	2.9885	1.3770
61	1.2953	0.7515	2.0596	1.0421	3.0031	1.3859
62	1.2822	0.7472	2.0461	1.0397	3.0175	1.3949
63	1.2690	0.7429	2.0324	1.0372	3.0318	1.4040
64	1.2559	0.7385	2.0186	1.0346	3.0459	1.4132
65	1.2427	0.7339	2.0048	1.0321	3.0599	1.4226
66	1.2297	0.7293	1.9910	1.0295	3.0737	1.4321
67	1.2166	0.7246	1.9772	1.0269	3.0872	1.4418
68	1.2037	0.7198	1.9637	1.0243	3.1005	1.4515
69	1.1909	0.7149	1.9502	1.0218	3.1134	1.4614
70	1.1781	0.7099	1.9370	1.0193	3.1258	1.4714
71	1.1655	0.7047	1.9240	1.0169	3.1378	1.4814
72	1.1529	0.6995	1.9112	1.0145	3.1491	1.4914
73	1.1405	0.6941	1.8986	1.0122	3.1597	1.5014
74	1.1280	0.6886	1.8862	1.0099	3.1693	1.5112
75	1.1156	0.6830	1.8740	1.0077	3.1779	1.5209
76	1.1032	0.6772	1.8619	1.0055	3.1852	1.5302
77	1.0908	0.6712	1.8499	1.0033	3.1911	1.5391
78	1.0783	0.6649	1.8378	1.0010	3.1953	1.5474
79	1.0656	0.6585	1.8257	0.9985	3.1975	1.5550
80	1.0527	0.6518	1.8132	0.9960	3.1975	1.5618
81	1.0395	0.6448	1.8004	0.9931	3.1949	1.5675
82	1.0259	0.6375	1.7870	0.9900	3.1895	1.5719
83	1.0118	0.6299	1.7728	0.9864	3.1809	1.5748
84	0.9972	0.6218	1.7576	0.9823	3.1687	1.5759
85	0.9818	0.6134	1.7412	0.9776	3.1524	1.5750
86	0.9656	0.6045	1.7233	0.9721	3.1316	1.5717
87	0.9485	0.5951	1.7036	0.9656	3.1059	1.5657
88	0.9302	0.5852	1.6817	0.9581	3.0747	1.5567
89	0.9106	0.5747	1.6573	0.9493	3.0374	1.5442
90	0.8895	0.5635	1.6299	0.9390	2.9935	1.5278

% mass alcohol	MeOH @ 25 °C	MeOH @ 50 °C	EtOH @ 25 °C	EtOH @ 50 °C	2-PrOH @ 25 °C	2-PrOH @ 50 °C
91	0.8668	0.5516	1.5992	0.9270	2.9424	1.5070
92	0.8421	0.5390	1.5646	0.9131	2.8833	1.4814
93	0.8154	0.5255	1.5256	0.8970	2.8155	1.4504
94	0.7864	0.5112	1.4817	0.8784	2.7383	1.4134
95	0.7547	0.4959	1.4322	0.8570	2.6509	1.3698
96	0.7202	0.4796	1.3765	0.8325	2.5524	1.3189
97	0.6825	0.4621	1.3139	0.8045	2.4420	1.2601
98	0.6413	0.4435	1.2436	0.7726	2.3187	1.1925
99	0.5964	0.4237	1.1648	0.7365	2.1815	1.1155
100	0.5474	0.4025	1.0768	0.6957	2.0294	1.0281

Trend lines used to calculate values

Aqueous alcohol mixture	Equation
MeOH @ 25 °C	$y = 0.89227 + 0.01916x + 5.64878\text{E-}4x^2 - 2.53957\text{E-}5x^3 + 2.11567\text{E-}7x^4 + 4.75229\text{E-}10x^5 - 8.42297\text{E-}12x^6$
MeOH @ 50 °C	$y = 0.55272 + 0.00794x + 2.26501\text{E-}4x^2 - 1.14902\text{E-}5x^3 + 1.44501\text{E-}7x^4 - 6.16918\text{E-}10x^5$
EtOH @ 25 °C	$y = 0.876 + 0.0343x + 4.92899\text{E-}4x^2 - 5.66731\text{E-}6x^3 - 4.84268\text{E-}7x^4 + 8.74958\text{E-}9x^5 - 4.15599\text{E-}11x^6$
EtOH @ 50 °C	$y = 0.5446 + 0.01861x - 5.17531\text{E-}4x^2 + 2.5185\text{E-}5x^3 - 6.4992\text{E-}7x^4 + 7.10627\text{E-}9x^5 - 2.77903\text{E-}11x^6$
2-PrOH @ 50 °C	$y = 0.88243 + 0.03651x + 0.00118x^2 - 3.39779\text{E-}5x^3 + 1.16986\text{E-}7x^4 + 3.59574\text{E-}9x^5 - 2.79821\text{E-}11x^6$
2-PrOH @ 50 °C	$y = 0.54678 + 0.02126x - 6.9043\text{E-}4x^2 + 3.78584\text{E-}5x^3 - 9.60045\text{E-}7x^4 + 1.07597\text{E-}8x^5 - 4.41913\text{E-}11x^6$

APPENDIX F

Alcohol % mass compositions of aqueous microgel mixtures

(a) First batches of N2 and VL tested in MeOH or EtOH at 25 °C

Alcohol % volume	N2 microgel		VL microgel	
	Alcohol concentration (% mass)			
	MeOH	EtOH	MeOH	EtOH
0	0	0	0	0
20	16	16	16	16
40	34	34	34	34
60	54	54	54	54
80	76	76	76	76
90	88	87	88	88

(b) Second batches of N2 and VL tested in MeOH, EtOH or 2-PrOH at 25 and 50 °C

Alcohol (% volume)	N2 microgel			VL microgel		
	Alcohol (% mass)					
	MeOH	EtOH	2-PrOH	MeOH	EtOH	2-PrOH
0	0	0	0	0	0	0
10	8	8	8	8	8	8
20	16	17	17	17	16	17
30	25	25	25	24	25	25
40	33	35	34	34	34	34
50	43	44	39	43	44	44
60	53	54	54	53	54	53
70	64	64	64	64	65	65
80	75	76	75	76	76	76
85	81	82	81	82	82	82

APPENDIX G

Calculation of theoretical number of particles in *P*-SO$_3^-$, *P*-COO$^-$ and *P*-NH$_3^+$ dispersions and theoretical number of surface charged groups on each particle

To calculate the number of charged groups present on the surface of a particle, both the number of particles in dispersion and the number of radicals formed during synthesis must be known. The theoretical number of microgel particles produced in a synthesis reaction can be calculated from the mass of reagents used, density of the particles (Equation G.1), equation for the volume of a sphere (Equation G.2) and measured particle radius (at 50 °C when the particles adopt a collapsed conformation). Table G.1 shows the theoretical number of particles in the -SO$_3^-$, *P*-COO$^-$ and *P*-NH$_3^+$ dispersions and Table G.2 shows the theoretical number of radical groups per particle.

$$Density = \rho = \frac{m}{V} \quad \text{where } m = \text{mass and } V = \text{volume}$$

[Equation G.1]

$$Volume\ of\ a\ sphere = V = \frac{4}{3}\pi r^3 \quad \text{where } r = \text{particle radius (hydrodynamic radius)}$$

[Equation G.2]

Table G.1 Theoretical number of particles

Microgel dispersion	*P*-SO$_3^-$ (N4)	*P*-COO$^-$ (N5)	*P*-NH$_3^+$ (N6)
Total mass reagents (g)[†]	6.00380	6.00320	6.00124
Volume H$_2$O (mL)[††]	1000.15	1000.15	1000.07
Particle diameter @ 50 °C (nm)	249	224	219
Particle radius, *r* (nm)	124.5	112.0	109.5
Particle radius, *r* (m)	1.25 x 10^{-7}	1.12 x 10^{-7}	1.10 x 10^{-7}
Particle volume, *V* (m^3)[‡]	8.08 x 10^{-21}	5.88 x 10^{-21}	5.50 x 10^{-21}
Particle density, ρ (kg/m^3)[‡‡]	1090	1090	1090
Particle mass (kg)[§]	8.81 x 10^{-18}	6.41 x 10^{-18}	5.99 x 10^{-18}
Particle mass (g)	8.81 x 10^{-15}	6.41 x 10^{-15}	5.99 x 10^{-15}
Total no. particles in dispersion	6.81 x 10^{14}	9.36 x 10^{14}	1.00 x 10^{15}
No. particles/mL	6.81 x 10^{11}	9.36 x 10^{11}	1.00 x 10^{12}

[†] Total mass of monomer, cross-linker and initiator used in synthesis; [††] Total volume of water used in synthesis; [‡] Calculated from Equation G.2; [‡‡] From Ref. [1]; [§] Calculated from particle volume and density using Equation G.1.

Table G.2 Theoretical number of radical charged groups per particle

Initiator	KPS	CVA	MPA
Mass initiator (g)	0.50	0.50	0.50
Relative molecular mass (RMM) initiator	270.32	280.28	271.19
No. moles initiator (mol)[†]	0.00186	0.00179	0.00184
No. initiator molecules [††]	1.12×10^{21}	1.08×10^{21}	1.11×10^{21}
No. radicals[‡]	2.23×10^{21}	2.15×10^{21}	2.22×10^{21}
Total no. particles in dispersion[4]	6.81×10^{14}	9.36×10^{14}	1.00×10^{15}
No. radical groups per particle[5]	3.28×10^{6}	2.30×10^{6}	2.22×10^{6}

[†] Where no. moles = mass/RMM; [††] Where no. molecules = no. moles x Avogadro's number (6.022 x 10^{23}); [‡] Two radicals are formed from every initiator molecule, therefore no. radicals = 2 x no. initiator molecules; [‡‡] Values from Table 7A.2; [§] Calculated by dividing no. radicals by no. particles.

[1] Chiklis, C. K., Grasshof, J. M. (1970) *Journal of Polymer Science, Part A-2*, **8**, 1617–1626. *In*: Meunier, F., Elaïssari, A., Pichot, C. (1995) *Polymers for Advanced Technologies*, B6B, 489–496.

APPENDIX H

Charts illustrating effect of increasing concentrations of NaCl, MgCl$_2$ and LaCl$_3$ electrolyte upon the particle size of *P*-SO$_3^-$, *P*-COO$^-$ and *P*-NH$_3^+$ at 6 and 25 °C

At 6 °C:
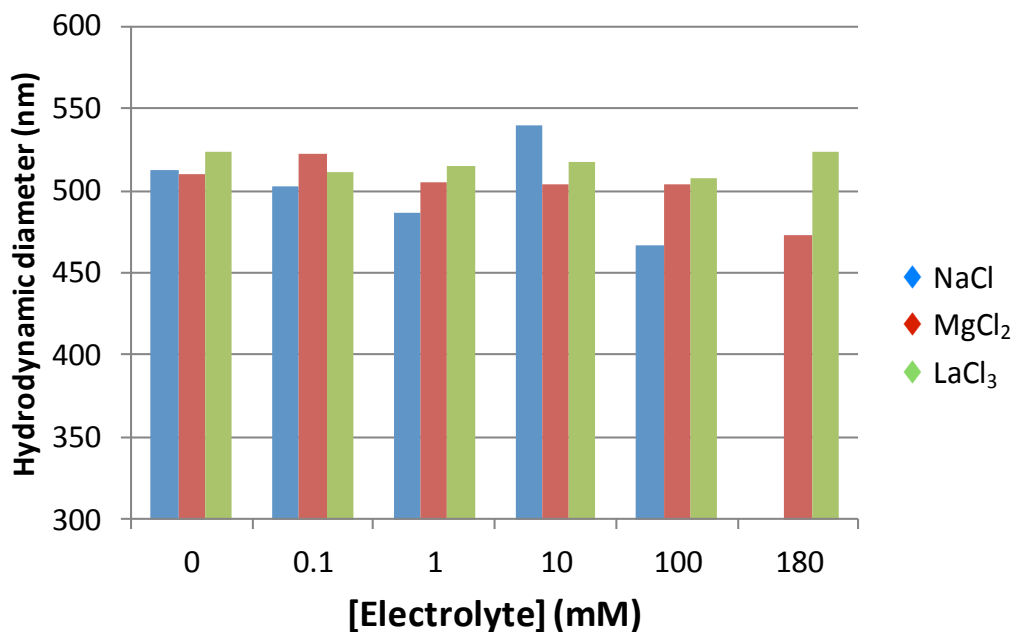
Figure 7B.1 *D*$_H$ of dispersed *P*-SO$_3^-$ particles at 6 °C in NaCl, MgCl$_2$ and LaCl$_3$
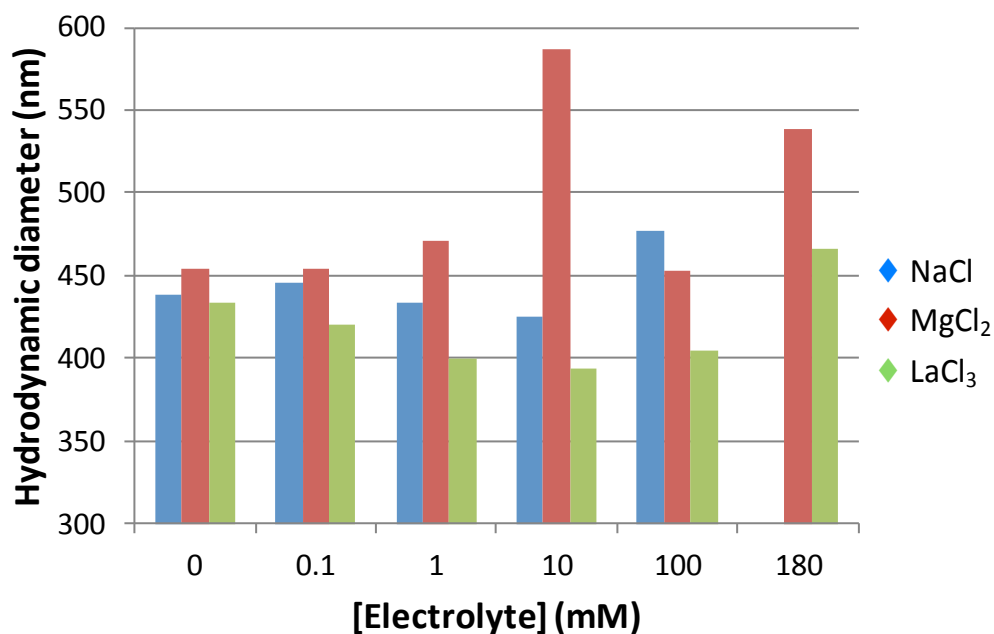

Figure 7B.2 *D*$_H$ of dispersed *P*-COO$^-$ particles at 6 °C in NaCl, MgCl$_2$ and LaCl$_3$
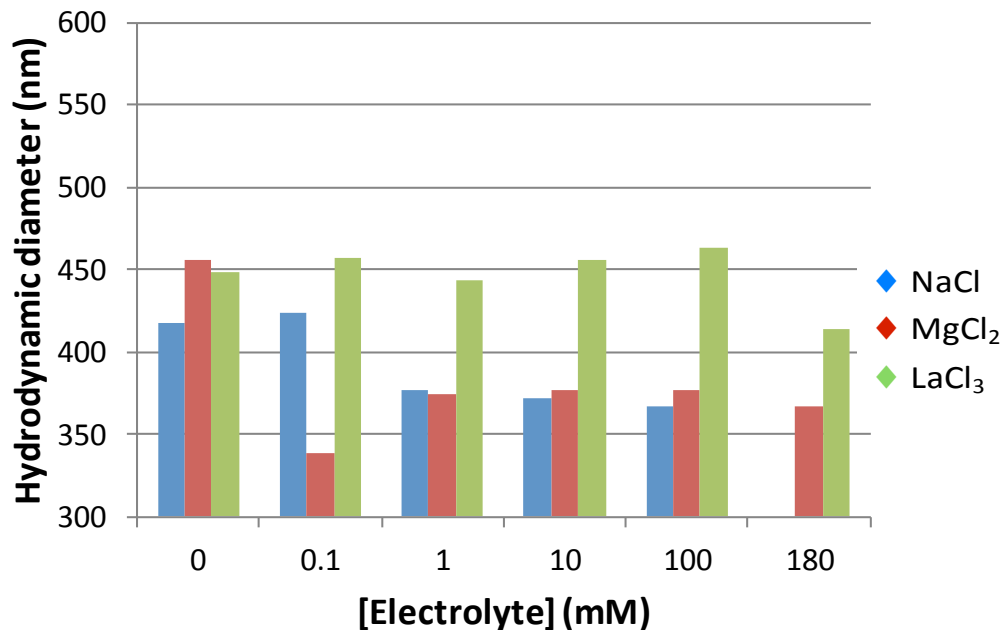
Figure 7B.3 D_H of dispersed P-NH$_3^+$ particles at 6 °C in NaCl, MgCl$_2$ and LaCl$_3$
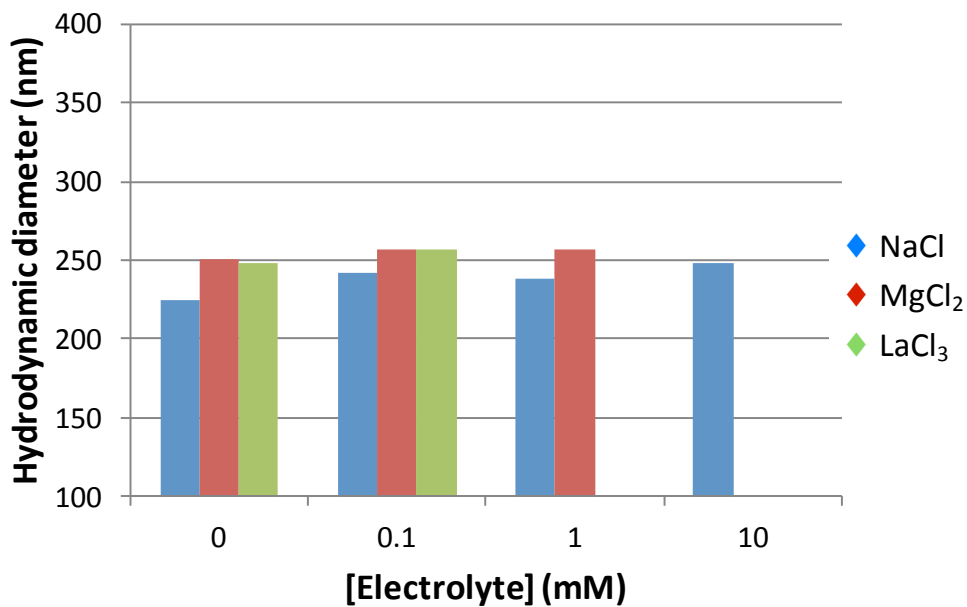
At 50 °C:

Figure 7B.4 D_H of dispersed P-SO$_3^-$ particles at 50 °C in NaCl, MgCl$_2$ and LaCl$_3$
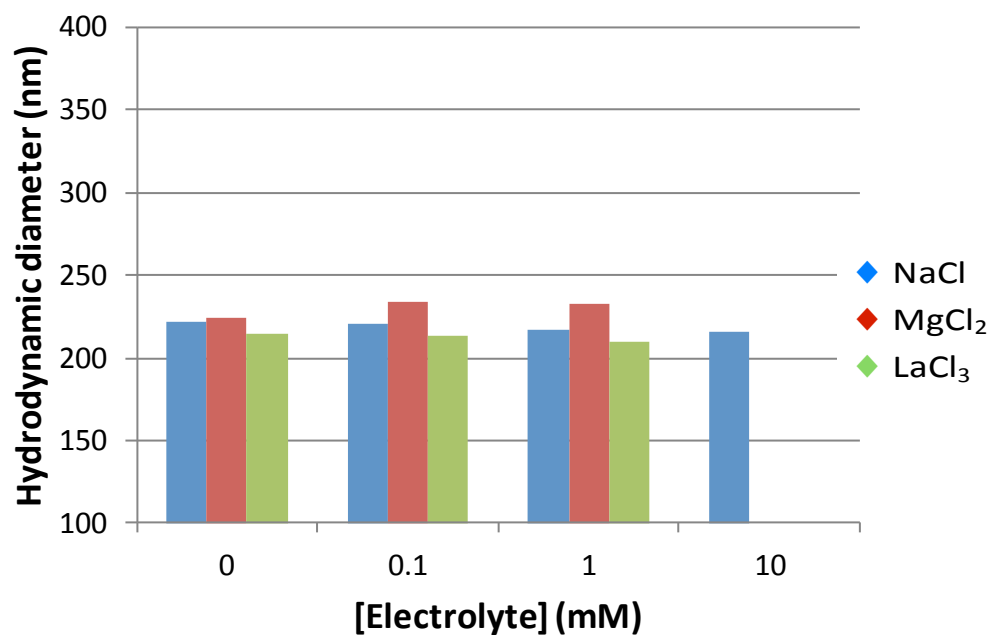
Figure 7B.5 D_H of dispersed *P*-COO$^-$ particles at 50 °C in NaCl, MgCl$_2$ and LaCl$_3$
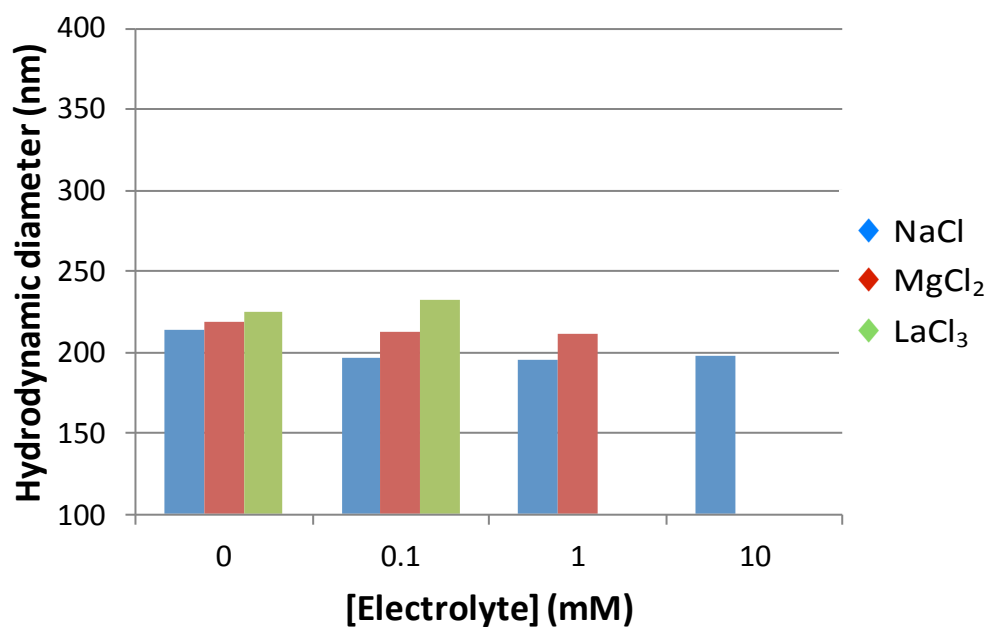

Figure 7B.6 D_H of dispersed *P*-NH$_3^+$ particles at 50 °C in NaCl, MgCl$_2$ and LaCl$_3$

APPENDIX I

Publication relating to work contained within this thesis

ORIGINAL CONTRIBUTION

Microgel applications and commercial considerations

Joanna B. Thorne · George J. Vine · Martin J. Snowden

Abstract The term microgel has been used to describe a variety of particles that differ substantially in structure, physicochemical properties, preparation and application and has been used interchangeably with terms such as nanogel, microsphere and macrogel. Many excellent and wide-ranging reviews have been published on the numerous particle types considered to fall within the broad sphere of nano-/microparticles. The aim of this review is to focus on applications of microgel particles that are synthesised by polymerisation, are of colloidal size and exhibit conformational changes in response to changes in environmental conditions. It is not the intention to attempt to cover every potential microgel application; instead, a selected range of areas will be covered and the commercial implications of scaling up the production of microgels for such purposes will be discussed. A brief description of the characteristics of microgel particles is followed by discussion of applications such as enhanced oil recovery, biomaterials and catalysis, before issues of commercialising microgel production are considered.

Keywords Microgel · Applications · Commercial implications · Properties · Poly(NIPAM) · Nanoparticles

Abbreviation

2-PrOH	2-Propanol
4-VP	4-Vinylpyridine
AA	Acrylic acid
AAPBA	3-Acrylamidophenylboronic acid
AM	Acrylamide
AMPS	2-Acrylamido-2-methyl-1-propanesulphonic acid
APBA	3-Aminophenylboronic acid
BDDA	1,4-Butanediol diacrylate
BuA	Butyl acrylate
CRP	Controlled/'living' radical polymerization
DLS	Dynamic light scattering
DVB	Divinylbenzene
EA	Ethylacrylate
EDC	N-ethyl-N'-dimethylaminopropyl-carbodiimide
EOR	Enhanced oil recovery
ERF	Electrorheological fluid
EtOH	Ethanol
Fig	Figure
HEMA	2-Hydroxyethyl methacrylate
KPS	Dipotassium persulphate
LCST	Lower critical solution temperature
LFRP	Living free radical polymerisation
MAA	Methacrylic acid
MBA	N,N'-Methylene bisacrylamide
MeOH	Methanol
MIPs	Molecularly imprinted polymers
MMA	Methylmethacrylate
NIPAM	N-Isopropylacrylamide
nm	Nanometre
o/w	Oil/water
pK_a	Acid dissociation constant
POEGMA	Poly-oligo(ethylene glycol) methacrylates
SDS	Sodium dodecyl sulphate
SFEP	Surfactant-free emulsion polymerisation
TEM	Transmission electron microscope
VP	Vinylpyridine
VPTT	Volume phase transition temperature

J. B. Thorne · G. J. Vine · M. J. Snowden (✉)
School of Science, University of Greenwich,
Chatham Maritime,
Kent ME4 4TB, UK
e-mail: M.J.Snowden@greenwich.ac.uk

w/o   Water/oil

μm   Micrometre

Introduction

The last three decades have witnessed huge interest in microgels due to their potential for applications across a wide range of industries. Many excellent and wide-ranging reviews of various aspects of microgel preparation, characteristics and applications already exist in the literature, which encompass the many different particle types that can be considered to fall within the broad sphere of nano-/microparticles [1–14]. The intention of this particular review is not to attempt to cover every aspect; instead, the aim is to focus on a selected range of application areas and consider the commercial implications of bringing such potential applications to the market place.

In particular, this review focuses on particles that meet the following criteria:

–   Have colloidal dimensions, i.e. 1 nm–1 μm
–   Result from a polymerisation reaction
–   Exhibit the ability to react to external stimuli such as pH or temperature

The term 'microgel' has been used to describe a broad range of particles that differ substantially in size, composition, structure, synthesis method, dispersion medium, properties and applications. It has also been used interchangeably with terms such as microsphere, nanogel, hydrogel, macrogel and hydrogel sphere. For example, there is a common misinterpretation regarding the terms 'microgel', 'hydrogel' and 'macrogel'. 'Hydrogel' is used to describe the formation of a polymer in which the disperse phase (e.g. colloid) has combined with the continuous phase (e.g. water) to produce a partially solvated polymer/water solution. Macrogels have a large, cross-linked structure often referred to as a 'bowl of jelly' [6], whereas microgels are much smaller, cross-linked, discrete particles. Both microgels and macrogels are types of hydrogel, having similar polymer chemistry but different physical molecular arrangements (Fig. 1). In general, microgel particles can be defined as a disperse phase of discrete, intra-molecularly cross-linked polymeric gel particles that are uniformly dispersed in a solvent medium and swollen by a good solvent [1, 15]. This review is concerned with microgel particles and hybrid microgel particles, mostly in aqueous dispersion.

The most widely studied water-swellable microgel system is based on the monomer N-isopropylacrylamide (NIPAM) [2]. Poly(NIPAM) microgel particles may be prepared by surfactant-free emulsion polymerisation (SFEP) and exhibit both hydrophilic and hydrophobic characteristics that are derived from the charged surface groups or carbon backbone
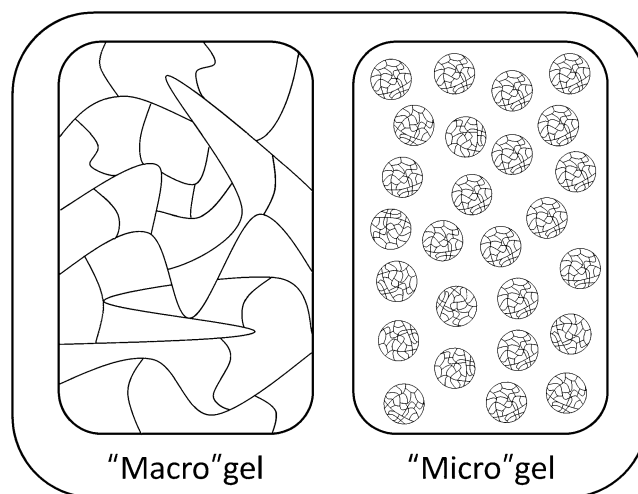

Fig. 1 Illustration of the fundamental difference between macrogels and microgels

plus methyl groups, respectively [16, 17]. The internal structure of the particles resembles a typical cross-linked network, with a porous, 'sponge-like' structure [1]. Poly (NIPAM) was first prepared in 1986 by Pelton and Chibante [15], who observed the formation of aqueous poly(NIPAM) lattices that were swollen below the lower critical solution temperature (LCST) of linear poly(NIPAM) (32 °C) but shrunken at temperatures above the LCST [15]. Further investigations revealed that the shrinking and swelling behaviour exhibited occurred in response to changes in environmental conditions such as pH, ionic strength and temperature [1]. This meant microgel particles could be tailored to enable them to be applied to a wide range of uses under specific conditions [2]. For example, by controlling the extent of cross-linking within the particle network, the extent to which a microgel particle swells can be influenced (Fig. 2) [2]. The presence of cross-linkers means that microgels, in addition to having a finite structure, are not strictly soluble but instead form colloidal dispersions [1].

Similar microgel particles have been prepared from other monomers/co-monomers, with great effect. These include methylmethacrylate, methacrylic acid (MAA), styrene, divinylbenzene, acrylic acid (AA), N,N'-methylene bisacrylamide (MBA) and ethylene glycol dimethacrylate [2]. NIPAM may be co-polymerised with other monomers, such as butyl acrylate (BuA) and/or MAA; Lopez et al. found that the resultant particles had potential to act as transdermal delivery agents for drugs such as ibuprofen and salicylate [19, 20]. Alternative acrylamide (AM) monomers have been used to prepare temperature-sensitive microgels, e.g. Lowe et al. [21] used N-ethyl-acrylamide, whilst Duracher et al. [22] used N-isopropyl-methacrylamide. The key characteristic of these monomers is the presence of at least one vinyl group which can
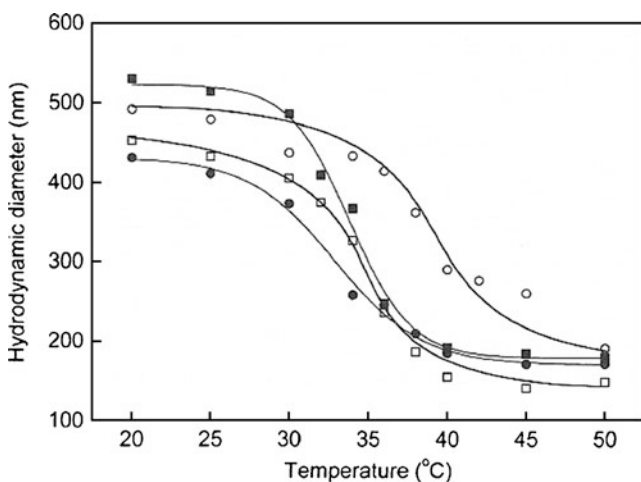
Fig. 2 Hydrodynamic diameter vs temperature plots for poly(NIPAM) microgel dispersions prepared with cross-linker (MBA) densities of 5% (*filled square*), 10% (*empty square*), 20% (*filled circle*) and 30% (*empty circle*) obtained from light scattering data. Reprinted from [18] with permission from ACS

participate in polymerisation/cross-linking [2, 6]. Non-acrylamide-based monomers have also been utilized, such as *N*-[(2-hydroxy-3-trimethylammonium)propyl] chitosan chloride [23] and *N*-vinylcaprolactam [24, 25], which both resulted in pH-responsive microgels. The monomeric composition of a microgel will determine whether the particles are swellable in aqueous or non-aqueous solvents [1].

The use of alternative synthesis methods enables the preparation of particles in different dispersion media and with very different structures. Such synthesis methods include emulsion polymerisation, living free radical polymerisation (LFRP) and radiation polymerisation [5, 6]. A wide range of different structures can be prepared, such as star microgels from LFRP, core–shell hybrids and micro-gels filled or covered with inorganic nanoparticles [6, 10].

Microgel dispersions have a range of physicochemical properties derived from the monomer(s), cross-linker and initiator from which they are prepared. For example, poly (NIPAM)-based microgels prepared by SFEP are discrete, gel-like particles in dispersion, typically prepared at a concentration of 0.5% (*w/v*) [1], with low viscosities, very high surface areas and rapid thermal and solution responses [3, 6]. They display interesting electrical properties that result from the presence of covalently bonded charged groups originating from the initiator and vary with changes in conditions, such as temperature and electrolyte [3]. The 'sponge-like' structure enables the colloidal particles to behave like 'microsponges', absorbing solvated materials under one set of conditions then undergoing rapid conformational changes and releasing them again following certain environmental changes [6].

Stimuli-responsive behaviour

Temperature

Figure 3a illustrates the typical thermoresponsive behaviour of poly(NIPAM). At room temperature, the particle is swollen [15], with its polymer networks extended into a soft, porous structure. Such polymer networks, immersed in a good solvent, will take in solvent molecules until the chemical potential inside and outside the structure is balanced. Swelling therefore continues until the elastic forces of the cross-links that restrict swelling are equal to the osmotic force imposed by the solvent [6]. As the temperature increases, the particle collapses, adopting a tightly packed structure more like a hard particle such as a polystyrene latex [5].

Figure 3b illustrates a typical plot of the change in microgel particle size (hydrodynamic diameter) as a function of temperature. The point at which the particle switches between swollen and collapsed conformations is known as the volume phase transition temperature (VPTT) [6, 15, 26]. It is usually taken to be the midpoint of the particle diameter versus temperature curve [2], determined by taking the first derivative, and is 34 °C for poly(NIPAM) [5]. The swelling behaviour results from the temperature dependence of hydrogen bonding and hydrophobic interactions between the polymer chains and the solvent (water) [27].

pH

Ionic (or polyelectrolyte) microgels contain at least one co-monomer that carries a charge when the pH approaches the pK_a for that species and therefore display pH sensitivity [9, 28]. By combining a polyelectrolyte co-monomer such as AA with a temperature-sensitive monomer such as NIPAM, it is possible to prepare microgel particles sensitive to both pH and temperature, i.e. multi-responsive microgels [28–30]. Figure 4 illustrates the conformational change of a microgel containing polyelectrolyte groups driven by changes in pH.

The mechanism controlling the pH-driven swelling of microgel particles is governed by the internal osmotic pressure resulting from mobile counterions within the particle, which oppose the internal electrostatic repulsion [6]. As the pH rises above the pK_a, the polyelectrolyte groups within the microgel structure become dissociated (ionised) and repel one another, causing the particle to swell. Below the pK_a, the associated (deionised) groups facilitate the adoption of a more compact structure [6, 28].

Ionic strength

The presence of electrolyte influences the size and stability of microgel particles, particularly when polyelectrolyte
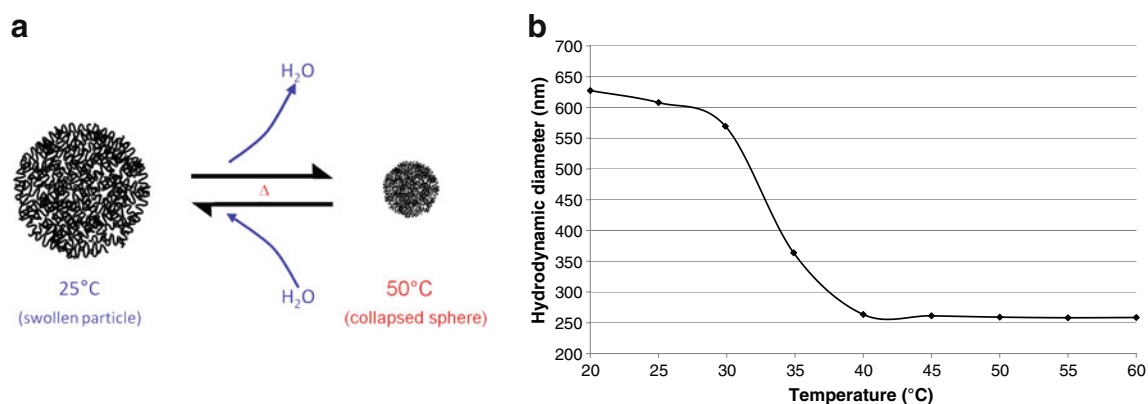
Fig. 3 **a** Illustration of typical thermoresponsive behaviour of poly(NIPAM) microgel particles; **b** associated change in hydrodynamic diameter of poly(NIPAM) microgel particles as a function of temperature (previously unpublished data)

groups are incorporated by co-polymerisation. For example, Snowden et al. [28] demonstrated that the hydrodynamic diameter of poly(NIPAM-co-AA) microgels decreases in the presence of increasing NaCl concentration (Fig. 5). This is a result of the electrolyte screening the internal charge repulsion; the effect is reversible by removing the electrolyte. The effect of electrolyte upon the stability/flocculation behaviour of microgels is described in the section on dispersion stability below, but it is worth noting at this point that temperature influences the response to changes in ionic strength due to the conformational changes that result from increased temperature. For example, in the presence of an electrolyte such as NaCl, dilute microgel dispersions are colloidally stable, even when heated above the VPTT, provided the ionic strength is not high [9]. However, at higher ionic strengths, aggregation may occur, especially above the VPTT.
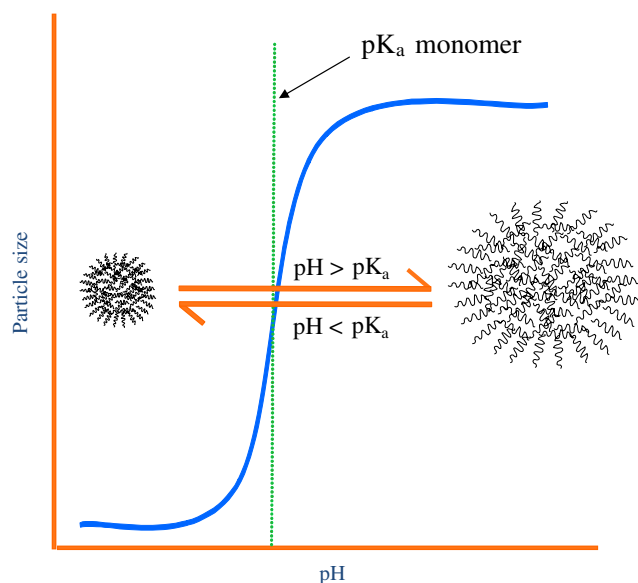
Alcohol addition

The swelling of poly(NIPAM) microgel particles can be controlled by other factors, e.g. addition of alcohols [31]. Several groups have investigated poly(NIPAM) swelling behaviour in the presence of short-chain alcohols [31–35]. For example, Crowther and Vincent [31] studied the swelling behaviour of poly(NIPAM) microgel particles (produced by SFEP with 9% MBA cross-linker and ammonium persulphate initiator) in aqueous mixtures of methanol (MeOH), ethanol (EtOH) and 2-propanol (2-PrOH) using dynamic light scattering. At 25 °C, as the volume fraction of alcohol increased, the microgel particles collapsed (de-swelling) to a minimum size at low volume fractions but in the higher, alcohol-rich region, the particles re-swelled (re-entrant swelling), as shown in Fig. 6. The volume fraction at which the greatest degree of collapse was reached was affected by the alcohol carbon chain

Fig. 4 Conformational changes of a polyelectrolyte microgel as a function of pH. Adapted from [6] with permission of CRC Press conveyed through Copyright Clearance Centre, Inc
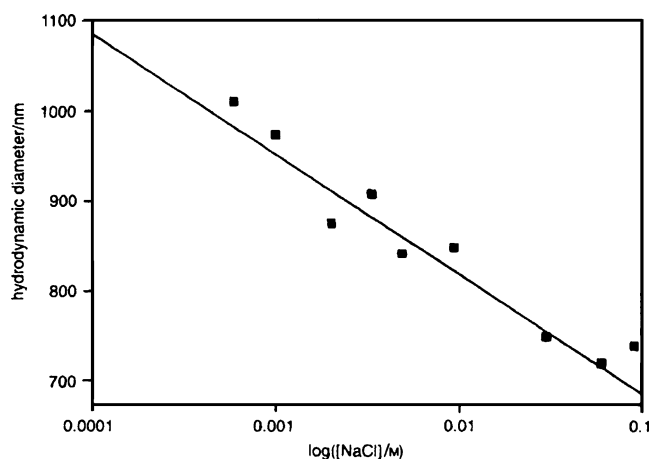

Fig. 5 Hydrodynamic diameter of poly(NIPAM-co-AA) (95:5%) microgel particles as a function of ionic strength of NaCl at pH 6 and 25 °C at a microgel concentration of 0.07% (*w/w*). Reproduced from [28] by permission of The Royal Society of Chemistry
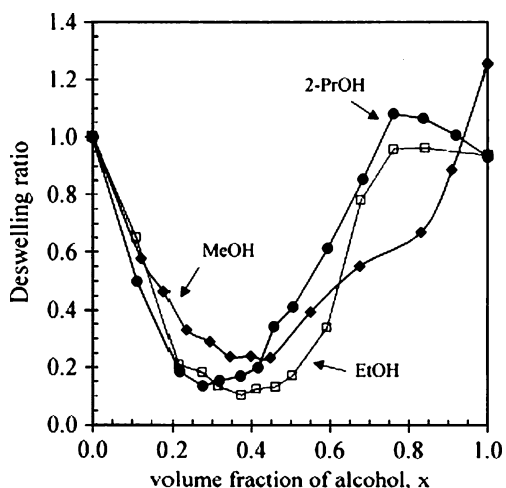
Fig. 6 Change in the de-swelling ratio of poly(NIPAM) (9% MBA) microgel particles as a function of increasing volume fraction of three alcohols. The alcohols investigated are MeOH (*filled diamond*), EtOH (*empty square*) and 2-PrOH (*filled circle*). Reproduced with permission from [31]

length, with smaller volumes of the longer chain alcohols required to achieve the maximum degree of collapse.

This de-swelling/re-entrant swelling behaviour has been explained by co-non-solvency and clathrate structure formation [31]. Co-non-solvency is the term used to describe the fact that individually solvents such as water and alcohol can be good solvents for particles such as microgels but in combination, over certain concentration ranges, become a poor solvent for the same particles [36]. Clathrates are disordered tetrahedral cage-like structures of water molecules that form around an alcohol molecule [37]. In pure water, it has been suggested that water molecules form cage-like structures around hydrophobic regions of the poly(NIPAM) chains [17, 31]. Otake et al. [17] described two phenomena that occur when hydrophobic solutes are added to water. Firstly, water molecules form cage-like structures around the hydrophobic solutes, and this 'hydrophobic hydration' makes the non-polar molecules soluble in water. Secondly, the non-polar molecules associate with each other through 'hydrophobic interaction'.

Crowther and Vincent [31] proposed that the collapse observed at low alcohol volume fractions is a consequence of the effect of added alcohol on the environment of the poly(NIPAM) chains. Water molecules are removed from the particles to form clathrate structures around the alcohol molecules, thereby promoting hydrophobic bonding between poly(NIPAM) chains (i.e. excluding them from the binary water–alcohol mixture) and encouraging chain collapse [31, 36]. At higher alcohol volume fractions, the clathrate structure disruption frees up water molecules to re-solvate the polymer chains, contributing to the re-entrant swelling [31]. The re-entrant chain swelling is also promoted by direct interaction of the freed alcohol molecules with hydrophobic groups within the poly (NIPAM) macromolecular structure [36]. This is termed 'co-non-solvency' and results from an intricate balance of interactions [36].

Dispersion stability

The stability of microgel particles dispersed in a solvent medium is a key physicochemical property to be taken into account when investigating the suitability of a dispersion for a particular application [38, 39]. Dispersion stability is governed by a balance of interactions that occur between microgel particles themselves and between particles and the solvent [38]. These interactions include electrostatic repulsion, steric stabilization and attractive van der Waals forces [40]. When dispersed particles inevitably collide, if they remain in contact afterwards, they aggregate and precipitate out of dispersion; permanent (irreversible) contact is termed coagulation, whereas temporary contact is termed flocculation or association [38]. Mixed-charge colloidal dispersions (i.e. containing differently charged particles) may exhibit stronger aggregation, known as heteroaggregation (heteroflocculation), than dispersions containing only a single type of particle [38]. The form and strength of aggregation of microgel particles can be manipulated by the addition of polymer and/or simple electrolytes [41], as well as by varying the microgel's own composition, which means particles can be tailored to suit particular processes.

Excellent detailed reviews of the theory of colloidal stability can be found elsewhere [38] so only a brief description of the forces governing aggregation will be given here to support the main discussion of applications of *flocculating* microgel systems. In an aqueous dispersion of a single microgel type at room temperature, the swollen particles exhibit substantial hydrogen bonding with solvent molecules [36]. In addition, some polymer chains extend outwards from the particle into the solvent (known as the 'hairy layer') providing steric stabilization, and longer-range electrostatic repulsion forces between the charged groups that reside primarily at the particle surface help ensure the colloidal stability of the particles in the aqueous solvent [3, 15]. The Hamaker constant of the particles is very closely matched to that of the solvent, so the particles exhibit a very low van der Waals attractive force and the forces favouring aggregation remain minimal [40].

However, when the temperature rises above the VPTT of the particles, their collapse results in an increase in the particle Hamaker constant [2, 40]. This in turn leads to increased van der Waals attractive forces and favours particle aggregation [42]. Electrostatic repulsion increases due to the increased surface charge density [3, 15], but in the presence of relatively high electrolyte concentrations

(e.g. >0.05 mol dm^{-3} NaCl), aggregation occurs; the electrostatic charges that previously favoured stability below the VPTT are screened by the electrolyte ions, which reduces the Debye length of the electrical double layer and facilitates aggregation [40]. The aggregation is typically reversible (i.e. a flocculation) on cooling the dispersion back below the VPTT, where the particles redisperse [40].

In mixed-charge systems, such as the mixture of cationic microgel particles and anionic polystyrene latex studied by Islam et al. [40, 42], stable and unstable heteroflocculation may be observed above the VPTT of the particles. Below the VPTT, electrostatic and steric repulsion forces between the particles are sufficient to prevent attraction, but above the VPTT charge density and subsequent electrostatic attraction increase such that heteroaggregation may take place [40]. However, the formation of stable dispersions of macro-complexes was also observed above the VPTT, when the cationic microgel particles were in excess relative to the latex particles. The anionic latex particles were surrounded by the cationic microgel particles, giving rise to
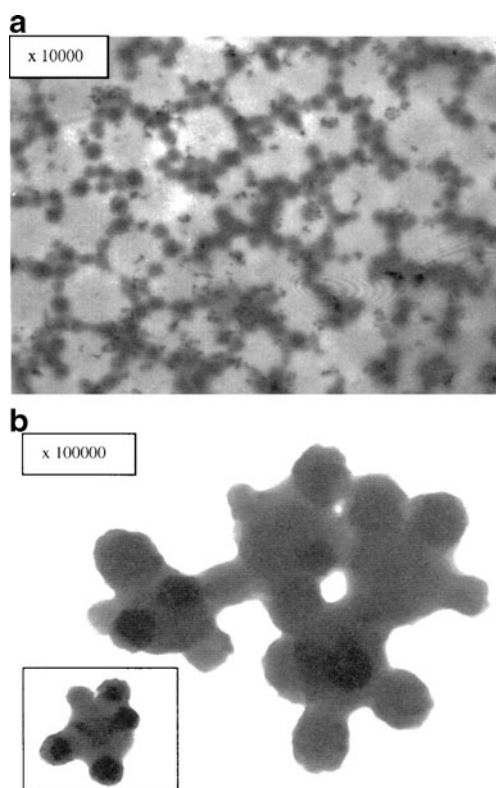
heteromacroparticles with a net positive charge that remained dispersed [40, 42] (Fig. 7).

As previously mentioned, dispersion stability can be influenced by the addition of electrolyte and/or free polymer [41]. For example, the work of Hall et al. [40] described above demonstrated that heteroaggregation can be influenced by the relative concentration of microgel particles, pH, electrolyte concentration and temperature. The presence of relatively high concentrations of electrolytes such as NaCl screens electrostatic repulsion forces, favouring particle aggregation [40], whilst the presence of free polymer can promote both stabilization and aggregation by steric mechanisms [41]. Figure 8 illustrates some effects of the presence of polymer on particulate dispersion stability, which alternates between stabilization and flocculation as the polymer concentration increases.

Other flocculation processes include incipient flocculation, where particles sterically stabilized by adsorbed polymer flocculate as a result of decreasing solvent quality; bridging flocculation, where an adsorbed polymer forms a bridge between two particles; charge-patch flocculation, where adsorbed polymer creates discrete anionic and cationic patches that attract neighbouring particles; and depletion

Fig. 7 **a** TEM image of equal concentrations of anionic poly(NIPAM) and cationic poly(NIPAM-co-4-vinylpyridine) (4-VP) in deionised water at pH 3. Samples were dried at room temperature; **b** TEM image of equal concentrations of anionic poly(NIPAM) and cationic 4-VP-co-poly(NIPAM) in deionised water at pH 3. Samples were dried on a hot plate at 45 °C (*inset*: single heteromacroparticle from the same sample). Reprinted from [40] with permission from Elsevier
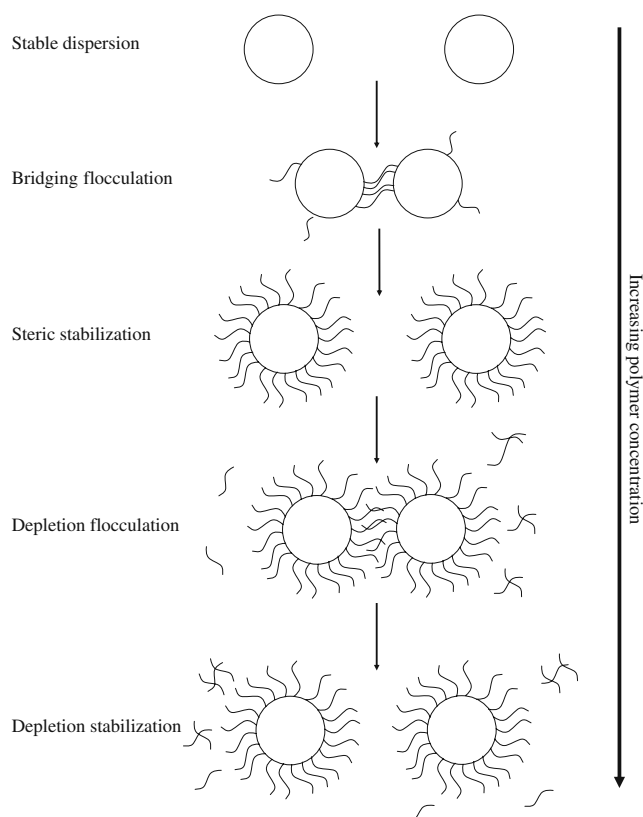
Fig. 8 Illustration of the potential effects of increasing polymer concentration on the stability of a particulate dispersion. Redrawn from [41] with permission from Elsevier

flocculation, when non-adsorbing polymer is excluded from the interstitial spaces between particles, exerting an osmotic pressure that forces the particles together [41, 43].

Other influences

Other influences or triggers for inducing the swelling behaviour of microgels include light and magnetism [44], examples of which are included in the discussion of applications below.

Applications

The fact that the shrinking/swelling response can be tailored to occur in response to specific environmental conditions means that these 'smart nanoparticles' show great potential in a wide variety of applications. They have already been utilized in a wide range of industries, including areas such as paints, ink-jet printing, cements, enzyme immobilization, oil recovery, molecular separation, environmentally sensitive display devices and on/off molecular switches [6]. The role of microgel particles in a variety of applications will be discussed, followed by a consideration of some commercial implications involved. Table 1 lists selected microgels and their potential applications.

Heteroflocculants

Waste water treatment/water purification

Flocculation and coagulation have proved to be extremely important in wastewater treatment over thousands of years, with clarifying agents such as crushed seeds known to have been used in treating potable water since ancient times [43]. Today, coagulation and flocculation are key processes for removing suspended fine particles, colloids, turbidity, natural organic matter and dissolved inorganic/organic contaminants during most water treatment [45]. Synthetic or natural polymers (polyelectrolytes) are commonly utilized, either adsorbing to and binding adjacent colloid particles to cause bridging flocculation, or by attracting and adsorbing oppositely charged materials, thereby decreasing the potential energy of repulsion between adjacent colloids and allowing flocculation to occur [43]. As microgels are capable of the sorption/desorption of a variety of materials [3] and can also be tailored to flocculate under specific environmental conditions [40], they show promise in assisting in wastewater treatment [46]. Note: A polymer coagulant is a polyelectrolyte—a 'polymer composed of macromolecules in which a substantial portion of the constitutional units contains ionic or ionizable groups, or both' [47].

Snowden et al. [48] demonstrated that thermosensitive microgel dispersions of poly(NIPAM) with cationic or anionic surface charges absorb significant quantities of ions from aqueous solution at 25 °C: ammonium/lead/cadmium nitrates, aluminium citrate and HCl. The study showed that the nature of the initiator used during microgel synthesis, which determines the surface charge group of the resulting particles, strongly influences the adsorptive characteristics. For example, cationic poly(NIPAM) (containing quaternary ammonium groups from 2,2-azobis-(2-amidinopropane)) removed more than three times more ammonium nitrate than carboxylated poly(NIPAM) (containing carboxylate groups from 4′4-azobis(cyanopentanoic acid)). At 50 °C, in most cases, microgel shrinkage led to the release of around 60% of the absorbed ions, indicating the potential value of these particles in wastewater treatment and water purification. The retained material is believed to be electrostatically bound to the microgel, whose polymer chains have low affinity for the aqueous solvent and have a considerably decreased surface area.

Morris et al. [46] demonstrated that poly(NIPAM-co-AA) microgel particles reversibly adsorb hydrolysable lead ions. The extent of adsorption/desorption could be controlled by pH adjustment, modifying the AA content of the microgels and changing temperature. In particular, the temperature-induced flocculation observed when the particles were in the collapsed state showed potential for water purification as the flocculated, lead-ion-containing microgels at high temperatures could be more easily recovered, then cooled to release the lead ions.

Other studies, although not necessarily directly concerned with water purification, also suggest microgels could play a role in such processes. For example, Peng and Wu [25] made a fundamental study of controllable interactions between metal cations (Hg^{2+}, Cu^{2+}, Ca^{2+} and Na^+) and thermosensitive poly(N-vinylcaprolactam-co-AA) microgels, with a view to biomedical applications such as the immobilization of proteins and drugs. As mandatory threshold parameters are prescribed for the presence of ions such as these are specified in regulations such as the European Directive (Council Directive 98/83/EC) [45], microgels with affinities for such ions could potentially find use in water purification.

Enhanced oil recovery

Nowadays, in response to the ever increasing world oil market and the rapid depletion of 'easy' oil reserves, many more unconventional oil reservoirs [49], such as heavy oil reservoirs, low-permeable oilfields, offshore oilfields etc., have been developed. In order either to stabilize the oil production of mature oilfields or to exploit the heavy oil reservoirs effectively, enhanced oil recovery (EOR) pro-

Table 1 Selected microgels and their potential applications

Microgel	Application	Ref
NIPAM	Wastewater treatment	[46, 48]
	EOR	[50]
	Water removal from biodiesel	[51]
	Tissue engineering	[61]
	Capillary occlusion	[63]
	Cancer hyperthermia treatment	[64]
	Molecular imprinting	[84]
	Paper-supported biosensors	[91]
	pH switch	[97]
	Catalysis	[97, 99]
	Temperature-sensitive thickener	[63]
NIPAM/BuA	Transdermal drug delivery agent	[19, 20]
NIPAM/MAA	Transdermal drug delivery agent	[19, 20]
		[19, 20]
Poly(N-ethylacrylamide)	High VPTT microgel	[21]
Poly(N-[(2-hydroxy-3-trimethylammonium)propyl] chitosan chloride)	pH-sensitive microgel	[23]
Poly(N-vinylcaprolactam)	pH-sensitive microgel	[24, 25]
NIPAM/AA	Multi-responsive microgels (temp/pH/ionic strength)	[28–30]
	Lead adsorption	[46]
Cationic NIPAM/4-VP with anionic NIPAM	Flocculation/aggregation	[40]
Cationic NIPAM with anionic PS	Potential for regeneration	[42]
NVCL/AA	Metal cation absorption	[25]
	Immobilization of protein and drugs	[25]
POEGMA	Biomaterial	[54]
PEG	Increased bioavailability	[55]
MAA derivatives	Injectable replacement for damaged soft tissue	[56]
EA/MAA/BDDA	Replacement for load-bearing soft tissue	[57]
NIPAM/HEMA/AA	Injectable cell scaffold	[58]
Polyglycerol	Highly biocompatible biomaterials	[59]
AM	Encapsulation of magnetic particles	[67]
	Molecular imprinting	[83]
Polyelectrolyte NIPAM	Encapsulation	[69]
Cationic chitosan/anionic citrate-modified ferroferric oxide	Targeted controlled drug release and diagnostics	[71]
NIPAM/BuA/AA	pH-controlled oral insulin drug delivery	[76]
L-Lactic acid/D-lactic acid co-polymers	Protein drug delivery	[78]
NIPAM/AAPBA	Glucose sensing	[87]
Polystyrene/cyclam	Cu(II) ion sensing	[11]
Styrene/BuA	Catalysis	[96]
Dimethylacrylamide-co-2-acrylamide-2-methyl-1-propanesulphonic acid	Rheological modifier	[101]
Epoxy-acrylic	Electrodeposition paint	[105, 106]
AA	Cosmetic/pharmaceutical thickener	[109]
AMPS	pH-triggered cosmetic thickener	[111, 113–115]
MAA	Electrorheological fluid	[63]
4-VP/silica	Emulsifier	[118–121]
NIPAM/MAA	pH-triggered emulsifier	[122, 123]

cesses are indispensable. Polyacrylamide has a long history in oilfield application to guarantee stable oil production in a variety of forms. In the form of spheres, such polymers have numerous useful properties, including nanosize, water absorbing selectivity, brine tolerance, high water absorptivity, good dispersion in water, low aqueous solution viscosity etc. They can therefore easily migrate into the interior layers of the reserve to accomplish in depth profile control, water shutoff and flooding, aiming to improve the sweep efficiency. However, to some extent, the application of polyacrylamide nanospheres in EOR faces constraints as a result of low polymer content and high cost of production.

Poly(NIPAM) microgels offer potential as an intelligent secondary oil recovery system [50]. When an oil field comes to the end of its working life, secondary oil recovery methods are employed because as much as 40% of the oil within a reservoir can still be trapped underground. Initially, oil is extracted by drilling a number of wells into the reservoir (Fig. 9). Injector wells are used to pump a fluid (e.g. seawater) into the reservoir, which pushes oil out through a producer well. Over time, the seawater which is sweeping the reservoir, pushing the oil out of the producer well, will also begin to exit from the producer well. The sweep of the reservoir can be improved by blocking porous channels within the reservoir so that the seawater flow will take the path of least resistance (i.e. through porous channels) between the injector and producer. If this path of least resistance is blocked, then the flow of water will be diverted and sweep different areas of the reservoir. Currently polymer floods can be used to achieve a block,
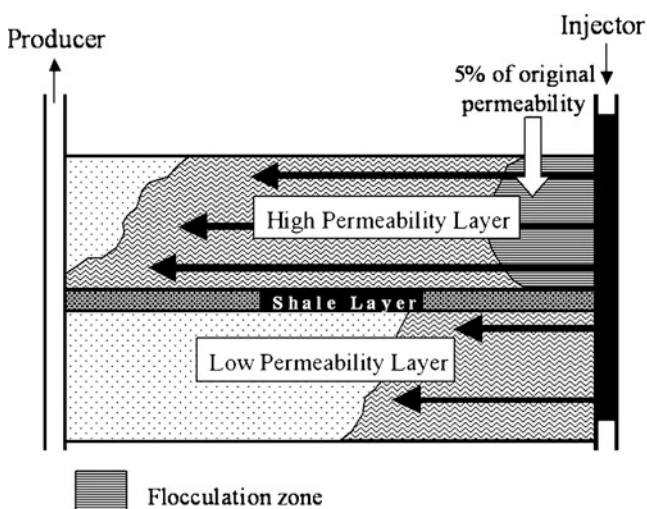

Fig. 9 Model of enhanced oil recovery with microgels. Initially the flow of water from the injector well passes through the high permeability layer. Upon injection of microgel, the permeability of this layer decreases to 5% of the original value, forcing the flow of water through the low permeability layer, therefore increasing reservoir sweep

by injecting them into the reservoir where they are allowed to cure. Effectively, these are polymers that have low viscosity under injection but change to a high viscosity over time. One drawback is the increase in viscosity is not reversible and the block is either permanent or cannot be moved rapidly. The ability to move a block is advantageous as it allows for a more efficient sweep of the reservoir.

The process relies on the charged microgel particles forming stable dispersions below their VPTT. When injected into the ground, the microgels flocculate in response to the higher temperatures prevalent in oil-bearing rock (above the VPTT) and the presence of electrolytes in the pumping material, e.g. seawater. The colloidal aggregates block channels of high permeability, enabling the oil in the less permeable areas to be mobilized. The process relies on the strength of the aggregation, i.e. its ability to endure large shear forces resulting from high pressures. Mixed-charge colloidal dispersions can exhibit stronger aggregation characteristics than can be achieved with the simple van der Waals forces of single-charge systems because electrostatic attractive forces also contribute to the robustness of the resulting aggregates.

Microgels can utilize this ability to flocculate and cause a blockage for EOR. Upon injection into the well, the microgel is cooled below the VPTT, and in the resultant swollen state, the microgel dispersion is a low viscosity fluid, with the particle size and density such that it permits passage through porous rock. As the microgel dispersion is pumped down into the reservoir, a temperature gradient is met (generally the greater the depth, the higher the temperature). When heated, poly(NIPAM) microgels in seawater undergo rapid flocculation, so when the injected microgel reaches a temperature above its VPTT, it will flocculate and cause a blockage. Flocculation of a poly(NIPAM) microgel is reversible, and it is thought that as the oil front moves, the temperature front will move in conjunction with it. The microgel block would effectively track the temperature front through the reservoir and provide an enhanced sweep compared to a static block.

Water removal from biodiesel

Nur et al. [51] demonstrated that poly(NIPAM)-based microgels are capable of removing water from the organic solvent hexane, suggesting that it shows potential for absorbing water from biodiesel prepared from rape seed. A range of co-polymer poly(NIPAM) microgels were shown to precipitate in hexane, but on the drop-wise addition of water, the precipitated microgel particles soaked up the water molecules and formed a gel, which could be easily recovered for re-use by filtration and centrifugation. The same microgels were shown to successfully remove water from biodiesel.

Biomaterials/biomedical applications

Another application area in which microgels show promise is in biomaterials, which can be defined as 'any systemically, pharmacologically inert substance or combination of substances utilized for implantation within or incorporation with a living system to supplement or replace functions of living tissues or organs' [52]. Biomaterials have been developed for many regions of the body, including contact lenses, degradable sutures and prosthetic joints [53]. The most fundamental requirement of any biomaterial is that it is biocompatible, i.e. that it should be able to co-exist with its tissue environment without having any undesirable or inappropriate effect on each other [53].

The toxicity of microgel base monomers such as NIPAM presents a problem when considering the potential of NIPAM-based microgels for biomedical/biotechnology applications, so there is substantial interest in alternative base monomers that show greater biocompatibility. For example, Hu et al. [54] highlighted the advantages of microgels based on poly-oligo(ethylene glycol) methacrylates (POEGMA), which include greater biocompatibility and resistance to absorption of proteins than NIPAM. Poly (ethylene glycol) coatings have been shown to substantially prolong the circulation time of polymeric nanoparticles in the blood stream [55].

Despite this requirement, microgel-based biomaterials are under development. For example, Freemont and Saunders [56] described the design of injectable microgel dispersions containing MAA that are capable of providing structural support for damaged soft tissue such as intervertebral discs and enable tissue regeneration in the longer term (Fig. 10). Saunders et al. [57] demonstrated the ability of pH-responsive microgel particles to restore the mechanical properties of load-bearing soft tissue. Gelled, dispersions of poly(ethylacrylate-co-methacrylic acid-co-1,4-butanediol diacrylate) (poly(EA/MAA/BDDA)) microgels were injected into artificially degenerated, model intervertebral discs, and then swelling was induced by changing pH. Results showed that pH-induced swelling of the microgels restored the mechanical properties of the degen-
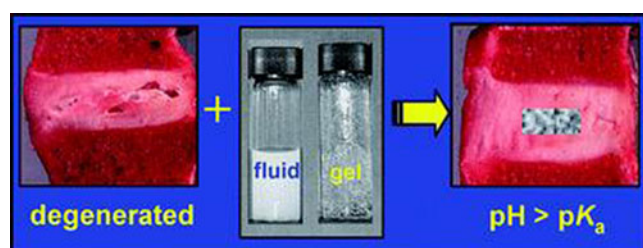

Fig. 10 Illustration of the role of pH-responsive MAA-containing microgels in repairing degenerated intervertebral discs. Reproduced from [56] with permission of The Royal Society of Chemistry

erated discs to similar values to those of normal, non-degenerated discs.

More recently, Gan et al. [58] investigated the potential of poly(NIPAM-co-2-hydroxyethyl methacrylate-co-acrylic acid) microgels to act as injectable cell scaffolds. Results showed successful culture and proliferation of HepG2 cells in poly(NIPAM/HEMA/AA) hydrogels with a low degree of syneresis (i.e. the expulsion of liquid from a gel), the extent of which could be controlled by adjusting the AA content. Sisson and Haag [59] produced highly biocompatible, biodegradable polyglycerol nanogels that could be surface functionalized and readily internalized by cells by endocytic mechanisms. The authors believe that polyglycerol nanogels are likely to find use in a broad range of biomedical applications. Panda et al. [60] fabricated large numbers of cell-laden microgel particles using stop-flow lithography, which could be used in generating three-dimensional tissue constructs for drug delivery or tissue engineering.

The potential of microgels for the detachment and delivery of human cells has also been demonstrated: Hopkins et al. [61] modified poly(NIPAM) microgels with a cell-adhesive peptide (GRGDS), which bound to cell surface integrins on dermal fibroblasts and entholial cells. Above their LCST, the microgels removed the cells from their normal culture substrate then, on cooling, released the viable cells to grow on new substrates. The authors suggest that such systems will have wide-ranging applications in cell biology and tissue engineering.

Microgels based on synthetic polymers have been investigated as synovial fluid substitutes [62]. In some inflammatory diseases, the polymeric component of synovial fluid, hyaluronic acid, becomes degraded and is unable to provide the necessary degree of viscosity. Hyaluronic acid injections are costly and have short-lived effect, but microgels can simulate the viscoelastic properties of hyaluronic acid and, due to their resistance to radical-induced degradation, could provide a longer-term effect. The potential for poly(NIPAM) to act as an artificial embolus by swelling above the LCST to occlude capillaries has also been investigated (Matsumura et al. 1994 in [63]).

Microgels have also been tested for application as slimming aids [62]. Microgels were embedded with a cationic fat-binding agent in an edible, sugar-free matrix, which disintegrates in the digestive tract. The microgels swell (up to 100 times the dry volume) in the stomach, creating a feeling of fullness and hence satiety. The cationic fat-binding agent scavenges fatty acids, reducing absorption in the intestine.

Microgels can be used to improve the efficiency of other biomaterials/drug delivery systems/treatments. For example, Aqil et al. [64] investigated the potential of NIPAM-based microgels for increasing the stealthiness of magnetic

iron oxide nanoparticles in hyperthermia treatments. Magnetic fluid hyperthermia shows promise in the treatment of cancers, where magnetic nanoparticles are injected into a tumour, which is then subjected to an alternating magnetic field that induces the nanoparticles to generate heat and destroy the tumour [65]. Aqil et al. [64] demonstrated that coating the iron oxide nanoparticles with NIPAM-based co-polymers—poly(AA)-b-poly(NIPAM) and poly(AA)-b-poly(NIPAM)-b-poly(acrylate methoxy poly(ethylene oxide))—resulted in increased stealthiness of the nanoparticles, making them suitable for biomedical applications.

Colloidal dispersions of magnetic nanoparticles in water, known as aqueous magnetic fluids, have a number of applications in biosciences, including magnetic resonance imaging contrast agents, the magnetic guidance of drugs/radioisotopes and for cell-sorting processes [66, 67]. Ménager et al. [67] demonstrated a free radical polymerisation in inverse emulsion technique to encapsulate magnetic particles inside a hydrophilic AM gel. The resulting microgels (Fig. 11) demonstrated a rapid and reversible response to a weak magnetic field, homogenous distribution of the magnetic colloid and solvent swelling without release of the magnetic content, all of which suggest potential biotechnological applications.

Encapsulation/carrier systems

The previous examples of microgel-based magnetic nanoparticle biomedical applications illustrate the role microgel systems can play as carrier systems due to their tunable size, high loading capacity, high stability (compared to micelles), responsiveness to environmental factors and large surface area capable of multivalent bioconjugation [68]. The particles are capable of 'carrying' a wide variety of materials/biomaterials.

For example, Sukhorukov et al. [69] reported a novel form of designer capsule (100 nm–10 μm) in which a wide variety of materials could be encapsulated, making them suitable for a wide variety of applications in medicine,

pharmacy, biotechnology, food technology, cosmetics or detergency. Consecutive layers of oppositely charged polyelectrolytes were adsorbed onto a colloidal particle, e.g. a poly(NIPAM)-based microgel, which could later be sacrificed, leaving a micron-sized hollow polyelectrolyte capsule (see Fig. 12). Various materials, such as enzymes, could then be encapsulated by using pH to reversibly switch the permeability of the capsule (Fig. 13). In addition to applications in encapsulation and release, the capsules also showed potential for processes in microcompartments, for example, in biotechnology or diagnostics. The possibility of a role as artificial cell organelles was also postulated, for example, with encapsulated protected enzymes capable of communicating with the cell cytoplasm.

Substantial research on nanocapsules has continued, creating nanocapsules based on a wide variety of polyelectrolytes and sacrificial colloidal particles. For example, Cao et al. [70] prepared thermosensitive poly(NIPAM)-based nanocapsules with a hydrophilic core of an aqueous cobalt tetrafluoroborate solution. Mu et al. [71] prepared superparamagnetic pH-sensitive multilayer hybrid hollow microspheres for targeted controlled drug release or in diagnostics. The nanocapsules were created from cationic chitosan and anionic citrate-modified ferroferric oxide nanoparticles, on sacrificial polystyrene sulphonate microsphere-etched templates. Pastorino et al. [72] used nano-engineered polymeric capsules to successfully encapsulate and release the anticancer agent paclitaxel.

Related to the suggestion by Sukhorukov et al. [69] that hollow nanocapsules could act as artificial cell organelles, Hammer and Discher [73] discussed the potential of functionalized colloidal or polymeric microspheres with cell-like adhesive properties, which could contribute to building complex hierarchies characteristic of biological cells, but incorporating novel and possibly superior properties of material strength, specific targeting and controlled release.

Microgel particles can also be considered not only to have potential for 'carrying' materials, such as inks and dyes, then releasing them in a controlled way, but also for 'containing' or

Fig. 11 Optical micrographs of magnetic microgels (5 wt.% MBA/AM) prepared in water in oil emulsion and dispersed in water **a** without magnetic field and **b** under magnetic field ($B=$ 200 G). The scale bar measures 20 μm. Reproduced from [67] with permission from Elsevier
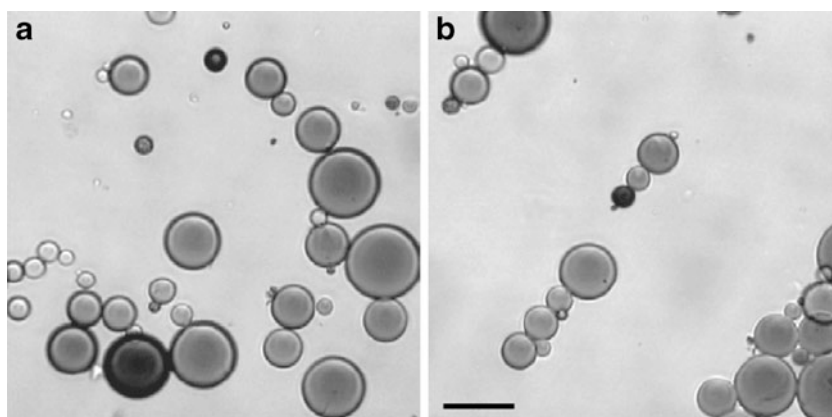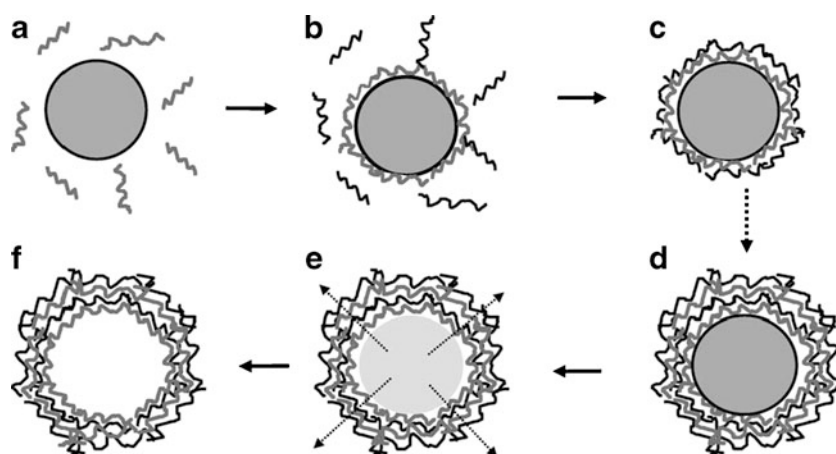
'enclosing' reactions. For example, Sanson and Rieger [68] noted that microgels can be used as nanoreactors capable of modulating the catalytic activity of metal nanoparticles.

Drug delivery

An increasing field of research is the development of devices that can control the release of rapidly metabolized drugs or have the ability to protect sensitive drugs. Conventional delivery systems suffer from limitations of dose dumping, i.e. the delivery of a high dose of therapeutic in one go. What is actually required is an elevated therapeutic drug plasma concentration over a long period of time, known as controlled release. Microgels have been used to achieve both zero-order and pulsatile release patterns [20]. They can also confer protection to sensitive drugs (e.g. proteins and DNA) against harsh environmental conditions such as pH. Microgels can fulfil the requirements for controlled release and protection due to the fact that, in response to temperature modulation, ionic strength, pH values, solvents, and even light, they undergo a rapid conformational change from a closed structure and swell to an open structure, potentially releasing entrapped therapeutics.

Microgels are being studied with the aim of developing oral drug delivery systems in which the option to cast the microgel as a thin, rapidly absorbing film is possible [74, 75]. Currently, insulin has to be injected intravenously because passage through the low pH of the stomach degrades insulin, rendering it useless. A co-polymer microgel of poly(NIPAM/butyl methacrylate/AA) has been

investigated as a delivery vehicle that protects insulin from low pH [76]. The hydrophobic butyl methacrylate facilitates the uptake of insulin into the interior of the microgel, and the incorporation of AA sensitizes the microgel to pH via protonation and de-protonation of the carboxylic acid groups above and below its pK_a (pH 4.4). Below the pK_a of AA (approximately pH 2), the microgel adopts a closed network structure within which insulin can be entrapped. Upon raising the pH above the pKa (approximately pH 7.4), the conformation changes to one of an open network structure as the intermolecular charge repulsion causes expansion. Over time, insulin was released from the open network structure via osmosis. This delivery system could be used for delivery of an oral therapeutic, whereby the therapeutic will be protected from stomach acid (closed conformation at pH 2) but on moving out of the stomach into the GI tract, the pH increases, causing the microgel to change conformation and release the therapeutic.

Delivery of protein therapeutics is challenging because biomacromolecules are sensitive to their environment and easily degraded by organic solvents and temperature. A novel biodegradable microgel has been prepared for the post-fabrication encapsulation of biomacromolecules that has a VPTT between 4 °C and 37 °C [77, 78]. A principal advantage of the entrapment of these biomacromolecules is that microparticles enable administration via injection, whilst fabrication from biodegradable polymer microgels, which more closely resemble natural living tissues due to their high water content and soft, rubbery consistencies, minimises irritation to surrounding tissues. This microgel
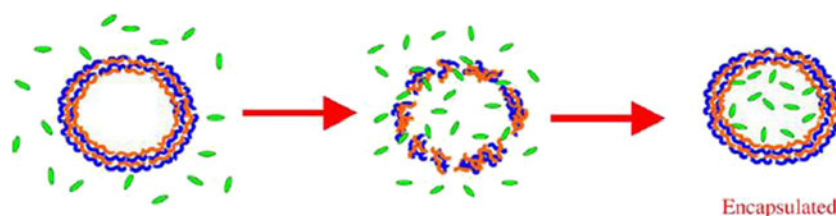
system has the ability to load a biomacromolecule at 4 °C, when the conformation is an open network, and becomes encapsulated by increasing the temperature to 37 °C. Release is achieved by the degradation of the network structure. Polymers such as poly(l-lactic acid) and its co-polymers with D-lactic acid or glycolic acid provide a wide range of degradation periods (weeks to years) resulting in the eventual release of the therapeutic [78].

The use of microgels for transdermal drug delivery has been reported [19, 20]. For example, microgels could be used in wound dressings where controlled release of a therapeutic is advantageous. The synthesis of poly(NIPAM/BuA) in the presence of ibuprofen (Fig. 14) has been investigated as a model drug delivery system across a silicone membrane and human skin. It was shown that the transport rate of ibuprofen is significantly lower by two orders of magnitude, compared with the rate of flux from a saturated solution [19]. The authors concluded that the microgel may act as a reservoir of the drug and facilitate its slow, zero-order release.

Molecular imprinting

Microgels have proven to be valuable materials to use in combination with molecular imprinting technology [5]. Molecular imprinting is a synthetic approach by which a molecular receptor is assembled by template-guided synthesis [79]. The technique permits the creation of three-dimensional cavities with tailored recognition properties [80]. Molecularly imprinted polymers can be described as tailor-made biomimetic receptors that have target molecule binding sites with affinities and specificities on a par with those of natural receptors such as antibodies or enzymes [81]. This technology enables particles such as microgels to be molecularly imprinted to target specific molecules.

For example, Wulff et al. [82] demonstrated successful, efficient molecular imprinting of single-molecule nanogels (~20 nm), which proved to be catalytically active enzyme mimics. Alternative applications for molecularly imprinted

particles include assays and biomimetic sensors [79]. Pasetto et al. [83] prepared novel acrylamide-based micro-gels incorporating functional arginine and tyrosine side chains. The microgels were molecularly imprinted using a phosphate template that generated particles capable of carbonate hydrolysis.

In 2006, Tominey et al. [84] reported the preparation of polyanionic poly(NIPAM)-based microgels containing neg-atively charged tetrazole binding sites that possessed the ability to bind various protonated amines, including the local anaesthetic dibucaine and the β-blocker propranolol (Fig. 15). Previously, similar microgels had only been prepared in non-aqueous media, so this preparation in aqueous media represented a significant step forward, by addressing the key issue of particle solubility.

Chemical sensing

Molecules which are capable of sensing the presence of another chemical species (or a change in species) have many applications in science and industry. The following describes two potential applications of microgels in this area; however, more examples can be found in the literature [85, 86].

Microgels may play a role in the development of a viable implantable glucose sensor to assist in the management of diabetes mellitus, by continuously monitoring glucose levels. Microgels which have the ability to sense glucose have already been reported [87]. For example, poly(NIPAM) (core)/poly(NIPAM-co-3-acrylamidophenylboronic acid) (poly(NIPAM-AAPBA)) (shell) microgels were synthesised by the modification of poly(NIPAM) (core)/poly(NIPAM-AA) (shell) microgels with 3-aminophenylboronic acid (APBA). The resulting core/shell microgel showed glucose-induced swelling when the microgel was above its VPTT (17–28 °C).

Boronic acid-based optical glucose sensors utilizing fluorescence as a detection method have also been developed [88]. The sensor operates under physiological

Fig. 14 TEM images of micro-gel dispersions prepared in the presence and absence of ibupro-fen. Reproduced from [20] with permission of Elsevier

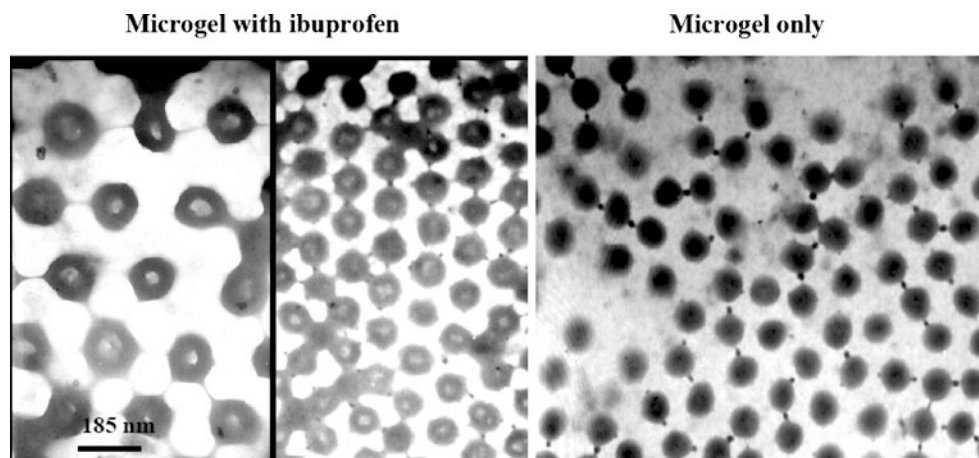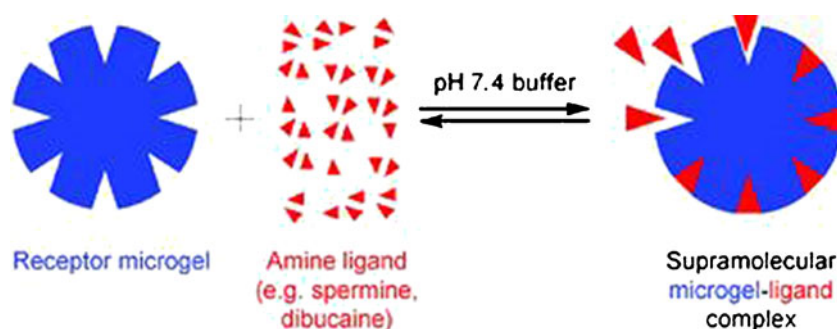Microgel with ibuprofen   Microgel only

185 nm

Fig. 15 Illustration of a microgel binding amine ligands to form a supramolecular microgel–ligand complex. Reproduced from [84] by permission of The Royal Society of Chemistry

Receptor microgel + Amine ligand (e.g. spermine, dibucaine) → pH 7.4 buffer → Supramolecular microgel-ligand complex

conditions and gives a reproducible signal in vitro. Current research is directed towards the synthesis of thin film polymers for an implantable chemical sensor that is selective for glucose.

Sensing methods based on fluorescence techniques are attracting increasing attention due to its sensitivity and the various useful analytical information it can provide [89]. Recent studies have demonstrated that dye-loaded amphiphilic core–shell particles exhibit several advantages such as higher brightness, improved photostability, faster detection and better dispersing ability of the hydrophobic fluorescence dye in aqueous solution over conventional fluorescent sensing dyes [90]. The incorporation of a dye into a smart microgel which will change its conformation upon an environmental stimuli could produce a chemical sensor.

These improved properties are attributed to the fact that the particle core can provide a hydrophobic environment to stabilize hydrophobic fluorescent dyes and confine them for efficient energy transfer. At the same time, the shell can attach ligands for selective binding of an analyte, resulting in the quenching of fluorescence intensity via energy transfer processes. Another advantage of using dye-loaded microgels is that they provide a large surface area-to-volume ratio as well as surface functional groups for binding different types of fluorescent probes for multiple analyte detections. Therefore, the incorporation of fluorescent probe(s) within the amphiphilic core–shell particle is an attractive strategy to build a convenient, effective and economical chemosensor. For a review of fluorescent dyes which have been incorporated into microgels with hydrophobic cores, see Ho et al. [11].

One novel suggestion for the use of a microgel biosensor is as a 'smart ink' that can be applied to chromatographic paper [91]. Biosensing inks for inexpensive paper-based biodetection are paper strips printed with carboxylic poly(NIPAM) microgels that are modified to enable ligand binding to a specific host; in the case of this author, an antibody (biotinylated IgG) and a DNA aptamer were used.

The printed microgel remains stationary during chromatographic elution (Fig. 16) while the microgel-supported molecular recognition elements are accessible to their intended targets present in the elution solution. This work indicates that microgels large enough to isolate the biosensors from the paper surface are sufficiently hydrophilic to be wetted during chromatographic elution, exposing the gel-supported affinity probes to their targets.

Poly(NIPAM)-based microgels can act as temperature-dependent adsorbents of proteins such as immunoglobulin and lysozyme [63, 92, 93]. Microgels are also capable of protein detection, such as the poly(NIPAM-co-AA) microgels functionalized with biotin which were used to prepare bioresponsive hydrogel microlenses capable of detecting proteins [94].

Catalysis

Streigler [95] notes how highly cross-linked soluble microgels are not only useful platforms for molecular recognition and biosensing but also as colloids that participate in catalysis. By combining inorganic nanoparticles and organic microgel, it is possible to prepare hybrid microgels with optical, magnetic or catalytic properties; nanoparticles based on silver, gold or palladium can provide catalytic activity, whilst nanoparticles based on magnetite, nickel or cobalt can provide magnetic properties [44].

For example, Gichingaa et al. [96] prepared a poly(styrene-co-BuA) microgel in which transition metal catalysts (pentadentate salen-type ligands) were immobilized, creating a macromolecular oxidation catalyst in aqueous media. Chen et al. [97] synthesised a water-soluble, biocompatible catalytic system based on poly(NIPAM), with a switchable response to pH change that mimics horseradish peroxidise enzymes. Gua et al. [98] produced chlorogenic acid surface-imprinted magnetic nanoparticles and demonstrated that not only could they be used to successfully separate chlorogenic acid from the extract of the traditional Chinese medicine honeysuckle but the particles could also be re-used and regenerated. Cornelius et al. [99] prepared poly(NIPAM)-based microgel particles incorporating imidazole functional groups that complex with haem groups (iron(III) protoporphyrin centres). The haem–microgel complex produced showed potential for reversibly binding oxygen and carbon monoxide (e.g. in mammalian respiration) and potential as a catalyst.

Fig. 16 Paper-supported biosensor. A microgel is derivitised to express streptavidin with *N*-ethyl-*N'*-dimethylaminopropyl-carbodiimide as the coupling agent. Biotinylated IgG can then be attached to the streptavidin. The IgG antibody is then ready to bind to specific ligands (*targets*). Reproduced from [91] with permission of Elsevier
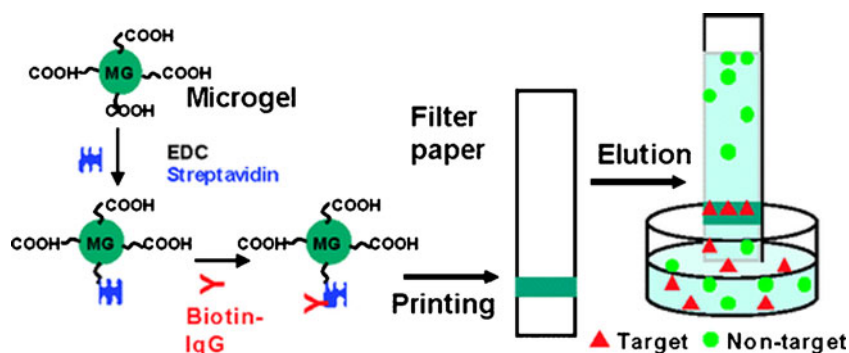
The structure of hybrid microgels, i.e. how the inorganic nanoparticles are combined with the organic component, influences the resultant behaviour [44]. In an excellent review of the synthesis and characterisation of inorganic/organic hybrids, Karg and Hellweg [44] discuss three main classes of hybrids (Fig. 17):

– Core–shell hybrids, where a nanoparticle core is surrounded by a microgel shell, e.g. hybrid microgels with gold, silver or other metal nanoparticle cores may be used to prepare photonic crystals with a temperature-tunable band gap
– Microgel particles filled with nanoparticles, e.g. poly (styrene-co-NIPAM) core–shell microgels loaded with palladium particles, which show catalytic properties [4]
– Microgel particles covered with nanoparticles, e.g. poly (NIPAM) covered with positively and negatively charged magnetic nanoparticles (based on iron and poly(sodium 4-styrenesulphonate)) which show promise for remotely controlled drug carriers [100]
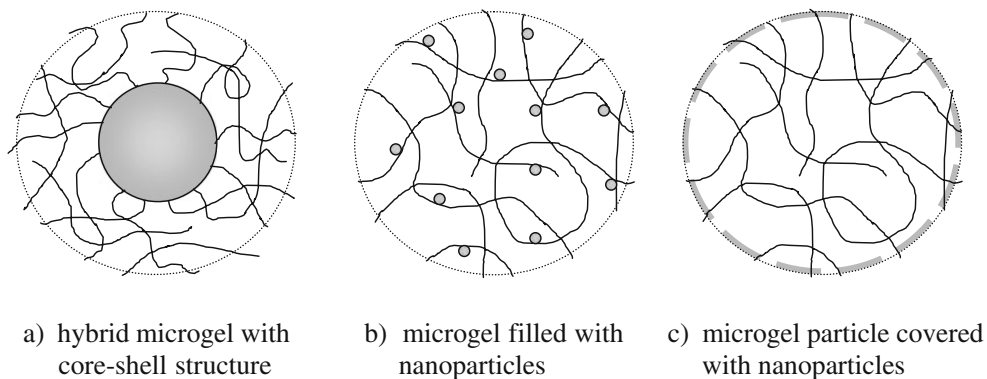
Thickeners, paints and surface coatings

The rheological behaviour of dilute and concentrated microgel dispersions has been studied in some detail. In general, the rheological behaviour is equivalent to that of hard particles with a thin, soft shell; at low concentrations,

the dispersions exhibit Newtonian flow properties, showing no change in viscosity with increasing shear rate, whilst at high concentrations, the dispersions are highly shear thinning [5]. The work of Kaneda and Sogabe [101] on a poly(dimethylacrylamide-co-2-acrylamide-2-methyl-1-propanesulphonic acid) microgel showed that at the highest concentrations, the microgel behaved as a bulk gel. The dispersion viscosity is also influenced by solvent quality, interaction with linear polymers and temperature; these collectively influence the extent of microgel swelling, which in turn dominates the shear-thinning rheology [5, 63, 102]. Microgel particles, which undergo volume changes with environmental conditions, can therefore be used to modify dispersion viscosity because it is directly proportional to the particles' hydrodynamic size [63].

As a consequence of the excellent rheological control that can be achieved with microgel dispersions, they have found numerous related applications in the surface coatings, printing and personal care product industries [6, 103]. For example, microgel additives have been used to improve the rheological properties of industrial coatings and the weather/shock resistance of films [1, 104].

In response to US regulations requiring a reduction in the use of a volatile component of automotive surface coatings, microgels have been used as a replacement [5, 9]. Simply reducing the volatile component led to an unacceptably low viscosity. However, using the non-volatile shear-thinning microgel particles provided rheological

Fig. 17 Illustration of hybrid microgel types. Adapted from [44] with permission of Elsevier

a) hybrid microgel with core-shell structure

b) microgel filled with nanoparticles

c) microgel particle covered with nanoparticles

control, good film-forming properties and favoured the alignment of added metallic flakes parallel to the substrate surface. Their rheological and reinforcing properties mean that polymeric microgels are excellent building blocks for formulating high performance organic coatings [105]. For example, cationic microgels based on a cationic polyepoxide-amine reaction product and a polyepoxide cross-linking agent have been identified for electrodeposition of coatings on automobiles, farm machinery and electrical appliances, with improved edge coverage and crater control [106]. Kim et al. [105] prepared electrodeposition paint containing epoxy-acrylic microgels which showed increased edge protection and excellent corrosion resistance, both important aspects in maintaining rust-free steel panels.

It has been shown that microgels can be applied as emulsifiers/stabilizers in a variety of complex coatings [68]. For example, microgel particles also have application in decorative paints due to the depletion interactions they exhibit, causing them to act as associative thickeners [107]. By further increasing the self-association of microgel particles utilized in decorative paints, it is possible to produce highly swellable gels or 'super absorbers' that can be used in disposable diapers and other sanitary products [107].

Polymers have frequently been used as gelating agents for gel systems and consistency excipients in emulsions and creams [108], and microgel particles have been used as thickeners in cosmetics, pharmaceuticals and personal care products [6]. For example, Carbopol 941 is a microgel based on poly(AA) that is widely used in cosmetics and pharmaceutical products and offers advantages over linear polymer thickeners, which influence the viscosity of a system by a different mechanism [109]. At high concentration (above the overlap concentration), linear polymer molecules interpenetrate and entangle, causing rapid increase in viscosity with concentration. However, microgel particles do not interpenetrate extensively, instead becoming close-packed at the overlap concentration and undergoing steric confinement by neighbouring particles, which in turn leads to an even greater increase in viscosity with concentration and causes microgel dispersions to display solid-like behaviour at low stresses [109, 110].

A further advantage of microgels over linear polymers, from a cosmetic product point of view, is that they avoid the 'sticky feeling' that results from entanglement of the linear chains; with far fewer free chain lengths to entangle, microgels provide a more desirable handling sensation [111]. Kaneda and Yanaki [112] studied the rheology of microgel particles prepared from agar, which has been used as a cosmetic thickener [111]. The study showed that the effectiveness of the particles as thickeners increased as the particle size decreased, with the apparent viscosity of the microgel dispersion depending upon the 'hardness' of the individual particles. Microgel particle size can therefore be used to adjust the extent to which a cosmetic is thickened.

Kaneda et al. [111] went on to investigate a microgel based on 2-acrylamido-2-methyl-1-propanesulphonic acid (AMPS). The previously mentioned Carbopol, although commonly used, will only thicken under basic conditions; however, personal care products/cosmetics need to remain stable over a wide pH range. Kaneda et al. [111] tested whether the incorporation of AMPS, itself a strong acid, would result in microgel particles capable of thickening under acidic and basic conditions. Several AMPS-based cosmetic thickeners were prepared [113–115]. Thermosensitive microgels such as those based on poly(NIPAM) demonstrate a thickening effect in response to changes in temperature, offering an alternative to the pH-sensitive thickeners [63].

Electrorheological fluids, whose rheological properties can be controlled using an electric field, show potential in use as novel switches or actuators, where the particles align themselves in response to the application of a voltage; poly(MAA) microgels are one example to be investigated [63].

Stimuli-responsive particulate emulsifiers

Emulsions can be defined as 'an opaque, heterogenous system of two immiscible liquid phases… where one of the phases is dispersed in the other as drops of microscopic or colloidal size' [116]. Emulsions prepared by the agitation of pure immiscible liquids are very unstable but may be stabilized by the addition of surface-active materials (surfactants) [116]. It has been shown that colloidal particles act in many similar ways to surfactant molecules, particularly at fluid–fluid interfaces, but they do not aggregate into micelles and are strongly held at interfaces [117]. Pickering emulsions are emulsions stabilized by particles [117], and a number of studies have demonstrated the emulsion-stabilizing effect of microgel particles. As emulsions are the end products in a wide range of industries, such as food, cosmetics and pharmaceuticals [118], this suggests that microgels could potentially find emulsifier applications in many areas.

Binks et al. [119] found that lightly cross-linked poly(4-VP)/silica nanocomposite microgels could be used as the sole emulsifier of methyl myristate and water and offered potential advantages over conventional surfactants. These included improved stability against coalescence and a reduced rate of creaming/sedimentation due to the enhanced viscosity of the continuous phase. An earlier study by Fujii et al. [120] demonstrated that the same particles were also effective oil/water (o/w) emulsifiers of *n*-dodecane and water/oil (w/o) emulsifiers of 1-undecanol. Temperature-induced phase inversion of o/w to w/o emulsions is possible [118], whilst in situ demulsification of o/w emulsions can be induced by decreasing pH [121]. Ngai et al. [122, 123] prepared poly(NIPAM)-stat-poly(MAA) co-polymer micro-

gels cross-linked with MBA, which acted as emulsifiers at high pH at 25 °C and 60 °C but not at low pH, i.e. further evidence of pH-dependent emulsification.

Commercialisation of microgel synthesis

The list of potential applications for microgels is extensive, and they provide an exciting opportunity to develop systems which are reactive (smart) with respect to environmental stimuli. Previous reviews and this one describe many elegant solutions to a wide range of problems/applications that have been proposed; however, when considering taking a microgel product to the next stage of development, a new set of factors must be considered.

Commercialisation and scale-up of any product requires the researcher look at the process of synthesis, storage, processing and, above all, cost, in a way which may not be familiar to a developmental researcher. The synthesis and characterisation of the homopolymer poly(NIPAM) microgel has been examined and published extensively and is therefore a good candidate as a case study for commercialisation and scale-up. The potential problems and unresolved issues which act as a barrier to commercialisation are hence discussed for poly(NIPAM) microgels.

Currently, no polymer manufacturers make thermosensitive poly(NIPAM) on a regular basis or in large quantities. To the authors' knowledge, no temperature-sensitive microgels at all are commercially produced. With the list of potential applications wide and diverse, it begs the question why it is that none is commercially made? To answer this question, the process of synthesis through to product delivery must be examined with commercialisation in mind, so that barriers can be identified and overcome.

Synthesis

Details of the synthesis of poly(NIPAM) by SFEP have been extensively published; however, the development of this
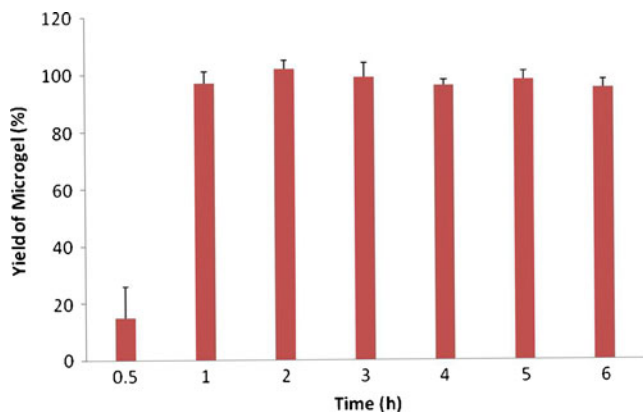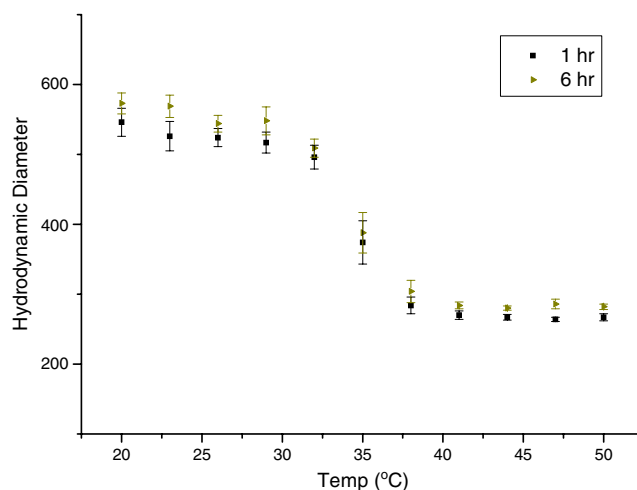
Fig. 19 Comparison of a microgel made via SFEP with 1 and 6 h synthesis times (unpublished data)

method has not been carried out with commercialisation in mind. The duration quoted for a poly(NIPAM) synthesis is 6 h at 70 °C. This yields approximately 98% conversion of monomers and other constituents into microgel. The predominant factor to consider here is time. Can the synthesis time be reduced without adversely affecting the physicochemical properties of the microgel? Unpublished work (Fig. 18) shows that the synthesis time can be reduced to 1 h, whilst still retaining a high yield. The physicochemical properties of a 1-h microgel are similar to that of a 6-h microgel (Fig. 19). A saving of 5 h could significantly reduce the cost in terms of energy and production man hours.

Consideration must also be given to the synthesis temperature. If using a thermally initiated initiator such as dipotassium persulphate, the minimum temperature at which the initiator thermally degrades but also adequately produces a microgel should be sought. However, this needs to be balanced with the reaction time. Figure 20 shows that the consumption of NIPAM and MBA is temperature dependent.
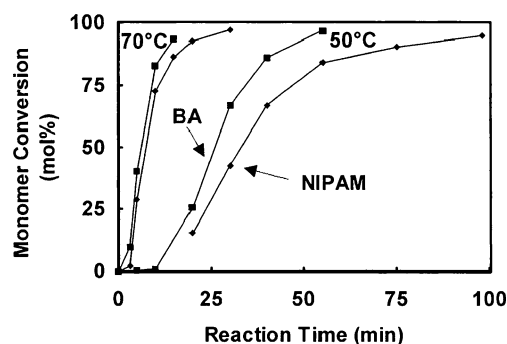
Fig. 18 Yield of microgel over a 6-h period (unpublished data)

Fig. 20 Monomer consumption vs time during microgel synthesis. Reproduced with permission from [124]
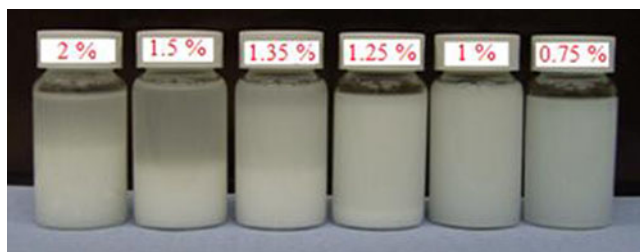
Fig. 21 Stability of a range of microgels with increasing polymer concentration

Fig. 23 Effect of surfactant on microgel particle diameter. Reproduced from [32] with permission of Elsevier

Low polymer content

Commercially available latexes typically contain 30–60% (w/v) solid, whereas SFEP of poly(NIPAM) results in a solid concentration of just 0.5% (w/v). The commercial production of such a low concentration product is not desirable to polymer manufacturers and is only suitable for the very highest value-added applications. It has been suggested [125] that the volume fraction of microgel synthesised can be increased by adding surfactant. However, it may be difficult to increase the concentration above 1% (w/v; Fig. 21) without surfactant, or 5% with surfactant, without dramatically altering the synthesis route. One possible route to increase the concentration could be the use of an inverse emulsion synthesis (Fig. 22).

It is conceivable that making a microgel inside a water droplet which is part of a stable emulsion (e.g. w/o) could stabilize the growing microgel particles at a high concen-

tration because of the repulsive forces between the individual water droplets. If the microgel particles were not kept apart by the emulsion, then the high concentration of particles would agglomerate (Fig. 22).

Apart from inverse emulsion, a number of other novel techniques are available which may allow for the increased concentration of microgel synthesis [126]. A new method has been developed to prepare smart polymeric microgels that consist of well-defined temperature-sensitive cores with pH-sensitive shells. The microgels were obtained directly from aqueous graft co-polymerizations of NIPAM and MBA from water-soluble polymers containing amino groups such as poly(ethyleneimine) and chitosan. The gel diameters ranged from 300 to 400 nm. The unique core–shell nanostructures, which had narrow size distributions, exhibited tuneable responses to pH and temperature. The method of synthesis

Fig. 22 Comparison of a SFEP and w/o EP. Proposed mechanism of stability in a high concentration of polymer

employed above has scope for increasing the percentage weight of monomer in solution [127–129].

The development of controlled/'living' radical polymerization (CRP) synthesis of nanogels/microgels, developed in the mid-1990s, allows for the easy synthesis of complex macromolecular structures with a high degree of functionality and compositional variety. Applying CRP techniques, their synthesis can be carried out at much higher monomer and cross-linker concentrations (or stopped at higher monomer conversion) as gelation is retarded [130–133]. It is indeed possible to synthesise low molar mass branched polymers in solution at monomer concentrations as high as 20 wt.% in the presence of CRP and up to 10 mol% cross-linker [134, 135]. It is important to stress, however, that a straightforward synthetic approach that is feasible at large production scales will be needed in order to bring these fascinating products to the market.

Cleaning

The cleaning of a synthesised microgel dispersion is a major problem. Microgel polymerisation can yield not only microgel but also un-reacted monomer constituents and oligomeric linear or branched chains. Ultracentrifugation followed by decantation and re-dispersion in clean water can be used to clean samples. Membrane dialysis is also commonly used, but both methods have drawbacks because they cannot easily remove high molecular weight contaminants and are long and tedious processes. This is because dialysis relies on passive osmotic diffusion for the removal of contaminants, and extensive ultracentrifugation is necessary because the density of microgels is close to that of water. Ion exchange beds, which are commonly used to clean polystyrene latex [136], cannot be used to remove non-ionic contaminants.

Contamination of the microgel with surfactant becomes an issue when surfactants are employed to increase the active concentration of microgel. The removal of surfactants is important for two reasons: It may confer a toxicological hazard to a microgel preparation which is intended for use within the pharmaceutical industry, and the presence of a surfactant can change the hydrodynamic diameter (Fig. 23) and VPTT of the microgel [125].

Sodium dodecyl sulphate (SDS) binding isotherms [137, 138] have been published for ionic surfactant solutions in equilibrium with polymer solutions, polymer microgels and macrogels. The interaction of the surfactant with the microgel particles takes place in a two-step process. The surfactant binds above a critical surfactant concentration; then, after a plateau is reached, a new binding step evolves in the isotherm. The hydrodynamic diameter of the particles also increases in a stepwise manner, in correlation with the binding isotherm. The surfactant binds in the gel as small

aggregates with different aggregation numbers in a two-step binding process, which is a consequence of the inhomogeneous inner structure of the particles. The binding starts in an outer shell of the particles followed by surfactant binding in the particle core. Surfactants can generally be removed by repeated washing; however, the complete reversibility of SDS binding has not been proved for SDS or other surfactants. Commercial scale production must overcome the cleaning problem for it to become a viable product.

Storage and transportation

Microgels which are synthesised currently have a low active concentration, approximately 0.5% (w/v). Consequently, if microgels were to be made in large quantities, then the majority of the dispersion is water. Storage and shipping of such large volumes of essentially water is not economical, and methods will have to be developed, which, if the active concentration cannot be raised during synthesis, will have to concentrate the microgel in post-production processing. A paper has been published [139] in which freeze-dried then rehydrated microgel is compared to untreated microgel. The results showed that the freeze-drying process does not adversely affect the microgels' physicochemical properties. However, freeze drying can be costly, especially for very large volumes, but there are many other techniques which could be used to reduce the water content of a microgel dispersion. Tangential flow on a commercial scale could be used to concentrate a dispersion or alternatively the dispersion could be quickly and easily spray dried. The pit falls of spray drying sub-micron microgel particles are unknown but should at the very least include inhalation and explosion hazards.

Concluding remarks

The literature available for the potential applications of microgels, whether they are smart materials with an environmental stimuli or simply a viscosity enhancer, is vast. Over the last 20 years, microgels have become more exotic in nature, and as a result, the potential applications have also become diverse. An increased knowledge of the fundamental physicochemical properties of the microgel itself and how it interacts with its environment has allowed the researcher to make bespoke microgels with a particular function or characteristic. It is this tunability and the wide variety of co-monomers which can be used that makes microgels an exciting area to study. However for all the benefits and potential applications set out in this review, currently there are no stimuli-responsive microgels commercially available. The barriers to scale-up, in particular low polymer concen-

tration dispersions and difficulties in removing un-reacted constituents, will need to be overcome. Time and effort must be put in to overcoming these barriers in order to convince commercial entities, especially polymer manufacturers, that microgels have commercial potential arising from their unique properties.

References

1. Murray MJ, Snowden MJ (1995) Adv Colloid Interface Sci 54:73–91
2. Saunders BR, Vincent B (1999) Adv Colloid Interface Sci 80:1–25
3. Pelton R (2000) Adv Colloid Interface Sci 85:1–33
4. Ballauff M, Lu Y (2007) Polymer 48:1815–1823
5. Gracia LH, Snowden MJ (2007) Preparation, properties and applications of colloidal microgels. In: Williams PA (ed) Handbook of industrial water soluble polymers. Blackwell, Oxford, pp 268–297
6. Kausar N, Chowdhry BZ, Snowden MJ (2008) Microgels from smart polymers. In: Galaev I, Mattiasson B (eds) Smart polymers: applications in biotechnology and biomedicine (2nd). CRC, Boca Raton, pp 137–175
7. Tan BH, Tam KC (2008) Adv Colloid Interface Sci 136:25–44
8. Fernández-Barbero A, Suárez IJ, Sierra-Martín B, Fernández-Nieves A, Javier de las Nieves F, Marquez M, Rubio-Retama J, López-Cabarcos E (2009) Adv Colloid Interface Sci 147–148:88–108
9. Saunders BR, Laajam N, Daly E, Teow S, Hu X, Stepto R (2009) Adv Colloid Interface Sci 147–148:251–262
10. Karg M, Hellweg T (2009) J Mater Chem 19:8714–8727
11. Ho KM, Li WY, Wong CH, Li P (2010) Colloid Polym Sci 288:1503
12. Texter J (2009) Colloid Polym Sci 287:313–321
13. Liu R, Fraylich M, Saunders BR (2009) Colloid Polym Sci 287:627–643
14. Schexnailder P, Schmidt G (2009) Colloid Polym Sci 287:1–11
15. Pelton RH, Chibante P (1986) Colloids Surf 20:247–256
16. Zhang J, Pelton R (1999) Colloid Surf A Physicochem Eng Aspects 156:111–122
17. Otake K, Inomata H, Konno M, Saito S (1990) Macromol 23:283–289
18. Woodward NC, Chowdhry BZ, Snowden MJ, Leharne SA, Giffiths PC, Winnington AL (2003) Langmuir 19:3202–3211
19. Lopez VC, Raghavan SL, Snowden MJ (2004) React Funct Polym 58:175–185
20. Lopez VC, Hadgraft J, Snowden MJ (2005) Intern J Pharm 292:137
21. Lowe JS, Chowdhry BZ, Parsonage JR, Snowden MJ (1998) Polym 39:1207–1212
22. Duracher D, Elasïssari A, Pichot C (1999) J Polym Sci A Polym Chem 37:1823–1837
23. Zhang H, Mardyani S, Chan WCW, Kumacheva E (2006) Biomacromol 7:1568–1572
24. Peng S, Wu C (2000) Macromol Sympos 159:179–186
25. Peng S, Wu C (2001) Polym 42:6871–6876
26. Ma X, Xi J, Huang X, Zhao X, Tang X (2004) Mater Lett 58:3400–3404
27. Liu HY, Zhu XX (1999) Polym 40:6985–6990
28. Snowden MJ, Chowdhry BZ, Vincent B, Morris GE (1996) J Chem Soc Faraday Trans 92:5013–5016
29. Das M, Kumacheva E (2006) Colloid Polym Sci 284:1073–1084
30. Saunders BR (2004) Langmuir 20:3925–3932
31. Crowther HM, Vincent B (1998) Colloid Polym Sci 276:46–51
32. McPhee W, Tam KC, Pelton R (1993) J Colloid Interfac Sci 156:24–30
33. Mukae K, Sakuri M, Sawamura S, Makino K, Kim SW, Ueda I, Shirahama K (1993) J Phys Chem 97:737–741
34. Mielke M, Zimehl R (1998) Prog Colloid Polym Sci 111:74–77
35. Saunders BR, Crowther HM, Vincent B (1997) Macromol 30:482–487
36. Zhu PW, Napper DH (1996) J Colloid Interface Sci 177:343–352
37. Soper AK, Finney JL (1993) Phys Rev Lett 71:4346–4349
38. Islam AM, Chowdhry BZ, Snowden MJ (1995) Adv Colloid Interface Sci 62:109–136
39. Eastman J (2005) Colloid stability. In: Cosgrove T (ed) Colloid science: principles, methods and applications. Blackwell, Oxford, pp 36–49
40. Hall RJ, Pinkrah VT, Chowdhry BZ, Snowden MJ (2004) Colloid Surf A Physicochem Eng Asp 233:25–38
41. Snowden MJ (1994) Flocculants. In: Bloor D, Brook RJ, Flemings MC, Mahajan S (eds) The encyclopedia of advanced materials. Pergamon, Oxford, pp 858–862
42. Islam AM, Chowdhry BZ, Snowden MJ (1995) J Phys Chem 99:14205–14206
43. Bratby J (2006) Coagulation and flocculation in water and wastewater treatment, 2nd edn. IWA, London
44. Karg M, Hellweg T (2009) Curr Opin Colloid Interface Sci 14:438–450
45. Parsons S, Jefferson B (2006) Introduction to potable water treatment processes. Blackwell, Oxford
46. Morris GE, Vincent B, Snowden MJ (1997) J Colloid Interf Sci 190:198–205
47. IUPAC (2006) Compendium of Chemical Terminology (2nd) (the "Gold Book"). Compiled by McNaught, AD, Wilkinson, A. Blackwell Scientific Publications, Oxford (1997). XML on-line corrected version: http://goldbook.iupac.org (2006-) created by Nic, M, Jirat, J, Kosata, B; updates compiled by Jenkins, A. ISBN 0-9678550-9-8. doi:10.1351/goldbook. Last update: 2009-09-07; version: 2.1.5. doi of this term: doi:10.1351/goldbook.P04728
48. Snowden MJ, Thomas D, Vincent B (1993) Analyst 118:1367–1369
49. Collings AG, Wright CC (1985) Enhanced oil recovery injection waters. In: Donaldson EC, Chilingarian GV, Yen TF (eds) Enhanced oil recovery, fundamentals and analyses. Elsevier Science, New York, pp 151–217
50. Wang L, Zhang GC, Ge JJ, Li GH, Zhang JQ, Ding BD (2010) Int Oil Gas Conf Exhibition 8:10
51. Nur H, Snowden MJ, Cornelius VJ, Mitchell JC, Harvey PJ, Benée LS (2009) Colloid Surf A Physicochem Eng Asp 335:133–137
52. Bhat SV (2002) Biomaterials. Kluwer, Dordrecht
53. Basu B, Katti DS, Kumar A (eds) (2009) Advanced biomaterials: fundamentals, processing and applications. Wiley, Hoboken
54. Hu Z, Cai T, Chi C (2010) Soft Matter 6:2115–2123
55. Delgado C, Pedley RB, Herraez A, Boden R, Boden JA, Keep PA, Chester KA, Fisher D (1996) Br J Cancer 73:175–182
56. Freemont TJ, Saunders BR (2008) Soft Matter 4:919–924
57. Saunders JM, Tong T, Le Maitre CL, Freemont TJ, Saunders BR (2007) Soft Matter 3:486–494
58. Gan T, Guan Y, Zhang Y (2010) J Mater Chem 20:5937–5944
59. Sisson AL, Haag R (2010) Soft Matter 6:4968–4975

60. Panda P, Ali S, Lo E, Chung BG, Hatton TA, Khademhosseini A, Doyle PS (2008) Lab Chip 8:1056–1061
61. Hopkins S, Carter SR, Haycock JW, Fullwood NJ, MacNeil S, Rimmer S (2009) Soft Matter 5:4928–4937
62. Rosiak JM, Janik I, Kadlubowski S, Kozicki M, Kujawa P, Stasica P, Ulanski P (2003) Nucl Instrum Methods Phys Res 208:325–330
63. Kawaguchi H (2000) Prog Polym Sci 25:1171–1210
64. Aqil A, Vasseur S, Duguet E, Passirani C, Benoit JP, Jerome R, Jerome C (2008) J Mater Chem 18:3352–3360
65. Philips JL (2005) A topical review of magnetic fluid hyperthermia. University of Alabama. http://bama.ua.edu/~joshua/archive/aug05/Jennifer%20Phillips.pdf. Accessed 10 Oct 2010
66. Billotey C, Wilhelm C, Devaud M, Bacri JC, Bittoun J, Gazeau F (2003) Magn Reson Med 49:646–654
67. Ménager C, Sandre O, Mangili J, Cabuil V (2004) Polym 45:2475–2481
68. Sanson N, Reiger J (2010) Polym Chem 1:965–977
69. Sukhorukov G, Fery A, Möhwald H (2005) Prog Polym Sci 30:885–897
70. Cao Z, Ziener U, Landfester K (2010) Macromol 43:6353–6360
71. Mu B, Liu P, Dong Y, Lu C, Wu X (2010) J Polym Sci A Polym Chem 48:3135–3144
72. Pastorino L, Erokhina S, Caneva-Soumetz F, Ruggiero C (2009) J Nanosci Nanotechnol 9:6753–6759
73. Hammer DA, Discher DE (2001) Annu Rev Mater Res 31:387–404
74. Yoshida M, Asano M, Suwa T, Katakai R (1999) Radiat Phys Chem 55:677–680
75. Khan MZ, Prebeg Z, Kurjakovic N (1999) J Control Release 58:215
76. Ramkissoon-Ganorkar C, Liu F, Baudys M, Kim SW (1999) J Controlled Release 59:287
77. Zhu W, Wang B, Zhang Y, Ding J (2005) Eur Polym J 41:2161–2170
78. Zhang Y, Zhu W, Wang B, Ding J (2005) J Control Release 105:260–268
79. Ye L, Cormack PAG, Mosbach K (2001) Anal Chim Acta 435:187–196
80. Flavin K, Resmini M (2009) Anal Bioanal Chem 393:437–444
81. Bompart M, Haupt K (2009) Aust J Chem 62:751–761
82. Wulff G, Chong B-O, Kolb U (2006) Angew Chem Int Ed 45:2955–2958
83. Pasetto P, Maddock SC, Resmini M (2005) Anal Chim Acta 542:66–75
84. Tominey A, Andrew D, Oliphant L, Rosair GM, Dupré J, Kraft A (2006) Chem Commun 23:2492–2494
85. Prodi L (2005) New J Chem 29:20–31
86. Mancin F, Rampazzo E, Tecilla P, Tonellato U (2006) Chem Eur J 12:1844–1854
87. Luo Q, Liu P, Guan Y, Zhang Y (2010) ACS Appl Mater Interfaces 2:760–767
88. Gamsey S, Suri JT, Wessling RA, Singaram B (2006) Langmuir 22:9067–9074
89. Wolfbeis OS (2005) J Mater Chem 15:2657–2669
90. Chen J, Zeng F, Wu S, Su J, Zhao J, Tong Z (2009) Nanotechnology 20:365502
91. Su S, Ali MM, Filipe CD, Li Y, Pelton R (2008) Biomacromolecules 9:935–941
92. Kawaguchi H, Fujimoto K, Mizuhara Y (1992) Colloid Polym Sci 270:53–57
93. Fujimoto K, Mizuhara Y, Tamura N, Kawaguchi H (1993) J Intell Mater Syst Struct 4:184–189
94. Kim J, Nayak S, Lyon LA (2005) J Am Chem Soc 127:9588–9592
95. Streigler S (2009) MiniRev Org Chem 6:234–240
96. Gichingaa MG, Streigler S, Dunawaya NA, Barnetta JD (2010) Polymer 51:606–615
97. Chen Z, Xu L, Liang Y, Zhao M (2010) Adv Mater 22:1488–1492
98. Gua X, Xua R, Yuana G, Lua H, Gub B, Xiea H (2010) Anal Chim Acta 675:64–70
99. Cornelius VJ, Snowden MJ, Silver J, Fern GR (2004) React Funct Polym 58:165–173
100. Wong JE, Gaharwar AK, Müller-Schulte D, Bahadur D, Richtering W (2008) J Colloid Interfac Sci 324:47–54
101. Kaneda I, Sogabe A (2005) Colloid Surf A Physicochem Eng Asp 270–271:163–170
102. Wolfe MS (1992) Prog Org Coat 20:487–500
103. Siedel J, Pinkrah VPT, Mitchell JC, Chowdhry BZ, Snowden MJ (2004) Thermochim Acta 414:47–52
104. Bartsch E, Kirsch S, Lindner P, Scherer T, Stölken S (1998) Ber Busengesellschaft für Physikaliscge Chem 102:1597–1602
105. Kim YB, Kim H-K, Hong J-W (2002) Surf Coat Technol 153:284–289
106. Corrigan VG, Zawacky SR (1992) Cationic microgels and their use in electrodeposition. US Patent 5096556
107. Goodwin J (2009) Colloids and interfaces with surfactants and polymers, 2nd edn. Wiley, Chichester
108. Valenta C, Auner BG (2004) Eur J Pharm Biopharm 58:279–289
109. Ketz RJ, Prud'homme RK, Graessley WW (1988) Rheol Acta 27:531–539
110. Naé HN, Reichert WW (1992) Rheol Acta 31:351–360
111. Kaneda I, Sogabe A, Nakajima H (2004) J Colloid Interface Sci 275:450–457
112. Kaneda I, Yanaki Y (2002) J Soc Rheol 30:89–94
113. Kaneda I, Miyazawa K, Yanaki T (2001a) Japanese Patent 2001–114641
114. Kaneda I, Miyazawa K, Yanaki T (2001b) Japanese Patent 2001–114642
115. Kaneda I, Miyazawa K, Yanaki T (2001c) Japanese Patent 2001–115135
116. Binks BP (1998) Emulsions—recent advances in understanding. In: Binks BP (ed) Modern aspects of emulsion science. Royal Society of Chemistry, Cambridge, pp 1–55
117. Binks BP (2002) Curr Opin Colloid Interface Sci 7:21–41
118. Binks BP, Murakami R, Armes SP, Fujii S (2005) Angew Chem Int Ed 44:4795–4798
119. Binks BP, Murakami R, Armes SP, Fujii S (2006) Langmuir 22:2050–2057
120. Fujii S, Read ES, Binks BP, Armes SP (2005) Adv Mater 17:1014
121. Fujii S, Randall DP, Armes SP (2004) Langmuir 20:11329
122. Ngai T, Behrens SH, Auweter H (2005) Chem Commun 3:331–333
123. Ngai T, Auweter H, Behrens SH (2006) Macromol 39:8171–8177
124. Wu X, Pelton RH, Hamielec AE, Woods DR, McPhee W (1994) Colloid Polym Sci 272:467
125. Pelton R (2004) Macromol Symp 207:57–65
126. Sansona N, Rieger J (2010) Polym Chem 1:965
127. Li P, Zhu J, Sunintaboon P, Harris FW (2002) Langmuir 18:8641
128. Li P, Zhu J, Sunintaboon P, Harris FW (2003) J Disp Sci Technol 24:607
129. Zhu J, Li P (2003) J Polym Sci A Polym Chem 41:3346
130. Gao H, Miasnikova A, Matyjaszewski K (2008) Macromolecules 41:7843–7849
131. Gao H, Wenwen L, Matyjaszewski K (2008) Macromolecules 41:2335–3340
132. Bannister I, Billingham NC, Armes SP, Rannard SP, Findlay P (2006) Macromolecules 39:7483–7492

133. Gao H, Polanowski P, Matyjaszewski K (2009) Macromolecules 42:5925–5932
134. Poly J, Wilson DJ, Destarac M, Taton R (2008) Macromol Rapid Commun 29:1965–1972
135. Taton D, Baussard JF, Dupayage L, Poly J, Gnanou Y, Ponsinet V, Destarac M, Mignaud C, Pitois C (2006) Chem Commun 18:1953–1955
136. Wilkinson MC, Hearn J, Steward PA (1999) Adv Colloid Interface Sci 81:77–165
137. Gilányi T, Varga I, Mészáros R, Filipcsei G, Zrínyi M (2001) Langmuir 17:4764–4769
138. Mears S, Deng Y, Cosgrove T, Pelton R (1997) Langmuir 13:1901
139. Agbugba CB, Hendriksen BA, Chowdhry BZ, Snowden MJ (1998) Colloids Surf 137:155–164